

## **Acknowledgements**

Not to sound too dramatic, but coming to Scotland to study for a PhD degree was a life-changing event for me and the person making it possible and indeed enjoyable was my supervisor, Prof Eva Hevia. She has given me the opportunity to work on amazing projects but also endless amounts of support, encouragement, optimism (apparently I am a bit pessimistic), ideas and understanding. It was not all work with Eva. We had great fun during our celebratory nights out, parties and conference trips. I don't think my next boss can ever live up to the standard set by Eva!

Another person who really made the difference for me was my second supervisor Prof Mulvey with his constant encouragements, helpful suggestions, generosity (I will just say Hawaii!) and a quick quip.

I also wish to thank the other academics in the group, Dr O'Hara and Dr Robertson for their helpful insights and comments, as well as Dr Hernán-Gómez for all his help and training in the lab. He was, and still is, my go-to-person when things get tricky. Although they are not sharing offices with us, I got the pleasure to work and learn from Dr Alan Kennedy and Dr David Armstrong who were always helpful and supportive. I can only hope I wasn't a constant test of their patience. Helping hands also came from abroad (Barcelona) from Prof Aromí and my friend Ivana who greatly contributed with their expertise in development of the manganese project. Greatly appreciated was also the help from Marco Amores, a final year student who I hadn't had the pleasure to work directly with but his contribution to the project was indisputable.

During my time at Strathclyde I got the opportunity to work with some amazing people who I can't thank enough for making me feel belonging here. There are so many to mention (it's been four years after all) and I am dreading to miss someone, so I would just like to thank them all collectively for the great welcome they had given me and even better (if possible) memories I'll be leaving with. I am lucky to have worked with such a great group of people! I must single out a few people, and first on that list is by all means Donna (or Dr Ramsay for future generations). It was an instant friendship we have struck, but I can say for certain it won't be a short lived one. Donna, Jenni, Sarah and Emma made me a part of their bunch which got bigger

and merrier with the arrival of Laia, Sam and Vicky. I can't even begin to tell the stories we have. Another very important person for me was Marco who I have met on my first day at work and very soon became good friends with. We have experienced together all the highs and lows of a PhD and travelled across the world together. It will be difficult getting use to not seeing his happy face every day. The most quiet of my pals (as Glaswegians would say) is Lewis who started alongside Marco and me. It took me a while to get to know him, but luckily I had 4 years to try and now I can't even remember the days when I didn't know him or attended his infamous parties.

And finally my family! I want to thank my parents for everything they have done for me during my whole life. The person I am today is their merit and I hope they are happy with who they see. Thanks also to my big brother Marko, for being my best friend and my strongest ally since I can remember; and to my uncle who always told me interesting stories, I credit him for getting me interested in science even before I knew what was happening; and lastly, my friend Ivana, my added member of the family. We met as undergraduates and have been through thick and thin since then, forming a bond of friendship as strong as that of sisters. I would never be here if it wasn't for her because she is the one who encouraged me and made me believe I can successfully complete a PhD.

In the end, all I can say is that I cannot believe that I am at the end of this journey. It's been great and even though I am looking forward to see what the future holds I can't help but feel uneasy about leaving. Where could I possibly find as good friends as I have found here?

Luckily, Eva helped me out with this one as well, at least for a wee short while longer, by giving me a postdoc position.

## Abstract

This project sought to extend the concept of enhanced cooperative reactivity in bimetallic chemistry to metals beyond Mg, Zn or Al, especially, Ga and Mn.

Towards new applications of trisalkylgallium in synthesis, studies on gallium NHC (N-heterocyclic carbene) chemistry afforded a novel series of normal, abnormal and anionic NHC complexes derived from  $\text{Ga}(\text{CH}_2\text{SiMe}_3)_3$ . These complexes proved excellent platforms for accessing functionalised *a*NHC ligands *via* metallation/electrophilic interception and/or thermal isomerisation. Capitalising on these advances, a new FLP system incorporating  $\text{Ga}(\text{CH}_2\text{SiMe}_3)_3$  and bulky NHCs as effective Lewis acid Lewis base combinations was developed. By exploring their reactivity towards carbonyl compounds two distinct types of FLP activation processes were uncovered. Adding the FLP pair across the C=O functionality can occur, forming new C-C and Ga-O bonds, in which NHC can participate through its normal or abnormal position. Alternatively, C-H bond activation can proceed by treating enolizable ketones, or other C-H acidic substrates such as nitriles or terminal alkynes, with the same mixture.

Exporting such steric incompatibility into bimetallic chemistry a new multicomponent LiTMP/GaR<sub>3</sub> metallating mixture that works in a tandem manner has been established. Lack of co-complexation between the bulky lithium amide LiTMP and trisalkylgallium facilitates substrate deprotonation by LiTMP (the base) and anion trapping by GaR<sub>3</sub> (the trap). Thus, introducing the concept of gallium *trans-metal-trapping*, for the first time formal gallation of aromatic substrates (*i.e.* diazines and anisole) has been accomplished.

The project also developed alkali-metal manganate chemistry. A new family of homoleptic alkali-metal manganates has been prepared and characterized by X-ray crystallographic, EPR spectroscopic and SQUID magnetometric studies. Intriguing structural/synthetic/magnetic correlations were revealed in which aggregation and reactivity of different manganates were largely determined by the alkali-metal. Furthermore, addressing the issue of ill-defined manganese species participating in organic transformations, lithium manganate  $[(\text{TMEDA})_2\text{Li}_2\text{Mn}(\text{CH}_2\text{SiMe}_3)_4]$  was disclosed as an effective reagent to promote direct Mn-I exchange and homocoupling processes.

## Publications

1. “Rational synthesis of normal, abnormal and anionic NHC-gallium alkyl complexes: structural, stability and isomerization insights” **Marina Uzelac**, Alberto Hernán-Gómez, David R. Armstrong, Alan R. Kennedy and Eva Hevia, *Chem. Sci.* **2015**, 6, 5719.
2. “Structural and Magnetic Diversity in Alkali-Metal Manganate Chemistry: Evaluating Donor and Alkali-Metal Effects in Co-complexation processes” **Marina Uzelac**, Ivana Borilovic, Marco Amores, Thomas Cadenbach, Alan R. Kennedy, Guillem Aromí and Eva Hevia, *Chem. Eur. J.* **2016**, 22, 4843.
3. “Understanding the Subtleties of Frustrated Lewis Pair Activation of Carbonyl Compounds by N-Heterocyclic Carbene/Alkyl Gallium Pairings” **Marina Uzelac**, David R. Armstrong, Alan R. Kennedy and Eva Hevia, *Chem. Eur. J.* **2016**, 22, 15826.
4. “Heavier alkali-metal gallates as platforms for accessing functionalized abnormal NHC carbene-gallium complexes” **Marina Uzelac**, Alan R. Kennedy, Alberto Hernán-Gómez, M. Ángeles Fuentes and Eva Hevia, *Z. Anorg. Allg. Chem.* **2016**, DOI: 10.1002/zaac201600310
5. “Transforming LiTMP lithiation of challenging diazines via gallium alkyl trans-metal-trapping” **Marina Uzelac**, Alan R. Kennedy, Eva Hevia and Robert E. Mulvey, *Angew. Chem. Int. Ed.* **2016**, 55, 13147.

## Other Publications not related to this work

6. “Zincate-Mediated Arylation Reactions of Acridine: Pre and Postarylation Structural Insights” Alberto Hernán-Gómez, Emma Herd, **Marina Uzelac**, Thomas Cadenbach, Alan R. Kennedy, Ivana Borilovic, Guillem Aromí and Eva Hevia, *Organometallics*, **2015**, 34, 2614.



## Conference Presentations

1. “From Normal to Abnormal: New Main Group-Metal Mediated Functionalizations Of N-Heterocyclic Carbenes”; Universities of Scotland Inorganic Conference (USIC), Glasgow University, September **2014**
2. “Rational Design of Normal, Abnormal and Anionic NHC-Ga Complexes”; WestCHEM Research Day, Glasgow University, August **2015** [prize for the best talk]
3. “Rational Design of Normal, Abnormal and Anionic NHC-Ga Complexes”; Pacificchem, Honolulu, Hawaii, December **2015**.
4. “Trans-metal-trapping (TMT) gallation of N-heterocyclic molecules”; Universities of Scotland Inorganic Conference (USIC), University of Strathclyde, Glasgow, August **2016**.

## Conference Poster Presentations

1. “Synthesis and Structural Elucidation of Novel Gallates”; 20<sup>th</sup> EuCheMS Conference on Organometallic Chemistry, St.Andrews, June **2013**.
2. “Synthesis and Structural Elucidation of Novel Gallates”; Universities of Scotland Inorganic Conference (USIC), University of Edinburgh, Edinburgh, July **2013**.
3. “Synthesis and Structural Elucidation of Novel Gallates”; RSC Main Group Chemistry Annual Meeting, Oxford, September **2013**.
4. “Synthesis and Structural Elucidation of Novel Gallates”; Hot Topics in Contemporary Crystallography - HTCC2014, Šibenik, Croatia, May **2014**.
5. “Synthesis of Triorgano Alkali-Metal Manganates: “Donor-Controlled Structural Variations in Mixed-Metal Chemistry”; XXVI International Conference on Organometallic Chemistry (ICOMC 2014), Sapporo, Japan, July **2014**.
6. “N-Heterocyclic Carbene-Stabilised Lithium Gallates: Synthetic, Structural and Reactivity Insights”; Dalton Division Poster Symposium, London, April **2015** [prize for the best poster]

7. “Synthesis of Triorgano Alkali-Metal Manganates: “Donor-Controlled Structural Variations in Mixed-Metal Chemistry”; Universities of Scotland Inorganic Conference (USIC), Heriot-Watt University, Edinburgh, September **2015**.
8. “N-Heterocyclic Carbene-Stabilised Lithium Gallates: Synthetic, Structural and Reactivity Insights”; Pacificchem, Honolulu, Hawaii, December **2015**.
9. “Transforming LiTMP lithiation of challenging diazines via gallium alkyl trans-metal-trapping (TMT)”; Universities of Scotland Inorganic Conference (USIC), University of Strathclyde, Glasgow, August **2016**.

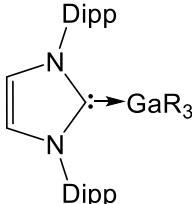
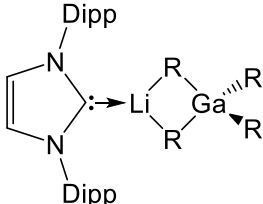
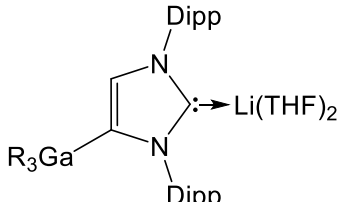
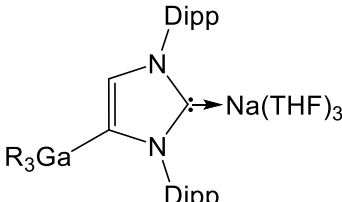
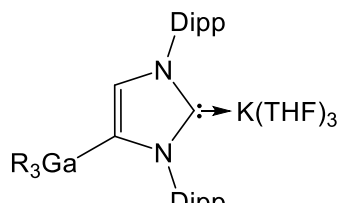
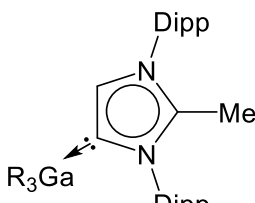
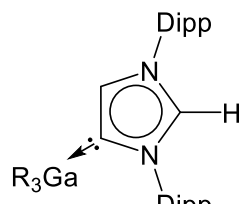
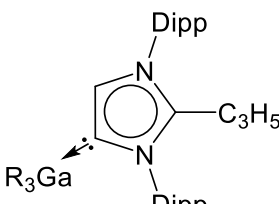
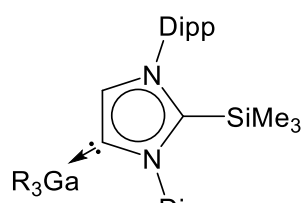
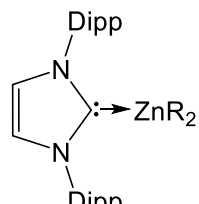
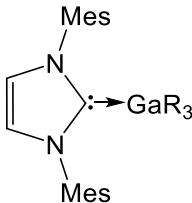
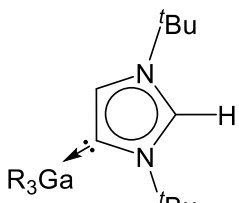
## List of Common Abbreviations

<b>AMMM</b>	Alkali-metal-mediated metallation
<b>AMMAI</b>	Alkali-metal-mediated alumination
<b>AMMMg</b>	Alkali-metal-mediated magnesiation
<b>AMMMn</b>	Alkali-metal-mediated manganation
<b>AMMZn</b>	Alkali-metal-mediated zincation
<b><math>\alpha</math>NHC</b>	Abnormal N-Heterocyclic carbene
<b>Ar</b>	Aryl
<b><i>i</i>Bu</b>	<i>iso</i> -butyl
<b><i>n</i>Bu</b>	<i>n</i> -butyl
<b><i>t</i>Bu</b>	<i>tert</i> -butyl
<b>btz</b>	benzothiazole
<b>CCDB</b>	Cambridge Crystallographic Database
<b>CIP</b>	Contacted ion-pair
<b>CIPE</b>	Complex Induced Proximity Effect
<b>D</b>	Diffusion coefficient
<b>DA</b>	Diisopropylamide
<b>DABCO</b>	1,4-diazabicyclo[2.2.2]octane
<b>DFT</b>	Density functional theory
<b>Dipp</b>	2,6-diisopropylphenyl
<b>DoM</b>	Directed <i>ortho</i> -metallation
<b>DOSY</b>	Diffusion ordered NMR spectroscopy
<b>E<sup>+</sup></b>	electrophile
<b>EPR</b>	Electron paramagnetic resonance
<b>Et</b>	ethyl
<b>Et<sub>2</sub>O</b>	diethyl ether
<b>FG</b>	functional group
<b>FLP</b>	Frustrated Lewis Pair
<b>FW</b>	formula weight
<b>HMDS</b>	hexamethyldisilazane
<b>HOMO</b>	Highest occupied molecular orbital
<b>HSAB</b>	Hard and soft Lewis acids and bases
<b>IAd</b>	1,3- <i>bis</i> -(adamantyl)imidazol-2-ylidene

<b>I<sup>t</sup>Bu</b>	1,3-bis( <i>tert</i> -butyl)imidazol-2-ylidene
<b>IMes</b>	1,3- <i>bis</i> -(2,4,6-trimethylphenyl)imidazol-2-ylidene
<b>im</b>	imidazole
<b>IPr</b>	1,3-bis-(2,6-di- <i>iso</i> propylphenyl)imidazol-2-ylidene
<b>IPr*</b>	:C{[N(2,6- <sup><i>i</i></sup> Pr <sub>2</sub> C <sub>6</sub> H <sub>3</sub> )] <sub>2</sub> CHC}
<b>iPr</b>	<i>iso</i> -propyl
<b>LA</b>	Lewis acid
<b>LB</b>	Lewis base
<b>LDA</b>	lithium diisopropylamide
<b>LICKOR</b>	alkyllithium/potassium alkoxide Superbase
<b>LiHMDS</b>	lithium hexamethyldisilazane
<b>LiTMP</b>	lithium tetramethylpiperidine
<b>LUMO</b>	Lowest Unoccupied Molecular Orbital
<b>M</b>	Metal
<b>Me</b>	methyl
<b>MeOTf</b>	methyl trifluoromethanesulfonate
<b>NBO</b>	Natural Bond Orbital
<b>NHC</b>	<i>N</i> -Heterocyclic carbene
	Nuclear magnetic resonance
	s - singlet
	d - doublet
<b>NMR</b>	t - triplet
	q - quartet
	mult - multiplet
	br - broad
<b>Np</b>	neopentyl group
<b>Nu</b>	nucleophile
<b>PEPPSI</b>	Pyridine-Enhanced Pre-catalyst Preparation Stabilisation and Initiation
<b>Ph</b>	phenyl
<b>PMDETA</b>	<i>N,N,N',N',N''</i> -pentamethyldiethylenetriamine
<b>ppm</b>	parts per million
<b>Pr</b>	propyl
<b>R</b>	CH <sub>2</sub> SiMe <sub>3</sub> <sup>-</sup> group
<b>r<sub>0</sub></b>	initial rate
<b>SI<sup>t</sup>Bu</b>	1,3-bis( <i>tert</i> -butyl)imidazoline-2-ylidene
<b>SQUID</b>	Superconducting quantum interference device

<b>SSIP</b>	Solvent separated ion-pair
<b>THF</b>	Tetrahydrofuran
<b>TMEDA</b>	<i>N,N,N',N'</i> -tetramethylethylenediamine
<b>TMP</b>	2,2,6,6-tetramethylpiperidide
<b>TMP(H)</b>	2,2,6,6-tetramethylpiperidine
<b>TMS</b>	tetramethylsilane
<b>TMT</b>	Trans-metal-trapping
<b>V</b>	Volume
<b>WBI</b>	Wiberg Bond Index
<b>X<sup>-</sup></b>	halide

## Table of Numbered Compounds

No	Compound	No	Compound
1		2	
3		4	
5		6	
7		8	
9		10	
11		12	

No	Compound	No	Compound
13		14	
15		16	
17		18	
19		20	
21		22	
23		24	

No	Compound	No	Compound
25		26	
27		28	
29		30	
31		32	
33		34	
35		36	
37		38	



No	Compound	No	Compound
39		40	
41		42	
43		44	
45			
46		47	
48		49	
50			

## Table of Contents

Acknowledgements.....	I
Abstract.....	III
Publications.....	IV
Other Publications not related to this work.....	IV
Conference Presentations.....	V
Conference Poster Presentations.....	V
List of Common Abbreviations.....	VII
Table of Numbered Compounds.....	X
<b>1. Introduction to state of the art cooperative chemistry .....</b>	<b>1</b>
1.1. Development of mixed-metal polar organometallic reagents .....	1
1.2. Deprotonative Metallation .....	7
1.2.1. Bimetallic compounds for NHC functionalisation.....	12
1.3. The less common metals .....	15
1.3.1. Organogallium chemistry .....	15
1.3.2. Organomanganese chemistry .....	18
1.4. Aims and structure of this thesis .....	21
1.5. Bibliography .....	22
<b>2. Rational synthesis of normal, abnormal and anionic NHC-gallium alkyl complexes</b>	<b>27</b>
2.1. Introduction to N-heterocyclic carbene chemistry .....	27
2.2. Aims of the chapter .....	31
2.3. NHC-stabilised lithium gallate complexes .....	32
2.4. Electrophilic interception reactions: accessing abnormal NHC-Ga complexes	40
2.5. Thermal isomerisation.....	49
2.6. DFT calculations.....	54
2.7. Mechanistic implications .....	56
2.8. Conclusions .....	62
2.9. Experimental procedures .....	63
2.10. Bibliography.....	71
<b>3. Introducing Ga complexes to Frustrated Lewis Pair (FLP) Chemistry.....</b>	<b>75</b>
3.1. Introduction to FLP Chemistry .....	75

3.2.	Aims of the chapter .....	78
3.3.	Reactions with aldehydes.....	79
3.5.	Reactions with ketones: C4 insertion vs C-H activation.....	92
3.6.	C-H activation of other substrates bearing acidic protons .....	100
3.7.	Conclusions and future work .....	105
3.8.	Experimental procedures.....	106
3.9.	Bibliography.....	114
<b>4.</b>	<b>Transforming LiTMP lithiation of challenging N-heterocyclic substrates via gallium alkyl trans-metal-trapping .....</b>	<b>119</b>
4.1.	Introduction.....	119
4.2.	Establishing GaR <sub>3</sub> as a trapping agent .....	123
4.3.	Applying TMT for pyrazine functionalisation.....	131
4.4.	Expanding the scope of TMT to other sensitive heterocycles .....	138
4.5.	Conclusion and future work.....	146
4.6.	Experimental procedures.....	146
4.7.	Bibliography .....	149
<b>5.</b>	<b>Structural and magnetic diversity in alkali-metal manganate chemistry: Evaluating donor and alkali-metal effects in co-complexation processes.....</b>	<b>152</b>
5.1.	Introduction.....	152
5.2.	Aim of the chapter .....	152
5.3.	Syntheses .....	152
5.3.1.	Synthesis of lower order sodium and potassium manganates .....	152
5.3.2.	A homologous series of tetraorgano alkali-metal manganates.....	166
5.4.	EPR and magnetic susceptibility .....	169
5.4.1.	Lower order manganates.....	169
5.4.2.	Higher order manganates .....	177
5.5.	Exploring the ability of [(TMEDA) <sub>2</sub> Li <sub>2</sub> MnR <sub>4</sub> ] to promote Mn-I exchange and homocoupling processes.....	179
5.6.	Conclusions .....	186
5.7.	Experimental procedures .....	188
5.8.	Bibliography.....	191
<b>6.</b>	<b>Conclusions and Outlook.....</b>	<b>197</b>
<b>7.</b>	<b>General experimental techniques and procedures .....</b>	<b>200</b>
7.1.	Schlenk Techniques .....	200
7.2.	Glove box.....	201

7.3.	Solvent purification.....	202
7.4.	Commercial reagents.....	202
7.5.	Standardisation of organometallic reagents .....	202
7.6.	Analytical procedures .....	203
7.7.	Synthesis of common starting materials .....	204
7.8.	Bibliography .....	210

## 1. Introduction to state of the art cooperative chemistry

Today's ease of access to information combined with the internationalisation of the scientific community has had a profound influence on modern science, primarily by elevating it from small confined areas of research to interest that pools together different backgrounds across different disciplines. In that aspect, progress made in polar organometallic chemistry has benefitted from an improved communication and collaboration between the inorganic and organic chemists. For this reason, to cover all progress made in the area would be impractical in an introduction of limited length, so therefore only the key developments relevant to the work presented in this thesis will be briefly introduced in this opening chapter. Completing this general section, at the beginning of each chapter, more specific introductions to the presented work will be given.

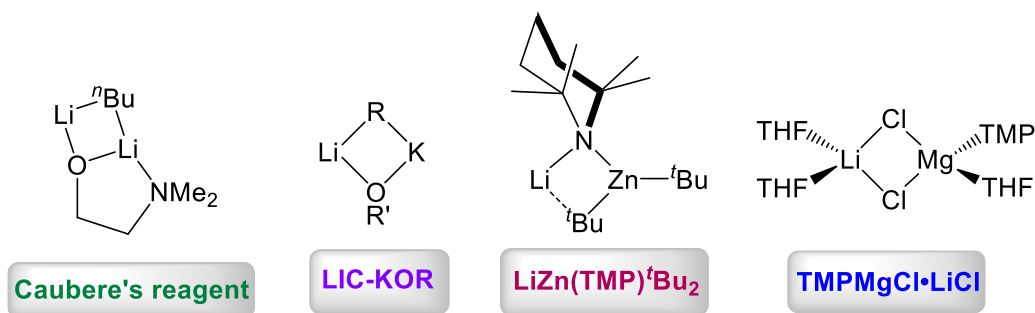
### 1.1. Development of mixed-metal polar organometallic reagents

Single-metal organometallic species such as alkyllithium  $(\text{LiR})_n$  and lithium amide  $(\text{LiNR}_2)_n$  reagents have long been deemed reagents of choice in several cornerstone organic transformations such as deprotonative metallation, metal-halogen exchange, transmetallation and carbometallation reactions.<sup>[1,2]</sup> The widespread utility of these reagents, evidenced in their commercial availability from companies such as Sigma Aldrich, Rockwood Lithium (now Albermarle) or Alfa Aesar, is due primarily to their high reactivity caused by the high polarity of the carbon-metal ( $\text{Li}^{\delta+}-\text{C}^{\delta-}$ ) bond ( $\chi(\text{Li}) = 0.98$  vs  $\chi(\text{C}) = 2.55$ , according to Pauling).<sup>[3,4]</sup>

Whereas high reactivity is sought after in a reagent, in organolithium reagents it often comes tainted with the lack of functional group tolerance and/or selectivity. Examples are side reactions from the attack of the electrophilic substituents and incompatibility with ethereal solvents. In many cases this imposes the need for strict reaction conditions including extremely low temperatures. Some of these drawbacks can be avoided or at least minimised by the use of Grignard reagents  $(\text{RMgX})_n$  which exhibit better functional group tolerance, compatibility with transition-metal catalysed cross-coupling reactions and tolerate higher temperatures.<sup>[5]</sup> However,

these group 2 reagents can be limited by their diminished reactivity in comparison to alkyllithiums, poor solubility in non-etheral solvents and complicated solution-state equilibria (most commonly Schlenk equilibria).<sup>[6]</sup>

A developing synthetic strategy, that aims to overcome the limitations of polar organometallic reagents, is the use of bimetallic compounds containing two metals of distinct polarities. These were often pioneered sporadically in early studies, the most notable examples being the Lochmann-Schlosser superbases<sup>[7,8]</sup> and Caubere's reagents<sup>[9]</sup> both in the late 1960s. More recently, mixtures of this type have been studied more systematically including Knochel's turbo Grignard and related salt-supported reagents<sup>[10-13]</sup> and the lithium zincate<sup>[14-16]</sup> and aluminate<sup>[16-18]</sup> reagents introduced by Kondo and Uchiyama (**Scheme 1.1**).



**Scheme 1.1:** Simplistic representation of a selection of bimetallic compounds.

The Lochmann-Schlosser superbases (LICKOR),<sup>[7,8]</sup> for instance, most commonly represents an equimolar mixture of *n*-butyllithium and potassium *tert*-butoxide, but other mixtures are possible as well. The exact structure of this powerful mixture is not known, however as it exhibits reactivity higher than that of <sup>n</sup>BuLi, but lower than that of <sup>n</sup>BuK it implies that a co-complexation rather than a complete transmetallation is taking place. The basicity of the Lochmann-Schlosser reagent is increased in a way such that even arenes with low acidity, for example benzene, can be deprotonated, but with this enhanced reactivity it lacks selectivity and often mixtures of products are obtained. Note that a neo-pentyl analogue [Li<sub>x</sub>K<sub>y</sub>(CH<sub>2</sub><sup>t</sup>Bu)<sub>z</sub>(O<sup>t</sup>Bu)<sub>x+y-z</sub>] was prepared and structurally defined in 2016 by Klett showing a complex structural motif (**Figure 1.1**).<sup>[19]</sup>

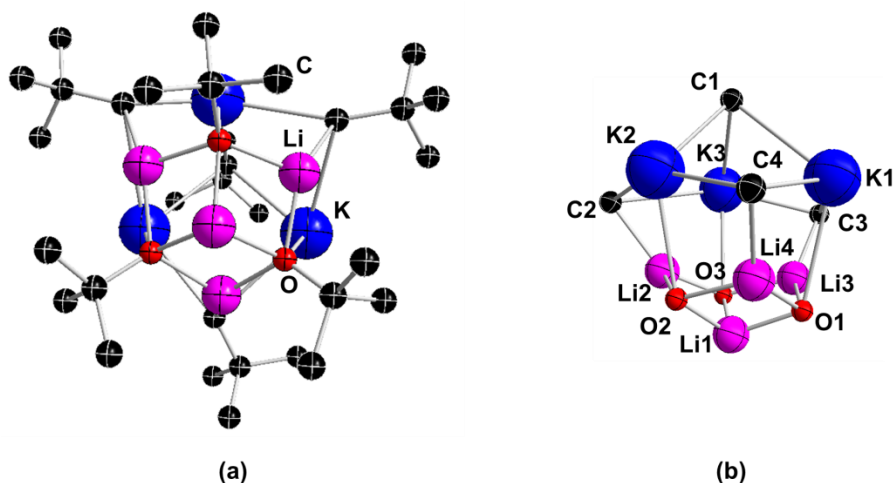
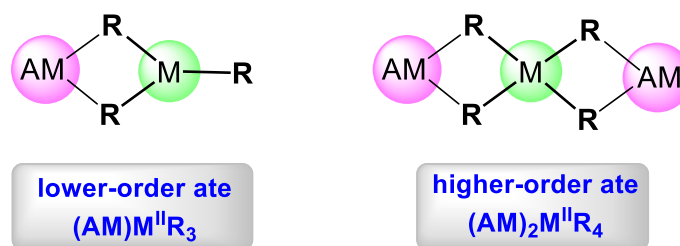


**Figure 1.1:** a) Ball and stick model of  $[\{Li_4(O'Bu)_3\}^+\{K_3Np_4\}^-]$ ; b) Framework of  $[\{Li_4(O'Bu)_3\}^+\{K_3Np_4\}^-]$  with O'Bu and Np substituents omitted for clarity (Np = neopentyl).<sup>[19]</sup>

Closely related alternatives to LICKOR are other heterobimetallic compounds which incorporate two metals of markedly different polarities held together by an array of ligands within one molecule.<sup>[20]</sup> These so-called ate compounds, strategically combine the high reactivity of the electropositive metal with the high selectivity and better functional group tolerance of the less polar metal, thus exhibiting greatly enhanced performances over their homometallic counterparts.<sup>[16,20–22]</sup>

Most typically encountered are mixtures of alkali-metal (usually Li, Na, K) and a second, less electropositive metallic centre (such as Zn, Mg or Al) with a variety of anionic ligands (e.g., alkyl, amido or alkoxy groups) combined in a way that the metal with stronger Lewis acidity can accept more (Lewis) basic ligands.<sup>[20–22]</sup> Such constitution arises from localisation of the anionic charge on the part of the molecule containing the more electronegative metal. Depending on the ratio of the alkali-metal (AM) and the subordinate metal ( $M^{II}$ ), two different common formulations of ates can be obtained, namely triorganometallates  $(AM)M^{II}R_3$  or tetraorganometallates  $(AM)_2M^{II}R_4$ , which can also be referred to as lower-order and higher-order ates, respectively (**Scheme 1.2**).



**Scheme 1.2:** Simplistic representation of lower and higher order formulations of ates.

Whereas these general formulae are given as examples of the most commonly employed stoichiometries, 1:1 and 2:1, and for ates which contain a divalent subordinate metal (e.g., Mg, Zn) they are by no means the only possibility. Employing the same stoichiometries but with trivalent metals, such as for instance group 13 metals, the corresponding formulations would be  $(AM)M^{III}R_4$  and  $(AM)_2M^{III}R_5$ . Illustrating a more unusual stoichiometry, Carmona<sup>[23]</sup> and Hevia<sup>[24,25]</sup> have independently reported “zinc-rich” zincates  $[M^+Zn_2R_5^-]$  ( $R = C_5H_5, Et$ ) where unusually the amount of subordinate metal (i.e., zinc) is increased over the amount of alkali-metal (**Figure 1.2**).

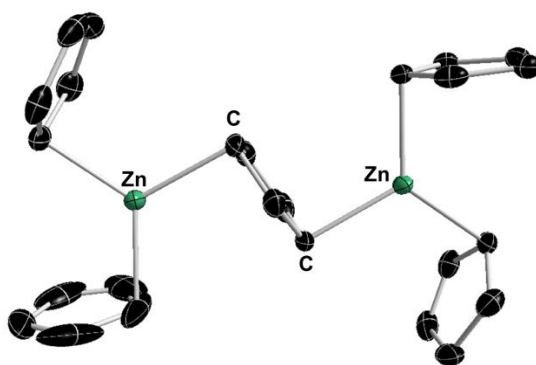


**Figure 1.2:** Structure of the  $[Zn_2(C_5H_5)_5]^-$  ion of  $[Na(THF)_6]^+[Zn_2(C_5H_5)_5]^-$  with 50% probability displacement ellipsoids. All hydrogen atoms and  $[Na(THF)_6]^+$  counterion have been omitted for clarity.<sup>[23]</sup>

The most common preparative methodologies for accessing ate compounds are (i) interlocking co-complexation where the two homometallic reagents self-assemble in an appropriate stoichiometry and (**Scheme 1.3a**) (ii) salt-metathesis where an excess of polar organometallic reagent is reacted with a halide salt of the low polarity metal (**Scheme 1.3b**). In both methods, the relative stoichiometry of the starting material

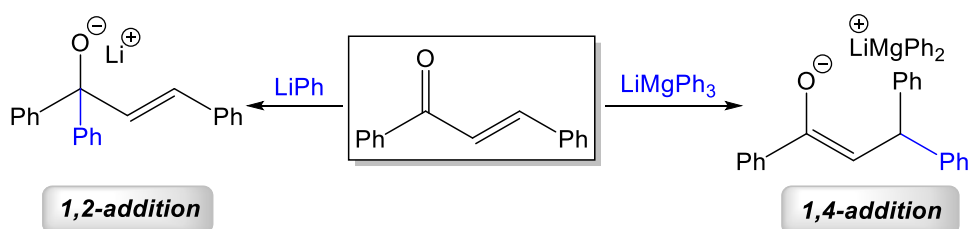


will generally determine whether the triorganometallate or tetraorganometallate will be formed, though in rare cases the structures produced do not match the stoichiometry of the reaction.



**Scheme 1.3:** General representation of methods for accessing homoleptic triorganometallates in a) co-complexation method; and (b) metathesis, respectively.

Although the oldest known bimetallic compound “NaZnEt<sub>3</sub>” dates to the work of Wanklyn,<sup>[26,27]</sup> it was Nobel laureate Wittig who coined the term ‘ate’ for the mixed Li/Mg aryl compound [LiMgPh<sub>3</sub>] in 1951 prepared by directly combining PhLi and Ph<sub>2</sub>Mg.<sup>[28,29]</sup> Furthermore, Wittig observed, even if not unambiguously stated, the synergic regioselectivity of the prepared magnesiate species towards benzalacetophenone which favoured the 1,4-addition product over the competing 1,2-addition product obtained with PhLi (**Scheme 1.4**).



**Scheme 1.4:** Contrasting reactivities of homometallic LiPh and bimetallic LiMgPh<sub>3</sub> towards benzalacetophenone.

Despite displaying intriguing properties and reactivities, ates had been somewhat overlooked by the synthetic community until recently. Close to the turn of the century, the development of powerful analytical techniques such as X-ray diffraction analysis enabled inorganic chemists to determine the true solid-state constitutions of various ‘ate complexes. In his seminal review, Weiss reflects on the importance of the structural information whose value to the field of synthetic chemistry comes from enabling a better understanding of the reaction mechanisms.<sup>[30]</sup> Ates are known to exhibit either contacted ion-pair (CIP) or solvent separated ion-pair (SSIP) structures.<sup>[31]</sup> Contacted ion-pair motifs (**Fig. 1.3a**) where both metals are connected

via bridging ligands are favoured in the absence of strongly coordinating Lewis donors (as for example THF or TMEDA). A solvent-separated ion-pair structure (**Fig. 1.3b**) contains well-defined cationic and anionic moieties, where the cation is made up by the most electropositive metal, usually solvated by donor solvent molecules and the anion comprises the most electronegative metal coordinated by the anionic ligands.

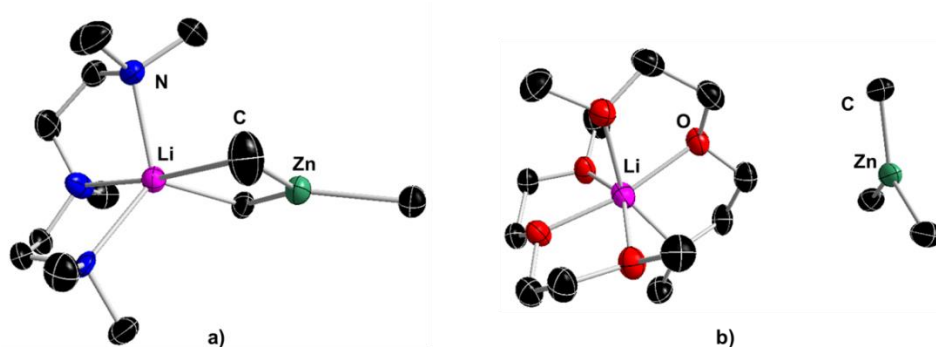


**Figure 1.3:** Crystal structures of (a) CIP lithium zincate  $\{(PMDTA)LiZnMe_3\}$ ; b) SSIP lithium zincate  $[\{Li(diglyme)_2\}^+\{ZnMe_3\}^-]$ . Ellipsoids are drawn at 50% probability level and all hydrogen atoms have been omitted for clarity.<sup>[32]</sup>

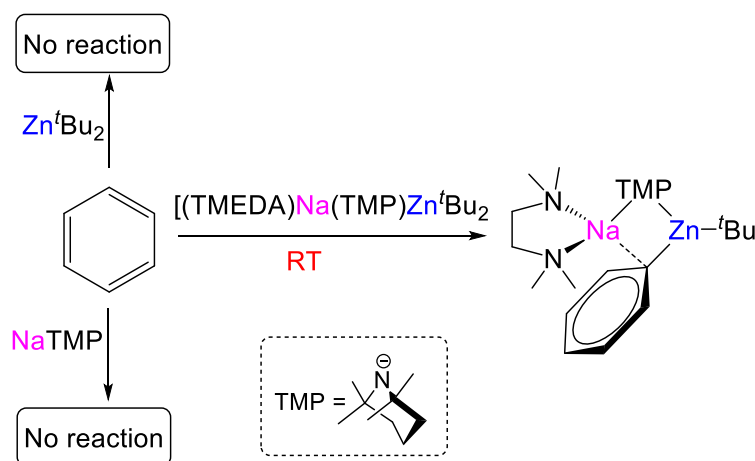
Nowadays, by switching on cooperative effects, this family of bimetallic reagents has found widespread applications in many fundamentally important organic transformations, displaying better functional group tolerance and enabling the use of ambient temperatures as their metallo-intermediates are generally multiple orders of magnitude more stable than the corresponding lithio-intermediates.

The results obtained by application of these versatile reagents in foremost central organic transformations (*i.e.*, deprotonative metallation, nucleophilic addition and metal-halogen exchange reactions) have been highlighted in many review articles<sup>[12,16,20,31,33]</sup> and book chapters.<sup>[5]</sup> For the sake of brevity, only developments in the area of deprotonative metallation will be considered here as this type of reactions will be discussed in detail latter in the thesis.

## 1.2. Deprotonative Metallation

Globally, deprotonative metallation is one of the most practised reactions. It is used as an approach for the transformation of commonly encountered, but relatively inert C-H bonds into more reactive carbon-metal bonds.<sup>[20]</sup> Subsequent reactivity of the C-M bond can allow formation of new a carbon-carbon or carbon-heteroatom bond which is central to the field of organic synthesis. Commonly employed reagents for these transformations are alkylolithiums (*n*-butyllithium is the best known) and bulky lithium amides, where the high reactivity of the predominantly ionic Li-C or Li-N bond enables direct proton abstraction from a myriad of organic substrates. The “softer”, less reactive metals, such as organozinc or organoaluminium, were always regarded as being unable to perform such tasks.

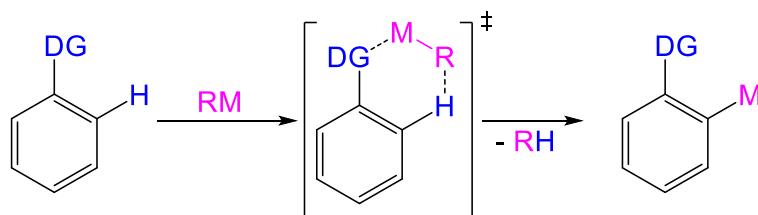
The development of heterobimetallic ‘ate compounds introduced a new approach for metallation of aromatic substrates where the softer metal in the presence of alkali-metal performs the deprotonation of the substrate in the process termed *Alkali-Metal-Mediated Metallation*.<sup>[20,21]</sup> While it is the less reactive metal that performs the actual M-H exchange process, the presence of the alkali-metal in close proximity is crucial for the reaction to take place. This synergic behaviour of metals can be illustrated on the example of benzene which is a very challenging substrate to deprotonate due to the low acidity of its C-H bonds (its  $pK_a$  is high at 44.7)<sup>[34]</sup> and was found to be inert to both NaTMP and  $Zn^tBu_2$ .<sup>[35]</sup> However, by combining the two homometallic compounds in a single heterobimetallic complex [(TMEDA)Na(TMP)Zn<sup>t</sup>Bu<sub>2</sub>] and switching on cooperative effects, benzene can be readily deprotonated (**Scheme 1.5**).<sup>[35]</sup> This metallation is formally a zincation, as the position previously filled by an H atom is now occupied in the final product by Zn. However, since the presence of sodium is required for the metallation process to take place, this special type of reaction can be described as alkali-metal mediated zincation (AMMZn). Metallation of benzene was previously achieved by employing LICKOR superbases (*vide supra*), however this AMMZn approach represents improvement as it is executed at room temperature.



**Scheme 1.5:** Contrasting reactivities of homometallic components NaTMP and  $\text{Zn}^t\text{Bu}_2$  with the heterobimetallic sodium zincate  $[(\text{TMEDA})\text{NaZn}(\text{TMP})^t\text{Bu}_2]$ .<sup>[35]</sup>

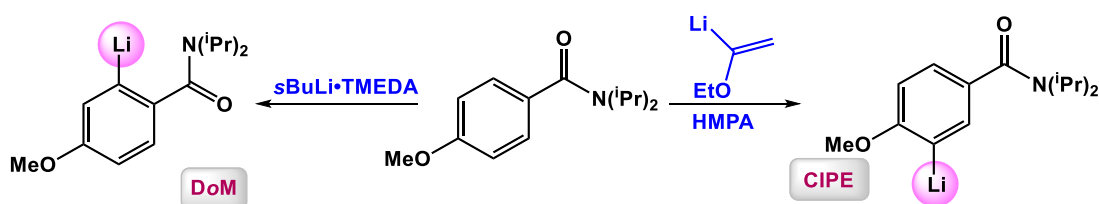
As mentioned before, the fundamental importance of direct metallation lies in the abundance of C-H bonds in any substrate, however this same abundance challenges the selectivity of the process. This challenge was met in the seminal discovery of “directed *ortho*-metallation” (DoM) independently developed by Gilman<sup>[36]</sup> and Wittig<sup>[37]</sup> while studying metallation of anisole, which has since then greatly developed as it applies irrespective of the nature of the metallating reagent.

The concept of DoM relies on the presence of substituent on the aromatic substrate which acts as a docking site for the approaching Lewis acidic metallating reagent, thus by coordination activating the adjacent (*ortho*) C-H bond (**Scheme 1.6**).<sup>[38]</sup> In addition to determining the position of the metallation, (hence the name directing group), the substituent can also weaken that same C-H bond through electronic effects making it more susceptible to undergo direct M-H exchange. Depending on the nature of the directing group (DG), primarily its coordinating and electron-withdrawing ability, DGs can be classified as weak (*e.g.*, alkyl), moderate (*e.g.*, alkoxy) or strong (*i.e.*, amido,  $[\text{R}_2\text{N}(\text{O}=\text{C})^-]$ ).



**Scheme 1.6:** General mechanism of DoM.

Building on these findings, a thought-provoking perspective by Snieckus and Beak introduced the theory of “complex-induced proximity effect” (CIPE) explaining how in special cases lithiation can occur at C-H bonds which are formally remote (through bond connections), but are conformationally (through space) in proximity of the DG substituent (**Scheme 1.7**).<sup>[39]</sup>

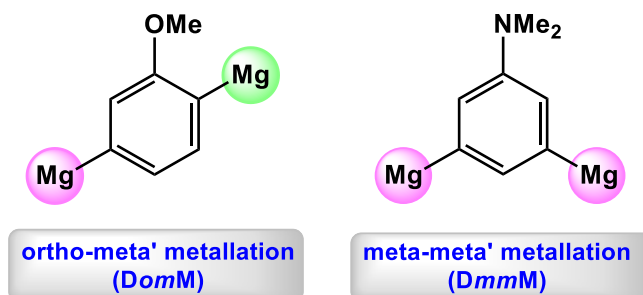


**Scheme 1.7:** Regioselectivity of lithiation of *N,N*-diisopropyl-4-methoxybenzamide with different lithium reagents illustrating the difference between the DoM and CIPE control.<sup>[39]</sup>

In one aspect, DoM is extremely beneficial as it enables selectivity in subsequent synthetic transformations, however the selectivity takes place only at one specific position (that is *ortho*) and although deviations from the rule exist, they are rare. Opening up site access within aromatic and heteroaromatic frameworks beyond ortho- or proximal C-H bonds is one of the foremost challenges currently exercising the minds of chemists worldwide. To date, most of the advances accomplishing such outlying site-selectivity have centred on late transition metal methodologies, which, while effective with certain substrates in specific catalytic transformations, have not yet come close to the ultimate goal of general applicability.<sup>[40–52]</sup> Furthermore, they often require significant pre-catalytic synthetic steps (e.g., attaching covalent linker groups to arene frameworks) and come with common, intrinsic limitations of late transition metals such as high cost, low abundance, limited sustainability and toxicity issues.<sup>[53]</sup>

Addressing this issue from a main group perspective, seminal report by Mulvey and O’Hara has introduced an innovative approach in controlling the regioselectivity attainable in the aromatic C-H metallation chemistry through the structure of the metallating agent.<sup>[54]</sup> By using a donor solvent-free sodium magnesiate  $[\text{Na}_4\text{Mg}_2(\text{TMP})_6(\text{tBu})_2]$  in hydrocarbon solvent unprecedented ortho-meta’ and meta-

meta' dimetallations of anisole and *N,N'*-dimethylaniline, respectively, have been accomplished in very high yields (**Scheme 1.8** and **Figure 1.4**)



**Scheme 1.8:** Simplistic representation of *DomM* of anisole and *DmmM* of aniline achieved with sodium magnesiate  $[\text{Na}_4\text{Mg}_2(\text{TMP})_6(\text{tBu})_2]$ .<sup>[54]</sup>

The major driving force behind these dimetallations is the preorganised structure of the base which with its inverse crown topology instigates the template mechanism, while the presence of the two pendant butyl ligands on two magnesium atoms ensures deprotonation. Note that the identity of the DG still plays a role as its spatial nature directs the deprotonation towards either ortho-meta' (*DomM*) or meta-meta' (*DmmM*) sites.

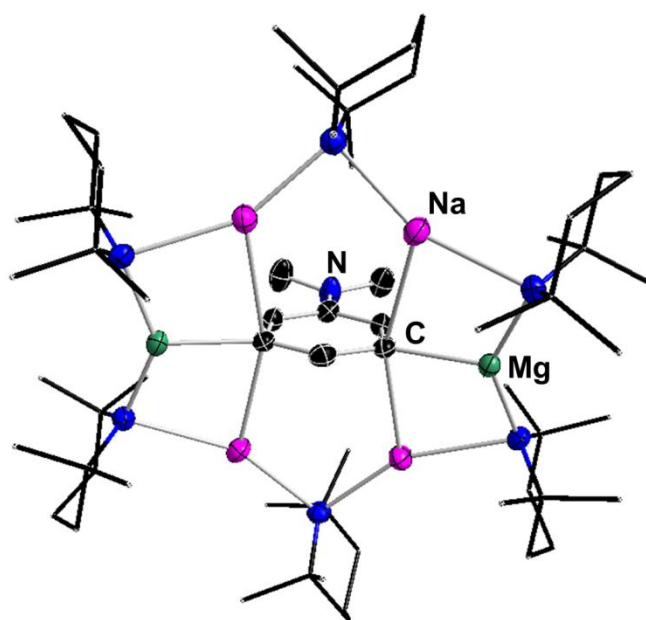


**Figure 1.4:** Molecular structure of  $\text{Na}_4\text{Mg}_2(\text{TMP})_6(\text{C}_6\text{H}_3\text{NMe}_2\text{-}3,5)$  with 50 % displacement ellipsoids. All hydrogen atoms have been omitted for clarity and TMP ligands are represented with wire model for clarity.<sup>[54]</sup>

The advances in metallation chemistry achieved by heterobimetallic reagents presented so far were executed by composite reagents where the two metals working together are incorporated within one molecule. The concept of AMMZn and AMMMg was exported to the branch of aluminium chemistry.

In 2004, Uchiyama and co-workers reported that a mixture of LiTMP and Al<sup>*i*</sup>Bu<sub>3</sub> was capable of regio- and chemoselective direct alumination of functionalised aromatics and heteroaromatics.<sup>[17,18]</sup> The *in situ* prepared mixture was found to be effective and regioselective for a variety of substrates bearing both electron-donating and electron-withdrawing groups and aluminated species were shown to undergo copper- and palladium catalysed heterocouplings in high yields and with high chemo- and regioselectivities. Notably, the metallation occurred with the suppression of nucleophilic addition to a carbonyl group or halogen-exchange reaction at iodine, which was unique to this system, because neither conventional metal bases (RLi) nor even TMP zincates can coexist with aryl iodides.

Further work by Mulvey and Hevia revealed that these remarkable transformations are, in fact, a product of stepwise LiTMP lithiation followed immediately by trapping by alkylaluminium complex.<sup>[55]</sup> Synergic cooperation between the two separate monometallic reagents present in the mixture has highlighted that two-metal synergistic reactions are not confined to concerted, synchronised processes where the metals belong within the same reagent, but can be extended to tandem, stepwise processes involving two separately added reagents that do not form a co-complex. To further illustrate the synthetic utility of this *trans-metal-trapping* approach, the authors successfully employed another, closely related LiTMP/TMPAl<sup>*i*</sup>Bu<sub>2</sub> pairing to metallate ferrocene in good yields (**Figure 1.5**).<sup>[22]</sup>

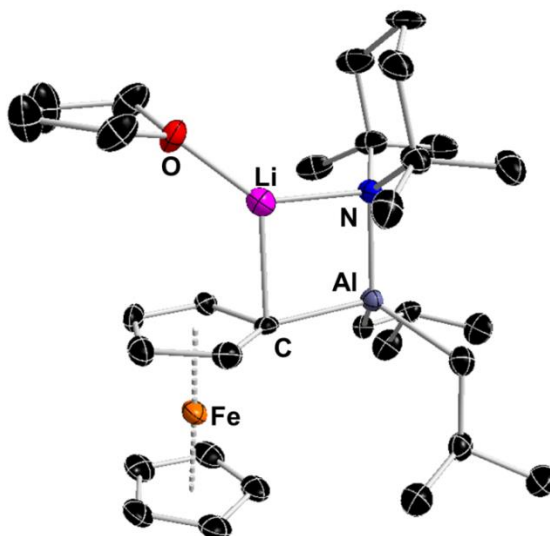


**Figure 1.5:** Molecular structure of monoaluminated ferrocene  $[\text{THF}\cdot\text{Li}(\mu\text{-TMP})\{\mu\text{-(C}_5\text{H}_4\text{)Fe(C}_5\text{H}_5\text{)}\}\text{Al}(\text{i-Bu})_2]$  with 50 % displacement ellipsoids. All hydrogen atoms have been omitted for clarity.<sup>[22]</sup>

### 1.2.1. Bimetallic compounds for NHC functionalisation

Progressing from laboratory curiosities and phosphine alternatives, N-heterocyclic carbenes (NHCs) have established themselves as pivotal ligands with applications in key areas of modern chemistry including organic and transition-metal catalysis,<sup>[56–59]</sup> stabilisation of low valent main-group compounds<sup>[60–65]</sup> and development of frustrated Lewis pair systems,<sup>[66,67]</sup> to name just a few. These commodity ligands are extremely versatile, which is primarily due to the possibility of fine tuning the steric and electronic properties by modifying substituents on N-atoms or the backbone of the imidazole ring.<sup>[68]</sup> Surprisingly, examples of selective metallation of the backbone of NHCs are scarce.

It was as recent as 2010 when Robinson reported the first straightforward lithiation of 1,3-bis(2,6-diisopropylphenyl)imidazol-2-ylidene (IPr) with  $n\text{BuLi}$ .<sup>[69]</sup> The single crystal X-ray analysis of the isolated product revealed a polymeric structure of Li cations connected by anionic NHC moieties employing simultaneously their C2 and C4 sites (**Figure 1.6**).



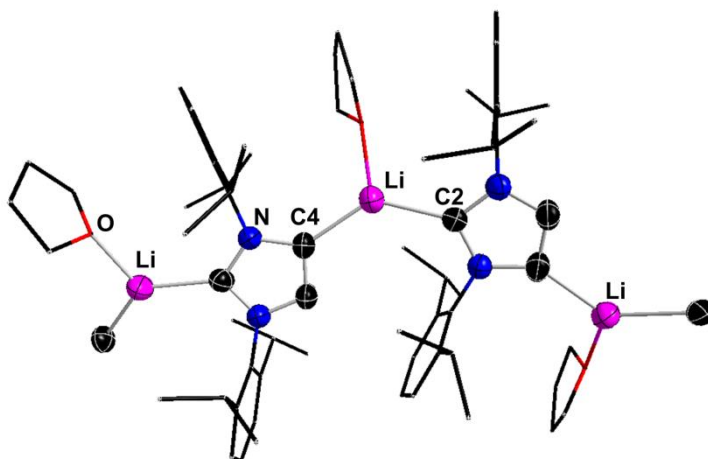
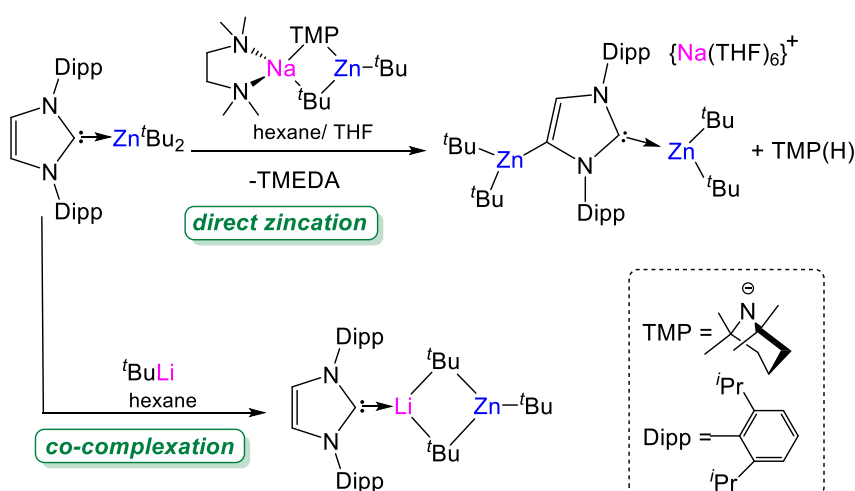


**Figure 1.6:** Wire model representation of a portion of a polymeric structure of  $[\{:\text{C}\{\text{N}(2,6\text{-}i\text{Pr}_2\text{C}_6\text{H}_3)_2\text{CH}\}\text{Li}(\text{THF})\}_\infty]$  with Li and atoms of the imidazole ring drawn with ellipsoids set at 50% probability.<sup>[69]</sup>

Exporting the developing idea of cooperative bimetallic bases to the evolving area of functionalization of NHCs, the group of Hevia has found that bimetallic base  $[\text{NaZn}(\text{TMP})\text{Bu}_2(\text{TMEDA})]$  can promote direct zincation of both free IPr and NHC complex at C4 position.<sup>[70]</sup> Particularly interesting was their finding that the  $\text{Zn}^i\text{Bu}_2\text{-IPr}$  which readily undergoes zincation with the bimetallic base fails to undergo metallation with  $^i\text{BuLi}$ , but instead formed a co-complex of NHC and lithium zincate, products of which have been isolated and structurally characterised (**Scheme 1.9**).



**Scheme 1.9:** Contrasting reactivities of homometallic organolithium reagent  $^i\text{BuLi}$  and heterobimetallic lithium zincate towards a Zn-NHC complex.<sup>[70]</sup>

Introducing heterobimetallic magnesiate bases to the handful of metals that can directly metallate NHC, Mulvey *et al.* found that using higher order solvent-free sodium-magnesiate  $[\text{Na}_4\text{Mg}_2(\text{TMP})_6(\text{tBu})_2]$  it is possible to dideprotonate IPr (**Fig.1.7**).<sup>[71]</sup>

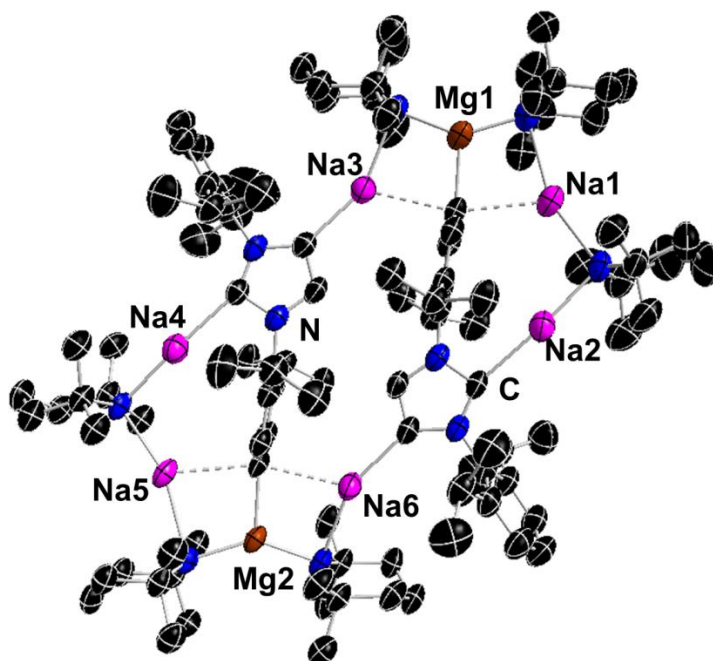
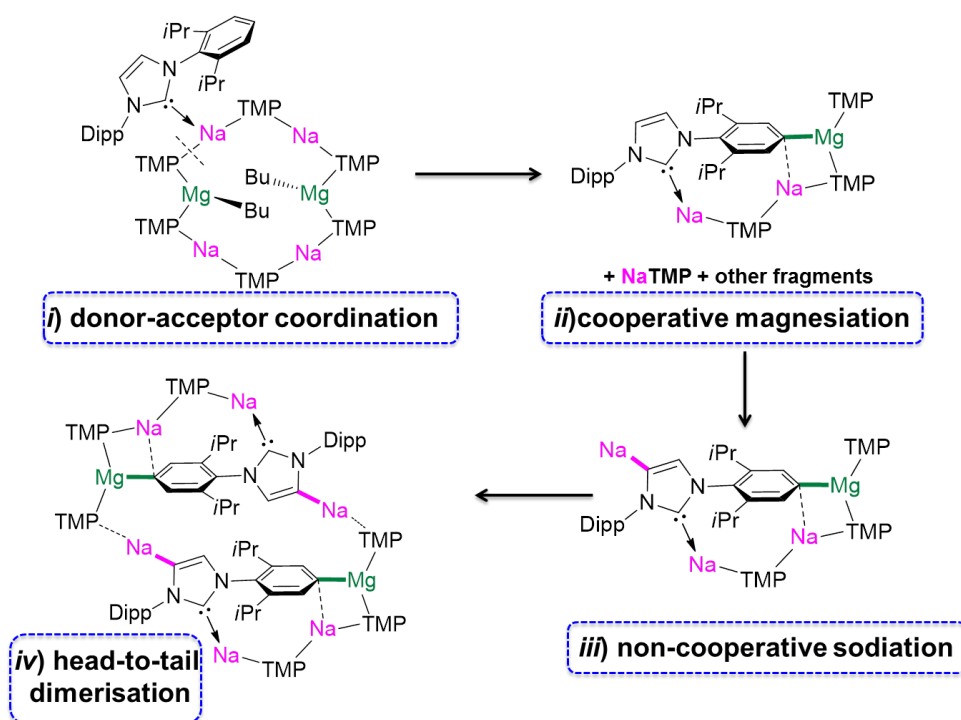


**Figure 1.7:** Molecular structure of the inverse  $[\{\text{Na}_3\text{Mg}(\text{TMP})_3(\text{IPr}^{2-})\}_2]$  of one of the two crystallographically independent molecules with 50 % displacement ellipsoids. All hydrogen atoms have been omitted for clarity.<sup>[71]</sup>

This remarkable result is believed to originate from the steric incompatibility of the substrate (NHC) and the inverse-crown template base which sets in motion a chain of reactions (**Scheme 1.10**) affording a product containing a dative C-Na bond at the normal (C2), sodiation at the abnormal (C4) and magnesiation at the *para*-position of the pendant Dipp substituent on N-atom.<sup>[71]</sup>



**Scheme 1.10:** Proposed stages in dideprotonation of IPr with  $[\text{Na}_4\text{Mg}_2(\text{TMP})_6(\text{Bu})_2]$ .<sup>[71]</sup>

### 1.3. The less common metals

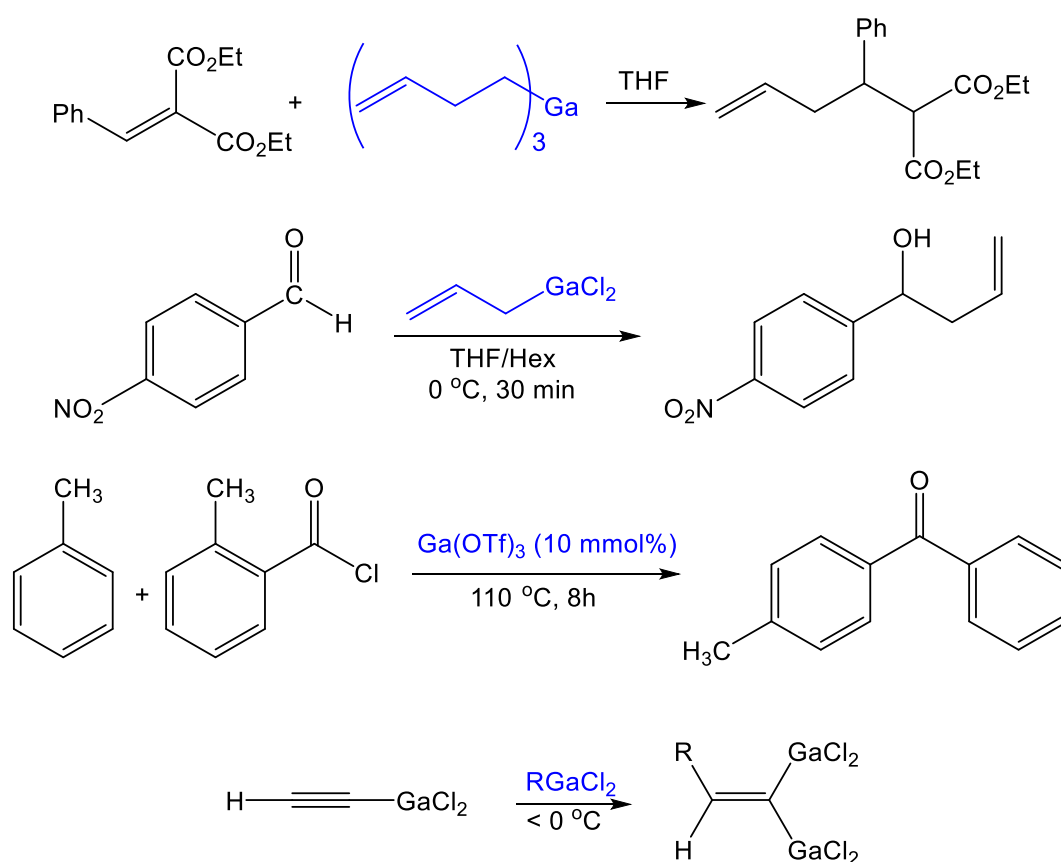
Most of the studies discussed so far have focused on main-group metal systems which combine an alkali-metal with a more electronegative metal such as Mg, Zn (pseudo main group because of its  $s^2 \rightarrow s^0$  reactivity) or Al.<sup>[31,33,72]</sup>

The main aim of this PhD project was however to develop systems which combine alkali-metals with less commonly employed low polarity metals, in particular Mn(II) and Ga(III). Therefore, the next few pages will very shortly present the relevance of these metals in organic synthesis and why they attracted our interest.

#### 1.3.1. Organogallium chemistry

The organometallic chemistry of group 13 is still heavily dominated by the chemistry of organoaluminium compounds, whilst gallium and indium derivatives are still under-explored and confined primarily to academic research.<sup>[6]</sup>

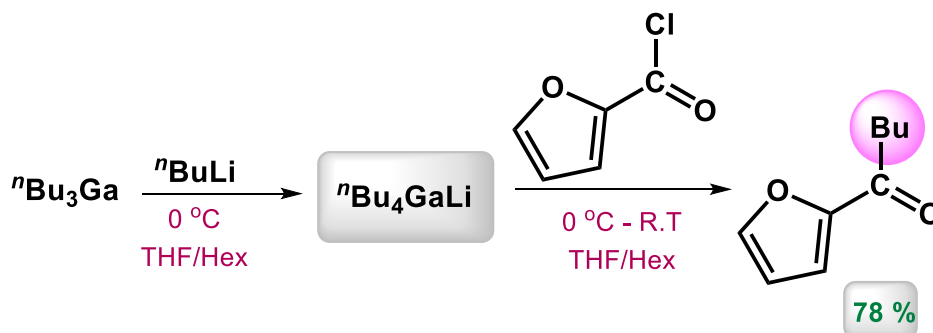
Pioneering work by Dennis *et al.* reporting the synthesis and isolation of the first gallium alkyl compounds,<sup>[73]</sup> initiated the interest in organogallium compounds. Although they have found applications in a wide range of fields such as homogeneous catalysis,<sup>[74,75]</sup> and chemotherapeutics,<sup>[76]</sup> their use in organic synthesis has become more prominent.<sup>[77,78]</sup> Accordingly, organogallium reagents have been successfully employed as selective alkylating reagents in addition reactions to activated olefins,<sup>[79,80]</sup> aldehydes and ketones,<sup>[81,82]</sup> as Lewis acid catalyst for transformations such as Friedel-Crafts alkylation and acylation,<sup>[83]</sup> along with promoting carbometallation of carbon-carbon triple bonds<sup>[84–87]</sup> (**Scheme 1.11**).



**Scheme 1.11:** Selected examples of application of organogallium compounds in organic synthesis: addition to olefins and aldehydes, Friedel-Crafts acylation and carbogallation of alkynes, respectively.

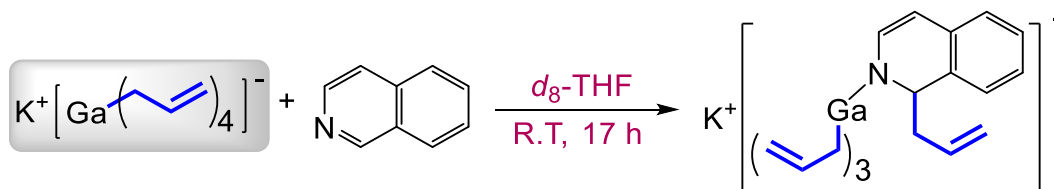
Within the context of mixed-metal chemistry, although gallates have not been studied to the same extent as aluminates, there are few structurally characterised alkali-metal gallates as well as some studies on their applications in organic chemistry. *In situ* prepared lithium tetraorganogallates have been employed to produce ketones from acyl chlorides as an alternative to organocopper and

organocadmium compounds.<sup>[88]</sup> It has been shown that lithium gallates can react selectively under mild conditions to transfer only one alkyl or aryl group in excellent yields in the presence of other sensitive functional groups like olefin, ether and nitro groups (**Scheme 1.12**).



**Scheme 1.12:** *In situ* prepared lithium tetraorganogallate employed in addition to acyl chloride.

More recently, Okuda *et al.* have reported an extensive study on the preparation and characterisation of neutral, cationic and anionic allylgallium compounds.<sup>[89]</sup> Reactivities of these related compounds were compared and the first example of 1, 2 insertion reactions of isoquinoline mediated by potassium tetra(allyl)gallates has been described (**Scheme 1.13**).



**Scheme 1.13:** Reactivity of potassium tetrakis(allyl)gallate towards isoquinoline.

Our own group has prepared novel unsolvated tetraorganogallate species using non-polar hexane/arene solvent mixtures (**Figure 1.8**).<sup>[90]</sup> X-ray crystallographic studies reveal that these gallates exhibit novel polymeric arrangements, with the lithium and sodium derivatives sharing the same linear chain structure, made up exclusively of M–C and Ga–C bonds. The potassium derivative has incorporated benzene into its constitution and displays a more open structural motif. Multinuclear NMR spectroscopic studies suggest that in deuterated benzene solutions these compounds

exist as discrete solvent separated ion-pair  $[\{M(\text{solvent})_x\}^+\{\text{Ga}(\text{CH}_2\text{SiMe}_3)_4\}]$  species.

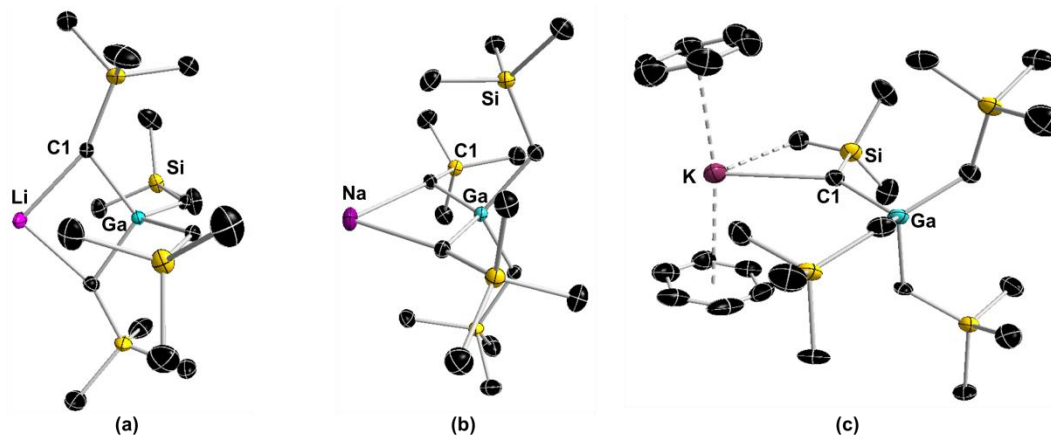
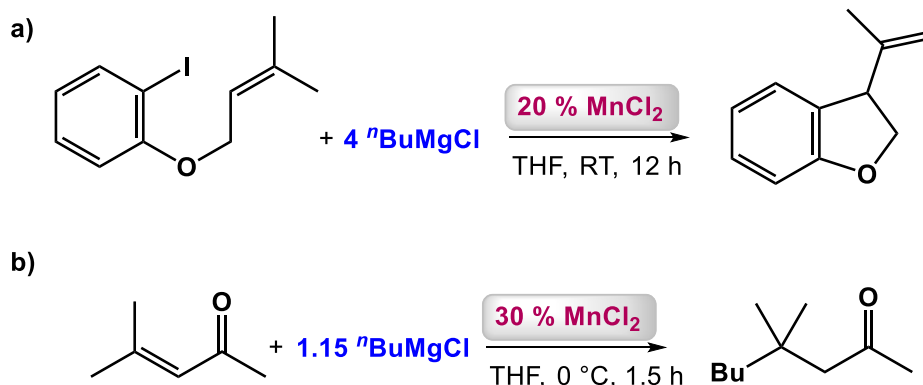


**Figure 1.8:** Asymmetric units of a) lithium, b) sodium and c) potassium gallates with 50 % displacement ellipsoids. All hydrogen atoms have been omitted for clarity.<sup>[90]</sup>

### 1.3.2. Organomanganese chemistry

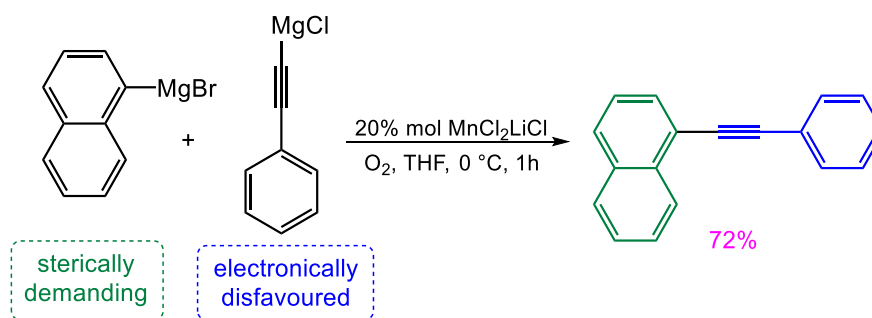
The chemistry of heterobimetallic systems which incorporate a transition metal as the divalent partner for the alkali-metal is still in its infancy; however it is attracting attention due to certain advantages that could be encountered. By incorporating a transition metal as a subordinate partner, possibilities for new and attractive reactivity such as redox chemistry or catalytic behaviour emerge, as well as some specific, sought-after properties (*e.g.* magnetic) all of which are, in general, uncharacteristic for the main group chemistry. Manganese could be considered an excellent candidate as transition metal incorporated in an ate for several reasons. Relatively inexpensive, toxicologically benign and readily available due to its high abundance (12<sup>th</sup> most abundant metal in the Earth's crust), manganese embodies a great appeal to industry.<sup>[91]</sup> More importantly, the organometallic chemistry of manganese in oxidation state +2 has been shown to be more comparable to that of main-group metals than to d-block metals due to the presence of predominantly ionic Mn-C bonds.<sup>[92]</sup> Additional likeness arises from similar values of the ionic radii<sup>[93]</sup> of  $\text{Mn}^{2+}$  and  $\text{Mg}^{2+}$  (0.81 Å vs 0.86 Å) which is evident through the isolation of some molecularly isostructural compounds (*i.e.*  $[\text{M}\{\text{N}(\text{SiMe}_3)_2\}_3\text{Li}(\text{THF})]$ , where  $\text{M} = \text{Mn}^{[94]}$  or  $\text{Mg}^{[95]}$ ).

Focusing on Mn(II), lithium tri- and tetra-alkyl manganates (usually prepared *in situ* via salt-metathesis or Mn insertion protocols)<sup>[92,96,97]</sup> have proved to be efficient reagents in organic synthesis for bringing about key transformations including radical cyclizations, 1,4-additions, Mn-halogen exchange and homo- and cross-coupling processes to name just a few (**Scheme 1.14**).<sup>[91][98–100]</sup>



**Scheme 1.14:** a) Mn-catalysed dehalogenative radical cyclizations of aryl iodides; b) 1,4-addition of Grignard reagents to conjugated enones.<sup>[91]</sup>

In 2007, Cahiez reported a manganese-catalysed homocoupling of aryl, alkenyl and alkynyl Grignard reagents using dry air as an oxidant.<sup>[101]</sup> The reactions were performed under mild conditions (RT, 45 min) and were found to be chemo- (*i.e.*, ester, nitrile and nitro groups tolerant) and stereoselective. During these studies, the authors have noted the coupling was rapid, however the reaction rate was highly dependent on the steric and electronic nature of the organic group of RMgX. Elegantly exploiting this observation, by combining an electron-rich but bulky aryl group with an alkynyl group that couples more slowly but is not sterically demanding, the formation of homocoupled products was overpowered by the formation of heterocoupled product (**Scheme 1.15**).<sup>[102]</sup>



**Scheme 1.15:** Mn-catalysed heterocoupling of Grignard reagents.<sup>[102]</sup>

Surprisingly, despite these, and several other, excellent organic studies which highlight the synthetic utility of these bimetallic compounds, the information on the nature of and constitution of the reactive manganese species is very limited.

In the context of better understanding of reactive organomanganese species, Mulvey successfully extended the developing idea of alkali-metal-mediated metallation to manganese by employing structurally defined [(TMEDA)LiMn(TMP)(CH<sub>2</sub>SiMe<sub>3</sub>)<sub>2</sub>] to directly manganese ferrocene.<sup>[103]</sup> The unique crystal structure of 1,1'-dimetallated ferrocene (**Fig. 1.9**) has unveiled the reactivity of all three arms (two alkyl and one amido) as bases making this lithium manganese exceptionally atom-economical and superior in comparison to related magnesitates or zincates which typically use only two arms.

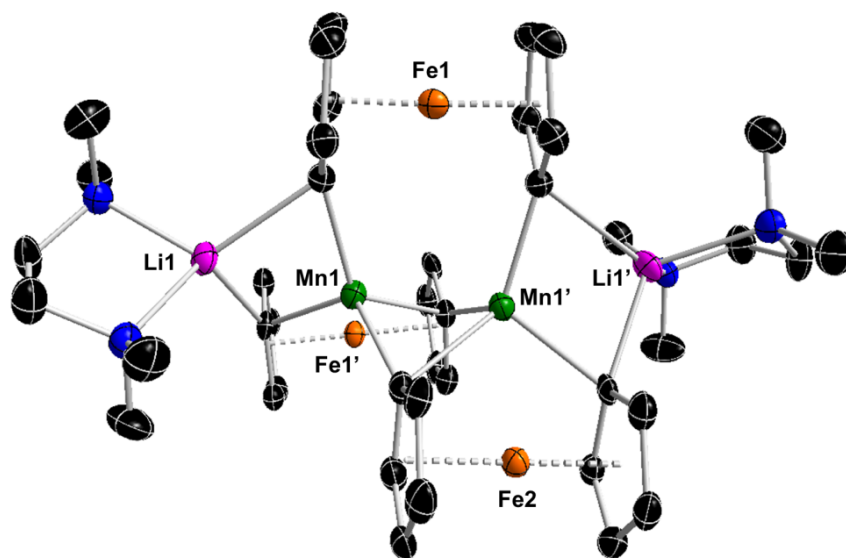
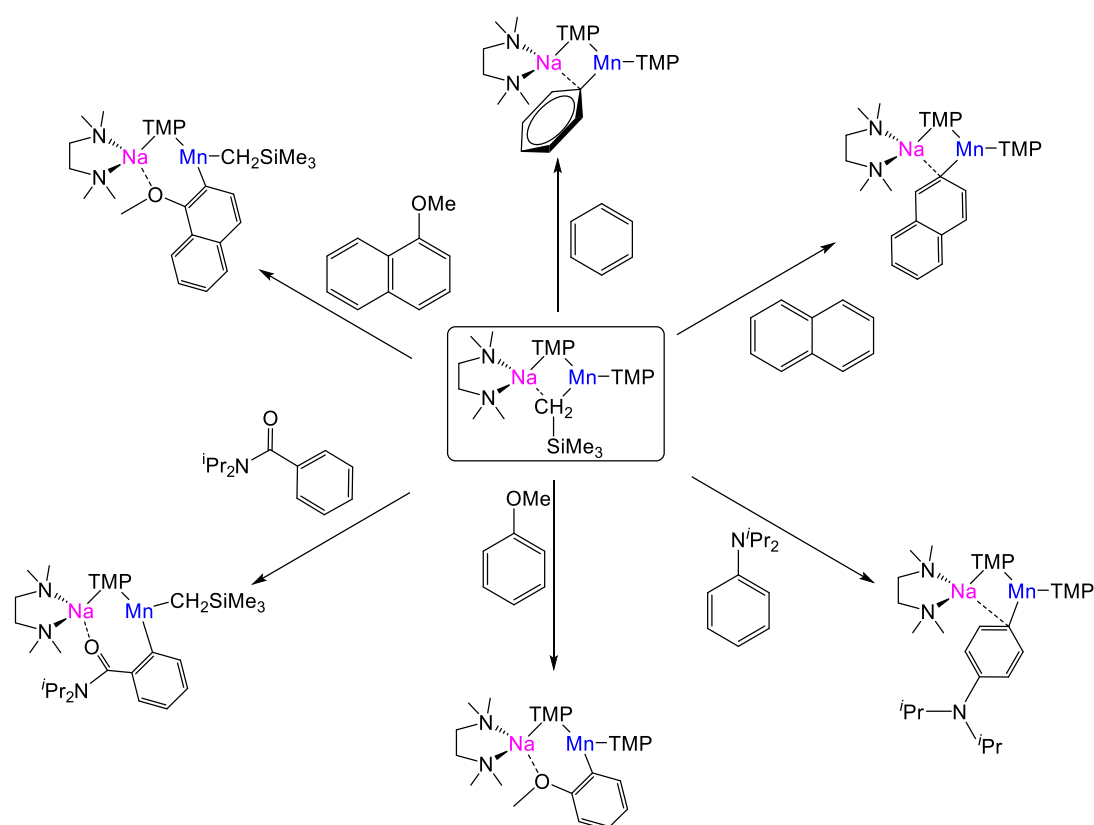


**Figure 1.9:** Molecular structure of [(TMEDA)<sub>2</sub>Li<sub>2</sub>Mn<sub>2</sub>{Fe(C<sub>5</sub>H<sub>4</sub>)<sub>2</sub>}]<sub>3</sub> with selective atom labelling and 50% probability displacement labelling.<sup>[103]</sup>

In the framework of the research developing AMMMn, Mulvey recently demonstrated the ability of the structurally related sodium manganese [(TMEDA)NaMn(TMP)<sub>2</sub>(CH<sub>2</sub>SiMe<sub>3</sub>)] to promote direct Mn-H exchange reactions of various aromatics (**Scheme 1.16**),<sup>[104–106]</sup> mimicking in some cases reactivities previously reported for related alkali-metal magnesiate systems. This particular base proved to be a versatile manganeseating reagent, capable of displaying both alkyl and amido basicity as shown in **Scheme 1.16**.





**Scheme 1.16:** An overview of direct Mn-H exchange reactions achieved by sodim manganate [(TMEDA)NaMn(TMP)<sub>2</sub>(CH<sub>2</sub>SiMe<sub>3</sub>)].<sup>[104–106]</sup>

#### 1.4. Aims and structure of this thesis

Building on recent developments in cooperative organometallic chemistry, this thesis presents our findings in developing new applications of organogallium and organomanganese reagents. **Chapter 2** will focus on progressing gallium NHC chemistry by introducing new methodologies for the rational synthesis of Ga complexes containing anionic, normal and abnormal NHC. Building on these results, **Chapter 3** explores the potential of Ga/NHC partnership to promote small molecule activation processes via FLP reactivities. With our focus still on organogallium chemistry, but exploiting metal-metal stepwise cooperativity, **Chapter 4** will investigate a mixture of LiTMP/GaR<sub>3</sub> for metallation of pharmaceutically relevant *N*-heterocyclic molecules. Moving our focus to alkali-metal manganates, **Chapter 5** presents a systematic study into the structural diversity of a series of homoalkyl alkali-metal manganates. **Chapter 6** provides overall conclusions of the work presented here, while **Chapter 7** details general experimental techniques and preparation of starting materials.

## 1.5. Bibliography

- [1] J. Clayden, *Organolithiums: Selectivity for Synthesis*, Pergamon, Oxford, **2002**.
- [2] M. Schlosser, *Organometallics in Synthesis*, New York, **2002**.
- [3] L. Pauling, *The Nature of the Chemical Bond*, Ithaca, **1960**.
- [4] A. L. Allred, *J. Inorg. Nucl. Chem.* **1961**, *17*, 215–221.
- [5] P. Knochel, *Handbook of Functionalized Organometallics*, Wiley-VCH Verlag GmbH & Co. KGaA, Boschstr. 12, 69469 Weinheim, Germany, **2005**.
- [6] C. Elschenbroich, *Organometallics*, Wiley-VCH, Weinheim, **2005**.
- [7] M. Schlosser, *J. Organomet. Chem.* **1967**, *8*, 9–16.
- [8] L. Lochmann, J. Pospisil, D. Lim, *Tetrahedron Lett.* **1966**, *7*, 257–262.
- [9] P. Caubere, *Chem. Rev.* **1993**, *93*, 2317–2334.
- [10] A. Krasovskiy, P. Knochel, *Angew. Chem. Int. Ed.* **2004**, *43*, 3333–3336.
- [11] D. Tilly, F. Chevallier, F. Mongin, P. C. Gros, *Chem. Rev.* **2014**, *114*, 1207–1257.
- [12] B. Haag, V. Malakhov, P. Knochel, *Angew. Chem. Int. Ed.* **2011**, *50*, 9794–9824.
- [13] E. Hevia, R. E. Mulvey, *Angew. Chem. Int. Ed.* **2011**, *50*, 6448–6450.
- [14] T. Furuyama, M. Yonehara, S. Arimoto, M. Kobayashi, Y. Matsumoto, M. Uchiyama, *Chem. Eur. J.* **2008**, *14*, 10348–10356.
- [15] Y. Kondo, M. Shilai, M. Uchiyama, T. Sakamoto, *J. Am. Chem. Soc.* **1999**, *121*, 3539–3540.
- [16] R. E. Mulvey, F. Mongin, M. Uchiyama, Y. Kondo, *Angew. Chem. Int. Ed.* **2007**, *46*, 3802–3824.
- [17] M. Uchiyama, H. Naka, Y. Matsumoto, T. Ohwada, *J. Am. Chem. Soc.* **2004**, *126*, 10526–10527.
- [18] H. Naka, M. Uchiyama, Y. Matsumoto, A. E. H. Wheatley, M. McPartlin, J. V. Morey, Y. Kondo, *J. Am. Chem. Soc.* **2007**, *129*, 1921–1930.
- [19] P. Benrath, M. Kaiser, T. Limbach, M. Mondeshki, J. Klett, *Angew. Chem. Int. Ed.* **2016**, *55*, 10886–10889.
- [20] R. E. Mulvey, *Acc. Chem. Res.* **2009**, *42*, 743–755.
- [21] R. E. Mulvey, *Organometallics* **2006**, *25*, 1060–1075.
- [22] W. Clegg, E. Crosbie, S. H. Dale-Black, E. Hevia, G. W. Honeyman, A. R. Kennedy, R. E. Mulvey, D. L. Ramsay, S. D. Robertson, *Organometallics* **2015**, *34*, 2580–2589.

- [23] E. Alvarez, A. Grirrane, I. Resa, D. Del Río, A. Rodríguez, E. Carmona, *Angew. Chem. Int. Ed.* **2007**, *46*, 1296–1299.
- [24] W. Clegg, D. V. Graham, E. Herd, E. Hevia, A. R. Kennedy, M. D. McCall, L. Russo, *Inorg. Chem.* **2009**, *48*, 5320–5327.
- [25] D. R. Armstrong, W. Clegg, P. García-Alvarez, M. D. McCall, L. Nuttall, A. R. Kennedy, L. Russo, E. Hevia, *Chem. Eur. J.* **2011**, *17*, 4470–4479.
- [26] J. A. Wanklyn, *Justus Liebigs Ann. Chem.* **1858**, *108*, 67–79.
- [27] D. Seyferth, *Organometallics* **2001**, *20*, 2940–2955.
- [28] G. Wittig, F. J. Meyer, G. Lange, *Justus Liebigs Ann. Chem.* **1951**, *571*, 167–201.
- [29] G. Wittig, *Angew. Chemie* **1958**, *70*, 65–71.
- [30] E. Weiss, *Angew. Chem. Int. Ed.* **1993**, *32*, 1501–1670.
- [31] A. Harrison-Marchand, F. Mongin, *Chem. Rev.* **2013**, *113*, 7470–7562.
- [32] S. Merkel, D. Stern, J. Henn, D. Stalke, *Angew. Chem. Int. Ed.* **2009**, *48*, 6350–6353.
- [33] F. Mongin, A. Harrison-Marchand, *Chem. Rev.* **2013**, *113*, 7563–7727.
- [34] K. Shen, Y. Fu, J.-N. Li, L. Liu, Q.-X. Guo, *Tetrahedron* **2007**, *63*, 1568–1576.
- [35] P. C. Andrikopoulos, D. R. Armstrong, H. R. L. Barley, W. Clegg, S. H. Dale, E. Hevia, G. W. Honeyman, A. R. Kennedy, R. E. Mulvey, *J. Am. Chem. Soc.* **2005**, *127*, 6184–6185.
- [36] H. Gilman, R. L. Bebb, *J. Am. Chem. Soc.* **1939**, *61*, 109–112.
- [37] G. Wittig, G. Fuhrmann, *Berichte der Dtsch. Chem. Gesellschaft* **1940**, *73B*, 1197–1218.
- [38] V. Snieckus, *Chem. Rev.* **1990**, *90*, 879–933.
- [39] M. C. Whisler, S. MacNeil, V. Snieckus, P. Beak, *Angew. Chem. Int. Ed.* **2004**, *43*, 2206–2225.
- [40] D. Leow, G. Li, T.-S. Mei, J.-Q. Yu, *Nature* **2012**, *486*, 518–522.
- [41] R.-Y. Tang, G. Li, J.-Q. Yu, *Nature* **2014**, *507*, 215–220.
- [42] Y.-J. Liu, H. Xu, W.-J. Kong, M. Shang, H.-X. Dai, J.-Q. Yu, *Nature* **2014**, *515*, 389–393.
- [43] X.-C. Wang, W. Gong, L.-Z. Fang, R.-Y. Zhu, S. Li, K. M. Engle, J.-Q. Yu, *Nature* **2015**, *519*, 334–338.
- [44] N. Hofmann, L. Ackermann, *J. Am. Chem. Soc.* **2013**, *135*, 5877–5884.
- [45] Z. Dong, J. Wang, G. Dong, *J. Am. Chem. Soc.* **2015**, *137*, 5887–5890.

- [46] O. Saidi, J. Marafie, A. E. W. Ledger, P. M. Liu, M. F. Mahon, G. Kociok-Köhn, M. K. Whittlesey, C. G. Frost, *J. Am. Chem. Soc.* **2011**, *133*, 19298–19301.
- [47] J. Luo, S. Preciado, I. Larrosa, *J. Am. Chem. Soc.* **2014**, *136*, 4109–4112.
- [48] S. Bag, T. Patra, A. Modak, A. Deb, S. Maity, U. Dutta, A. Dey, R. Kancharla, A. Maji, A. Hazra, M. Bera, D. Maiti, *J. Am. Chem. Soc.* **2015**, *137*, 11888–11891.
- [49] P. X. Shen, X. C. Wang, P. Wang, R. Y. Zhu, J. Q. Yu, *J. Am. Chem. Soc.* **2015**, *137*, 11574–11577.
- [50] J.-Y. Cho, M. K. Tse, D. Holmes, R. E. Maleczka Jr., M. R. Smith III, *Science* **2002**, *295*, 305–308.
- [51] C. Cheng, J. F. Hartwig, *Science* **2014**, *343*, 853–857.
- [52] R. J. Phipps, M. J. Gaunt, *Science* **2009**, *323*, 1593–1597.
- [53] K. S. Egorova, V. P. Ananikov, *Angew. Chemie Int. Ed.* **2016**, 2–15.
- [54] A. J. Martínez-Martínez, A. R. Kennedy, R. E. Mulvey, C. T. O. Hara, *Science* **2014**, *346*, 834–837.
- [55] D. R. Armstrong, E. Crosbie, E. Hevia, R. E. Mulvey, D. L. Ramsay, S. D. Robertson, *Chem. Sci.* **2014**, *5*, 3031–3045.
- [56] M. Scholl, S. Ding, C. W. Lee, R. H. Grubbs, *Org. Lett.* **1999**, *1*, 953–956.
- [57] C. Valente, M. G. Organ, *Angew. Chem. Int. Ed.* **2012**, *51*, 3314–3332.
- [58] S. Diez-Gonzalez, N. Marion, S. P. Nolan, *Chem. Rev.* **2009**, *109*, 3612–3676.
- [59] D. Enders, O. Niemeier, A. Henseler, *Chem. Rev.* **2007**, *107*, 5606–5655.
- [60] Y. Wang, Y. Xie, P. Wei, R. B. King, H. F. Schaefer, P. von R Schleyer, G. H. Robinson, *Science* **2008**, *321*, 1069–1071.
- [61] A. Sidiropoulos, C. Jones, A. Stasch, S. Klein, G. Frenking, *Angew. Chem. Int. Ed.* **2009**, *48*, 9701–9704.
- [62] C. Jones, A. Sidiropoulos, N. Holzmann, G. Frenking, A. Stasch, *Chem. Commun.* **2012**, *48*, 9855–9857.
- [63] Y. Wang, Y. Xie, P. Wei, R. B. King, H. F. Schaefer, P. V. R. Schleyer, G. H. Robinson, *J. Am. Chem. Soc.* **2008**, *130*, 14970–14971.
- [64] M. Y. Abraham, Y. Wang, Y. Xie, P. Wei, H. F. Schaefer, P. V. R. Schleyer, G. H. Robinson, *Chem. Eur. J.* **2010**, *16*, 432–435.
- [65] H. Braunschweig, R. D. Dewhurst, K. Hammond, J. Mies, K. Radacki, A. Vargas, *Science* **2012**, *336*, 1420–1422.
- [66] D. W. Stephan, *Acc. Chem. Res.* **2015**, *48*, 306–316.

- [67] E. L. Kolychev, E. Theuergarten, M. Tamm, in *Frustrated Lewis Pairs II Expand. Scope* (Eds.: G. Erker, D.W. Stephan), Springer, Heidelberg, **2013**, pp. 121–156.
- [68] S. P. Nolan, *N-Heterocyclic Carbenes*, Wiley-VCH Verlag GmbH & Co. KGaA, Boschstr. 12, 69469 Weinheim, Germany, **2014**.
- [69] Y. Wang, Y. Xie, M. Y. Abraham, P. Wei, H. F. Schaefer III, P. v. R. Schleyer, G. H. Robinson, *J. Am. Chem. Soc.* **2010**, *132*, 14370–14372.
- [70] D. R. Armstrong, S. E. Baillie, V. L. Blair, N. G. Chabloz, J. Diez, J. Garcia-Alvarez, A. R. Kennedy, S. D. Robertson, E. Hevia, *Chem. Sci.* **2013**, *4*, 4259–4266.
- [71] A. J. Martínez-Martínez, M. Ángeles Fuentes, A. Hernán-Gómez, E. Hevia, A. R. Kennedy, R. E. Mulvey, C. T. O'Hara, *Angew. Chem. Int. Ed.* **2015**, *54*, 14075–14079.
- [72] T. Klatt, J. T. Markiewicz, C. Sämann, P. Knochel, *J. Org. Chem.* **2014**, *79*, 4253–4269.
- [73] L. M. Dennis, W. Patnode, *J. Am. Chem. Soc.* **1932**, *54*, 182–188.
- [74] R. J. Wehmschulte, J. M. Steele, J. D. Young, M. A. Khan, *J. Am. Chem. Soc.* **2003**, *55*, 1470–1471.
- [75] P. Horeglad, P. Kruk, J. Pécaut, *Organometallics* **2010**, *29*, 3729–3734.
- [76] M. R. Kaluđerović, G. N. Kaluđerović, S. Gómez-Ruiz, R. Paschke, A. Hemprich, J. Kühling, T. W. Remmerbach, *J. Inorg. Biochem.* **2011**, *105*, 164–170.
- [77] M. Yamaguchi, Y. Nishimura, *Chem. Commun.* **2008**, 35–48.
- [78] Y. Nishimoto, H. Ueda, M. Yasuda, A. Baba, *Chem. Eur. J.* **2011**, *17*, 11135–11138.
- [79] S. Araki, T. Horie, M. Kato, T. Hirashita, *Tetrahedron Lett.* **1999**, *40*, 2331–2334.
- [80] H. Yao-Zeng, Z. Cheng-Ming, *Tetrahedron Lett.* **1996**, *37*, 3347–3350.
- [81] Z. Wang, S. Yuan, C.-J. Li, *Tetrahedron Lett.* **2002**, *43*, 5097–5099.
- [82] T. Tsuji, S. Usugi, H. Yorimitsu, H. Shinokubo, S. Matsubara, K. Oshima, *Chem. Lett.* **2002**, *31*, 2–3.
- [83] G. K. S. Prakash, P. Yan, I. Bucsi, M. Tanaka, G. A. Olah, *Catal. Letters* **2003**, *85*, 1–6.
- [84] M. Yamaguchi, T. Sotokawa, M. Hirama, *Chem. Commun.* **1997**, 743–744.
- [85] K. Takai, Y. Ikawa, K. Ishii, M. Kumanda, *Chem. Lett.* **2002**, *84*, 172–173.
- [86] R. Amemiya, M. Yamaguchi, *European J. Org. Chem.* **2005**, *2005*, 5145–5150.
- [87] H. Zhou, G. Liu, C. Zeng, *J. Organomet. Chem.* **2008**, *693*, 787–791.
- [88] Y. Yao-Zeng, Huang; Tao, Wen-Tian; Fang, Lei; Han, *Tetrahedron Lett.* **1995**, *36*,

1287–1290.

- [89] C. Lichtenberg, T. P. Spaniol, J. Okuda, *Inorg. Chem.* **2012**, *51*, 2254–2262.
- [90] T. Cadenbach, E. Hevia, *Organometallics* **2013**, *32*, 480–489.
- [91] D. A. Valyaev, G. Lavigne, N. Lugan, *Coord. Chem. Rev.* **2015**, *308*, 191–235.
- [92] R. A. Layfield, *Chem. Soc. Rev.* **2008**, *37*, 1098–1107.
- [93] R. Fischer, H. Goerls, M. Friedrich, M. Westerhausen, *J. Organomet. Chem.* **2009**, *694*, 1107–1111.
- [94] B. D. Murray, P. P. Power, *Inorg. Chem.* **1984**, *23*, 4584–4588.
- [95] G. C. Forbes, A. R. Kennedy, R. E. Mulvey, P. J. A. Rodger, R. B. Rowlings, *J. Chem. Soc. Dalton Trans.* **2001**, 1477–1484.
- [96] P. Knochel, S. H. Wunderlich, *Angew. Chem. Int. Ed.* **2009**, *48*, 7256–7260.
- [97] J. M. Concellón, H. Rodríguez-Solla, V. del Amo, *Chem. Eur. J.* **2008**, *14*, 10184–10191.
- [98] G. Cahiez, C. Duplais, J. Buendia, *Chem. Rev.* **2009**, *109*, 1434–1476.
- [99] K. Oshima, *J. Organomet. Chem.* **1999**, *575*, 1–20.
- [100] G. Cahiez, F. Mahuteau-Betzer, *Manganese Organometallics for the Chemoselective Synthesis of Polyfunctional Compounds*, in *Handbook of Functionalized Organometallics: Applications in Synthesis*, Wiley-VCH, Weinheim, Weinheim, **2005**.
- [101] G. Cahiez, A. Moyeux, J. Buendia, C. Duplais, *J. Am. Chem. Soc.* **2007**, *129*, 13788–13789.
- [102] G. Cahiez, C. Duplais, J. Buendia, *Angew. Chem. Int. Ed.* **2009**, *48*, 6731–6734.
- [103] J. Garcia-Alvarez, A. R. Kennedy, J. Klett, R. E. Mulvey, *Angew. Chem. Int. Ed.* **2007**, *46*, 1105–1108.
- [104] L. M. Carrella, W. Clegg, D. V. Graham, L. M. Hogg, A. R. Kennedy, J. Klett, R. E. Mulvey, E. Rentschler, L. Russo, *Angew. Chem. Int. Ed.* **2007**, *46*, 4662–4666.
- [105] V. L. Blair, W. Clegg, B. Conway, E. Hevia, A. Kennedy, J. Klett, R. E. Mulvey, L. Russo, *Chem. Eur. J.* **2008**, *14*, 65–72.
- [106] V. L. Blair, W. Clegg, R. E. Mulvey, L. Russo, *Inorg. Chem.* **2009**, *48*, 8863–8870.

## 2. Rational synthesis of normal, abnormal and anionic NHC-gallium alkyl complexes

### 2.1. Introduction to N-heterocyclic carbene chemistry

Over the past two decades, *N*-heterocyclic carbenes (NHCs), in particular imidazol-2-ylidenes, have progressed from mere curiosities to commodity neutral  $\sigma$ -donor ligands with a multitude of applications in synthesis and materials.<sup>[1]</sup> Typically, the carbene centre is located between the two nitrogen atoms (C2 position) allowing  $\pi$ -donation by both adjacent N-heteroatoms into the empty  $p_\pi$  orbital of the carbene (**Figure 2.1**), which makes these ligands remarkably more stable than other non-cyclic, all-carbon counterparts.<sup>[2,3]</sup>

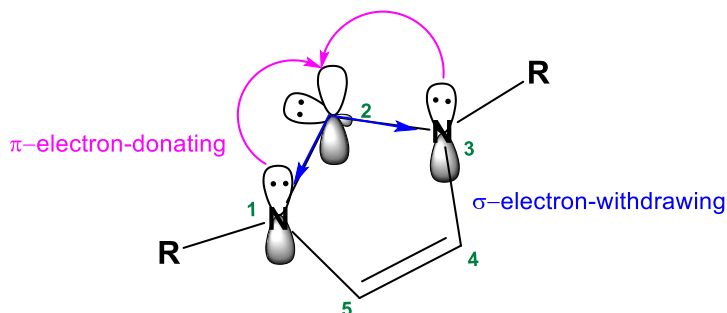


**Figure 2.1:** Ground-state electronic structure of imidazol-2-ylidenes with the  $\sigma$ -withdrawing and  $\pi$ -donating effects of nitrogen atoms contributing to the stabilisation depicted. IUPAC numbering system shown in green.

Acting as strong  $\sigma$ -donors, these versatile ligands have been pivotal to recent breakthroughs in transition-metal catalysis.<sup>[4–9]</sup> For example, Grubbs' 2<sup>nd</sup> generation catalyst (**Figure 2.2a**), where one of the two phosphine ligands has been replaced by a carbene, promotes olefin metathesis at very low catalyst loading (0.05 mol%).<sup>[4,10,11]</sup> The role of the carbene ligand is believed to be twofold: enhancing the catalyst performance by being a better donor than the phosphine ligand as well as slowing down its degradation due to the presence of more sterically demanding substituents.<sup>[12]</sup>

In terms of Pd-catalysed cross-coupling reactions, Organ's Pd-PEPPSI-NHC precatalyst complexes (PEPPSI = pyridine-enhanced precatalyst preparation, stabilisation and initiation) are now commercially available and have demonstrated excellent performance in cross-coupling reactions. In particular, Pd-PEPPSI-IPent

(**Figure 2.2b**) has been revealed as one of the most reactive and general catalysts for both carbon-carbon bond formation (*e.g.*, Suzuki-Miyaura, Negishi, and Stille-Migita couplings) and for carbon-heteroatom bond formation (*e.g.*, amination and sulfination reactions).<sup>[6]</sup>

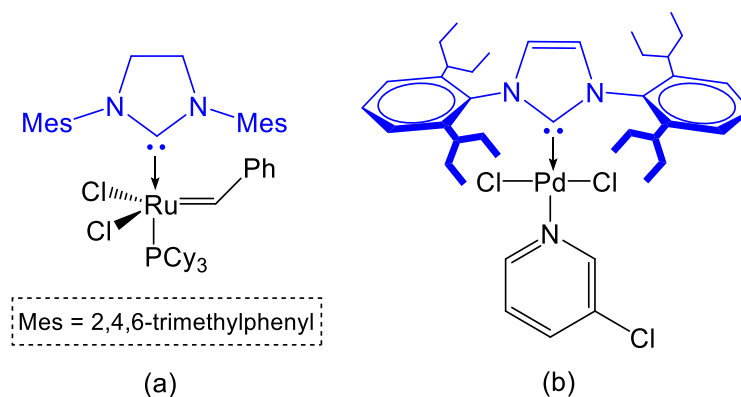
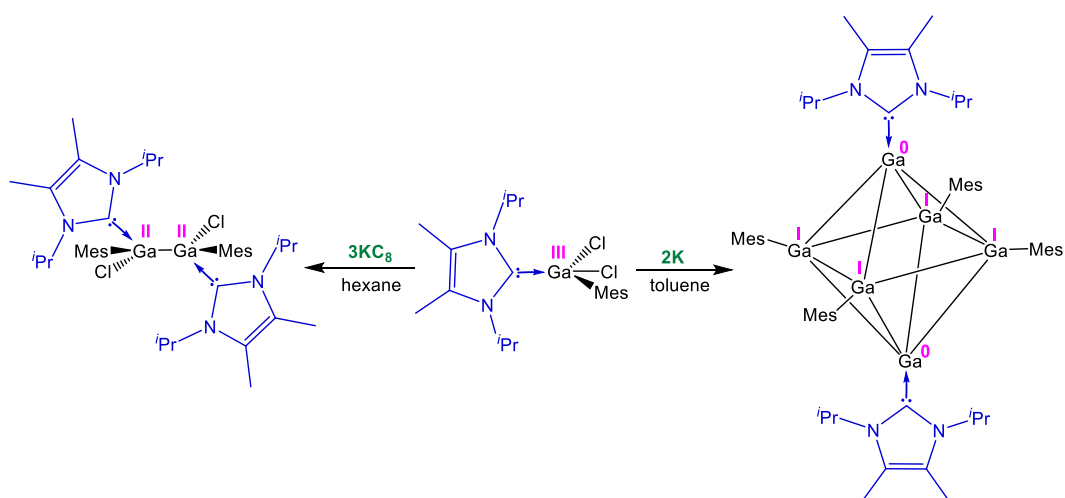


**Figure 2.2:** Incorporation of NHCs into catalysts for organic transformations: a) 2<sup>nd</sup> generation Grubbs' catalyst<sup>[4]</sup>; b) Organ's Pd-PEPPSI-IPent precatalyst complex.<sup>[6]</sup>

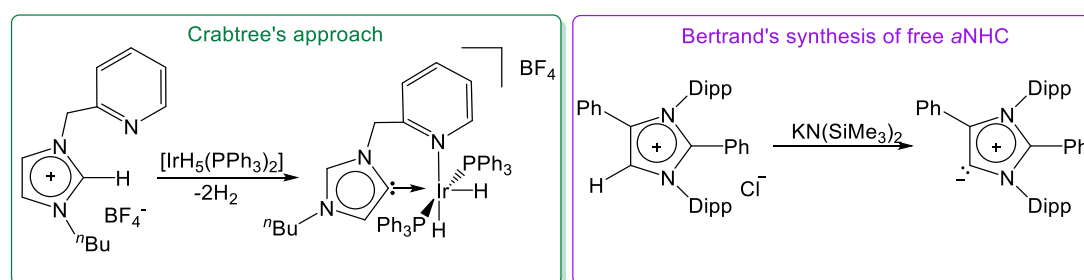
Furthermore, the application of NHCs to main group chemistry has enabled the stabilisation of novel low valent compounds,<sup>[13–20]</sup> as well as the development of several frustrated Lewis pair (FLP) systems.<sup>[21–23]</sup> By utilising NHCs as Lewis bases a group of highly reactive molecules including neutral diborines,<sup>[20]</sup> disilicon,<sup>[18]</sup> diphosphorus<sup>[14]</sup> and digermane<sup>[13]</sup> compounds have been stabilised and isolated. The role of the carbene is crucial as it provides the steric support to the newly generated element-element bonds whilst being unreactive towards the alkali-metal reduction method used in the synthesis of allotropes. Noteworthy are the examples of gallium clusters reported by Robinson and co-workers.<sup>[24]</sup> By reducing the carbene-complexed mesitylgallium dichloride with potassium graphite a dimeric compound comprising Ga(II) is formed, whilst when potassium is used the first example of a neutral aromatic Ga<sub>6</sub> octahedron with Ga(I) and Ga(0) is formed (**Scheme 2.1**).





**Scheme 2.1:** Preparation of gallium clusters with gallium centres in different oxidation states stabilised by NHCs.<sup>[24]</sup>

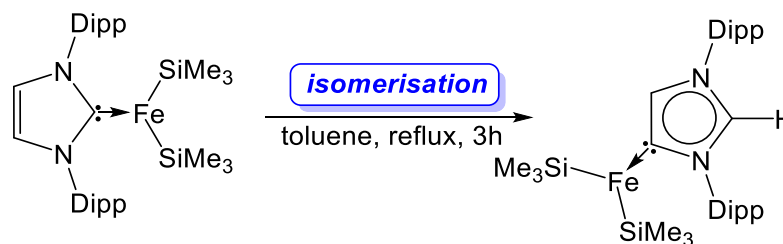
In parallel to these studies, a different type of NHC complex has been developed where the imidazole ring binds to the metal centre through its backbone. These less stabilised carbenes, where there is only one N-atom adjacent to their carbenic carbon<sup>[25]</sup> have been termed as *abnormal* (or mesoionic) NHCs (*a*NHCs).<sup>[26–28]</sup> Following Crabtree's seminal report in 2001 of the first transition-metal complex with an *a*NHC (**Scheme 2.2a**), several other examples have been prepared.<sup>[29–31]</sup> However, it was only in 2009 that Bertrand succeeded in the isolation of the first stable free *a*NHC by the elegant deprotonation of 1,2,3,4-tetraarylated imidazolium chloride (**Scheme 2.2b**).<sup>[32]</sup>



**Scheme 2.2:** Crabtree's<sup>[26]</sup> and Bertrand's<sup>[32]</sup> pioneering methods for the preparation of metal complex with an abnormal NHC and the free abnormal NHC, respectively.

Interestingly, experimental and theoretical studies point to *a*NHCs being better donors than their normal counterparts, which is in part attributed to their reduced steric congestion.<sup>[32–34]</sup> Thus Layfield has recently reported a thermally induced rearrangement of  $\text{IPr}\cdot\text{Fe}(\text{HMDS})_2$  [IPr = 1,3-bis-(2,6-diisopropylphenyl)imidazol-2-ylidene, HMDS = 1,1,1,3,3,3-

hexamethyldisilazide] which after 3h in refluxing toluene evolves to its *abnormal* isomer (**Scheme 2.3**).<sup>[35]</sup>



**Scheme 2.3:** Thermal isomerisation of  $\text{IPr}\cdot\text{Fe}(\text{HMDS})_2$  into  $a\text{IPr}\cdot\text{Fe}(\text{HMDS})_2$  reported by Layfield.<sup>[35]</sup>

Within main group chemistry, the number of complexes containing *a*NHCs remains very limited. The first example of an adduct of this type, a substituted phosphinidene complex resulting from coupling of complexes derived from singlet phosphinidenes (i.e.,  $[\text{Mn}_2(\text{CO})_8\{\mu\text{-P}(\text{N}^i\text{Pr}_2)\}]$ ) with free singlet carbenes (e.g., *t*Bu or IAd), was reported by Carty in 2006 (**Figure 2.3**).<sup>[36]</sup>

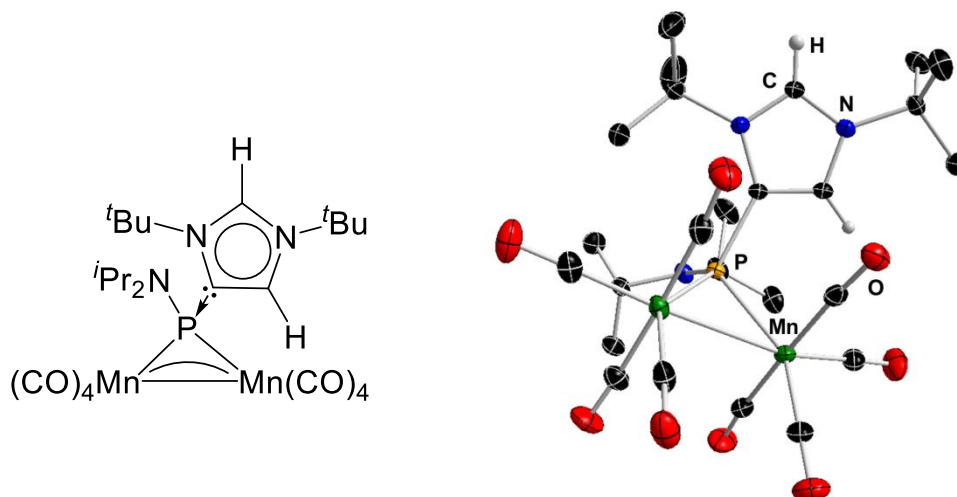
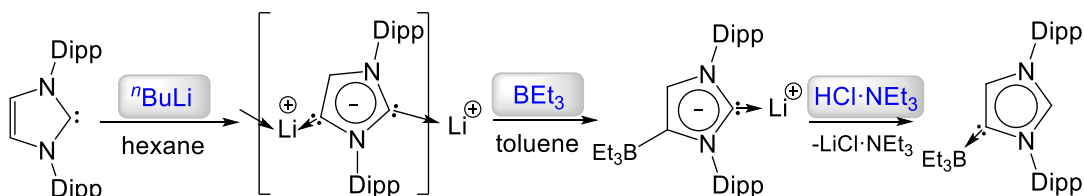


**Figure 2.3:** ChemDraw representation and X-ray structure of phosphinidene-*a*NHC complex.<sup>[36]</sup>

Thermal rearrangements related to that mentioned above in iron chemistry have been proposed for tris(pentafluorophenyl)borane NHC systems which exhibit FLP chemistry.<sup>[37–39]</sup> Similarly, within group 13 Dagorne has shown the isomerisation of *t*Bu·AlMe<sub>3</sub> [*t*Bu = 1,3-bis(*tert*-butyl)imidazol-2-ylidene] to its C4 bound isomer (*a**t*Bu·AlMe<sub>3</sub>) at room temperature in THF, although the mechanisms involved in these processes remain unclear.<sup>[40]</sup>

In addition to these isomerisation studies, Robinson has demonstrated that anionic NHCs, resulting from the lithiation of the imidazole backbone of

unsaturated NHCs,<sup>[41]</sup> can be employed as platforms to access *a*NHC-complexes of B and Zn by quenching the relevant anionic B or Zn complex with a suitable electrophile such as HCl·NEt<sub>3</sub> or MeOTf (Scheme 2.4).<sup>[42–44]</sup>



**Scheme 2.4:** Synthesis of *a*NHC complex of BEt<sub>3</sub> by electrophilic quenching of anionic mixed Li/B complex.<sup>[43]</sup>

Within the scope of gallium chemistry, there have been some examples of NHC-Ga complexes reported, however the majority of these were gallium hydrides and halides,<sup>[24,45–49]</sup> while organogallium examples remain scarce.<sup>[24,46,50]</sup> Some of the prepared complexes have demonstrated intriguing chemistry as exemplified by the work of Gandon who developed applications of some Ga-NHC adducts as  $\pi$ -acid catalysts.<sup>[48,49]</sup> However, all of these examples are examples of normal complexes, the only abnormal NHC complex known to date *a*IPr·GaCl<sub>3</sub><sup>[43]</sup> was reported as recently as 2014, although its synthesis is not straightforward as it was obtained by transmetalation of GaCl<sub>3</sub> with an anionic NHC mixed Li-B complex.

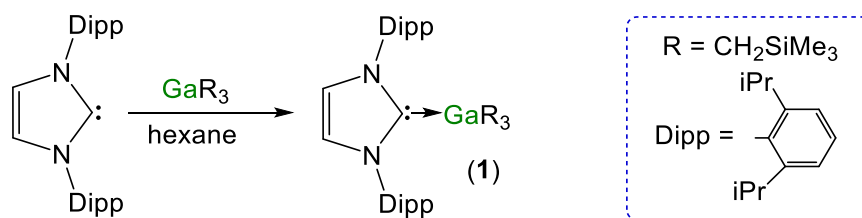
## 2.2. Aims of the chapter

Identifying a gap in knowledge in Ga-NHC chemistry and building on the most significant developments in the field of NHC chemistry, this chapter presents a systematic study into the rational synthesis of series of gallium-NHC complexes derived from the same metal fragment, tris(alkyl)gallium Ga(CH<sub>2</sub>SiMe<sub>3</sub>)<sub>3</sub> while using the unsaturated carbene IPr as a case study. The gallium reagent containing the heteroneopentyl ligand Me<sub>3</sub>SiCH<sub>2</sub><sup>-</sup> was selected due to its straightforward synthesis,<sup>[51]</sup> lack of  $\beta$ -hydrogen atoms, considerable steric bulk and electronic stabilization when compared to carbon-only-based alkyl groups that are prone to decomposition processes.<sup>[52,53]</sup> The constitution and stability of these complexes has been assessed by combining

X-ray crystallographic, kinetic and spectroscopic studies with theoretical investigations.

### 2.3. NHC-stabilised lithium gallate complexes

By reacting equimolar amounts of IPr and trimethylsilylmethylgallium(III)<sup>[51]</sup> ( $\text{GaR}_3$ ) at room temperature in non-polar hexane solvent a yellow suspension was formed which was gently heated into a solution and afforded colourless crystals of the adduct  $\text{IPr}\cdot\text{GaR}_3$  (**1**) in a 75% isolated yield (**Scheme 2.5**).



**Scheme 2.5:** Synthesis of normal adduct  $\text{IPr}\cdot\text{GaR}_3$  (**1**).

The molecular structure of **1** (**Fig. 2.4**) was elucidated by a single crystal X-ray diffraction analysis which revealed the formation of a complex with the four-carbon-coordinated gallium atom attached to three alkyl groups and the C2 (*i.e.*, C1 in **Fig. 2.4**) of a neutral carbene. A distorted tetrahedral geometry adopted by Ga centre is evidenced by the C-Ga-C bond angles which range from  $96.36(6)^\circ$  to  $119.43(7)^\circ$  (average angle  $108.79^\circ$ ). The Ga-C<sub>alkyl</sub> distances range from  $2.0034(15) \text{ \AA}$  to  $2.0164(16) \text{ \AA}$  (mean  $2.0106 \text{ \AA}$ ) which is elongated (by  $\sim 2.5\%$ ) when compared to parent monomeric  $\text{GaR}_3$  (Ga-C bonds ranging from  $1.952(4) \text{ \AA}$  to  $1.971(3) \text{ \AA}$ , average  $1.959 \text{ \AA}$ )<sup>[54]</sup> in agreement with the increase in the coordination number of Ga in **1**. Noticeably, the Ga-C<sub>NHC</sub> distance of  $2.1960(16) \text{ \AA}$  is significantly longer compared to that observed in the related Ga halide complex  $\text{IPr}\cdot\text{GaCl}_3$  ( $2.016(2) \text{ \AA}$ ).<sup>[47]</sup> This elongation can be rationalised in terms of a combination of the greater steric congestion in **1** imposed by the monosilyl groups as well as the stronger Lewis acidity of  $\text{GaCl}_3$  compared to  $\text{GaR}_3$ .

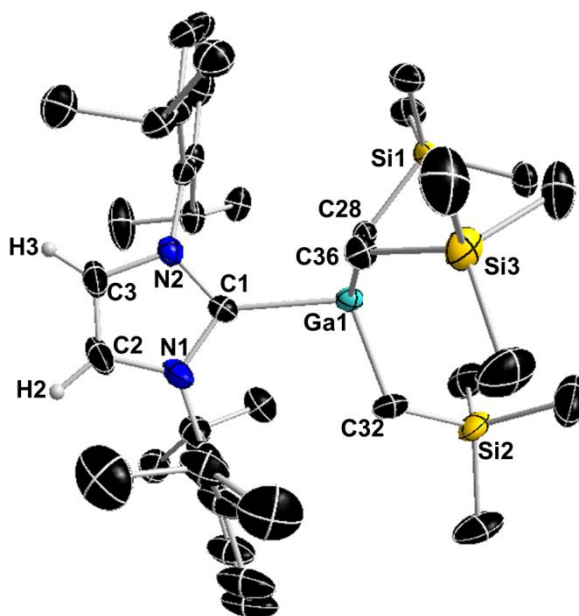


**Figure 2.4:** Molecular structure of **1** with 50% probability displacement ellipsoids. Minor disorder in one isopropyl group and one monosilyl group are omitted for clarity, as are all H atoms except for those on the imidazole ring. Selected bond distances (Å) and bond angles (°): Ga(1)-C(1) 2.1960(16), Ga(1)-C(28) 2.0034(15), Ga(1)-C(32) 2.0120(17), Ga(1)-C(36) 2.0164(16), C(28)-Ga(1)-C(1) 101.15(6), C(32)-Ga(1)-C(1) 106.27(7), C(36)-Ga(1)-C(1) 96.36(6), C(28)-Ga(1)-C(32) 114.89(7), C(28)-Ga(1)-C(36) 119.43(7), C(32)-Ga(1)-C(36) 114.63(7), N(1)-C(1)-N(2) 102.80(3).

Despite the long Ga-C1 distance, it should be noted that **1** retains its integrity in  $C_6D_6$  solution as evidenced by  $^1H$ -DOSY NMR studies, which show that the IPr and monosilyl groups belong to the same sized species, as the cross-point for both ligand resonances are aligned in the second dimension (average  $D$  value =  $6.2 \cdot 10^{-10} \text{ m}^2\text{s}^{-1}$ ; see **Fig. 2.5**). The most informative resonance in the  $^{13}C$  NMR spectrum is that for the carbenic carbon observed at 186.6 ppm (*vs.* 220.6 ppm for the free IPr), confirming a retention of the Ga-C bond in solution. Two singlets are observed for the monosilyl group at -0.95 (Ga- $CH_2$ ) and 0.18 ppm ( $Si(CH_3)_3$ ) contrasting with the  $^1H$  NMR spectrum of  $GaR_3$  in the same solvent where both signals coincidentally overlap displaying a singlet at 0.13 ppm.

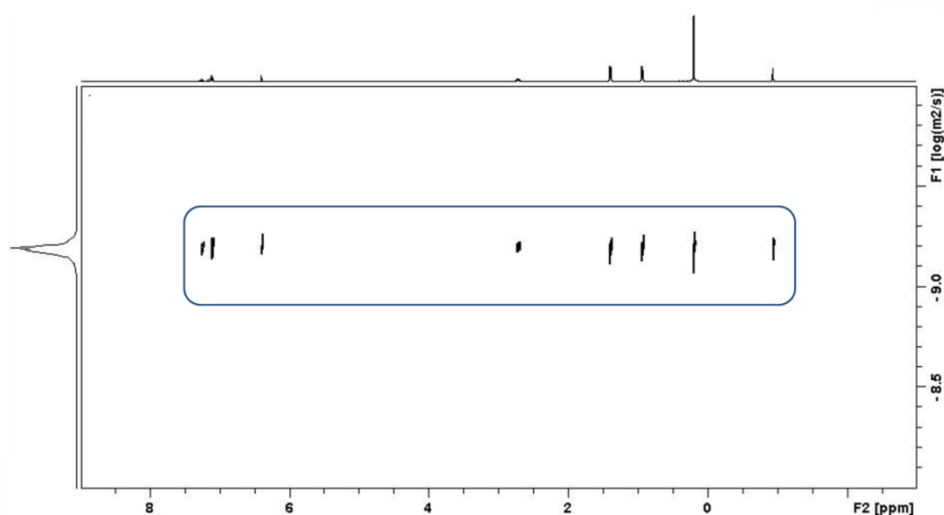
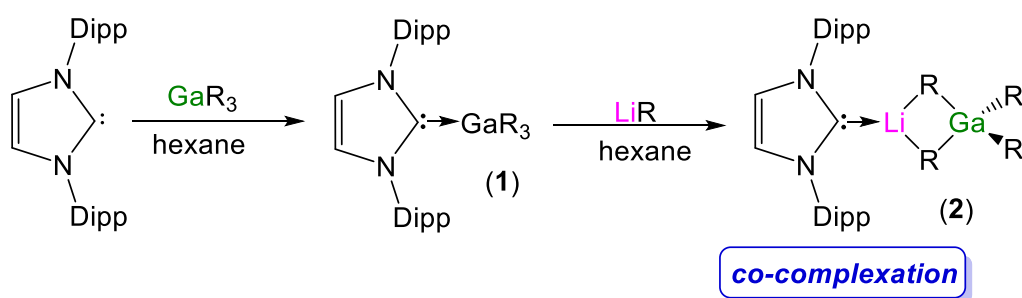


**Figure 2.5:**  $^1\text{H}$ -DOSY NMR spectrum of  $\text{IPr}\cdot\text{GaR}_3$  (**1**) at 25 °C in  $\text{C}_6\text{D}_6$  solution.

Next the reactivity of **1** towards  $\text{LiCH}_2\text{SiMe}_3$  was investigated. Previous work by Roesky and Stalke<sup>[55]</sup> has shown that when borane adduct  $\text{IPr}\cdot\text{BH}_3$  is treated with  $n\text{BuLi}$ , lithiation of the C4 position of the imidazole ring takes place affording an anionic NHC which binds through its C4 position to Li, leaving the B-C2 bond untouched.<sup>[55]</sup> Similar reactivity has also been described for the alkylborane  $\text{IPr}\cdot\text{BEt}_3$ .<sup>[41]</sup> Interestingly in our studies, the polar organometallic  $\text{RLi}$  fails to deprotonate the NHC ligand of **1**, affording instead lithium gallate  $[\text{IPr}\cdot\text{LiGa}(\text{CH}_2\text{SiMe}_3)_4]$  (**2**) in an isolated yield of 48% (**Scheme 2.6**).



**Scheme 2.6:** Synthesis of  $[\text{IPr}\cdot\text{LiGaR}_4]$  (**2**).

Single crystal X-ray diffraction analysis established the molecular structure of  $[\text{IPr}\cdot\text{LiGa}(\text{CH}_2\text{SiMe}_3)_4]$  which represents to the best of our knowledge the first example of an alkali-metal gallate stabilised by an NHC ligand (**Figure 2.6**). Unfortunately even after several attempts in crystallising, all four monosilyl groups of compound **2** were found to be disordered which obviously

compromises any discussion of geometrical parameters such as bond distances, however the crystallographic analysis does establish the connectivity.

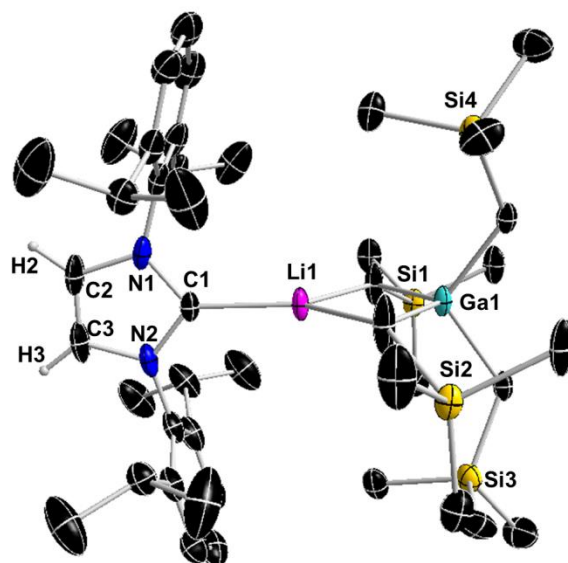
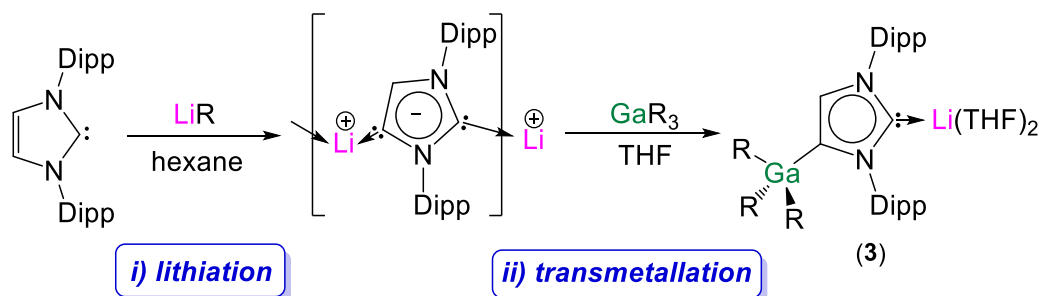


**Figure 2.6:** Molecular structure of **2** with 30% probability displacement ellipsoids. All  $\text{CH}_2\text{SiMe}_3$  groups are disordered and only one component of the disordered model is shown above. All hydrogen atoms except those on the imidazole ring have been omitted for clarity.

Compound **2** exhibits a contacted ion pair (CIP) motif where the two metals are connected by two bridging alkyl groups with the neutral NHC binding *via* its C2 (*i.e.*, C1) position to lithium. These findings show that under these reaction conditions the polar Li alkyl reagent preferentially co-complexes with  $\text{GaR}_3$ , to yield  $[\text{LiGaR}_4]^{[56]}$  which is then trapped and stabilised by the neutral NHC ligand, instead of lithiating the carbene backbone. Clearly the Ga atom favours coordination of another alkyl anion rather than a neutral IPr ligand. It should be noted that a similar reactivity has been reported by our group for the reaction of  $\text{IPr}\cdot\text{Zn}^t\text{Bu}_2$  with  $^t\text{BuLi}$  in hexane, which produces zincate complex  $[\text{IPr}\cdot\text{LiZn}^t\text{Bu}_3]^{[57]}$ . Gallate **2** can also be prepared by reacting polymeric  $[\{\text{LiGaR}_4\}_\infty]$  with free IPr. Solution state studies of **2** were hindered by poor solubility in arene solvents such as  $\text{C}_6\text{D}_6$ , whereas in coordinating THF the adduct dissociates into free IPr and multi-THF-solvated  $\text{LiGaR}_4$ , as evidenced by multinuclear NMR spectroscopy.

Contrastingly, if the order of the monometallic reactants is reversed, by treating first IPr with LiR followed by the addition of gallium alkyl  $\text{GaR}_3$  in THF, heteroleptic  $(\text{THF})_2\text{Li}[:\text{C}\{[\text{N}(2,6\text{-}^i\text{Pr}_2\text{C}_6\text{H}_3)]_2\text{CHCGa}(\text{CH}_2\text{SiMe}_3)_3\}]$  (**3**) was obtained in a 56% isolated yield. Formation of **3** can be rationalised in

terms of a stepwise indirect gallation process. IPr is first deprotonated at the C4 position by the highly polar  $\text{LiR}^{[41]}$  reagent (**I** in **Scheme 2.7**), which can then undergo fast transmetalation with the more electronegative Ga fragment, with the alkali-metal being trapped by the vacant C2 site of the carbene (**Scheme 2.7**).



**Scheme 2.7:** Two-step synthesis of heteroleptic lithium gallate **3**.

X-ray crystallographic studies established the CIP structure of **3** where the metals are now connected by an anionic NHC which coordinates as an asymmetric bridge *via* its normal C2 position to Li and its abnormal C4 position to Ga (**Figure 2.7**).

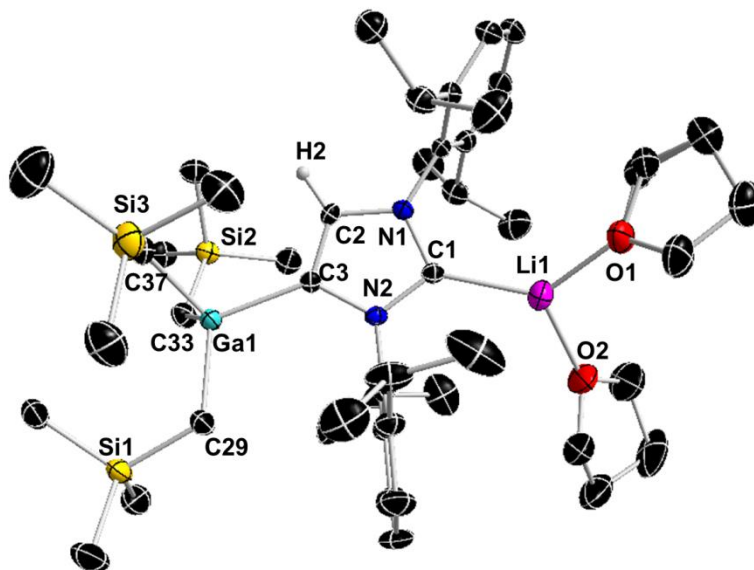


**Figure 2.7:** Molecular structure of **3** with 50% probability displacement ellipsoids. All hydrogen atoms except H2 on the imidazole ring and minor disorder of THF ligand have been omitted for clarity. Selected bond distances (Å) and bond angles (°): Ga(1)-C(3) 2.052(2), Ga(1)-C(29) 2.013(2), Ga(1)-C(33) 2.040(2), Ga(1)-C(37) 2.031(2), Li(1)-C(1) 2.093(5), C(29)-Ga(1)-C(3) 111.43(9), C(29)-Ga(1)-C(33) 108.63(10), C(29)-Ga(1)-C(37) 112.99(10), C(33)-Ga(1)-C(3) 110.96(9), C(37)-Ga(1)-C(3) 105.68(9), C(37)-Ga(1)-C(33) 107.06(10), N(1)-C(1)-N(2) 111.56(17).



The C2-Li (*i.e.*, C1 in **Fig. 2.7**) distance is 2.093(5) Å which is similar to those reported for related complexes containing anionic NHC bridged in a similar C2-Li/C4-M fashion to Li/Al and Li/B pairings.<sup>[41,43,55]</sup>

All four Ga-C bonds are similar in length ranging from 2.013(2) Å to 2.052(2) Å (average 2.034 Å) which is in good agreement with other tetra-coordinated gallate species such as {[K-dibenzo-18-c-6]<sup>+</sup>[Ga(η<sup>1</sup>-C<sub>3</sub>H<sub>5</sub>)<sub>4</sub>]<sup>-</sup>} (2.029 Å mean).<sup>[58]</sup> The Ga-C4 distance (*i.e.*, C3 in **Fig. 2.7**) of 2.052(2) Å is close in value with Ga-C<sub>alkyl</sub> bonds (average 2.028 Å) and understandably it is significantly shorter (by 0.144 Å) to that found in the neutral C2 bound IPr adduct **1**. It is noteworthy, that unlike in **1** where a pyramidalization of Ga coordination sphere was evident (*vide supra*), in **3** the gallium atom exhibits nearly ideal tetrahedral geometry with the average bond of 2.034 Å and mean angle of 109.46° (angles ranging from 105.68(9)° to 112.99(10)°). This decrease in distortion around the metal centre can be attributed to the relief of the steric congestion of **3** when compared to **1**. From the NMR data in *d*<sub>8</sub>-THF solutions, metallation of IPr was demonstrated by the large downfield chemical shift of the C4 resonance in the <sup>13</sup>C NMR spectrum (from 122.3 ppm in free IPr to 155.1 in **3**), as well as an informative singlet at 6.64 ppm (integral 1H) in the <sup>1</sup>H NMR spectrum of the imidazole CH (*versus* 7.19 ppm in free IPr), **Fig. 2.8**.

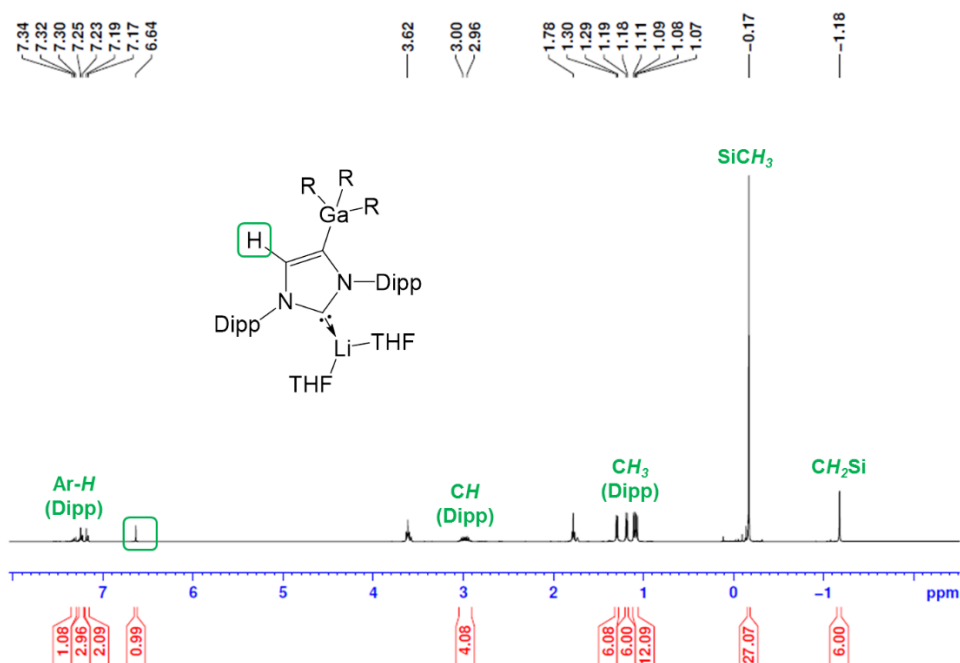
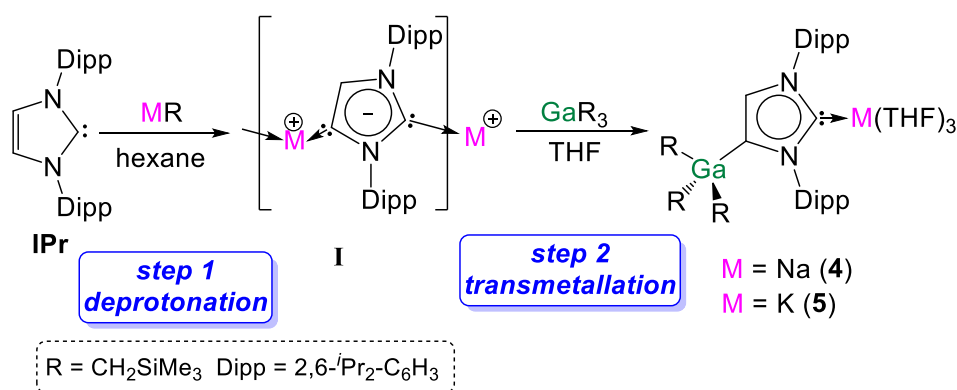


**Figure 2.8:** <sup>1</sup>H NMR spectrum of **3** in *d*<sub>8</sub>-THF solution.

In addition, a resonance in the  $^{13}\text{C}$  NMR spectrum at 201.4 ppm for carbenic C2 confirms the formation of an NHC complex. The loss of symmetry in the imidazole ring is evidenced in the  $^1\text{H}$  and  $^{13}\text{C}$  NMR spectra with the appearance of two distinct sets of Dipp signals.

Following this line of inquiry, treating a hexane suspension of IPr with heavier alkali-metal alkyls  $\text{MCH}_2\text{SiMe}_3$  ( $\text{M} = \text{Na}, \text{K}$ ) led to the instant formation of yellow solids which were completely insoluble even when using large amounts of the more polar solvent THF. Addition of  $\text{GaR}_3$ , however, solubilised this product allowing the isolation of heteroleptic alkali-metal gallates  $(\text{THF})_3\text{Na}[\text{C}\{\text{N}(2,6\text{-}^i\text{Pr}_2\text{C}_6\text{H}_3)_2\text{CHCGa}(\text{CH}_2\text{SiMe}_3)_3\}]$  (**4**) and  $(\text{THF})_3\text{K}[\text{C}\{\text{N}(2,6\text{-}^i\text{Pr}_2\text{C}_6\text{H}_3)_2\text{CHCGa}(\text{CH}_2\text{SiMe}_3)_3\}]$  (**5**) in 71 and 76% isolated yields respectively (**Scheme 2.8**).



**Scheme 2.8:** Synthesis of heavier alkaline metal gallates **4** and **5**.

Although the solids obtained by treating IPr with MR ( $\text{M} = \text{Na}, \text{K}$ ) cannot be characterised, due to their lack of solubility, the isolation of **4** and **5** provides compelling proof that these heavier alkaline metal alkyls can in fact metallate this NHC. While the relevant  $\text{M}^+\text{IPr}^-$  salts (**I** in **Scheme 2.8**) are obtained *via* direct metallation, it should be noted that Goicoechea has structurally characterised  $\text{K}^+\text{IPr}^- \cdot 2\text{THF}$  as the result of the reaction of the lithiated IPr with potassium *tert*-butoxide.<sup>[59]</sup>

Solid state structures of sodium (**4**) and potassium (**5**) gallates were elucidated by X-ray crystallographic studies (**Fig. 2.9**) which confirmed them to be molecularly isostructural with **3**. The Ga-C4 distances (i.e., C24 for **4** and C2 for **5** in **Fig. 2.9**) of

2.050(2) Å for **4** and 2.050(3) Å for **5** are close in value with the Ga-C<sub>alkyl</sub> bonds (average 2.027 Å and 2.028 Å for **4** and **5** respectively) and in excellent agreement with the bond distances found in **3**. The narrow variation observed for the Ga-C bond lengths together with very similar bond angles (mean angle 108.15° for **4** and 109.46° for **5**) reveal an almost ideal tetrahedral geometry of gallium centre in both compounds. With the virtually identical environment around Ga-atom, complexes **4** and **5** display their differences at the other end of the bridging ligand. Unsurprisingly, the M-C<sub>NHC</sub> bond distance found in **4** (2.530(3) Å) is significantly shorter than that of **5** (2.902(3) Å), which is in agreement with the increase in size of the alkali-metal. Both values compare well with those reported for other anionic complexes containing these alkali-metals.<sup>[56,57,60–62]</sup> Both sodium and potassium complete their coordination spheres by coordination of three molecules of THF, with more electropositive potassium gaining further stabilisation through electrostatic interaction with the *ipso* carbon of the pendant Dipp group on N2 (**Figure 2.9b**). This secondary contact (K1...C16 = 3.301(3) Å) is within the range of previously reported potassium  $\pi$ -interactions<sup>[63–68]</sup> and translates into a significantly more acute N2-C1-K1 angle (107.77(18)°) than N1-C1-K1 (150.71(19)°).

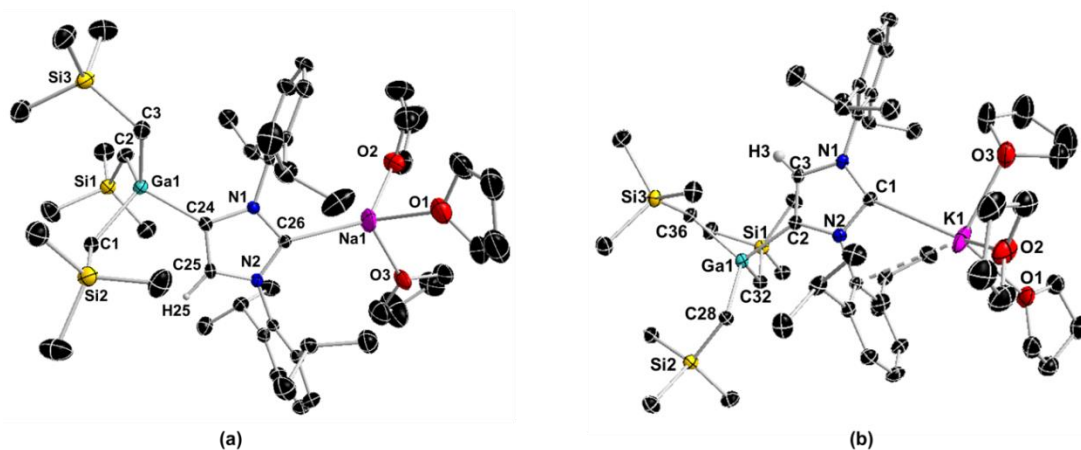


**Figure 2.9:** Molecular structure of **4** (a) and **5** (b) with 50% probability displacement ellipsoids. All hydrogen atoms except the one left on imidazole ring, and disorder components in THF ligands have been omitted for clarity. Dashed lines represent secondary interactions.

The NMR data of **4** and **5** in *d*<sub>8</sub>-THF solutions, follows the same trend observed for **3** with the large downfield shift of the C4-Ga resonance in the <sup>13</sup>C NMR spectra as well as with the presence of diagnostic singlets integrating 1H in the <sup>1</sup>H NMR

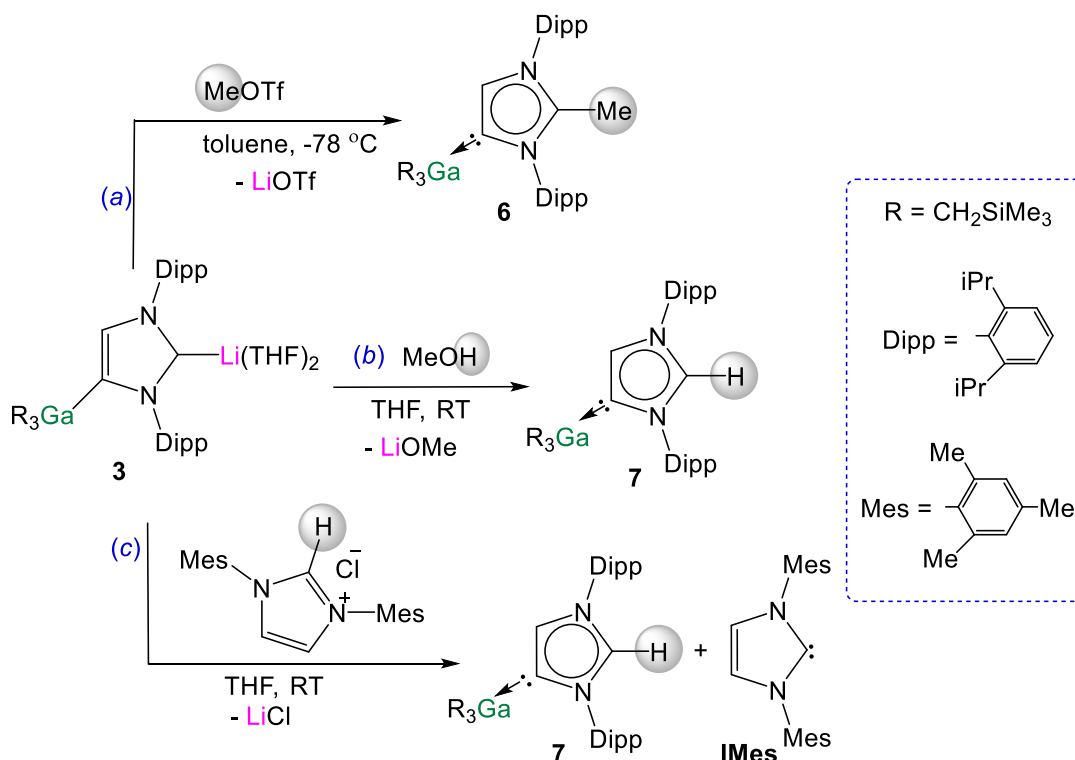
spectra for the imidazole *CH* (**Table 2.1**). In addition, the carbenic *C* atom attached to the alkali-metal can be observed at 202.8 and 210.7 ppm for **4** and **5** respectively, at similar values to those reported for other related complexes containing Na<sup>[57]</sup> and K.<sup>[59]</sup>

**Table 2.1:** Comparison of selected NMR chemical shifts (ppm  $\delta$ ) in *d*<sub>8</sub>-THF for alkali-metal gallates **3-5**.

	<b>3</b> (M = Li)	<b>4</b> (M = Na)	<b>5</b> (M = K)
$\delta^{13\text{C}}$ C2-M	201.4	202.8	210.7
$\delta^{13\text{C}}$ C4-Ga	155.1	155.2	153.6
$\delta^{1\text{H}}$ C5-H	6.64	6.64	6.59

#### 2.4. Electrophilic interception reactions: accessing abnormal NHC-Ga complexes

Recent studies have shown that certain anionic NHC complexes, when treated with an electrophile can be transformed into neutral abnormal adducts.<sup>[43,44]</sup> To explore this reactivity here, we treated **3** with a molar equivalent of MeOTf in toluene at -78 °C. The reaction occurred with the formation of a white precipitate (presumably LiOTf) furnishing a neutral *abnormal* NHC-Ga complex [CH<sub>3</sub>C{[N(2,6-*i*Pr<sub>2</sub>C<sub>6</sub>H<sub>3</sub>)]<sub>2</sub>CHCGa(CH<sub>2</sub>SiMe<sub>3</sub>)<sub>3</sub>}] (**6**) in a 68% yield (**Scheme 2.9a**).



**Scheme 2.9:** Electrophilic interception of anionic NHC complex **3** with a) MeOTf, b) MeOH and c) imidazolium salt IMes·HCl.

Complex **6** results from the selective C2 methylation of the anionic NHC leaving the Ga-C4 bond intact. It should be noted that although there are several examples of Ga-NHC adducts reported in the literature,<sup>[46,47,50]</sup> with some of them finding applications as  $\pi$ -acid catalysts,<sup>[48,49]</sup> the only abnormal NHC complex known to date  $a\text{IPr}\cdot\text{GaCl}_3$ <sup>[43]</sup> was reported as recently as 2014, although its synthesis is not straightforward.

The molecular structure of **6** was established by X-ray crystallographic studies (**Fig. 2.10**). The bond length of 1.538(6) Å for C2-C<sub>Me</sub> (*i.e.*, C1-C4 in **Fig. 2.10**) is consistent with a single bond, while the Ga-C4 (*i.e.*, C3 in **Fig. 2.10**) bond length of 2.087(3) Å is only slightly elongated compared to that found in the anionic variant **3** (2.052(2) Å), and significantly shorter than the Ga-C2 bond length in **1** (2.1960(16) Å). Reflecting the formation of a neutral abnormal complex, the <sup>13</sup>C NMR spectrum of **6** shows a resonance at 186.5 ppm for the C4 attached to Ga (*vs* 155.1 ppm in **3**) whereas the methylated carbon (originally C2 carbenic position in **3**) resonates significantly upfield at 124.4 ppm in comparison with that observed for **3** (at 201.1 ppm).

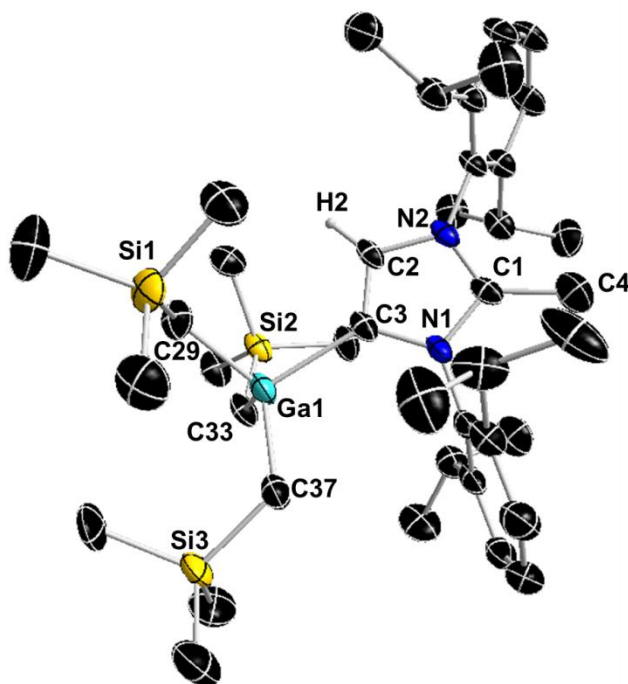


**Figure 2.10:** Molecular structure of **6** with 50% probability displacement ellipsoids. Only one component of disordered monosilyl groups is shown. All hydrogen atoms except the one on the imidazole ring have been omitted for clarity. Selected bond distances (Å) and bond angles (°): Ga(1)-C(3) 2.087(3), Ga(1)-C(29) 1.969(5), Ga(1)-C(33) 2.089(5), Ga(1)-C(37) 1.983(5), C(1)-C(4) 1.538(6), C(29)-Ga(1)-C(3) 107.34(18), C(29)-Ga(1)-C(33) 106.4(2), C(29)-Ga(1)-C(37) 117.3(2), C(33)-Ga(1)-C(3) 107.71(15), C(37)-Ga(1)-C(3) 109.77(17), C(37)-Ga(1)-C(33) 107.9(2), N(1)-C(1)-N(2) 107.6(3).

The use of methanol as a quenching reagent resulted in clean conversion of **3** to the abnormal adduct *aIPr*-GaR<sub>3</sub> (**7**) (**Scheme 2.9b**). Notably, **7** is also formed as a metallation product from the reaction of **3** with the imidazolium salt IMes·HCl (1,3-*bis*-(2,4,6-trimethylphenyl)imidazolium chloride) (**Scheme 2.9c**). These findings not only demonstrate that the C2 position of **3** in the imidazole ring is its preferred basic site, but also the high strength of its Ga-C4 bond as it is retained in **7**. Furthermore in view of these results it appears that for GaR<sub>3</sub> fragment *aIPr* is a better ligand than the related normal IMes carbene (obtained from deprotonation of the imidazolium salt, **Scheme 2.9c**), as no ligand exchange occurs. Compound **7** was isolated as a crystalline solid in a 61% yield and its molecular structure was established by X-ray crystallography (**Figure 2.11**).

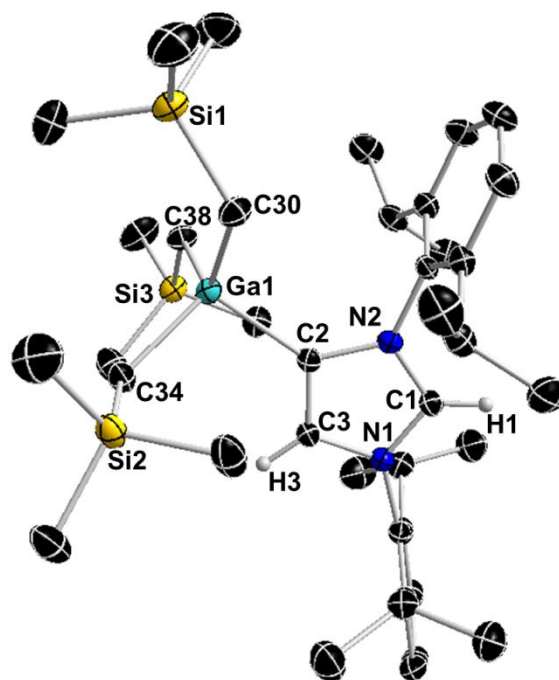


**Figure 2.11:** Molecular structure of **7** with 50% probability displacement ellipsoids. All hydrogen atoms except those on the imidazole rings have been omitted for clarity. Selected bond distances (Å) and bond angles (°): Ga(1)-C(2) 2.0759(16), Ga(1)-C(30) 2.0071(17), Ga(1)-C(34) 2.0262(17), Ga(1)-C(38) 2.0257(16), C(30)-Ga(1)-C(2) 106.54(7), C(34)-Ga(1)-C(2) 102.53(7), C(38)-Ga(1)-C(2) 109.08(7), C(30)-Ga(1)-C(38) 114.78(7), C(30)-Ga(1)-C(34) 112.42(7), C(38)-Ga(1)-C(34) 110.63(7), N(1)-C(1)-N(2) 107.51(14).

The Ga-C4 bond length (i.e., Ga-C2 in **Fig 2.11**) of 2.0759(16) Å in **7** is significantly shorter than the corresponding bond in the normal congener **1** (by 0.1201 Å), supporting previous studies which suggest that abnormal carbenes are stronger  $\sigma$ -donors, less sterically congested, and consequently are able to form stronger bonds with metal centres. In fact, as previously discussed for **6**, despite the neutral constitution of the *a*NHC ligand, the strength of this interaction is similar to that observed for the Ga-C bond of the anionic carbene present in **3**.

As mentioned above, the only example of an abnormal NHC Ga complex prior to this work was reported by Robinson,<sup>[43]</sup> where *a*IPr·GaCl<sub>3</sub> was formed while attempting the transmetalation of mixed lithium/boron anionic NHC complex with GaCl<sub>3</sub>. Interestingly the Ga-C<sub>carbene</sub> distance of this complex (1.978(3) Å) differs only by 0.097 Å to that found for **7** (2.0759(16) Å). This contrasts with the markedly different bond distances found when comparing the relevant normal isomer (Ga-C<sub>carbene</sub> bond distance in IPr·GaX<sub>3</sub>, 2.1960(16) Å when X=R (**1**); vs 2.016(2) Å when X=Cl), hinting that in the abnormal systems, due

to the increased steric space around the metal centre, the size of the anionic groups attached to Ga has a significantly smaller influence than in the normal adducts.

The  $^1\text{H}$  NMR spectrum of **7** in  $d_8$ -THF solution showed a diagnostic singlet at 9.00 ppm (**Fig. 2.12a**) belonging to the H attached to the C2 position of the carbene, whereas the remaining H in the imidazole ring resonates at 7.20 ppm. The significant downfield shift of this C2-H proton compared to the imidazole protons of **1** and **3** can be potentially correlated to its acidity as we have found that addition of LiR to **7** will cleanly and instantly yield **3**, whereas when we attempted deprotonation of **1** co-complexation took place affording **2** (*vide supra*). Similarly to that found in **6**, the  $^{13}\text{C}$  NMR spectrum shows two informative singlets at 162.8 and 124.4 ppm which can be assigned to Ga-C4 and NC(H)N respectively.

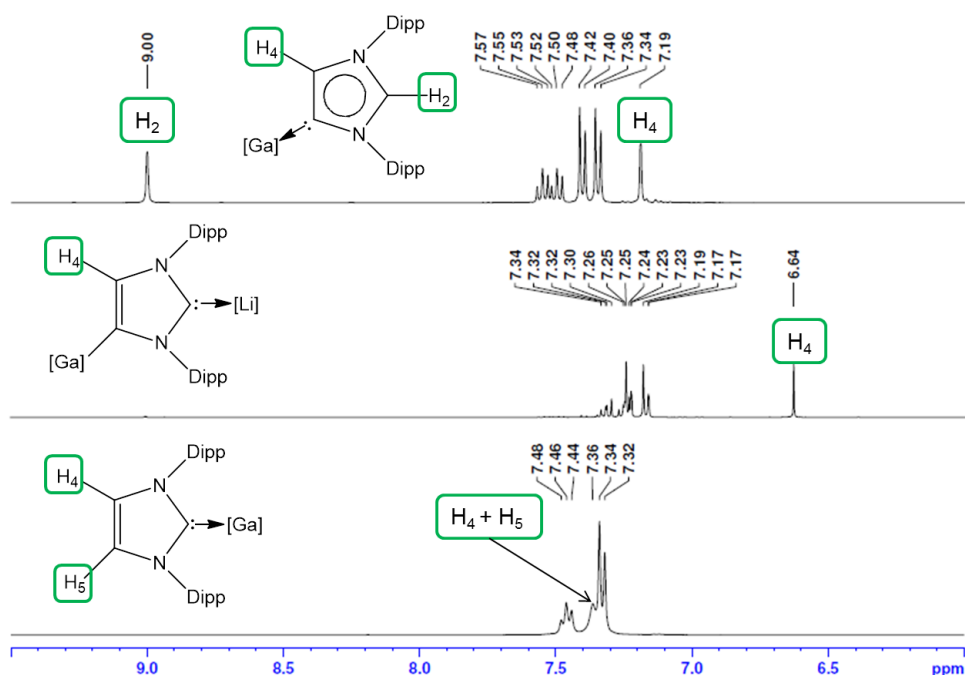
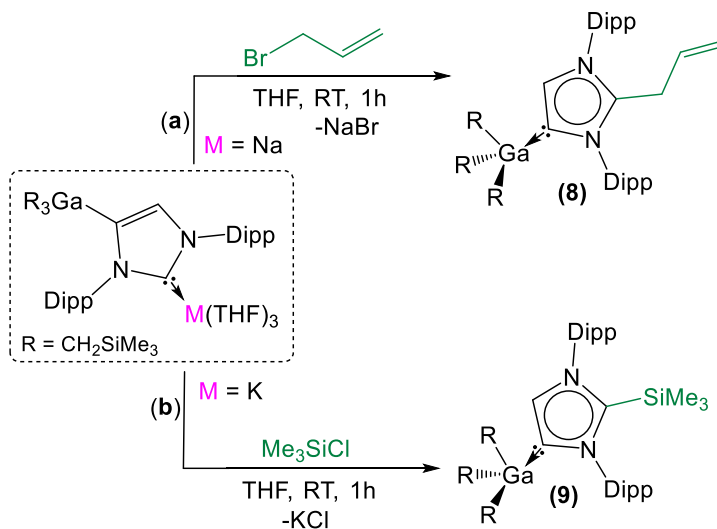


**Figure 2.12:** Comparison of the expanded aromatic region of  $^1\text{H}$  NMR spectra in  $d_8$ -THF solution of compounds **1** (bottom), **3** (middle) and **7** (top); [Ga] =  $\text{GaR}_3$ .

Illustrating the generality of these electrophilic interception reactions, we have next reacted **4** with an equimolar amount of allyl bromide and **5** with  $\text{Me}_3\text{SiCl}$  in THF at room temperature. In both cases the reaction proceeded with the formation of white precipitate (presumably alkali metal salts NaBr and KCl,



respectively) affording  $[\text{C}_3\text{H}_5\text{C}\{\text{N}(2,6\text{-}i\text{Pr}_2\text{C}_6\text{H}_3)_2\}\text{CHCGa}(\text{CH}_2\text{SiMe}_3)_3]$  (**8**) and  $[\text{Me}_3\text{SiC}\{\text{N}(2,6\text{-}i\text{Pr}_2\text{C}_6\text{H}_3)_2\}\text{CHCGa}(\text{CH}_2\text{SiMe}_3)_3]$  (**9**) in 42 and 61 % yields respectively (**Scheme 2.10**).



**Scheme 2.10:** Electrophilic interception of anionic NHC complexes (a) **4** with allyl bromide and (b) **5** with  $\text{Me}_3\text{SiCl}$ .

Compounds **8** and **9** are, like **6** and **7** before, neutral abnormal NHC Ga complexes obtained as a result of the selective allylation (for **8**) and silylation (for **9**) of the C2 position of the anionic NHC ligand present in **4** and **5**, leaving the C4-Ga left intact. The isolation of **9** contrasts with the reactivity reported by Arnold for a related mixed K/Y complex,<sup>[61]</sup> where the silylation occurs at the C4 position of the anionic carbene, instead of C2. Similar regioselectivity has been witnessed by Robinson for polymeric  $\text{Li}^+\text{IPr}^-$ , which in this case affords the C4- $\text{SiMe}_3$  substituted free carbene.<sup>[41]</sup> Interestingly, by adding borane to this lithium complex, it is possible to direct the selectivity of the quench with  $\text{SiMe}_3\text{Cl}$  towards the C2 position.<sup>[44]</sup>

The molecular structures of **8** and **9** have been established by X-ray crystallography (**Fig 2.13**). The Ga-C4 distances (i.e. C3 and C45 for **8** and **9** respectively) showed very little variation (2.0802(18) and 2.0887(16) Å) to that found in for instance **6** (2.0759(16) Å) where the C2 position of the carbene is occupied by a H atom, suggesting that the substituents on the C2 of the imidazole ring have little influence in the strength of the Ga-C4 bond.

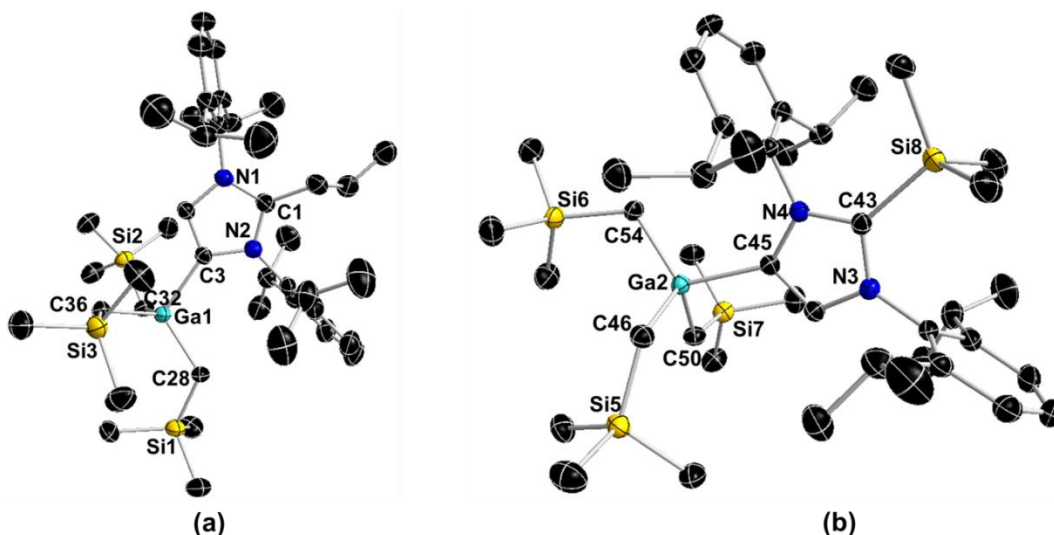


**Figure 2.13:** Molecular structure of **8** (a) and **9** (b) with 50% probability displacement ellipsoids. All hydrogen atoms have been omitted for clarity. For compound **8** only the  $\text{CH}_2\text{-CH=CH}_2$  fragment is shown. The unit cell of **9** contains three crystallographically independent molecules with identical connectivity. One of these molecules is shown here.

Structural analysis of **8** revealed it to be a cocrystal which contains  $\text{CH}_2\text{-CH=CH}_2$  and  $\text{CH=CH-CH}_3$  as substituents at the C2 of the carbene in approximately 2:3 ratio, arising from the partial allylic rearrangement. Mirroring this composition in solution, NMR spectroscopic analysis of **8** proved to be extremely complex in the allylic section (from 3 to 6 ppm); although it should be noted that no interconversion between these two isomers is observed over prolonged periods of time. Despite its complexity, the  $^1\text{H}$  NMR spectrum displays four septets for the *CH* of isopropyl groups, while an informative resonance at 163.4 ppm is observed for the carbenic carbon. A similar chemical shift is observed for **9** (167.6 ppm) along with another signal at 148.8 ppm, which can be assigned to the *C* of the imidazole ring that is now bonded to a  $\text{SiMe}_3$  group (**Fig. 2.14**).

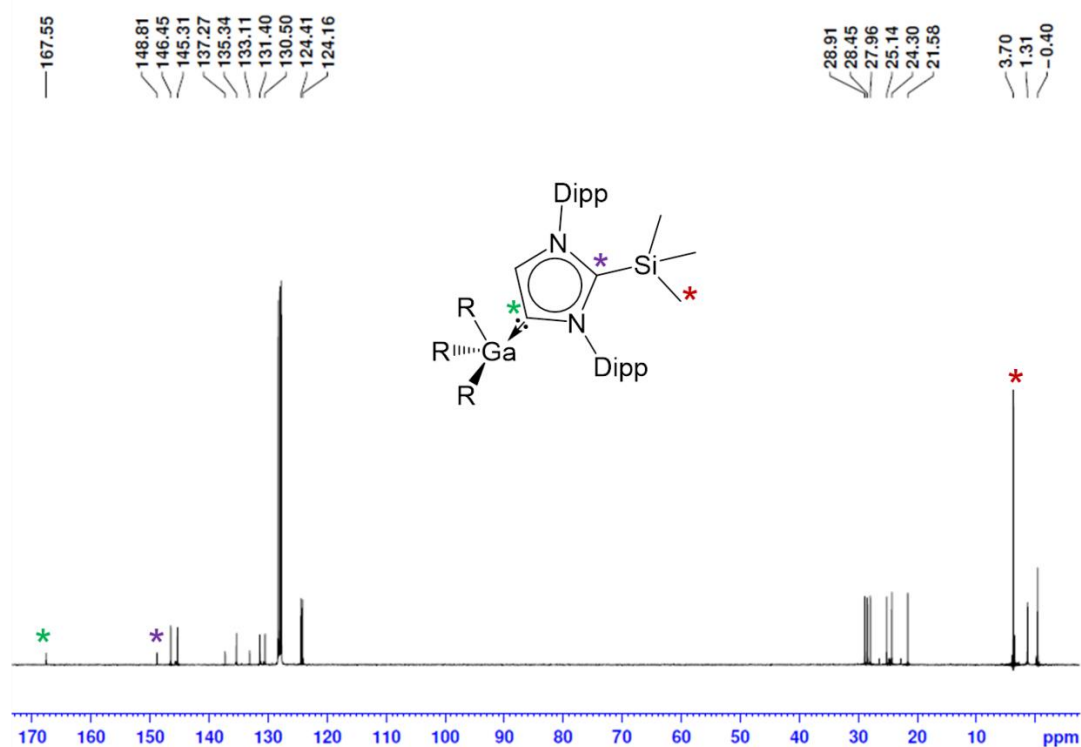


**Figure 2.14:**  $^{13}\text{C}$  NMR spectrum of **9** in  $\text{C}_6\text{D}_6$  solution.

Compound **7**, along with **1** and **3-5** constitutes a rare example of a series of normal, anionic and abnormal complexes incorporating the same metal-coligand partnership. As far as we can ascertain there are only two other examples containing the  $\text{BEt}_3$ <sup>[43,44,69]</sup> and  $\text{B}(\text{C}_6\text{F}_5)_3$  fragments.<sup>[37,39,70]</sup> Complementary DFT computational studies<sup>[71]</sup> were undertaken on these three compounds (i.e., **1**, **3** and **7**) employing the B3LYP method<sup>[72,73]</sup> and the 6-311G(d,p) basis set.<sup>[74]</sup> Natural bond orbital (NBO) analysis of the optimised structures of  $\text{IPr}\cdot\text{GaR}_3$  (**III**<sub>IPr</sub>),  $a\text{IPrGaR}_3$  (**IV**<sub>IPr</sub>) and  $(\text{THF})_2\text{Li}[:\text{C}\{\text{N}(2,6\text{-iPr}_2\text{C}_6\text{H}_3)_2\text{CHCGa}(\text{CH}_2\text{SiMe}_3)_3\}]$  (**V**<sub>IPr</sub>) suggest considerable covalent character of the Ga-C bonds. The Ga natural charges range from +1.43 to +1.35 and the Wiberg bond indices (WBIs) of the Ga-C bonds range from 0.45-0.64. Contrastingly reflecting the more ionic nature of the Li-C contact in **V**<sub>IPr</sub>, the natural charge of Li is +0.88 and the WBI of the Li-C is 0.08. In agreement with our experimental findings the estimated Ga-C4 bonds in **IV**<sub>IPr</sub> and **V**<sub>IPr</sub> are significantly shorter (2.146 and 2.054 Å, WBIs = 0.56 and 0.53 respectively) than the Ga-C2 bond in the normal complex **III**<sub>IPr</sub> (2.333 Å, WBI = 0.45), although it should be noted that for **III**<sub>IPr</sub> and **IV**<sub>IPr</sub>, the strength of these Ga-C bonds is somewhat underestimated (*vide infra*). A comparative

natural charges analysis of these three models shows that while in bimetallic  $\mathbf{V}_{\text{IPr}}$  the amount of electrons transfer to  $\text{GaR}_3$  unit is 0.34, in the case of adducts  $\mathbf{III}_{\text{IPr}}$  and  $\mathbf{IV}_{\text{IPr}}$  these values are 0.27 and 0.31 which is consistent with the neutral constitution of the NHC ligands.

**Figure 2.15** shows the highest occupied molecular orbitals (HOMOs) calculated for models  $\mathbf{III}_{\text{IPr}}$ ,  $\mathbf{IV}_{\text{IPr}}$  and  $\mathbf{V}_{\text{IPr}}$  which in all case correspond to the Ga-C bonding orbitals at the  $\text{CH}_2$  groups of the monosilyl ligands, involving also in the case of  $\mathbf{V}_{\text{IPr}}$  the C4 of the anionic NHC. For this bimetallic system, these calculations contrast with those reported for the related anionic lithium dicarbene  $[\text{C}\{\text{[N}(2,6\text{-iPr}_2\text{C}_6\text{H}_3)]_2\text{CHLi(THF)}\}]_n$  prepared by Robinson,<sup>[41]</sup> whose HOMO and HOMO-2 correspond to the two strongly polarised Li-C bonding orbitals at the C2 and C4 positions of the imidazole ring.

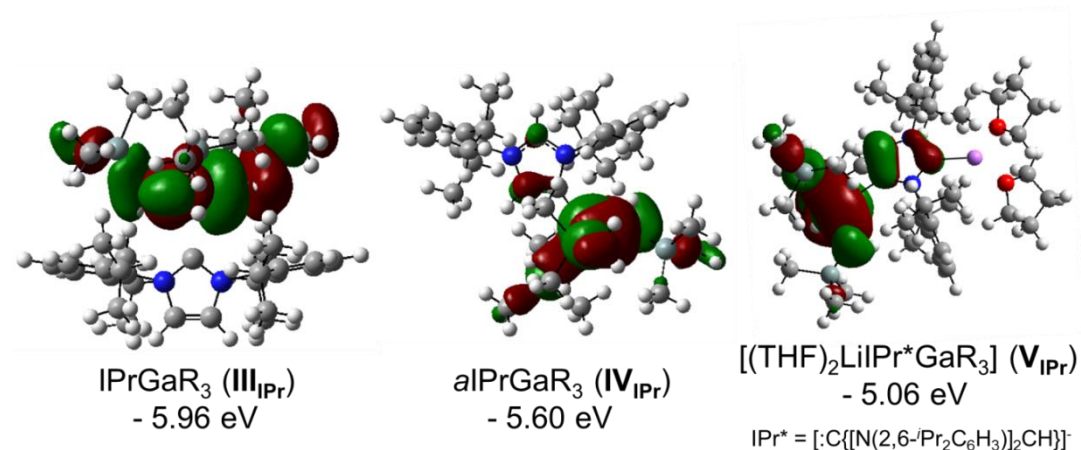


**Figure 2.15:** Calculated molecular orbitals HOMO of models  $\mathbf{III}_{\text{IPr}}$ ,  $\mathbf{IV}_{\text{IPr}}$  and  $\mathbf{V}_{\text{IPr}}$ .

Interestingly, calculations on the regioisomeric structure of  $[(\text{THF})_2\text{Li}\{\text{IPr}^*\text{GaR}_3\}]$  ( $\mathbf{V}_{\text{IPr}}$ ) with the positions of the  $\{\text{GaR}_3\}$  and  $\{\text{Li}(\text{THF})_2\}^+$  reversed, giving rise to Ga-C2 and Li-C4 coordination modes ( $[\text{GaR}_3\{\text{IPr}^*\text{Li}(\text{THF})_2\}]$ , model  $\mathbf{VI}_{\text{IPr}}$ ) showed that this model is significantly less stable (by  $11.7 \text{ kcal mol}^{-1}$ ) which is consistent with the formation of a significantly weaker (longer) Ga-C bond ( $2.272 \text{ \AA}$  for  $\mathbf{VI}_{\text{IPr}}$  vs  $2.054 \text{ \AA}$  for  $\mathbf{V}_{\text{IPr}}$ , **Figure 2.16**).

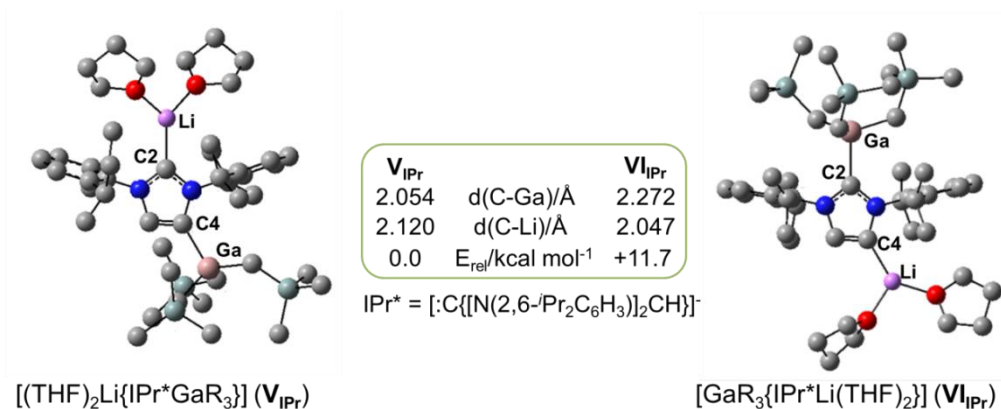
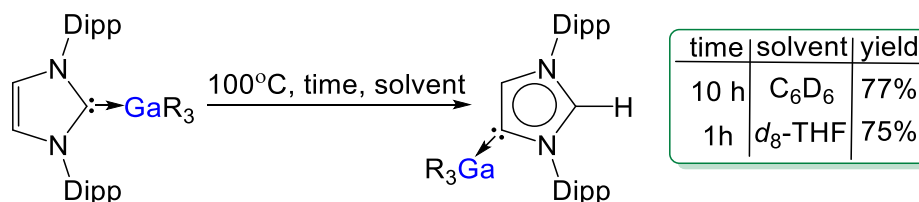


**Figure 2.16:** Comparison of regioisomeric structures  $V_{IPr}$  and  $VI_{IPr}$ .

## 2.5. Thermal isomerisation

It is rare to find examples where both normal and abnormal isomers have been structurally characterised.<sup>[75,76]</sup> Amongst them, intriguing studies from the groups of Layfield<sup>[35]</sup> and Dagonne<sup>[40]</sup> have shown that the systems IPr·Fe(HMDS)<sub>2</sub> and *t*Bu·AlMe<sub>3</sub> respectively, thermally isomerise to the relevant abnormal species although the possible reaction pathways for these transformations remain obscure. Similarly to our findings for complexes **1** and **7**, in these Fe and Al examples, analysis of the metal-carbon distances have revealed that the abnormal NHCs bind more strongly to the metal centres than the isomeric normal carbenes. These studies also suggest the formation of the abnormal-NHC complex is thermodynamically controlled with steric factors strongly influencing isomerisation processes. Since compound **7** was obtained using an indirect method (metallation/electrophilic interception), we pondered if such types of thermal rearrangement would also be in operation when **1** was heated in solution (**Scheme 2.11**).



**Scheme 2.11:** Thermally-induced rearrangement of **1** into **7**.

Indeed, heating a *d*<sub>6</sub>-benzene solution of **1** at 100 °C and monitoring progress by <sup>1</sup>H NMR, produced **7** in 77% yield after 10 h (**Fig 2.17** and **2.18**)

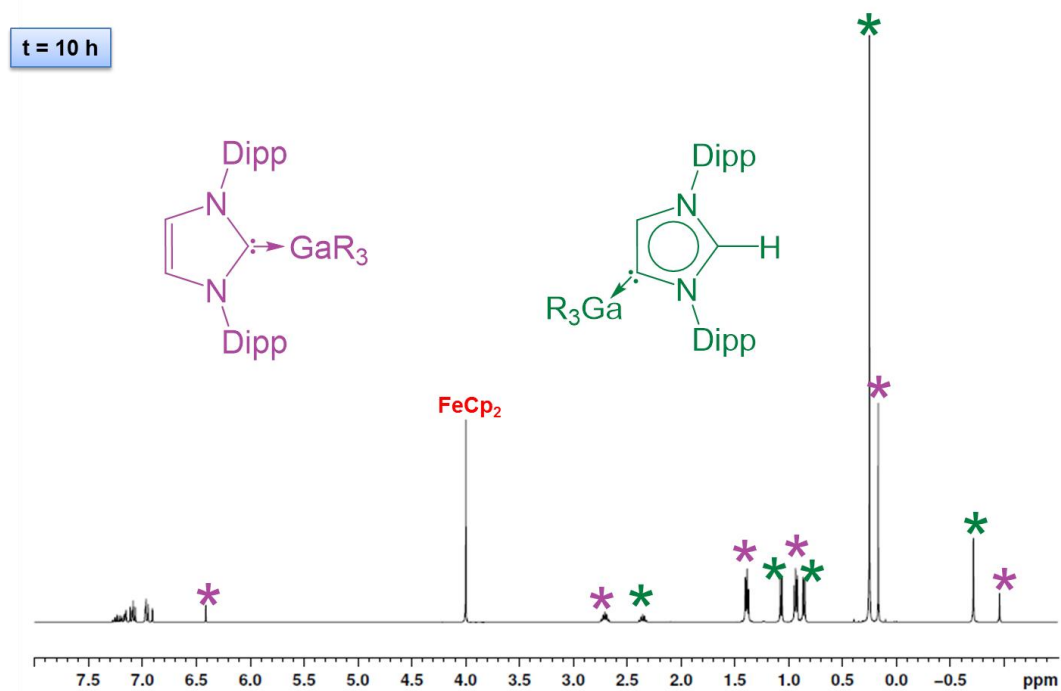


**Figure 2.17:**  $^1\text{H}$  NMR spectrum of mixture of **1** and **7** (77%) in  $\text{C}_6\text{D}_6$  solution obtained after 10h of heating of **1** at 100 °C.

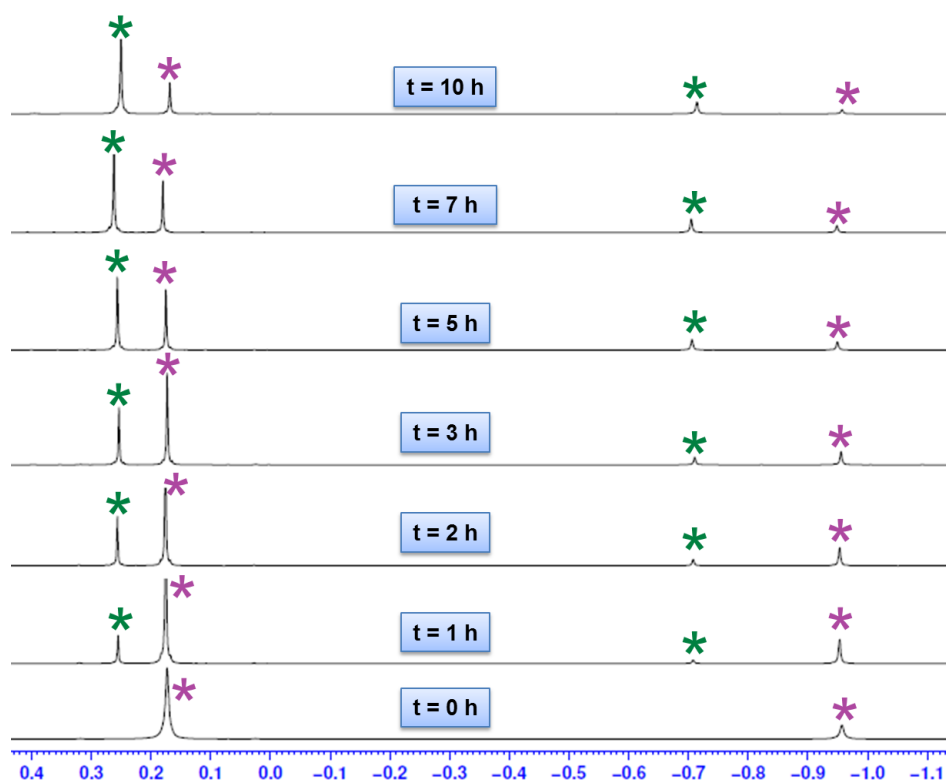


**Figure 2.18:** Expanded high field region of the  $^1\text{H}$  NMR spectra for the isomerisation of **1** into **7** in  $\text{C}_6\text{D}_6$ .

The reaction was greatly accelerated by using the more coordinating solvent  $d_8$ -THF (75% conversion in only 1 h). Under these conditions the maximum conversion observed of **1** to **7** was 75%, however extended reaction times (48h) did not lead to an increase in this conversion.

Previous studies on  $I^t\text{Bu}\cdot\text{AlMe}_3$  have shown that the isomerisation is much faster using a Lewis donor solvent such as THF, hinting that dissociation (at least partially) of the carbene from the metal must play a significant role in the process. Assessing the role of the metal fragment, related  $\text{IPr}\cdot\text{GaCl}_3$ ,<sup>[47]</sup>  $\text{MgR}_2\cdot\text{IPr}$ <sup>[77]</sup> and  $\text{ZnR}_2\cdot\text{IPr}$  [ $\text{R} = \text{CH}_2\text{SiMe}_3$ ] were prepared and heated in a sealed tube.  $\text{ZnR}_2\cdot\text{IPr}$  (**10**) was prepared by mixing equimolar amounts of  $\text{ZnR}_2$  and IPr in hexane and fully characterised by multinuclear NMR spectroscopy and X-ray crystallographic analysis (**Figure 2.19**).

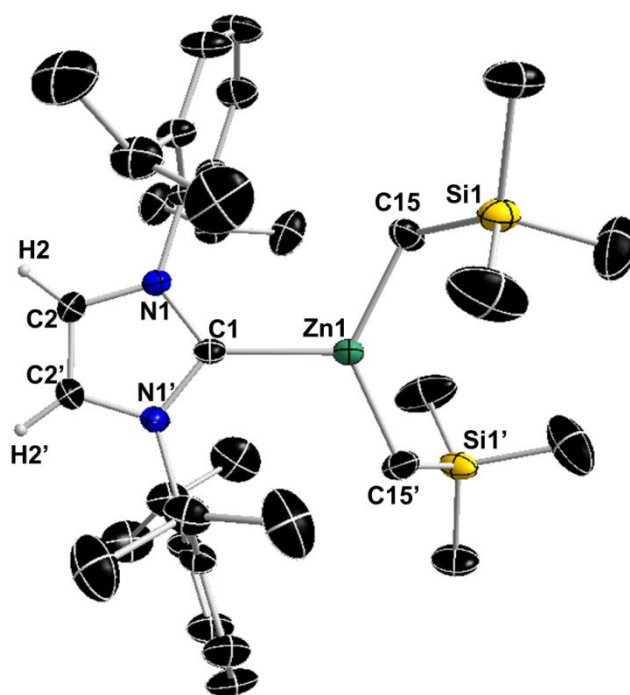


**Figure 2.19:** Molecular structure of **10** with 50% probability displacement ellipsoids. All hydrogen atoms except those on imidazole ring and minor disorder in isopropyl groups are omitted for clarity. Symmetry operator:  $-x, y, -z + 0.5$ . Selected bond distances (Å) and bond angles (°): Zn(1)-C(1) 2.141(3), Zn(1)-C(15) 2.008(2), C(15)-Zn(1)-C(15') 129.54(17), C(15)-Zn(1)-C(1) 115.23(9), N(1)-C(1)-N(1') 103.2(3).

Interestingly no isomerisation is observed for  $\text{IPr}\cdot\text{GaCl}_3$  when using smaller and stronger Lewis acid  $\text{GaCl}_3$ , as mentioned above, the carbene binds significantly more strongly to the Ga centre. Related to these findings, reflecting the relevance of the Lewis acidic character of the metal fragment,



using the alkyl compounds  $\text{MgR}_2\cdot\text{IPr}^{[77]}$  and  $\text{ZnR}_2\cdot\text{IPr}$  (**10**) no rearrangements were observed after 72 h at 100 °C.

The effect of the steric bulk of the substituents on the NHC ligand was assessed. By mixing equimolar amounts of 1,3-bis-(2,4,6-trimethylphenyl)imidazol-2-ylidene (IMes) and  $\text{GaR}_3$  in hexane at room temperature,  $\text{IMes}\cdot\text{GaR}_3$  (**11**) was isolated as a crystalline solid in 34% yield. The coordination of metal fragment to the carbene and formation of a NHC complex is best demonstrated by a resonance for the carbenic carbon at 182.2 ppm (vs 220.0 ppm in free IMes). Likewise, in  $^1\text{H}$  NMR spectrum splitting of the resonance for the methyl substituents and an upfield shift of the resonance for the imidazole backbone from 6.50 ppm in free IMes to 5.92 ppm in **11**, further supports the formation of the adduct.

Containing the less bulky (IMes) $^{[78]}$  carbene, **11** rearranges at a significantly slower rate than **1**, showing after 30 hours at 100°C in  $d_8$ -THF a modest 8% conversion to its abnormal isomer (**Figure 2.20**).

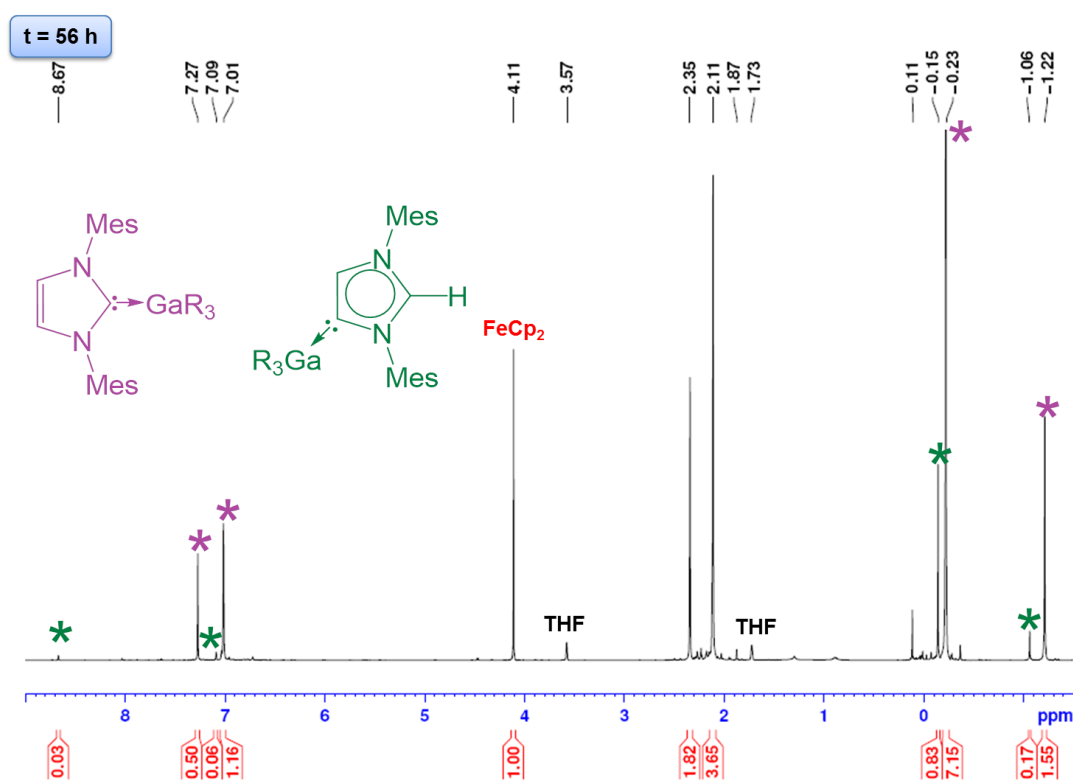


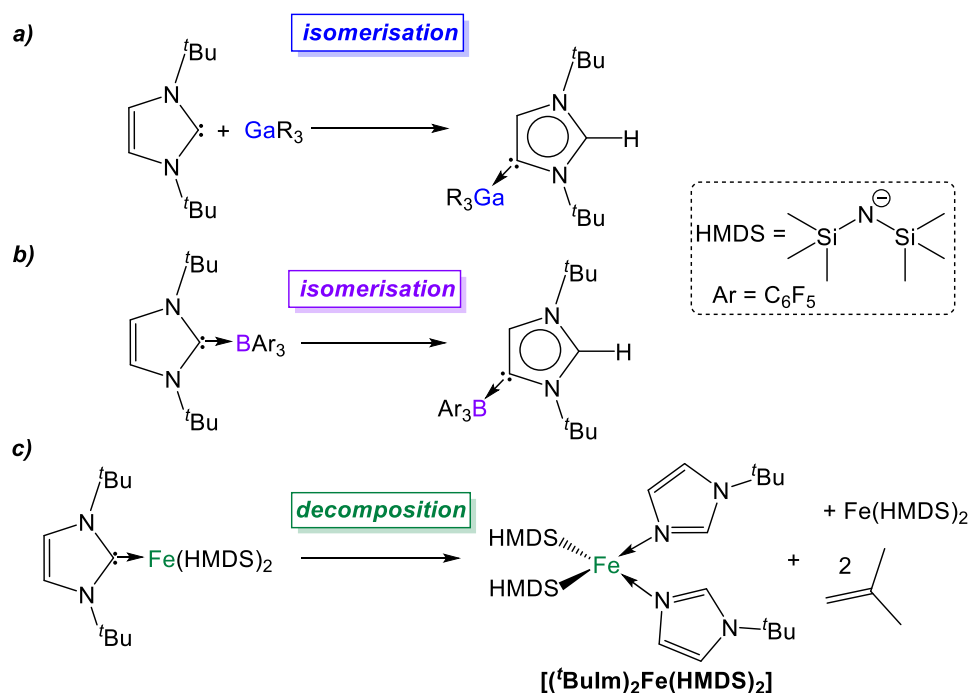
**Figure 2.20:**  $^1\text{H}$  NMR of mixture of **11** and its abnormal isomer (8 %) in  $d_8$ -THF solution obtained after 56 h of heating at 100 °C.

Contrastingly, 1,3-bis(*tert*-butyl)imidazol-2-ylidene (I<sup>t</sup>Bu) failed to form a normal adduct with  $\text{GaR}_3$ , furnishing instead only the abnormal isomer



$t\text{Bu}\cdot\text{GaR}_3$  (**12**) at room temperature within one hour. Isolated as a microcrystalline yield (43%, but almost quantitative in solution) **12** was not amenable to single crystal X-ray analysis, however it was characterised by multinuclear NMR spectroscopy. In the  $^1\text{H}$  NMR spectrum in  $d_8$ -THF solution two sharp singlets are observed at 1.60 and 1.67 ppm (each integrating for 9H) along with the two singlets at 7.07 and 8.36 ppm (1H each) attributed to inequivalent  $t\text{Bu}$  groups and imidazole protons, respectively. Furthermore, an informative resonance at 158.7 ppm for the C4-Ga is observed in  $^{13}\text{C}$  NMR spectrum which is in excellent agreement with the analogous bond in **7** (*cf.* 162.8 ppm).

This reactivity contrasts with that reported for the iron complex  $t\text{Bu}\cdot\text{Fe}(\text{HMDS})_2$  which undergoes thermal decomposition producing a bis(imidazole)iron complex  $[(t\text{BuIm})_2\text{Fe}(\text{HMDS})_2]$  accompanied with the extrusion of isobutene,<sup>[35]</sup> and appears to be more in line with that reported by Tamm for the  $\text{B}(\text{C}_6\text{F}_5)_3/t\text{Bu}$  frustrated Lewis pair system (FLP) which has been used for the activation of small molecules such as  $\text{H}_2$  or alkynes (**Scheme 2.12**). Although the two components fail to give an isolable normal complex, in the absence of other reactive substrates, the irreversible formation of the relevant abnormal carbene-borane adduct is observed.<sup>[37–39]</sup>



**Scheme 2.12:** Comparison of  $t\text{Bu}/\text{GaR}_3$  system with related  $t\text{Bu}/\text{BAr}_3$  and  $t\text{Bu}/\text{Fe}(\text{HMDS})_2$  systems.<sup>[35,39]</sup>

## 2.6. DFT calculations

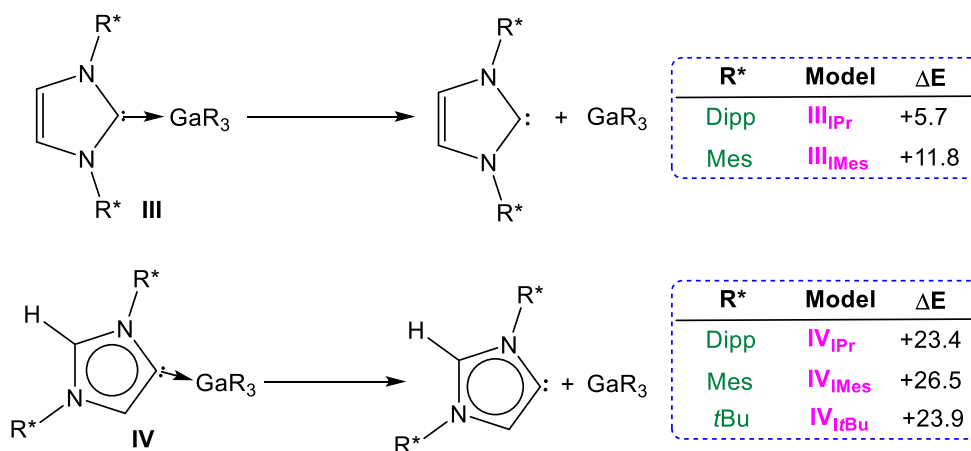
Encouraged by the formation of several *a*NHC-Ga complexes using this approach, we performed theoretical calculations at the DFT level<sup>[71]</sup> employing the B3LYP method<sup>[72,73]</sup> and the 6-311G(d,p) basis set<sup>[74]</sup> to optimize structures and to gain new insights into the thermodynamics involved in these processes. A comparison of geometrical parameters of optimised structures IPr·GaR<sub>3</sub> (**III**<sub>IPr</sub>) and *a*IPrGaR<sub>3</sub> (**IV**<sub>IPr</sub>) shows general good agreement with those found experimentally from the X-ray determinations of **1** and **7** respectively (**Table 2.2**) although for both models there is a slight underestimation of the strength of the Ga-C<sub>carbene</sub> interaction ( $\Delta[d(\text{Ga-C})_{\text{calc}} - d(\text{Ga-C})_{\text{exp}}] = 0.137$  and  $0.070$  Å for **1** and **7** respectively). Interestingly model **IV**<sub>IPr</sub> was computed to be more stable than **III**<sub>IPr</sub> by just  $1.5$  kcal mol<sup>-1</sup>.

**Table 2.2:** Modelled structures and relative energies of NHC-adducts IPr·GaR<sub>3</sub> (**III**<sub>IPr</sub>) and *a*IPr·GaR<sub>3</sub> (**IV**<sub>IPr</sub>).

	IPr·GaR <sub>3</sub>		<i>a</i> IPr·GaR <sub>3</sub>	
<i>E</i> <sub>relative</sub>	1.5 kcal mol <sup>-1</sup>		0.0 kcal mol <sup>-1</sup>	
	calculated ( <b>III</b> <sub>IPr</sub> )	experimental ( <b>1</b> )	calculated ( <b>IV</b> <sub>IPr</sub> )	experimental ( <b>7</b> )
Ga-C <sub>NHC</sub> (Å)	2.333	2.1960(16)	2.146	2.0759(16)
Ga-C <sub>R</sub> (Å)	2.038	2.0120(17)	2.045	2.0071(17)
	2.045	2.0164(16)	2.051	2.0257(16)
	2.036	2.0034(15)	2.051	2.0262(17)
N-C-N (°)	102.9	102.80(13)	108.6	107.51(14)

Using the same level of theory, free *a*IPr was also found to be  $16.2$  kcal mol<sup>-1</sup> less stable than its normal isomer IPr. Notably, the dissociation energy of **IV**<sub>IPr</sub> was found to be  $17.7$  kcal mol<sup>-1</sup> higher than for **III**<sub>IPr</sub> (**Scheme 2.13**), in agreement with our experimental findings which suggest a greater donor

ability of the abnormal NHC ligand for the  $\text{GaR}_3$  fragment when compared to its normal isomer.



**Scheme 2.13:** Estimated dissociation energies ( $\Delta E$ ) in  $\text{kcal mol}^{-1}$  of complexes **III** and **IV** ( $\text{R}^* = \text{Dipp, Mes, } t\text{Bu}$ ).

These studies were extended to the related carbenes  $\text{IMes}$  and  $\text{I}^t\text{Bu}$ . For  $\text{IMes}$ , which is less sterically demanding than  $\text{IPr}$ , the order of stability of **III** <sub>$\text{IMes}$</sub>  and **IV** <sub>$\text{IMes}$</sub>  is reversed; with the normal isomer **III** <sub>$\text{IMes}$</sub>  being  $2.1 \text{ kcal mol}^{-1}$  more stable (**Figure 2.21**). Interestingly, the energy difference between free  $a\text{IMes}$  and  $\text{IMes}$  of  $+16.8 \text{ kcal mol}^{-1}$  is almost identical to that for free  $a\text{IPr}$  and  $\text{IPr}$ . As shown in **Scheme 2.13**, the calculated values for the dissociation energies of **III** <sub>$\text{IMes}$</sub>  and **IV** <sub>$\text{IMes}$</sub>  follow the same trend as described for the  $\text{IPr}$  complexes, although now the dissociation of  $\text{IMes}\cdot\text{GaR}_3$  (**III** <sub>$\text{IMes}$</sub> ) is noticeably more endothermic (by  $6.1 \text{ kcal mol}^{-1}$ ) than in  $\text{IPr}\cdot\text{GaR}_3$  (**III** <sub>$\text{IPr}$</sub> ). These subtle but significant changes in the energy values could explain the lower conversions observed experimentally when  $\text{IMes}\cdot\text{GaR}_3$  (**11**) is heated in  $d_8$ -THF (max yield 8% for  $a\text{IMes}\cdot\text{GaR}_3$ , *vide supra*), as the dissociation of  $\text{IMes}\cdot\text{GaR}_3$  is more thermodynamically challenging.

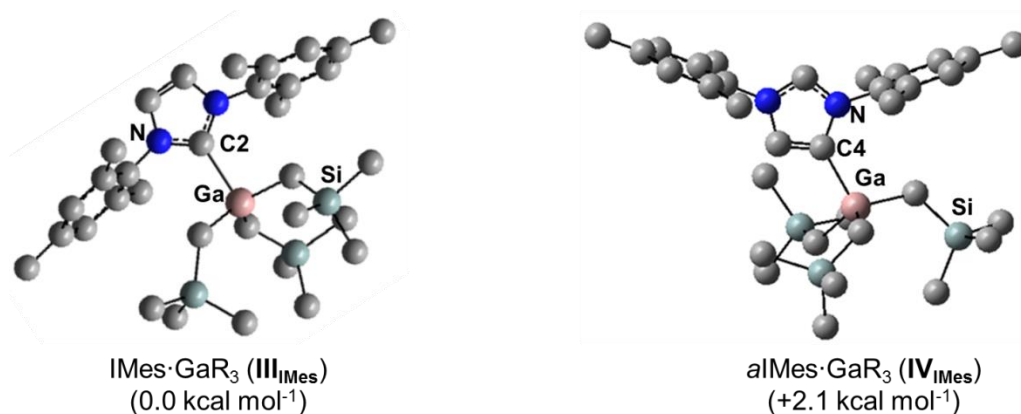


**Figure 2.21:** Modelled structures and relative energies of NHC-adducts  $\text{III}_{\text{IMes}}$  and  $\text{IV}_{\text{IMes}}$ .

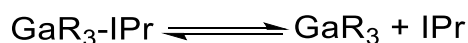
A more dramatic effect is observed for  $I^t\text{Bu}$ , which containing aliphatic  $t\text{Bu}$  substituents, is significantly bulkier than  $\text{IPr}$ , more basic and therefore a better donor, from an electronic perspective. Notably attempts to optimize the structure of  $I^t\text{Bu}\cdot\text{GaR}_3$  were unsuccessful, as all the obtained models showed no stabilisation compared to the separate constituents  $I^t\text{Bu}$  and  $\text{GaR}_3$ . This lack of coordination between  $I^t\text{Bu}$  and  $\text{GaR}_3$  can best be explained by steric incompatibility of  $t\text{Bu}$  and monosilyl groups and supports our experimental findings that when  $I^t\text{Bu}$  and  $\text{GaR}_3$  are mixed at RT  $aI^t\text{Bu}\cdot\text{GaR}_3$  (**12**) is formed. The dissociation energy for this abnormal complex was found to be +23.9 kcal mol<sup>-1</sup> (**Scheme 2.13**).

Collectively these computational results not only offer further support for the greater donor ability of abnormal NHC ligands compared to their normal isomers but also highlight the crucial role that the steric profile plays in these isomerisation processes. Thus, in the case of  $\text{IMes}$ , the less bulky of the carbenes investigated, it becomes slightly endothermic, whereas for  $\text{IPr}$  and  $I^t\text{Bu}$ , the formation of the abnormal complexes is thermodynamically favoured by -1.5 and -6.63 kcal mol<sup>-1</sup> respectively, in accord with their sizes.

## 2.7. Mechanistic implications

Both computational and spectroscopic studies suggest that the isomerisation of **1** into **7** may involve a dissociative step. Supporting this assumption, when a mixture of **1** and  $\text{GaR}_3$  (two equivalents) was heated at 100 °C in  $d_8$ -THF, the

formation of **7** becomes significantly slower (46% conversion observed after 1 h), which can be rationalised in terms of the effect that the excess of this reagent will have in the equilibrium depicted in **Equation 2.1**, namely shift it towards the left.



**Equation 2.1:** Proposed equilibrium of **1** and its free components in solution.

Contrastingly, when the reaction is carried out using an excess of IPr (2 equivalents), the isomerisation process occurs significantly faster (90% after 30 minutes). In order to shed some light on the mechanism involved in this isomerization process, kinetic analysis of a NMR scale reaction ( $[\mathbf{1}] = 0.22 \text{ M}$ ) performed at  $100^\circ\text{C}$  in  $d_8$ -THF revealed a pseudo-zeroth-order kinetics over a period of two-half lives (64% conversion). Under these conditions the maximum conversion observed of **1** to **7** was 75%, while the extended reaction times (48h) did not lead to an increase in this conversion. An identical experiment using  $\text{IPr}^{\text{D}}\cdot\text{GaR}_3$  (**1<sup>D</sup>**) ( $\text{IPr}^{\text{D}} = 1,3\text{-bis}(2,6\text{-di-isopropylphenyl})\text{-}4,5\text{-dideutero-imidazolin-}2\text{-ylidene}$ )<sup>[79]</sup> allowed the comparison of the subsequent zero order rate constants, revealing no observable KIE (**Figure 2.22**).

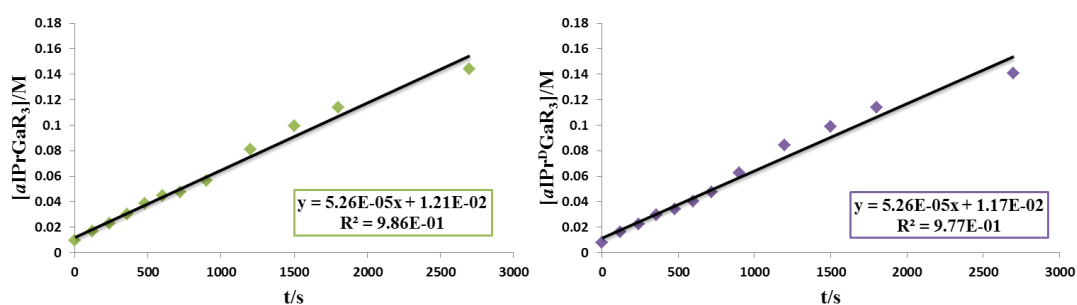
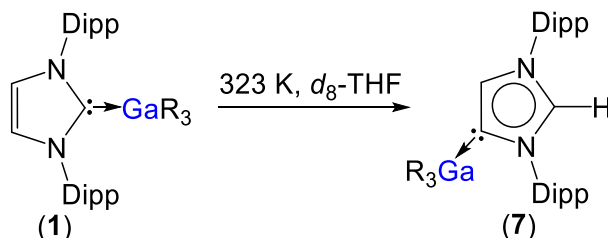


**Figure 2.22:** Kinetic analysis performed on the 0.22 M  $d_8$ -THF solution of **1** (left hand side) and **1<sup>D</sup>** (right hand side) at  $100^\circ\text{C}$ .

These findings suggest that the bond cleavage of the  $\text{C}_4\text{-H}$  in IPr ligand is unlikely to be rate-determining step in the isomerisation process. Encouraged by these findings we chose to study further the mechanism of this process using the method of initial rates.<sup>[80]</sup> Attempts to study transformation of **1** into **7** under pseudo-first-order conditions (using a 10 molar equivalent excess of

GaR<sub>3</sub> per complex **1**) completely inhibited the isomerisation process, however initial rate experiments could be successfully conducted. Isomerisation of **1** into **7** in *d*<sub>8</sub>-THF at 323K (**Scheme 2.14**) was monitored using *in situ* NMR spectroscopy by following the appearance of the resonance assigned to the new C<sub>carbene</sub>-H bond (9 ppm).



**Scheme 2.14:** Isomerisation of **1** into **7** at 323 K in *d*<sub>8</sub>-THF studied by initial rate experiments.

The percentage of conversion was restricted to 5–7 % in order to calculate the initial rate ( $r_0$ ) of the reaction. The data were plotted as molar concentration of the product *versus* time yielding straight lines, which were fitted by conventional linear regression ( $r^2 > 0.96$ ) and  $r_0$  values were obtained from the corresponding slopes. A sample plot is shown in **Figure 2.23**.

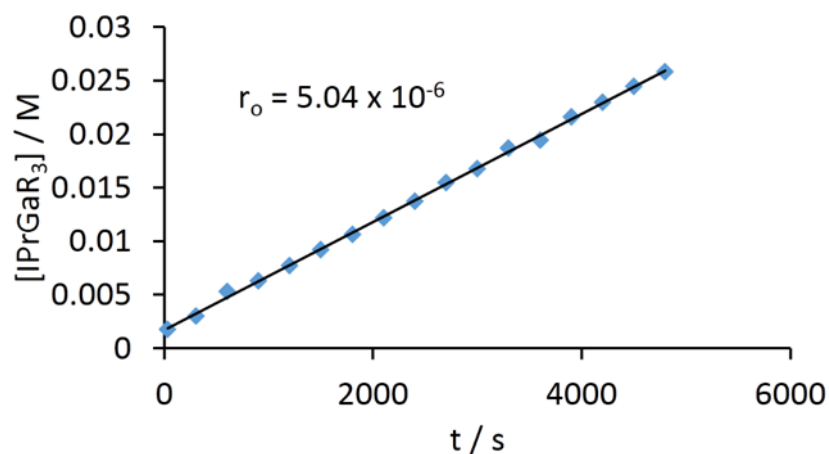


**Figure 2.23:** Initial rate over 4800 s (0.42 M [IPrGaR<sub>3</sub>]).

To investigate the effect of [IPrGaR<sub>3</sub>] (**1**) on the reaction rate, four experiment were carried out varying the concentration of **1** in the range 0.17–0.42 M and a first order dependence was revealed (**Figure 2.24**).

[1] M	$r_0 \cdot 10^6$ (Ms <sup>-1</sup> )
0.17	1.95 ± 0.08
0.29	3.26 ± 0.08
0.37	4.81 ± 0.03
0.42	5.04 ± 0.04

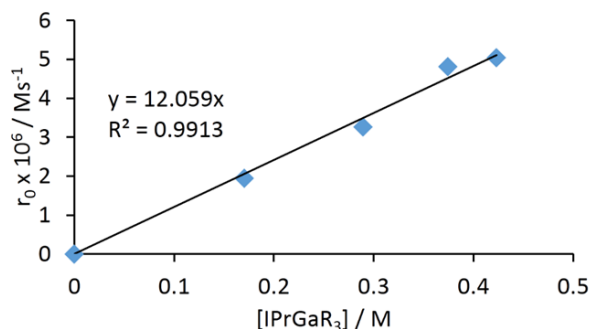


**Figure 2.24:** Initial rates *versus* concentration of IPr·GaR<sub>3</sub>, [1] for isomerisation of **1** into **7** in *d*<sub>8</sub>-THF at 323 K and at given initial concentration of **1**.

First-order dependence is also observed for the concentration of IPr ([IPr] = 0.29–0.55 M) as shown in **Figure 2.25**, which is consistent with the dissociative step previously discussed and the involvement of free IPr in the isomerization process.

[1] M	[IPr] M	$r_0 \cdot 10^6$ (Ms <sup>-1</sup> )
0.29		3.26 ± 0.08
0.29	0.07	4.67 ± 0.05
0.29	0.15	5.71 ± 0.15
0.29	0.26	6.40 ± 0.09

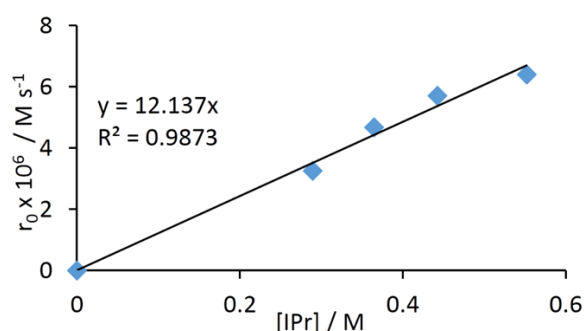


**Figure 2.25:** Initial rates *versus* concentration of [IPr] for isomerisation of **1** into **7** in *d*<sub>8</sub>-THF at 323 K and at given initial concentration of **1** and IPr.

By contrast to IPr, a negative order of -1 is observed for the concentration of GaR<sub>3</sub> ([GaR<sub>3</sub>] = 0.32–0.74 M) as shown in **Figure 2.26**.

[1] M	[GaR <sub>3</sub> ] M	$r_0 \cdot 10^6$ (Ms <sup>-1</sup> )
0.32	0.16	3.39 ± 0.04
0.32	0.31	2.30 ± 0.02
0.32	0.42	2.06 ± 0.04

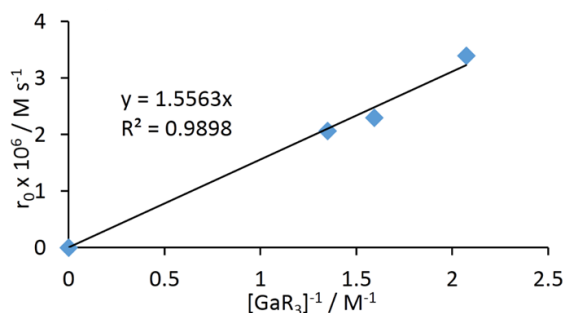
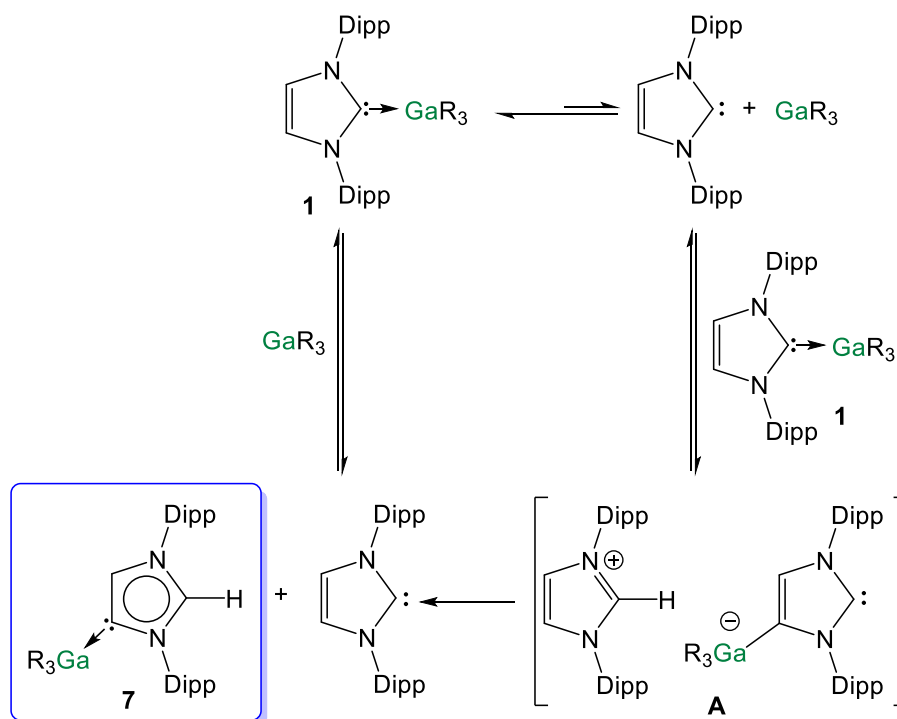


**Figure 2.26:** Initial rates *versus* concentration of [GaR<sub>3</sub>]<sup>-1</sup> for isomerisation of **1** into **7** in *d*<sub>8</sub>-THF at 323 K and at given initial concentration of **1** and GaR<sub>3</sub>.

A plausible interpretation of these results is that the isomerisation process takes place by the partial dissociation of **1** (which appears to be the rate-determining step of the reaction) to form free IPr that in turn can activate the H atom from the backbone of the NHC ligand coordinated to Ga in complex **1** (**Scheme 2.15**). Consistent with this interpretation, the formation of *a*I'BuGaR<sub>3</sub> (**12**) from an equimolar mixture of I'Bu and GaR<sub>3</sub> occurs under much milder conditions (room temperature, 60 minutes) than for **7**. In this case I'Bu and GaR<sub>3</sub> fail to form a stable normal adduct, thus a dissociation step is not required. NMR studies of equimolar amounts of IPr<sup>D</sup>·GaR<sub>3</sub> (**1<sup>D</sup>**) and IPr·GaR<sub>3</sub> (**1**) in *d*<sub>8</sub>-THF were carried out in order to assess if the transformation of **1** to **7** occurs *via* an intra- or intermolecular mechanism. However analysis of the NMR data proved to be inconclusive due to the overlapping of the signals from the protonated and deuterated species.

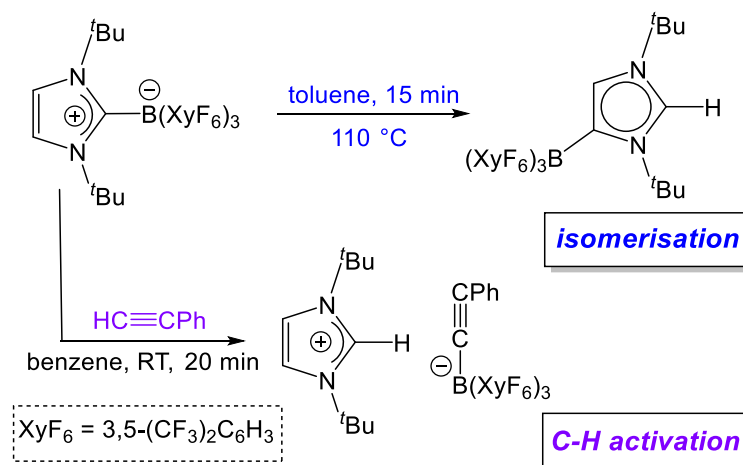


**Scheme 2.15:** Proposed mechanism for the isomerisation of **1** into **7**.

This proposed *modus operandi* is similar to that described for the activation of small molecules such as acetylenes, H<sub>2</sub> or amines using NHC/borane FLP systems, that, as mentioned before, in the absence of another substrate form the relevant abnormal *a*NHC-BAr<sub>3</sub> adducts (Ar = C<sub>6</sub>F<sub>5</sub> or XyF<sub>6</sub>).<sup>[37–39]</sup> In particular the reactivity of **1** can be related to that described by Tamm for



$t\text{Bu}\cdot\text{B}(\text{XyF}_6)_3$  that forms a stable normal adduct at room temperature but heating at  $110^\circ\text{C}$  isomerizes to  $aI\text{Bu}\cdot\text{B}(\text{XyF}_6)_3$ . This system exhibits FLP reactivity and can activate  $\text{CO}_2$ ,  $\text{HCCPh}$  and  $\text{THF}$  (**Scheme 2.16**).<sup>[39]</sup>



**Scheme 2.16:** The formation of abnormal NHC-borane complex and FLP activation of phenylacetylene by the same normal NHC-borane complex under different conditions.<sup>[39]</sup>

This could lead to the formation of the transient ion-pair species  $[\text{IPr}\text{-H}]^+[\text{IPr}^*\text{GaR}_3]^-$  (**A** in **Scheme 2.15**) ( $\text{IPr}^* = \text{:C}\{[\text{N}(2,6\text{-}i\text{Pr}_2\text{C}_6\text{H}_3)]_2\text{CHC}\}$ ), comprising an imidazolium cation and an NHC-gallate containing an anionic NHC (which on the basis of the constitution of lithium gallate **3**, it could be expected to have its Ga center coordinated to the C4 position).

This reactivity can be interpreted in terms of “thermally induced frustration”, a concept recently introduced by Pápai which refers to the thermal activation of strained dative bonds of bulky Lewis donor-acceptor pairs.<sup>[81]</sup> Intermediate **A** will evolve fast with the irreversible formation of abnormal complex **7** and the regeneration of free IPr. This proposed behaviour mirrors that described in **Scheme 2.9c**, for the protonation of the anionic carbene present in **3** by the imidazolium salt  $\text{IMes}\cdot\text{HCl}$ , which occurs at the C2 position, forming neutral  $a\text{IPrGaR}_3$  and free IMes. Since IPr is regenerated at the end of the process, it can then be envisaged that under the conditions studied it acts as a catalyst in the isomerization process. The proposed intermediate **A** as a transient species has never been experimentally observed, however a model for the energy of its formation has been calculated. The formation of intermediate **A** from two molecules of free IPr and a molecule of  $\text{GaR}_3$  was found to be endothermic by  $+11.7 \text{ kcal mol}^{-1}$  (**Figure 2.27**). Several models of the analogous intermediate, which would

be formed from free carbenes and has no GaR<sub>3</sub> coordinated, were attempted but their geometries were not possible to optimize.

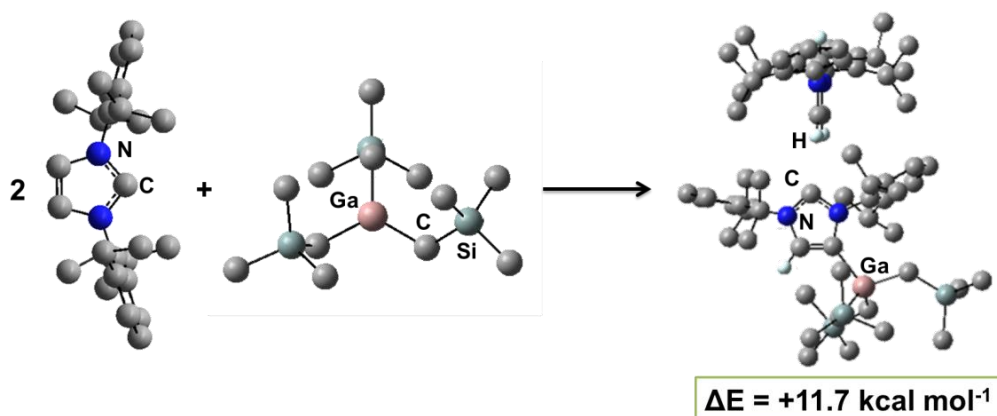


**Figure 2.27:** DFT study on the reaction of model systems **IPr** and GaR<sub>3</sub> to afford intermediate **A**.

## 2.8. Conclusions

Progressing main-group NHC chemistry, this systematic study of the synthesis and stability of abnormal NHC-gallium complexes has demonstrated two alternative and efficient methodologies to access *a*IPrGaR<sub>3</sub> (**7**). Studies investigating the synthesis of anionic NHC complexes have shown that the functionalization of the imidazole backbone can be achieved by sequentially treating IPr with the polar organometallic reagent LiR followed by GaR<sub>3</sub> addition (indirect stepwise gallation), to afford heteroleptic gallate (THF)<sub>2</sub>Li[:C{[N(2,6-*i*Pr<sub>2</sub>C<sub>6</sub>H<sub>3</sub>)]<sub>2</sub>CHCGa(CH<sub>2</sub>SiMe<sub>3</sub>)<sub>3</sub>}] (**3**). Electrophilic interception of **3** with MeOTf or the imidazolium salt IMes·HCl led to the isolation of neutral abnormal NHC (*a*NHC) complexes [CH<sub>3</sub>C{[N(2,6-*i*Pr<sub>2</sub>C<sub>6</sub>H<sub>3</sub>)]<sub>2</sub>CHCGa(CH<sub>2</sub>SiMe<sub>3</sub>)<sub>3</sub>}] (**6**) and *a*IPrGaR<sub>3</sub> (**7**). These studies disclose the preference of the anionic IPr ligand present in **3** to react with these electrophiles *via* its C2 position, leaving its Ga-C4 interaction intact. Compound **7** can also be accessed by a thermally induced rearrangement of its normal isomer IPr·GaR<sub>3</sub> (**1**). NMR spectroscopic studies coupled with theoretical calculations have revealed the importance of the donor ability of the solvent used in these thermal isomerisation processes as well as the steric

bulk of the substituents on the N atoms of the NHC ligands and the Ga reagent, suggesting that the relief of the steric hindrance by forming an abnormal complex is one of the main driving forces behind these rearrangements and hinting at the potential FLP reactivity that these systems may exhibit. Mechanistic studies intimate that these processes occur via a rate-determining dissociative step, supporting the formation of free NHC, which in turn can catalyse the isomerization process.

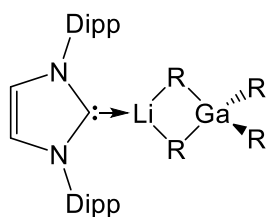
## 2.9. Experimental procedures

### 2.9.1. Synthesis of [IPrGa(CH<sub>2</sub>SiMe<sub>3</sub>)<sub>3</sub>] (1)

Equimolar amounts of Ga(CH<sub>2</sub>SiMe<sub>3</sub>)<sub>3</sub> (0.36 g, 1 mmol) and bis(2,6-diisopropylphenyl)imidazol-2-ylidene (IPr) (0.39 g, 1 mmol) were suspended in hexane (10 ml) and stirred for one hour at room temperature. The resulting yellow suspension was gently heated until all of the visible solid had dissolved. Slow cooling of the resulting solution afforded a crop of colourless crystals (0.54 g, 75%). Anal. Calcd for C<sub>39</sub>H<sub>69</sub>N<sub>2</sub>Si<sub>3</sub>Ga: C, 65.06; H, 9.66; N, 3.89. Found: C, 65.00; H, 10.08; N, 3.94.

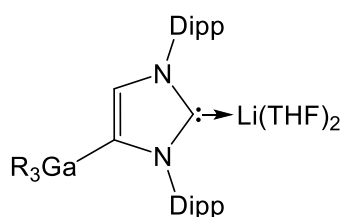
<sup>1</sup>H NMR (298 K, C<sub>6</sub>D<sub>6</sub>) δ -0.95 (6H, s, CH<sub>2</sub>SiMe<sub>3</sub>), 0.18 (27H, s, Si(CH<sub>3</sub>)<sub>3</sub>), 0.94 (12H, d, CH(CH<sub>3</sub>)<sub>2</sub>), 1.39 (12H, d, CH(CH<sub>3</sub>)<sub>2</sub>), 2.71 (4H, sept, CH(CH<sub>3</sub>)<sub>2</sub>), 6.40 (2H, s, imidazole backbone CH), 7.11 (4H, d, *m*-CH), 7.26 (2H, t, *p*-CH). <sup>13</sup>C{<sup>1</sup>H} NMR (298 K, C<sub>6</sub>D<sub>6</sub>) δ 0.4 (CH<sub>2</sub>SiMe<sub>3</sub>), 3.6 (Si(CH<sub>3</sub>)<sub>3</sub>), 23.0 (CH(CH<sub>3</sub>)<sub>2</sub>), 26.0 (CH(CH<sub>3</sub>)<sub>2</sub>), 29.0 (CH(CH<sub>3</sub>)<sub>2</sub>), 124.3 (*m*-CH), 124.4 (imidazole backbone CH), 130.7 (*p*-CH), 136.3 (*i*-C), 145.8 (*o*-C), 186.6 (C:).

<sup>1</sup>H NMR (298 K, *d*<sub>8</sub>-THF) δ -1.13 (6H, br s, CH<sub>2</sub>SiMe<sub>3</sub>), -0.20 (27H, s, Si(CH<sub>3</sub>)<sub>3</sub>), 1.14 (12H, d, CH(CH<sub>3</sub>)<sub>2</sub>), 1.36 (12H, br s, CH(CH<sub>3</sub>)<sub>2</sub>), 2.76 (4H, sept, CH(CH<sub>3</sub>)<sub>2</sub>), 7.32-7.48 (8H, mult, imidazole backbone CH + ArCH). <sup>13</sup>C{<sup>1</sup>H} NMR (298 K, *d*<sub>8</sub>-THF) δ 0.7 (CH<sub>2</sub>SiMe<sub>3</sub>), 3.4 (Si(CH<sub>3</sub>)<sub>3</sub>), 23.6 (CH(CH<sub>3</sub>)<sub>2</sub>), 25.9 (CH(CH<sub>3</sub>)<sub>2</sub>), 29.5 (CH(CH<sub>3</sub>)<sub>2</sub>), 124.7 (*m*-CH), 126.0 (imidazole backbone CH), 130.9 (*p*-CH), 137.5 (*i*-C), 146.7(*o*-C). Carbenic C could not be detected.

**2.9.2. Synthesis of [IPrLiGa(CH<sub>2</sub>SiMe<sub>3</sub>)<sub>4</sub>] (2)**

$\text{Li}(\text{CH}_2\text{SiMe}_3)$  (1M in pentane, 1 mL, 1 mmol) was added to a solution of  $\text{GaR}_3$  (0.33 g, 1 mmol in 10 mL hexane) and stirred for 1h at room temperature. To this suspension of  $[\text{LiGaR}_4]_\infty$ , an equivalent of IPr (0.39 g, 1 mmol) was added and the resulting orange suspension was stirred for another hour at room temperature. To the resulting orange suspension toluene was added dropwise with gentle heating until all of the visible solid has dissolved. Slow cooling of the resulting solution afforded X-ray quality crystals. The mixture was then concentrated and kept at  $-26\text{ }^\circ\text{C}$  for a couple of days to yield a crop of colourless crystals (0.39 g, 48%). Anal. Calcd for  $\text{C}_{43}\text{H}_{80}\text{N}_2\text{Si}_4\text{LiGa}$ : C, 63.36; H, 10.02; N, 3.44. Found: C, 63.01; H, 10.37; N, 3.54.

$^1\text{H NMR}$  (298 K,  $\text{C}_6\text{D}_6$ )  $\delta$  -0.96, -0.91 (8H, s,  $\text{CH}_2\text{SiMe}_3$ ), 0.21 (36H, s,  $\text{Si}(\text{CH}_3)_3$ ), 0.97 (12H, d,  $\text{CH}(\text{CH}_3)_2$ ), 1.32 (12H, d,  $\text{CH}(\text{CH}_3)_2$ ), 2.65 (4H, sept,  $\text{CH}(\text{CH}_3)_2$ ), 6.34 (2H, s, imidazole backbone CH), 7.08 (4H, d, *m*-CH), 7.22 (2H, t, *p*-CH).  $^7\text{Li NMR}$  (298 K,  $\text{C}_6\text{D}_6$ ):  $\delta$  0.80. Because of poor solubility  $^{13}\text{C}$  spectrum was not obtained. By switching to the donor solvent  $d_8$ -THF it was evident from  $^1\text{H}$  and  $^7\text{Li}$  that the co-complex was broken and the free IPr and  $\text{LiGaR}_4$  were identified.

**2.9.3. Synthesis of  $(\text{THF})_2\text{Li}[:\text{C}\{[\text{N}(2,6\text{-}i\text{-Pr}_2\text{C}_6\text{H}_3)]_2\text{CHCGa}(\text{CH}_2\text{SiMe}_3)_3\}]$** 

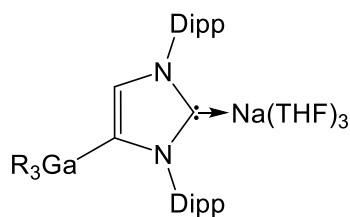
$\text{Li}(\text{CH}_2\text{SiMe}_3)$  (1 mL, 1M in pentane, 1 mmol) was added *via* syringe to a suspension of IPr (0.39 g, 1 mmol) in hexane (10 mL) at room temperature to form a white suspension. After stirring overnight, a hexane solution of  $\text{Ga}(\text{CH}_2\text{SiMe}_3)_3$  (0.33 g, 1 mmol in 5 mL hexane) was added *via* cannula and stirred for 3h at room temperature. The reaction mixture was then concentrated to approximately 5 mL and 1 mL of THF was added to afford a colourless solution. Overnight storage of the solution at  $-30\text{ }^\circ\text{C}$  provided a batch of colourless crystals (0.44 g, 56 %). Anal. Calcd for  $\text{C}_{47}\text{H}_{84}\text{N}_2\text{Si}_3\text{LiO}_2\text{Ga}$ : C, 64.88; H, 9.73; N, 3.22. Found: C, 65.00; H, 10.08; N, 3.65.

$^1\text{H NMR}$  (298 K,  $d_8$ -THF)  $\delta$  -1.18 (6H, s,  $\text{CH}_2\text{SiMe}_3$ ), -0.17 (27H, s,  $\text{Si}(\text{CH}_3)_3$ ), 1.07-1.11 (12H, mult,  $\text{CH}(\text{CH}_3)_2$ ), 1.18 (6H, d,  $\text{CH}(\text{CH}_3)_2$ ), 1.29

(6H, d,  $\text{CH}(\text{CH}_3)_2$ ), 3.0 (4H, mult,  $\text{CH}(\text{CH}_3)_2$ ), 6.64 (1H, s, imidazole backbone CH), 7.16-7.34 (6H, mult, *m*-CH + *p*-CH).  $^{13}\text{C}\{^1\text{H}\}$  NMR (298 K, *d*<sub>8</sub>-THF)  $\delta$  0.1 ( $\text{CH}_2\text{SiMe}_3$ ), 3.6 ( $\text{Si}(\text{CH}_3)_3$ ), 23.2 ( $\text{CH}(\text{CH}_3)_2$ ), 24.8 ( $\text{CH}(\text{CH}_3)_2$ ), 25.2 ( $\text{CH}(\text{CH}_3)_2$ ), 26.7 ( $\text{CH}(\text{CH}_3)_2$ ), 28.4 ( $\text{CH}(\text{CH}_3)_2$ ), 28.6 ( $\text{CH}(\text{CH}_3)_2$ ), 123.4 (*p*-CH), 124.0(*p*-CH), 127.8 (*m*-CH), 128.7 (*m*-CH), 129.2 (imidazole backbone CH), 140.1 (*i*-C), 143.6 (*i*-C), 147.1 (*o*-C), 147.3 (*o*-C), 155.0 (C-Ga), 201.5 (C:).  $^7\text{Li}$  NMR (298 K, *d*<sub>8</sub>-THF):  $\delta$  0.12.

$^1\text{H}$  NMR (298 K,  $\text{C}_6\text{D}_6$ )  $\delta$  -0.60 (6H, s,  $\text{CH}_2\text{SiMe}_3$ ), 0.40 (27H, s,  $\text{Si}(\text{CH}_3)_3$ ), 1.01 (12H, mult,  $\text{CH}(\text{CH}_3)_2$ ), 1.06 (8H, mult, THF), 1.27 (6H, d,  $\text{CH}(\text{CH}_3)_2$ ), 1.58 (6H, d,  $\text{CH}(\text{CH}_3)_2$ ), 2.56 (8H, mult, THF), 3.00 (2H, sept,  $\text{CH}(\text{CH}_3)_2$ ), 3.21 (2H, sept,  $\text{CH}(\text{CH}_3)_2$ ), 6.99 (1H, s, imidazole backbone CH), 7.0-7.2 (mult, ArCH overlapping with  $\text{C}_6\text{D}_6$ ).

#### 2.9.4. Synthesis of $(\text{THF})_3\text{Na}[:\text{C}\{[\text{N}(2,6\text{-}i\text{Pr}_2\text{C}_6\text{H}_3)]_2\text{CHCGa}(\text{CH}_2\text{SiMe}_3)_3\}]$



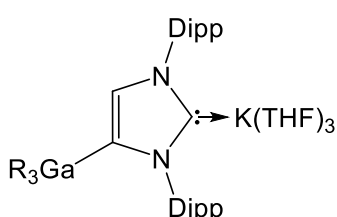
(4) Equimolar amounts of  $\text{Na}(\text{CH}_2\text{SiMe}_3)$  (0.22g, 2 mmol) and IPr (0.8 g, 2 mmol) were suspended in hexane (10 mL) and stirred for 2h at room temperature. To the obtained slurry, a hexane solution of  $\text{Ga}(\text{CH}_2\text{SiMe}_3)_3$  (0.66 g, 2 mmol in 10 mL hexane) was

added *via* cannula and stirred over night at room temperature. The reaction mixture was then concentrated to approximately 5 mL and 1 mL of THF was added to afford a straw solution. Overnight storage of the solution at  $-30\text{ }^\circ\text{C}$  provided a batch of colourless crystals (1.36 g, 71 %). It should be noted that two coordinated THF molecules are lost upon drying *in vacuo*. Anal. Calcd for  $\text{C}_{43}\text{H}_{76}\text{N}_2\text{Si}_3\text{NaOGa}$ : C, 63.44; H, 9.41; N, 3.44. Found: C, 63.21; H, 9.44; N, 3.70.

$^1\text{H}$  NMR (298 K,  $\text{C}_6\text{D}_6$ )  $\delta(\text{ppm})$  -0.62 (6H, s,  $\text{CH}_2\text{SiMe}_3$ ), 0.37 (27H, s,  $\text{Si}(\text{CH}_3)_3$ ), 1.04 (12H, d,  $\text{CH}(\text{CH}_3)_2$ ), 1.31 (20H, mult,  $\text{CH}(\text{CH}_3)_2$  + THF), 1.57 (6H, d,  $\text{CH}(\text{CH}_3)_2$ ), 3.00 (2H, sept,  $\text{CH}(\text{CH}_3)_2$ ), 3.09 (14H, mult, THF), 3.21 (2H, sept,  $\text{CH}(\text{CH}_3)_2$ ), 6.99 (1H, s, imidazole backbone CH), 7.08 (2H, *p*-CH), 7.16-7.21 (4H, mult, *m*-CH overlapping with  $\text{C}_6\text{D}_6$ ).  $^{13}\text{C}\{^1\text{H}\}$  NMR (298 K,  $\text{C}_6\text{D}_6$ )  $\delta(\text{ppm})$  0.2 ( $\text{CH}_2\text{SiMe}_3$ ), 3.8 ( $\text{Si}(\text{CH}_3)_3$ ), 23.3 ( $\text{CH}(\text{CH}_3)_2$ ), 24.8 ( $\text{CH}(\text{CH}_3)_2$ ), 25.3 ( $\text{CH}(\text{CH}_3)_2$ ), 25.5 ( $\text{CH}(\text{CH}_3)_2$ ), 27.9 ( $\text{CH}(\text{CH}_3)_2$ ), 28.1 ( $\text{CH}(\text{CH}_3)_2$ ), 123.4 (Ar-CH), 123.7 (Ar-CH), 124.5 (Ar-CH), 128.5 (Ar-CH), 129.2 (imidazole backbone CH), 139.1 (Ar-C), 142.7 (Ar-C), 146.8 (Ar-C), 146.9 (Ar-C), 156.0(C-Ga), 198.6 (C:).

**$^1\text{H}$  NMR (298 K,  $d_8$ -THF)  $\delta(\text{ppm})$**  -1.18 (6H, s,  $\text{CH}_2\text{SiMe}_3$ ), -0.17 (27H, s,  $\text{Si}(\text{CH}_3)_3$ ), 1.09-1.19 (12H, mult,  $\text{CH}(\text{CH}_3)_2$ ), 1.30 (6H, d,  $\text{CH}(\text{CH}_3)_2$ ), 3.0 (4H, mult,  $\text{CH}(\text{CH}_3)_2$ ), 6.64 (1H, s, imidazole backbone CH), 7.18-7.36 (6H, mult,  $m$ -CH +  $p$ -CH).  **$^{13}\text{C}\{^1\text{H}\}$  NMR (298 K,  $d_8$ -THF)  $\delta(\text{ppm})$**  0.2 ( $\text{CH}_2\text{SiMe}_3$ ), 3.7 ( $\text{Si}(\text{CH}_3)_3$ ), 23.3 ( $\text{CH}(\text{CH}_3)_2$ ), 25.1 ( $\text{CH}(\text{CH}_3)_2$ ), 25.3 ( $\text{CH}(\text{CH}_3)_2$ ), 26.4 ( $\text{CH}(\text{CH}_3)_2$ ), 28.5 ( $\text{CH}(\text{CH}_3)_2$ ), 28.6 ( $\text{CH}(\text{CH}_3)_2$ ), 123.6 (Ar-CH), 124.1 (Ar-CH), 127.9 (Ar-CH), 128.8 (Ar-CH), 129.5 (imidazole backbone CH), 139.1 (Ar-C), 142.7 (Ar-C), 147.3 (Ar-C), 147.5 (Ar-C), 155.2 (C-Ga), 202.8 (C:).

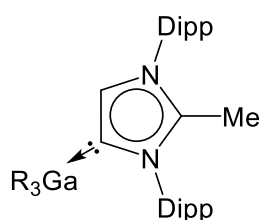
### 2.9.5. Synthesis of $(\text{THF})_3\text{K}[:\text{C}\{\text{N}(2,6\text{-}i\text{-Pr}_2\text{C}_6\text{H}_3)_2\text{CHCGa}(\text{CH}_2\text{SiMe}_3)_3\}]$



(5) Equimolar amounts of  $\text{K}(\text{CH}_2\text{SiMe}_3)$  (0.26 g, 2 mmol) and IPr (0.8 g, 2 mmol) were suspended in hexane (10 mL) and stirred for 2h at room temperature. To the obtained slurry, a hexane solution of  $\text{Ga}(\text{CH}_2\text{SiMe}_3)_3$  (0.66 g, 2 mmol in 10 mL hexane) was added via cannula and stirred over night at room temperature. The reaction mixture was then concentrated to approximately 5 mL and 1 mL of THF was added to afford a straw solution. Overnight storage of the solution at  $-30\text{ }^\circ\text{C}$  provided a batch of colourless crystals (1.48 g, 76 %). It should be noted that one coordinated THF molecule is lost upon drying *in vacuo*. Anal. Calcd for  $\text{C}_{47}\text{H}_{84}\text{N}_2\text{Si}_3\text{KO}_2\text{Ga}$ : C, 62.57; H, 9.38; N, 3.10. Found: C, 62.71; H, 9.62; N, 3.45.

**$^1\text{H}$  NMR (298 K,  $d_8$ -THF)  $\delta(\text{ppm})$**  -1.16 (6H, s,  $\text{CH}_2\text{SiMe}_3$ ), -0.17 (27H, s,  $\text{Si}(\text{CH}_3)_3$ ), 1.09 (12H, d,  $\text{CH}(\text{CH}_3)_2$ ), 1.17 (6H, d,  $\text{CH}(\text{CH}_3)_2$ ), 1.29 (6H, d,  $\text{CH}(\text{CH}_3)_2$ ), 3.02 (4H, mult,  $\text{CH}(\text{CH}_3)_2$ ), 6.59 (1H, s, imidazole backbone CH), 7.15-7.28 (6H, mult,  $m$ -CH +  $p$ -CH).  **$^{13}\text{C}\{^1\text{H}\}$  NMR (298 K,  $d_8$ -THF)  $\delta(\text{ppm})$**  0.2 ( $\text{CH}_2\text{SiMe}_3$ ), 3.7 ( $\text{Si}(\text{CH}_3)_3$ ), 23.2 ( $\text{CH}(\text{CH}_3)_2$ ), 24.9 ( $\text{CH}(\text{CH}_3)_2$ ), 25.3 ( $\text{CH}(\text{CH}_3)_2$ ), 26.4 ( $\text{CH}(\text{CH}_3)_2$ ), 28.4 ( $\text{CH}(\text{CH}_3)_2$ ), 28.6 ( $\text{CH}(\text{CH}_3)_2$ ), 123.2 (Ar-CH), 123.7 (Ar-CH), 127.6 (Ar-CH), 128.2 (Ar-CH), 128.6 (imidazole backbone CH), 140.8 (Ar-C), 144.3 (Ar-C), 147.3 (Ar-C), 147.4 (Ar-C), 153.6 (C-Ga), 210.7 (C:).

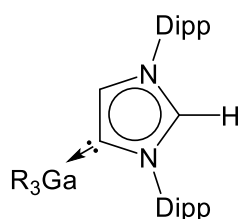
**2.9.6. Synthesis of  $[\text{CH}_3\text{C}\{\text{N}(2,6\text{-}i\text{-Pr}_2\text{C}_6\text{H}_3)_2\text{CHCGa}(\text{CH}_2\text{SiMe}_3)_3\}]$  (6)** A toluene solution of **3** (0.43 g, 0.5 mmol in 15 mL of toluene) was cooled down to  $-80\text{ }^\circ\text{C}$  and stirred for 20 min. To this slurry, a toluene solution of MeOTf (0.08 g, 0.5 mmol in 3 mL of toluene) was added dropwise and stirred for an



hour. The mixture was filtered through Celite to remove LiOTf and washed with more toluene (5 mL). The solvent was exchanged *in vacuo* to hexane (5 mL) to which 2 mL of fresh toluene were added. Obtained suspension was gently heated until a yellow solution was obtained which upon slow cooling afforded X-ray quality crystals. This mixture was then kept overnight at -30 °C to yield a crop of colourless crystals (0.25 g, 68%). Anal. Calcd for C<sub>40</sub>H<sub>71</sub>N<sub>2</sub>Si<sub>3</sub>Ga: C, 65.28; H, 10.00; N, 3.81. Found: C, 65.04; H, 9.91; N, 4.08.

**<sup>1</sup>H NMR (298 K, *d*<sub>8</sub>-THF)** δ -1.09 (6H, s, CH<sub>2</sub>SiMe<sub>3</sub>), -0.13 (27H, s, Si(CH<sub>3</sub>)<sub>3</sub>), 1.09 (6H, d, CH(CH<sub>3</sub>)<sub>2</sub>), 1.20 (6H, d, CH(CH<sub>3</sub>)<sub>2</sub>), 1.36 (6H, d, CH(CH<sub>3</sub>)<sub>2</sub>), 2.04 (3H, s, CH<sub>3</sub>), 2.51 (2H, sept, CH(CH<sub>3</sub>)<sub>2</sub>), 2.72 (2H, sept, CH(CH<sub>3</sub>)<sub>2</sub>), 7.13 (1H, s, imidazole backbone), 7.34-7.48 (mult, 6H, Ar-CH). **<sup>13</sup>C{<sup>1</sup>H} NMR (298 K, *d*<sub>8</sub>-THF)** δ 0.5 (CH<sub>2</sub>SiMe<sub>3</sub>), 3.5 (Si(CH<sub>3</sub>)<sub>3</sub>), 12.2 (CH<sub>3</sub>), 24.0 (CH(CH<sub>3</sub>)<sub>2</sub>), 24.4 (CH(CH<sub>3</sub>)<sub>2</sub>), 24.9 (CH(CH<sub>3</sub>)<sub>2</sub>), 25.4 (CH(CH<sub>3</sub>)<sub>2</sub>), 28.9 (CH(CH<sub>3</sub>)<sub>2</sub>), 29.3 (CH(CH<sub>3</sub>)<sub>2</sub>), 125.3 (*m*-CH), 125.8 (*m*-CH), 130.0 (*p*-CH), 131.7 (imidazole backbone CH), 132.1 (*p*-CH), 132.1 (*i*-C), 135.1 (*i*-C), 145.0 (NCMeN), 146.3 (*o*-C), 146.5 (*o*-C), 161.2 (C-Ga).

### 2.9.7. Synthesis of [aIPrGa(CH<sub>2</sub>SiMe<sub>3</sub>)<sub>3</sub>] (7)

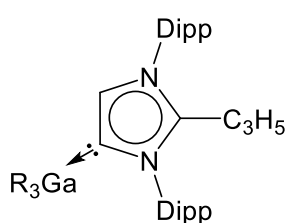


To a THF solution of **3** (0.43 g, 0.5 mmol in 10 mL of THF) IMesHCl (0.17 g, 0.5 mmol) was added from solid addition tube and stirred for 6h at room temperature. The mixture was filtered through Celite and washed with more THF (2 x 5 mL). Clear filtrate was concentrated to *ca.* 5 mL in volume to which 2 mL of hexane was added and stored at -30 °C to afford colourless crystals of title compound (0.22 g, 61%). Anal. Calcd for C<sub>39</sub>H<sub>69</sub>N<sub>2</sub>Si<sub>3</sub>Ga: C, 65.06; H, 9.66; N, 3.89. Found: C, 65.42; H, 9.76; N, 4.19.

**<sup>1</sup>H NMR (298 K, C<sub>6</sub>D<sub>6</sub>)** δ -0.67 (6H, s, CH<sub>2</sub>SiMe<sub>3</sub>), 0.29 (27H, s, Si(CH<sub>3</sub>)<sub>3</sub>), 0.85 (6H, d, CH(CH<sub>3</sub>)<sub>2</sub>), 0.91 (6H, d, CH(CH<sub>3</sub>)<sub>2</sub>), 1.07 (6H, d, CH(CH<sub>3</sub>)<sub>2</sub>), 1.41 (6H, d, CH(CH<sub>3</sub>)<sub>2</sub>), 2.37 (2H, sept, CH(CH<sub>3</sub>)<sub>2</sub>), 2.73 (2H, sept, CH(CH<sub>3</sub>)<sub>2</sub>), 6.93 (2H, d, *m*-CH), 6.94 (1H, s, imidazole backbone CH), 6.97 (1H, s, C2-H), 7.08 (2H, d, *m*-CH), 7.11-7.23 (2H, two triplets, *p*-CH).

**$^1\text{H}$  NMR (298 K,  $d_8$ -THF)**  $\delta$  -1.07 (6H, s,  $\text{CH}_2\text{SiMe}_3$ ), -0.13 (27H, s,  $\text{Si}(\text{CH}_3)_3$ ), 1.10 (6H, d,  $\text{CH}(\text{CH}_3)_2$ ), 1.18 (6H, d,  $\text{CH}(\text{CH}_3)_2$ ), 1.27 (6H, d,  $\text{CH}(\text{CH}_3)_2$ ), 1.38 (6H, d,  $\text{CH}(\text{CH}_3)_2$ ), 2.59 (2H, sept,  $\text{CH}(\text{CH}_3)_2$ ), 2.77 (2H, sept,  $\text{CH}(\text{CH}_3)_2$ ), 7.19 (1H, s, imidazole backbone CH), 7.35-7.41 (4H, two doublets,  $m$ -CH), 7.48-7.58 (2H, two triplets,  $p$ -CH), 9.00 (1H, s, C2-H).  
 **$^{13}\text{C}\{^1\text{H}\}$  NMR (298 K,  $d_8$ -THF)**  $\delta$  -0.1 ( $\text{CH}_2\text{SiMe}_3$ ), 3.4 ( $\text{Si}(\text{CH}_3)_3$ ), 22.9 ( $\text{CH}(\text{CH}_3)_2$ ), 24.6( $\text{CH}(\text{CH}_3)_2$ ), 24.9 ( $\text{CH}(\text{CH}_3)_2$ ), 26.7 ( $\text{CH}(\text{CH}_3)_2$ ), 29.1 ( $\text{CH}(\text{CH}_3)_2$ ), 29.3 ( $\text{CH}(\text{CH}_3)_2$ ), 124.6 ( $m$ -CH), 125.2 ( $m$ -CH), 131.1 ( $p$ -CH), 131.2 (imidazole backbone CH), 131.8 ( $p$ -CH), 132.1 ( $i$ -C), 135.6 ( $i$ -C), 139.2 (NCHN), 146.5 ( $o$ -C), 146.7 ( $o$ -C), 162.8 (C-Ga).

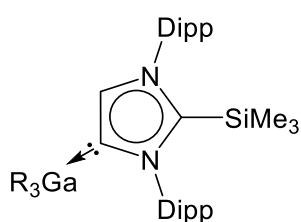
### 2.9.8. Synthesis of $[\text{C}_3\text{H}_5\text{C}\{\text{N}(2,6\text{-}i\text{-Pr}_2\text{C}_6\text{H}_3)\}_2\text{CHCGa}(\text{CH}_2\text{SiMe}_3)_3]$ (**8**)



To a THF solution of **4** (0.48 g, 0.5 mmol in 5 mL of THF) allyl bromide (0.06 g, 43  $\mu\text{L}$ , 0.5 mmol) was added inducing precipitation. Obtained suspension was stirred for 1h at room temperature and then filtered through Celite. Orange filtrate was layered with 3 mL of hexane and stored at -33  $^\circ\text{C}$  to afford colourless crystals of title compound (0.16 g, 42%). Anal. Calcd. for  $\text{C}_{42}\text{H}_{73}\text{N}_2\text{Si}_3\text{Ga}$ : C, 66.37; H, 9.68; N, 3.69. Found: C, 65.69; H, 9.66; N, 3.84. The NMR analysis is very complex and the reported chemical shifts are for both  $\text{CH}=\text{CH}-\text{CH}_3$  and  $\text{CH}_2-\text{CH}=\text{CH}_2$  fragments.

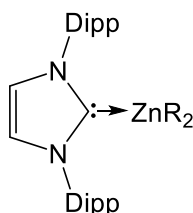
**$^1\text{H}$  NMR (298 K,  $d_8$ -THF)**  $\delta(\text{ppm})$  -0.67 (6H, mult,  $\text{CH}_2\text{SiMe}_3$ ), -0.29 and -0.33 (27H, s,  $\text{Si}(\text{CH}_3)_3$ ), 0.81-1.46 (24H, mult,  $\text{CH}(\text{CH}_3)_2$ ), 2.35 (0.8 H, mult,  $\text{CH}(\text{CH}_3)_2$ ), 2.51 (1.2 H, mult,  $\text{CH}(\text{CH}_3)_2$ ), 2.70 (0.8 H, mult,  $\text{CH}(\text{CH}_3)_2$ ), 2.85 (1.2 H, mult,  $\text{CH}(\text{CH}_3)_2$ ), 2.95 (0.5 H, d,  $\text{CH}=\text{CH}-\text{CH}_3$ ), [4.12, 4.36, 4.54, 4.67, 5.00, 5.60] ( $\text{CH}_2-\text{CH}=\text{CH}_2 + \text{CH}=\text{CH}-\text{CH}_3$ ), 6.88 (7H, mult, imidazole backbone CH + Ar-CH),  
 **$^{13}\text{C}\{^1\text{H}\}$  NMR (298 K,  $d_8$ -THF)**  $\delta(\text{ppm})$  0.3 ( $\text{CH}_2\text{SiMe}_3$ ), 3.6 ( $\text{Si}(\text{CH}_3)_3$ ), 22.6 ( $\text{CH}(\text{CH}_3)_2$ ), 22.8 ( $\text{CH}(\text{CH}_3)_2$ ), 23.0 ( $\text{CH}(\text{CH}_3)_2$ ), 23.7 ( $\text{CH}(\text{CH}_3)_2$ ), 23.8 ( $\text{CH}(\text{CH}_3)_2$ ), 23.9 ( $\text{CH}(\text{CH}_3)_2$ ), 24.4 ( $\text{CH}(\text{CH}_3)_2$ ), 24.5 ( $\text{CH}(\text{CH}_3)_2$ ), 24.6 ( $\text{CH}(\text{CH}_3)_2$ ), 26.4 ( $\text{CH}(\text{CH}_3)_2$ ), 28.3 ( $\text{CH}(\text{CH}_3)_2$ ), 28.4 ( $\text{CH}(\text{CH}_3)_2$ ), 28.5 ( $\text{CH}(\text{CH}_3)_2$ ), 28.7 ( $\text{CH}(\text{CH}_3)_2$ ), 30.1 ( $\text{CH}=\text{CH}-\text{CH}_3$ ), [114.2, 115.9, 120.3, 124.1, 124.4, 124.6, 124.7, 124.8, 125.1  $\text{CH}_2-\text{CH}=\text{CH}_2 + \text{CH}=\text{CH}-\text{CH}_3$ ], [130.1, 130.2, 130.5, 130.8, 130.9, 131.2, 131.4, 131.7 aromatic CH + imidazole backbone CH ], [134.1, 134.7, 136.6 Ar-C], 141.6 (C2-C), [143.7, 145.5, 145.6, 145.7 Ar-C], 163.4 (C-Ga).



**2.9.9. Synthesis of [Me<sub>3</sub>SiC{[N(2,6-*i*Pr<sub>2</sub>C<sub>6</sub>H<sub>3</sub>)]<sub>2</sub>CHCGa(CH<sub>2</sub>SiMe<sub>3</sub>)<sub>3</sub>] (9)**

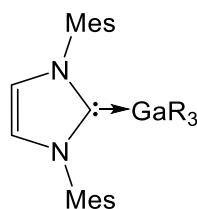
To a THF solution of **5** (0.49 g, 0.5 mmol in 5 mL of THF) dried TMSCl (0.05 g, 63  $\mu$ L, 0.5 mmol) was added inducing precipitation. Obtained suspension was stirred for 1h at room temperature and then filtered through Celite. Clear filtrate was layered with 2 mL of hexane and stored at -33 °C to afford colourless crystals of title compound (0.24 g, 61%). Anal. Calcd for C<sub>42</sub>H<sub>77</sub>N<sub>2</sub>Si<sub>4</sub>Ga: C, 63.68; H, 9.80; N, 3.54. Found: C, 62.89; H, 9.46; N, 3.60.

**<sup>1</sup>H NMR (298 K, C<sub>6</sub>D<sub>6</sub>)  $\delta$ (ppm)** -0.69 (6H, s, CH<sub>2</sub>SiMe<sub>3</sub>), -0.46 (9H, s, SiCH<sub>3</sub>), 0.33 (27H, s, Si(CH<sub>3</sub>)<sub>3</sub>), 1.03 (6H, d, CH(CH<sub>3</sub>)<sub>2</sub>), 1.09 (12H, d, CH(CH<sub>3</sub>)<sub>2</sub>), 1.40 (6H, d, CH(CH<sub>3</sub>)<sub>2</sub>), 2.40 (2H, sept, CH(CH<sub>3</sub>)<sub>2</sub>), 2.76 (2H, sept, CH(CH<sub>3</sub>)<sub>2</sub>), 6.95 (2H, d, Ar-CH), 7.04 (2H, d, Ar-CH), 7.12-7.21 (3H, mult, Ar-CH + CH imidazole backbone). **<sup>13</sup>C{<sup>1</sup>H} NMR (298 K, d<sub>8</sub>-THF)  $\delta$ (ppm)** -0.5 (SiCH<sub>3</sub>), 1.3 (CH<sub>2</sub>SiMe<sub>3</sub>), 3.7 (Si(CH<sub>3</sub>)<sub>3</sub>), 21.6 (CH(CH<sub>3</sub>)<sub>2</sub>), 24.3 (CH(CH<sub>3</sub>)<sub>2</sub>), 25.1 (CH(CH<sub>3</sub>)<sub>2</sub>), 28.0 (CH(CH<sub>3</sub>)<sub>2</sub>), 28.5 (CH(CH<sub>3</sub>)<sub>2</sub>), 28.9 (CH(CH<sub>3</sub>)<sub>2</sub>), 124.2 (Ar-CH), 124.4 (Ar-CH), 130.5 (Ar-CH), 131.4 (Ar-CH), 133.1 (Ar-C), 135.3 (imidazole backbone CH), 137.3 (Ar-C), 145.3 (Ar-C), 146.5 (Ar-C), 148.8 (C-SiMe<sub>3</sub>), 167.6 (C-Ga).

**2.9.10. Synthesis of [IPrZn(CH<sub>2</sub>SiMe<sub>3</sub>)<sub>2</sub>] (10)**

Zn(CH<sub>2</sub>SiMe<sub>3</sub>)<sub>2</sub> (0.92 mL, 0.54 M in hexane, 0.5 mmol) was added *via* syringe to a suspension of IPr (0.19 g, 0.5 mmol) in hexane (10 mL) at room temperature to form a white suspension and stirred for 15 min at room temperature. The reaction mixture was then gently heated until all of the visible solid had dissolved. Slow cooling of the resulting solution afforded X-ray quality crystals (0.22 g, 70%). Anal. Calcd for C<sub>35</sub>H<sub>58</sub>N<sub>2</sub>Si<sub>2</sub>Zn: C, 66.90; H, 9.30; N, 4.46. Found: C, 66.67; H, 9.46; N, 4.81.

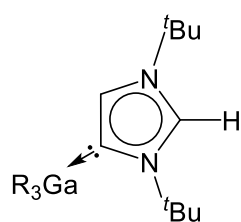
**<sup>1</sup>H NMR (298 K, C<sub>6</sub>D<sub>6</sub>)  $\delta$**  -0.99 (4H, s, CH<sub>2</sub>SiMe<sub>3</sub>), 0.10 (18H, s, Si(CH<sub>3</sub>)<sub>3</sub>), 1.00 (12H, d, CH(CH<sub>3</sub>)<sub>2</sub>), 1.34 (12H, d, CH(CH<sub>3</sub>)<sub>2</sub>), 2.82 (4H, sept, CH(CH<sub>3</sub>)<sub>2</sub>), 6.44 (2H, s, imidazole backbone CH), 7.11 (4H, d, *m*-CH), 7.23 (2H, t, *p*-CH). **<sup>13</sup>C{<sup>1</sup>H} NMR (298 K, C<sub>6</sub>D<sub>6</sub>)  $\delta$**  -0.8 (CH<sub>2</sub>SiMe<sub>3</sub>), 3.9 (Si(CH<sub>3</sub>)<sub>3</sub>), 23.4 (CH(CH<sub>3</sub>)<sub>2</sub>), 25.3 (CH(CH<sub>3</sub>)<sub>2</sub>), 28.7 (CH(CH<sub>3</sub>)<sub>2</sub>), 123.3 (*m*-CH), 124.5 (imidazole backbone CH), 130.5 (*p*-CH), 135.6 (*i*-C), 145.6 (*o*-C), 192.2 (C:).

**2.9.11. Synthesis of [IMes·Ga(CH<sub>2</sub>SiMe<sub>3</sub>)<sub>3</sub>] (11)**

Ga(CH<sub>2</sub>SiMe<sub>3</sub>)<sub>3</sub> (0.36 g, 1 mmol) and bis(1,3,5-trimethylphenyl)imidazol-2-ylidene (IMes) (0.30 g, 1 mmol) were mixed in hexane (10 ml) and stirred for one hour at room temperature. The resulting orange solution was concentrated to

the half of its volume and placed at -27 °C to yield a crop of orange crystals (0.22 g, 34%). Anal. Calcd for C<sub>33</sub>H<sub>57</sub>N<sub>2</sub>Si<sub>3</sub>Ga: C, 62.34; H, 9.04; N, 4.41. Found: C, 62.45; H, 9.52; N, 4.77.

<sup>1</sup>H NMR (298 K, C<sub>6</sub>D<sub>6</sub>) δ -0.91 (6H, s, CH<sub>2</sub>SiMe<sub>3</sub>), 0.22 (27H, s, Si(CH<sub>3</sub>)<sub>3</sub>), 1.99 (12H, s, CH<sub>3</sub>), 2.16 (6H, s, CH<sub>3</sub>), 5.92 (2H, s, imidazole backbone CH), 6.77 (4H, d, *m*-CH). <sup>13</sup>C{<sup>1</sup>H} NMR (298 K, C<sub>6</sub>D<sub>6</sub>) δ -0.6 (CH<sub>2</sub>SiMe<sub>3</sub>), 3.5 (Si(CH<sub>3</sub>)<sub>3</sub>), 18.2 (CH<sub>3</sub>), 21.1 (CH<sub>3</sub>), 122.9 (*m*-CH), 129.6 (imidazole backbone CH), 135.3 (*p*-CH), 135.9 (*i*-C), 139.6 (*o*-C), 182.2 (C:).

**2.9.12. Synthesis of [a<sup>t</sup>BuGa(CH<sub>2</sub>SiMe<sub>3</sub>)<sub>3</sub>] (12)**

Ga(CH<sub>2</sub>SiMe<sub>3</sub>)<sub>3</sub> (0.17 g, 0.5 mmol) and bis(tert-butyl)imidazole-2-ylidene (tBu) (0.09 g, 0.5 mmol) were mixed in 5 mL hexane. Obtained suspension was stirred for 2h at room temperature. Toluene (1 mL) was added and the mixture was gently heated until all of the visible solid had

dissolved. Slow cooling of the resulting solution afforded a crop of colourless crystals (0.11 g, 43 %). Anal. Calcd. for: C<sub>23</sub>H<sub>53</sub>GaN<sub>2</sub>Si<sub>3</sub>: C, 53.99; H, 10.44; N, 5.48. Found: C, 53.43; H, 10.07; N, 5.40.

<sup>1</sup>H NMR (298 K, *d*<sub>8</sub>-THF) δ -0.73 (6H, s, CH<sub>2</sub>SiMe<sub>3</sub>), -0.13 (27H, s, Si(CH<sub>3</sub>)<sub>3</sub>), 1.60 (9H, s, C(CH<sub>3</sub>)<sub>3</sub>), 1.67 (9H, s, C(CH<sub>3</sub>)<sub>3</sub>), 7.07 (1H, s, imidazole backbone CH), 8.36 (1H, s, C2-H). <sup>13</sup>C{<sup>1</sup>H} NMR (298 K, *d*<sub>8</sub>-THF) δ 1.9 (CH<sub>2</sub>SiMe<sub>3</sub>), 3.4 (Si(CH<sub>3</sub>)<sub>3</sub>), 29.9 (C(CH<sub>3</sub>)<sub>3</sub>), 30.8 (C(CH<sub>3</sub>)<sub>3</sub>), 57.8 (C(CH<sub>3</sub>)<sub>3</sub>), 59.8 (C(CH<sub>3</sub>)<sub>3</sub>), 127.0 (imidazole backbone CH), 130.1 (NCHN), 158.7 (C-Ga).

<sup>1</sup>H NMR (298 K, C<sub>6</sub>D<sub>6</sub>) δ -0.23 (6H, s, CH<sub>2</sub>SiMe<sub>3</sub>), 0.33 (27H, s, Si(CH<sub>3</sub>)<sub>3</sub>), 0.87 (9H, s, C(CH<sub>3</sub>)<sub>3</sub>), 1.33 (9H, s, C(CH<sub>3</sub>)<sub>3</sub>), 7.09 (1H, s, imidazole backbone CH), 7.21 (1H, s, C2-H). <sup>13</sup>C{<sup>1</sup>H} NMR (298 K, C<sub>6</sub>D<sub>6</sub>) δ 2.0 (CH<sub>2</sub>SiMe<sub>3</sub>), 3.6 (Si(CH<sub>3</sub>)<sub>3</sub>), 29.3 (C(CH<sub>3</sub>)<sub>3</sub>), 30.4 (C(CH<sub>3</sub>)<sub>3</sub>), 56.5 (C(CH<sub>3</sub>)<sub>3</sub>), 59.1 (C(CH<sub>3</sub>)<sub>3</sub>), 126.6 (imidazole backbone CH), 126.9 (NCHN), 160.1 (C-Ga).

## 2.10. Bibliography

- [1] D. Bourissou, O. Guerret, F. P. Gabbaï, G. Bertrand, *Chem. Rev.* **2000**, *100*, 39–92.
- [2] A. J. Arduengo, R. L. Harlow, M. Kline, *J. Am. Chem. Soc.* **1991**, *113*, 361–363.
- [3] A. J. Arduengo, H. V. R. Dias, D. A. Dixon, R. L. Harlow, W. T. Klooster, T. F. Koetzle, *J. Am. Chem. Soc.* **1994**, *116*, 6812–6822.
- [4] M. Scholl, S. Ding, C. W. Lee, R. H. Grubbs, *Org. Lett.* **1999**, *1*, 953–956.
- [5] W. A. Herrmann, *Angew. Chem. Int. Ed.* **2002**, *41*, 1290–1309.
- [6] C. Valente, S. Çalimsiz, K. H. Hoi, D. Mallik, M. Sayah, M. G. Organ, *Angew. Chem. Int. Ed.* **2012**, *51*, 3314–3332.
- [7] D. Enders, O. Niemeier, A. Henseler, *Chem. Rev.* **2007**, *107*, 5606–5655.
- [8] S. Diez-Gonzalez, N. Marion, S. P. Nolan, *Chem. Rev.* **2009**, *109*, 3612–3676.
- [9] S. P. Nolan, *N-Heterocyclic Carbenes*, Wiley-VCH, Weinheim, Germany, **2014**.
- [10] M. Scholl, T. M. Trnka, J. P. Morgan, R. H. Grubbs, *Tetrahedron Lett.* **1999**, *40*, 2247–2250.
- [11] L. Ackermann, A. Fürstner, T. Weskamp, F. J. Kohl, W. A. Herrmann, *Tetrahedron Lett.* **1999**, *40*, 4787–4790.
- [12] J. Huang, E. D. Stevens, S. P. Nolan, J. L. Petersen, *J. Am. Chem. Soc.* **1999**, *121*, 2674–2678.
- [13] A. Sidiropoulos, C. Jones, A. Stasch, S. Klein, G. Frenking, *Angew. Chem. Int. Ed.* **2009**, *48*, 9701–9704.
- [14] Y. Wang, Y. Xie, P. Wei, R. B. King, H. F. Schaefer, P. V. R. Schleyer, G. H. Robinson, *J. Am. Chem. Soc.* **2008**, *130*, 14970–14971.
- [15] M. Y. Abraham, Y. Wang, Y. Xie, P. Wei, H. F. Schaefer, P. V. R. Schleyer, G. H. Robinson, *Chem. Eur J.* **2010**, *16*, 432–435.
- [16] Y. Wang, G. H. Robinson, *Inorg. Chem.* **2011**, *50*, 12326–12337.
- [17] C. A. Dyker, G. Bertrand, *Science* **2008**, *321*, 1050–1051.
- [18] Y. Wang, Y. Xie, P. Wei, R. B. King, H. F. Schaefer, P. V. R. Schleyer, G. H. Robinson, *Science* **2008**, *321*, 1069–1071.
- [19] C. Jones, A. Sidiropoulos, N. Holzmann, G. Frenking, A. Stasch, *Chem. Commun.* **2012**, *48*, 9855–9857.
- [20] H. Braunschweig, R. D. Dewhurst, K. Hammond, J. Mies, K. Radacki, A. Vargas, *Science* **2012**, *336*, 1420–1422.

- [21] L. J. Hounjet, D. W. Stephan, *Org. Process Res. Dev.* **2014**, *18*, 385–391.
- [22] D. W. Stephan, *Acc. Chem. Res.* **2015**, *48*, 306–316.
- [23] D. W. Stephan, G. Erker, *Angew. Chem. Int. Ed.* **2015**, *54*, 6400–6441.
- [24] B. Quillian, P. Wei, C. S. Wannere, P. V. R. Schleyer, G. H. Robinson, *J. Am. Chem. Soc.* **2009**, *131*, 3168–3169.
- [25] R. Tonner, G. Heydenrych, G. Frenking, *Chem. Asian J.* **2007**, *2*, 1555–1567.
- [26] S. Gründemann, A. Kovacevic, M. Albrecht, J. W. Faller, R. H. Crabtree, *Chem. Commun.* **2001**, 2274–2275.
- [27] S. Gründemann, A. Kovacevic, M. Albrecht, J. W. Faller, R. H. Crabtree, *J. Am. Chem. Soc.* **2002**, *124*, 10473–10481.
- [28] L. N. Appelhans, D. Zuccaccia, A. Kovacevic, A. R. Chianese, J. R. Miecznikowski, A. Macchioni, E. Clot, O. Eisenstein, R. H. Crabtree, *J. Am. Chem. Soc.* **2005**, *127*, 16299–16311.
- [29] P. L. Arnold, S. Pearson, *Coord. Chem. Rev.* **2007**, *251*, 596–609.
- [30] O. Schuster, L. Yang, H. G. Raubenheimer, M. Albrecht, *Chem. Rev.* **2009**, *109*, 3445–3478.
- [31] R. H. Crabtree, *Coord. Chem. Rev.* **2013**, *257*, 755–766.
- [32] G. Bertrand, E. Aldeco-Perez, A. J. Rosenthal, B. Donnadiu, P. Parameswaran, G. Frenking, *Science* **2009**, *326*, 556–559.
- [33] J. B. Waters, J. M. Goicoechea, *Coord. Chem. Rev.* **2015**, *293–294*, 80–94.
- [34] M. Heckenroth, E. Kluser, A. Neels, M. Albrecht, *Angew. Chem. Int. Ed.* **2007**, *46*, 6293–6296.
- [35] B. M. Day, T. Pugh, D. Hendriks, C. F. Guerra, D. J. Evans, F. M. Bickelhaupt, R. A. Layfield, *J. Am. Chem. Soc.* **2013**, *135*, 13338–13341.
- [36] T. W. Graham, K. A. Udachin, A. J. Carty, *Chem. Commun.* **2006**, 2699–2701.
- [37] D. Holschumacher, T. Bannenberg, C. G. Hrib, P. G. Jones, M. Tamm, *Angew. Chem. Int. Ed.* **2008**, *47*, 7428–7432.
- [38] D. Holschumacher, T. Bannenberg, K. Ibrom, C. G. Daniliuc, P. G. Jones, M. Tamm, *Dalton Trans.* **2010**, *39*, 10590–10592.
- [39] E. L. Kolychev, T. Bannenberg, M. Freytag, C. G. Daniliuc, P. G. Jones, M. Tamm, *Chem. Eur. J.* **2012**, *18*, 16938–16946.
- [40] A.-L. Schmitt, G. Schnee, R. Weltera, S. Dagorne, *Chem. Commun.* **2010**, *46*, 2480–2482.
- [41] Y. Wang, Y. Xie, M. Y. Abraham, P. Wei, H. F. Schaefer, P. v. R. Schleyer, G. H.

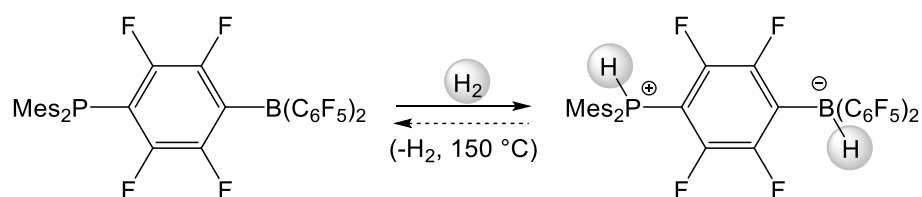
- Robinson, *J. Am. Chem. Soc.* **2010**, *132*, 14370–14372.
- [42] Y. Wang, Y. Xie, M. Y. Abraham, R. J. Gilliard, P. Wei, C. F. Campana, H. F. Schaefer, P. V. R. Schleyer, G. H. Robinson, *Angew. Chem. Int. Ed.* **2012**, *51*, 10173–10176.
- [43] M. Chen, Y. Wang, R. J. Gilliard, P. Wei, N. A. Schwartz, G. H. Robinson, *Dalton Trans.* **2014**, *43*, 14211–14214.
- [44] Y. Wang, M. Y. Abraham, R. J. Gilliard, P. Wei, J. C. Smith, G. H. Robinson, *Organometallics* **2012**, *31*, 791–793.
- [45] M. L. Cole, S. K. Furfari, M. Kloth, *J. Organomet. Chem.* **2009**, *694*, 2934–2940.
- [46] C. Fliedel, G. Schnee, T. Avilés, S. Dagherne, *Coord. Chem. Rev.* **2014**, *275*, 63–86.
- [47] N. Marion , E. C. Escudero-Adán , J. Benet-Buchholz , E. D. Stevens , L. Fensterbank, M. Malacria , S. P. Nolan, *Organometallics* **2007**, *26*, 3256–3259.
- [48] S. Tang, J. Monot, A. El-Hellani, B. Michelet, R. Guillot, C. Bour, V. Gandon, *Chem. Eur. J.* **2012**, *18*, 10239–10243.
- [49] C. Bour, J. Monot, S. Tang, R. Guillot, J. Farjon, V. Gandon, *Organometallics* **2014**, *33*, 594–599.
- [50] X. Li, J. Su, G. H. Robinson, *Chem. Commun.* **1996**, *3*, 2683–2684.
- [51] O. T. Beachley, R. Simmons, *Inorg. Chem.* **1980**, *19*, 1021–1025.
- [52] P. J. Davidson, M. F. Lappert, R. Pearce, *Acc. Chem. Res.* **1974**, *7*, 209–217.
- [53] P. J. Davidson, M. F. Lappert, R. Pearce, *Chem. Rev.* **1976**, *76*, 219–242.
- [54] M. U. Kramer, D. Robert, Y. Nakajima, U. Englert, T. P. Spaniol, J. Okuda, *Eur. J. Inorg. Chem.* **2007**, *2007*, 665–674.
- [55] A. Jana, R. Azhakar, G. Tavčar, H. W. Roesky, I. Objartel, D. Stalke, *Eur. J. Inorg. Chem.* **2011**, *2011*, 3686–3689.
- [56] D. R. Armstrong, E. Brammer, T. Cadenbach, E. Hevia, A. R. Kennedy, *Organometallics* **2013**, *32*, 480–489.
- [57] D. R. Armstrong, S. E. Baillie, V. L. Blair, N. G. Chabloz, J. Diez, J. Garcia-Alvarez, A. R. Kennedy, S. D. Robertson, E. Hevia, *Chem. Sci.* **2013**, *4*, 4259–4266.
- [58] C. Lichtenberg, T. P. Spaniol, J. Okuda, *Inorg. Chem.* **2012**, *51*, 2254–2262.
- [59] J. B. Waters, J. M. Goicoechea, *Dalton Trans.* **2014**, *43*, 14239–14248.
- [60] L. C. H. Maddock, T. Cadenbach, A. R. Kennedy, I. Borilovic, G. Aromí, E. Hevia, *Inorg. Chem.* **2015**, *54*, 9201–9210.
- [61] P. L. Arnold, S. T. Liddle, *Organometallics* **2006**, *25*, 1485–1491.

- [62] P. K. Majhi, G. Schnakenburg, Z. Kelemen, L. Nyulaszi, D. P. Gates, R. Streubel, *Angew. Chem. Int. Ed.* **2013**, *52*, 10080–10083.
- [63] F. Feil, S. Harder, *Organometallics* **2000**, *19*, 5010–5015.
- [64] G. C. Forbes, A. R. Kennedy, R. E. Mulvey, B. A. Roberts, B. Rowlings, *Organometallics* **2002**, *21*, 5115–5121.
- [65] K. L. Hull, I. Carmichael, B. C. Noll, K. W. Henderson, *Chem. Eur. J.* **2008**, *14*, 3939–3953.
- [66] M. S. Hill, G. Kociok-Köhn, D. J. MacDougall, *Inorg. Chem.* **2011**, *50*, 5234–5241.
- [67] M. I. Lipschutz, T. Chantarojsiri, Y. Dong, T. D. Tilley, *J. Am. Chem. Soc.* **2015**, *137*, 6366–6372.
- [68] M. Uzelac, I. Borilovic, M. Amores, T. Cadenbach, A. R. Kennedy, G. Aromí, E. Hevia, *Chem. Eur. J.* **2016**, *22*, 4843–4854.
- [69] Y. Yamaguchi, T. Kashiwabara, K. Ogata, Y. Miura, Y. Nakamura, K. Kobayashi, T. Ito, *Chem. Commun.* **2004**, 2160–2161.
- [70] S. Kronig, E. Theuergarten, C. G. Daniliuc, P. G. Jones, M. Tamm, *Angew. Chem. Int. Ed.* **2012**, *51*, 3240–3244.
- [71] W. Kohn, A. D. Becke, R. G. Parr, *J. Phys Chem* **1996**, *100*, 12974–12980.
- [72] A. D. Becke, *Phys. Rev. A* **1988**, *38*, 3098–3100.
- [73] C. Lee, W. Yang, R. G. Parr, *Phys. Rev. B* **1988**, *37*, 785–789.
- [74] A. D. McLean, G. S. Chandler, *J. Chem. Phys.* **1980**, *72*, 5639–5649.
- [75] T. Guo, S. Dechert, F. Meyer, *Organometallics* **2014**, *33*, 5145–5155.
- [76] M. Heckenroth, A. Neels, M. G. Garnier, P. Aebi, A. W. Ehlers, M. Albrecht, *Chem. Eur. J.* **2009**, *15*, 9375–9386.
- [77] A. R. Kennedy, J. Klett, R. E. Mulvey, S. D. Robertson, *Eur. J. Inorg. Chem.* **2011**, *2011*, 4675–4679.
- [78] H. Clavier, S. P. Nolan, *Chem. Commun.* **2010**, *46*, 841–861.
- [79] R. M. Stolley, H. A. Duong, D. R. Thomas, J. Louie, *J. Am. Chem. Soc.* **2012**, *134*, 15154–15162.
- [80] R. B. Jordan, *Reaction Mechanisms of Inorganic and Organometallic Systems*, Oxford University Press, Oxford, UK, **2007**.
- [81] T. A. Rokob, A. Hamza, A. Stirling, I. Pápai, *J. Am. Chem. Soc.* **2009**, *131*, 2029–2036.

### 3. Introducing Ga complexes to Frustrated Lewis Pair (FLP) Chemistry

#### 3.1. Introduction to FLP Chemistry

Nearly a century ago, G. N. Lewis offered a molecular-orbital-based principle for reactions describing dative donor-acceptor adducts where molecules are categorised as electron-pair donors and acceptors.<sup>[1]</sup> The concept for bonding involving filled HOMO (highest occupied molecular orbital) orbitals of a Lewis base and vacant LUMO (lowest unoccupied molecular orbital) orbitals of a Lewis acid is central to our understanding of much of modern chemistry, (for example, organic, organometallic, solid state chemistry and surface science). Early reports by Brown,<sup>[2]</sup> Wittig<sup>[3,4]</sup> and Tochtermann<sup>[5]</sup> revealed that there are exceptions from this rule and that steric incompatibility can prevent the formation of a simple Lewis adduct and rather afford unforeseen reactivity. These findings were, however, not further developed until the work of Stephan and co-workers, who while investigating the use of boranes and borate salts as activators for olefin polymerization, began to explore combinations of bulky phosphine-borane systems. It was these B/P systems that were shown to heterolytically cleave H<sub>2</sub> in a cooperative manner, displaying unique reactivities typically reserved for transition-metal complexes (**Scheme 3.1**).<sup>[6]</sup>

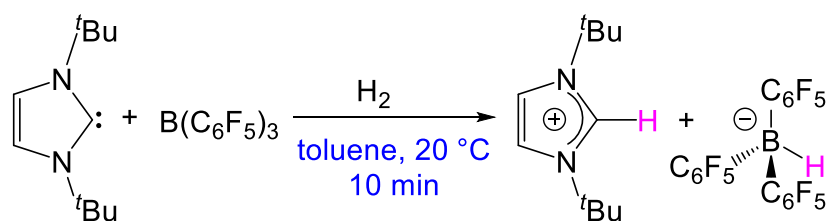


**Scheme 3.1:** Heterolytic cleavage of hydrogen by a bulky phosphine-borane system.<sup>[6]</sup>

Defined as a sterically encumbered Lewis pairs which evade self-quenching by formation of a “classical” Lewis adduct, “frustrated Lewis pairs (FLPs)” are “available” to react with a third molecule.<sup>[7–9]</sup> Stephan’s seminal work brought FLPs

to the forefront of main group chemistry, after which the field has, in less than a decade, snowballed due in part to the ever-growing scope of small molecules that can be activated (*e.g.*, H<sub>2</sub> and greenhouse gases), and also because of its progression from stoichiometric to catalytic processes.

Although the most powerful FLPs to date rely on the use of sterically hindered, electron-rich organophosphines as the Lewis base (LB) component,<sup>[6–12]</sup> *N*-heterocyclic carbenes (NHCs), which have a myriad of applications in their own right,<sup>[13]</sup> are increasingly gaining attention in this field. Exhibiting related coordination chemistry to that of phosphines, NHCs offer greater potential for subtle variations of their steric/electronic properties.<sup>[10,14–22]</sup> In addition to being a source of tuneability, the *N*-substituents are responsible for inducing “steric pressure” towards the Lewis acidic (LA) component by being directed towards the carbene lone pair.<sup>[10]</sup> Thus, in 2008, the groups of Stephan and Tamm have independently combined 1,3-di-*tert*-butylimidazole-2-ylidene (I<sup>t</sup>Bu) with B(C<sub>6</sub>F<sub>5</sub>)<sub>3</sub> for the activation of dihydrogen under mild reaction conditions (**Scheme 3.2**).<sup>[14,15]</sup>

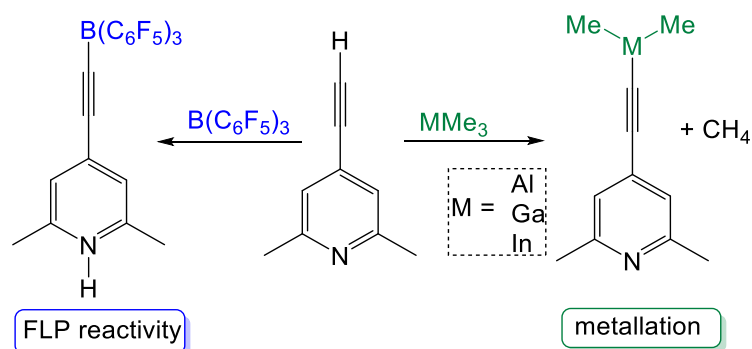


**Scheme 3.2:** Heterolytic cleavage of hydrogen by borane–NHC frustrated Lewis pair.<sup>[14,15]</sup>

Although the vast majority of these FLP studies employ boron complexes as Lewis acids, recent reports have also highlighted the potential of other group 13 complexes to exhibit related reactivities. Studies on aluminium species, for instance, have shown slow but steady growth in popularity with the notable work of Uhl<sup>[23–27]</sup> and Stephan,<sup>[19,28–32]</sup> amongst others.<sup>[33–36]</sup> By comparison, the use of heavier gallium Lewis acids (LA) has barely been touched upon. In this context, studies on the reaction of 4-ethynyl-2,6-lutidine with a range of group 13 compounds have revealed that while using B(C<sub>6</sub>F<sub>5</sub>)<sub>3</sub> leads to FLP activation processes, alkyl complexes of the heavier Al, Ga and In display a common but distinct reactivity, promoting

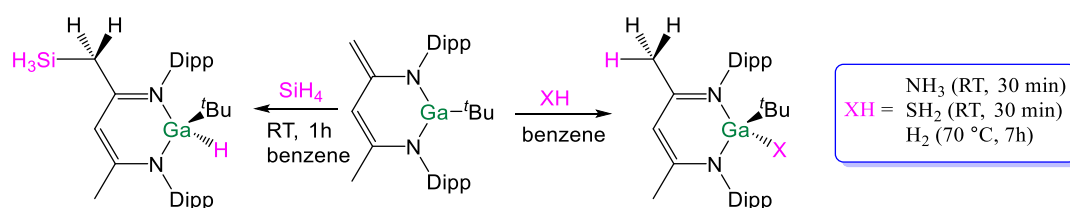


metallation of the ethynyl group with concomitant elimination of the relevant alkane (**Scheme 3.3**).<sup>[37]</sup>



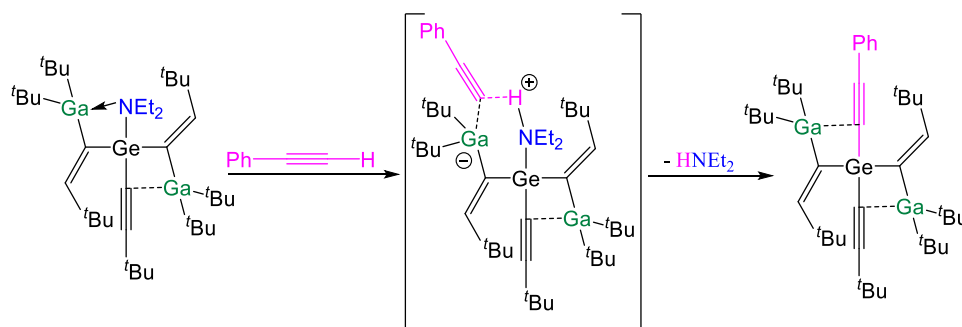
**Scheme 3.3:** Contrasting reactivity of 4-ethynyl-2,6-lutidine with group 13 compounds.<sup>[37]</sup>

Breaking new ground in the field, Aldridge has reported an ambiphilic gallium system, containing an activated  $\beta$ -diketiminato ligand, capable of cooperative activation of protic, hydridic and apolar H-X bonds (**Scheme 3.4**).<sup>[38]</sup> This work has not only demonstrated that a gallium species can in fact be a viable Lewis acid component of the FLP pair, but also that the obtained gallium hydride can act as a catalyst for the reduction of  $\text{CO}_2$  to MeOBpin using HBpin.



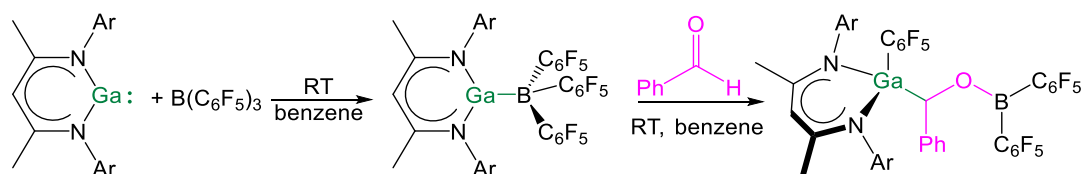
**Scheme 3.4:** Cooperative H-X bond activation using ambiphilic gallium system.<sup>[38]</sup>

Furthermore, the enhanced Lewis acidity of coordinatively unsaturated Ga alkyl fragments in close proximity to Lewis basic nitrogen atoms has proved to be key for promoting reactivity of mixed Ga/Ge complexes towards phenylacetylene and heterocumulenes (**Scheme 3.5**).<sup>[39]</sup>



**Scheme 3.5:** Reported FLP pair incorporating Ga species as a Lewis acid component for small molecule activation.<sup>[39]</sup>

Interesting recent work by Schulz has also uncovered the double agent role of Ga systems as they can reverse their role in FLP chemistry (**Scheme 3.6**). Being a part of a gallanediyl framework, acting in this case as a Lewis base component, when combined with  $[M(C_6F_5)_3]$  ( $M = B$  or  $Al$ ) LAs they have been found to facilitate insertion of benzaldehyde at room temperature.<sup>[40]</sup>



**Scheme 3.6:** Reported FLP system incorporating gallanediyl as a Lewis base component of FLP pair.<sup>[40]</sup>

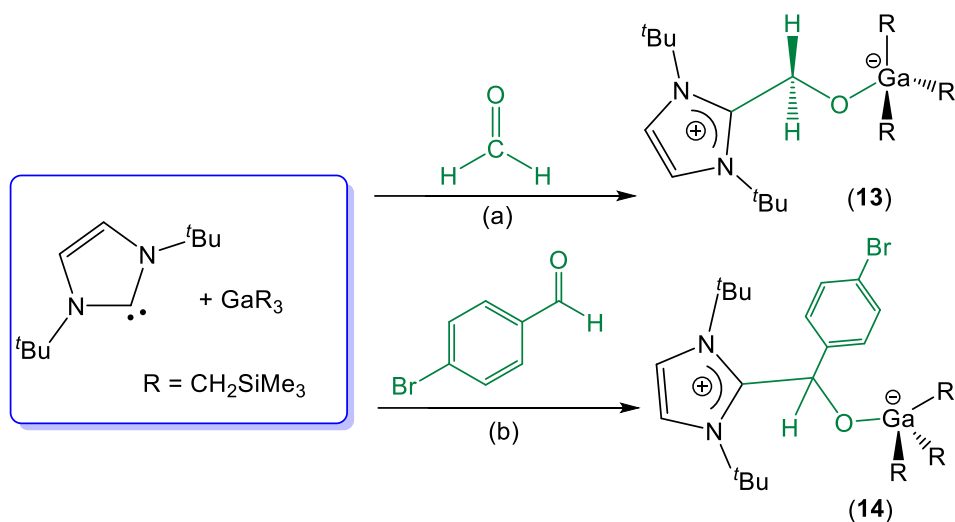
### 3.2. Aims of the chapter

Having established in our previous work (see **Chapter 2**) that steric incompatibility prevented trimethylsilylmethylgallium(III) ( $GaR_3$ ) and 1,3-bis(*tert*-butyl)imidazol-2-ylidene ( $tBu$ ) from forming a stable normal adduct, it seemed like a system with potential for FLP reactivity. This chapter details a systematic study probing the reactivity of these NHC/Ga combinations towards carbonyl compounds, an area where other, mostly, but not limited to,  $PR_3/B$  based FLP systems have shown considerable promise in synthesis and catalysis.<sup>[40–49]</sup> Combining X-ray crystallographic with spectroscopic and theoretical investigations, new insights are

provided into the intriguing chemoselectivities and mechanisms of these processes, which intensifies the potential of gallium tris(alkyl) complexes for FLP activation.

### 3.3. Reactions with aldehydes

Reacting  $\text{GaR}_3/\text{tBu}$  with the simplest and most reactive aldehyde, namely paraformaldehyde, in hexane suspension at  $0\text{ }^\circ\text{C}$  immediately produced a white precipitate which could be solubilised by addition of toluene to obtain X-ray amenable crystals of zwitterion  $[\text{tBuCH}_2\text{OGaR}_3]$  **13** in a 66% yield (**Scheme 3.7a**).



**Scheme 3.7:** FLP induced synthesis of zwitterionic compounds **13** (a) and **14** (b).

A single crystal X-ray diffraction analysis (**Fig. 3.1**) revealed the outcome of addition of the  $\text{tBu}/\text{GaR}_3$  pair across the  $\text{C}=\text{O}$  functionality forming a new, single carbon-carbon bond [i.e.  $\text{C1}-\text{C24}$ ,  $1.505(3)\text{ \AA}$ ] and an oxygen-gallium bond. The  $\text{C}_3\text{O}$ -tetracoordinated gallium atom adopts a distorted tetrahedral geometry as evidenced by the bond angles ranging from  $102.90(9)^\circ$  to  $116.28(11)^\circ$  with an average angle of  $109.16^\circ$ .  $\text{Ga}-\text{C}_{\text{alkyl}}$  and  $\text{Ga}-\text{O}$  bond distances (mean  $\text{Ga}-\text{C}$   $2.012\text{ \AA}$ ;  $\text{Ga1}-\text{O1}$   $1.9317(15)\text{ \AA}$ ) are in good agreement with literature values for other tetracoordinated gallium species.<sup>[50–52]</sup>

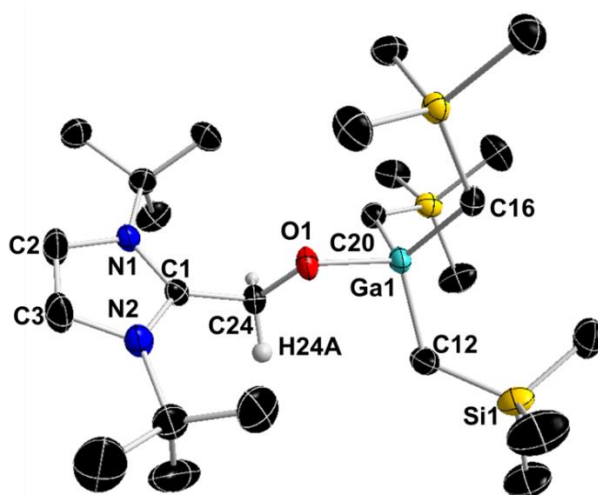


**Figure 3.1:** Molecular structure of **13** with 50% probability displacement ellipsoids. All hydrogen atoms except those on the reduced formaldehyde substrate are omitted for clarity. Selected bond distances (Å) and bond angles (°): Ga(1)-O(1) 1.9317(15), Ga(1)-C(12) 2.012(3), Ga(1)-C(16) 2.012(2), Ga(1)-C(20) 2.011(3), O(1)-C(24) 1.384(3), C(1)-C(24) 1.505(3), O(1)-Ga(1)-C(20) 103.41(9), O(1)-Ga(1)-C(12) 105.21(9), C(20)-Ga(1)-C(12) 110.86(13), O(1)-Ga(1)-C(16) 102.90(9), C(20)-Ga(1)-C(16) 116.27(11), C(12)-Ga(1)-C(16) 116.28(11), N(1)-C(1)-N(2) 107.50(19).

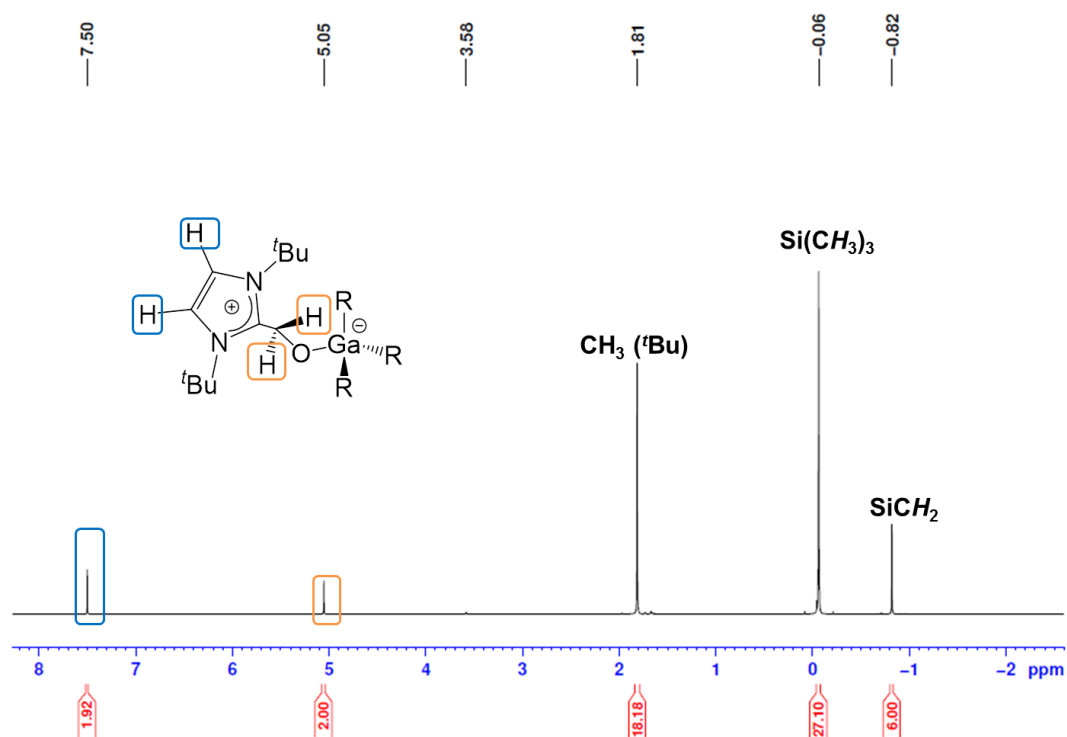


**Figure 3.2:**  $^1\text{H}$  NMR spectrum of **13** in  $d_8$ -THF solution.

The most informative resonance in the  $^1\text{H}$  NMR spectrum in  $d_8$ -THF (**Fig. 3.2**) is a singlet at 5.05 ppm for formerly aldehydic protons (*i.e.*, H24 in **Fig. 3.1**)

which displays a significant upfield shift (*vs.* 9.58 ppm in free formaldehyde). Similarly, in the  $^{13}\text{C}$  NMR spectrum, the resonances of former carbenic and C=O fragments are observed at 152.7 ppm and 58.1 ppm, respectively (*vs.* 213.2 ppm and 195.2 ppm in the free reagents).

Applying the same protocol to the aromatic aldehyde 4-bromobenzaldehyde afforded [tBuCH(*p*-Br-C<sub>6</sub>H<sub>4</sub>)OGaR<sub>3</sub>] (**14**) in 42% crystalline yield (**Scheme 3.7b**). As evidenced by X-ray crystallographic studies, **14** (**Fig 3.3**) has a similar molecular structure to **13** and displays similar gross structural features with an average angle of 109.15° around distorted tetrahedral gallium centre, an average Ga-C<sub>alkyl</sub> bond length of 2.018 Å and a Ga-O bond length of 1.9522(16) Å.

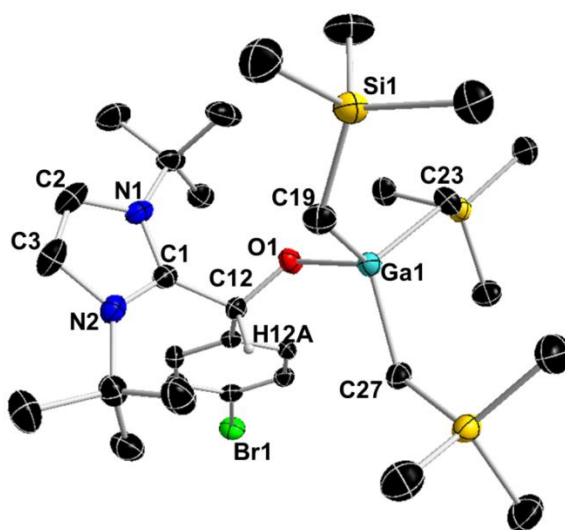
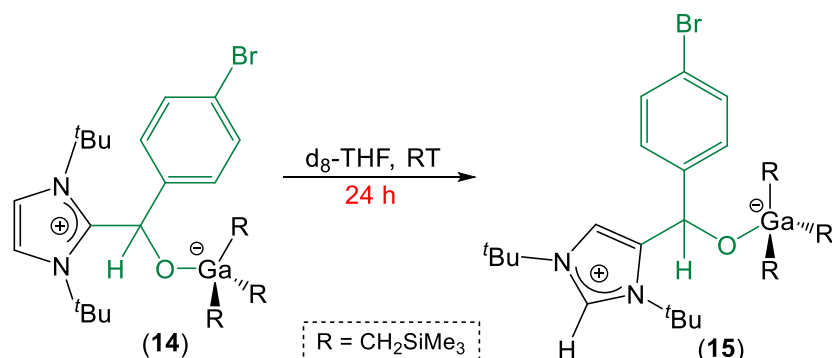


**Figure 3.3:** Molecular structure of **14** with 50% probability displacement ellipsoids. All hydrogen atoms except those on the reduced 4-bromobenzaldehyde substrate are omitted for clarity. Selected bond distances (Å) and bond angles (°): Ga(1)-O(1) 1.9522(16), Ga(1)-C(19) 2.021(2), Ga(1)-C(23) 2.005(2), Ga(1)-C(27) 2.027(2), O(1)-C(12) 1.372(3), C(1)-C(12) 1.525(3), O(1)-Ga(1)-C(23) 105.42(9), O(1)-Ga(1)-C(19) 103.48(9), C(23)-Ga(1)-C(19) 114.57(10), O(1)-Ga(1)-C(27) 102.42(8), C(23)-Ga(1)-C(27) 111.41(11), C(19)-Ga(1)-C(27) 117.58(10), N(1)-C(1)-N(2) 107.8(2).

Although in the solid state **14** has a molecular structure similar to that of **13**, NMR spectroscopic analyses revealed a much more complex scenario in solution. As **14** exhibited poor solubility in arene solvents such as C<sub>6</sub>D<sub>6</sub>, its solution studies were conducted in *d*<sub>8</sub>-THF solution where two different species containing reduced carbonyl group were observed together with the

free starting materials.<sup>[19]</sup> One species can be confidently assigned to complex **14**, displaying informative resonances in the <sup>13</sup>C NMR spectrum at 72.3 and 154.2 ppm for the OCH(Ar) and NCN fragments respectively. Interestingly, over the course of 24 hours,<sup>[20]</sup> **14** evolved completely into the new complex which could be isolated and structurally defined as  $[a^t\text{BuCH}(p\text{-Br-C}_6\text{H}_4)\text{OGaR}_3]$  (**15**) (Scheme 3.8).



**Scheme 3.8:** Solution state evolution of **14** into **15** in  $d_8$ -THF at room temperature.

Isomeric with **14**, complex **15** (Figure 3.4) also contains an OCHAR fragment coordinated to Ga, resulting from the addition of the carbene across the C=O bond of the aldehyde.

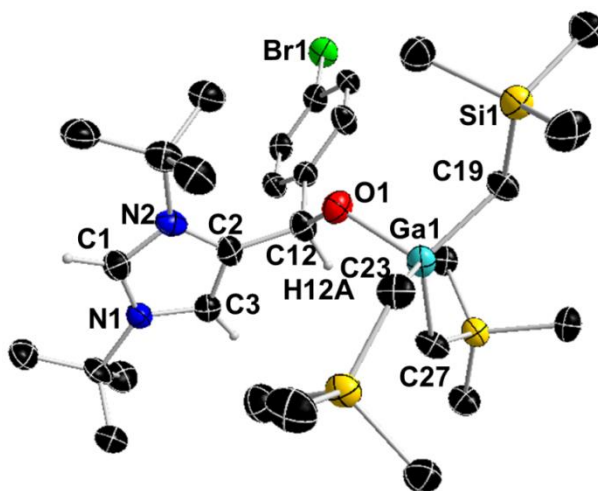


**Figure 3.4:** Molecular structure of **15** with 50% probability displacement ellipsoids. All hydrogen atoms except those on the imidazole ring and on the reduced 4-bromobenzaldehyde substrate are omitted for clarity. Selected bond distances (Å) and bond angles (°): Ga(1)-O(1) 1.943(5), Ga(1)-C(19) 2.019(8), Ga(1)-C(23) 2.020(7), Ga(1)-C(27) 2.012(8), O(1)-C(12) 1.335(9), C(2)-C(12) 1.541(10), O(1)-Ga(1)-C(27) 109.6(3), O(1)-Ga(1)-C(19) 102.0(3), C(27)-Ga(1)-C(19) 114.4(3), O(1)-Ga(1)-C(23) 102.8(3), C(27)-Ga(1)-C(23) 113.3(3), C(19)-Ga(1)-C(23) 113.3(3), N(1)-C(1)-N(2) 109.9(7).

However, in this case, this has occurred *via* one of the C atoms located at the backbone of the imidazole ring (so called abnormal<sup>[21a,22]</sup> or C4-position) [C2 in **Fig. 3.4**], whereas the former carbenic C in *t*Bu [C1 in **Fig. 3.4**] is now protonated.

Consistent with the lack of symmetry in the imidazole ring, <sup>1</sup>H NMR spectrum of **15** in d<sub>8</sub>-THF showed two singlets for the non-equivalent protons of the imidazole ring at 8.45 and 7.84 ppm (**Fig. 3.5**). Furthermore, the <sup>13</sup>C NMR spectrum displays a resonance at 72.7 ppm which can be assigned to the reduced C=O functionality (i.e., C12 in **Fig. 3.4**), whereas the formally C2 and C4 carbon atoms of *t*Bu (i.e., C1 and C2 in **Fig. 3.4**) resonate at 131.8 and 149.0 ppm respectively.

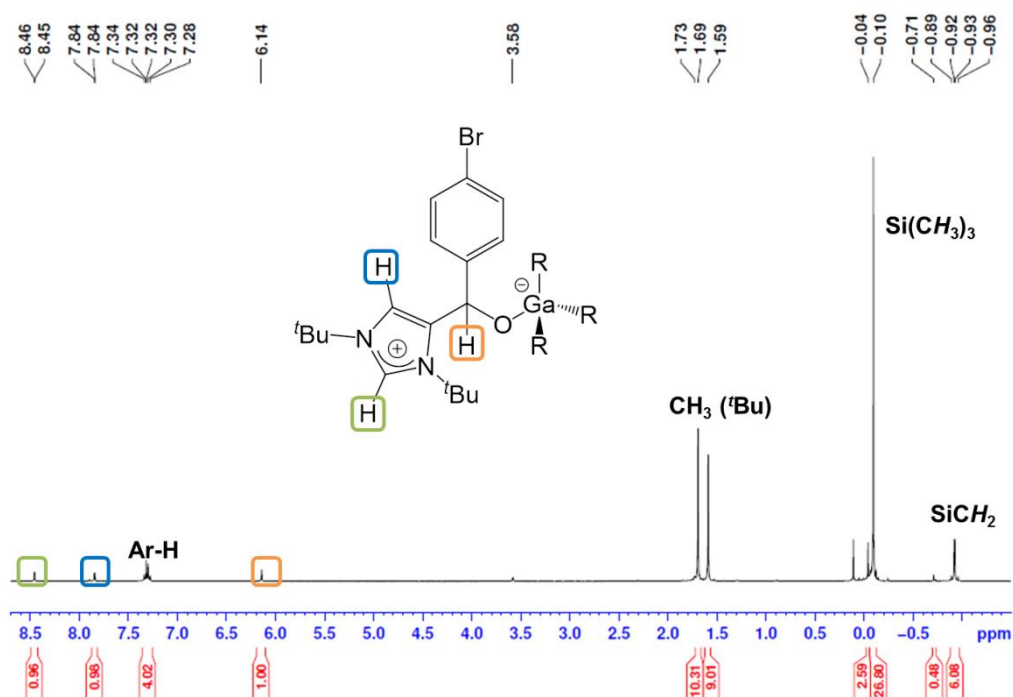


**Figure 3.5:** <sup>1</sup>H NMR spectrum of **15** in d<sub>8</sub>-THF solution.

Complexes **14** and **15** can be described as kinetic and thermodynamic products of the activation of 4-bromobenzaldehyde by GaR<sub>3</sub>/*t*Bu combinations. Supporting this interpretation, monitoring the reaction over a range of temperatures (230–323 K) revealed that at 230K, addition of *t*Bu led to the almost instantaneous formation of **14**. Gradual increase in temperature and recording of <sup>1</sup>H NMR spectra revealed an appearance of second set of

resonances at 303 K belonging to complex **15**. As the temperature was further increased, the relative amount of **15** has increased with the decrease in the amount of **14**, and after just 15 min at 323 K full conversion of **14** into **15** was evident (**Fig. 3.6**).

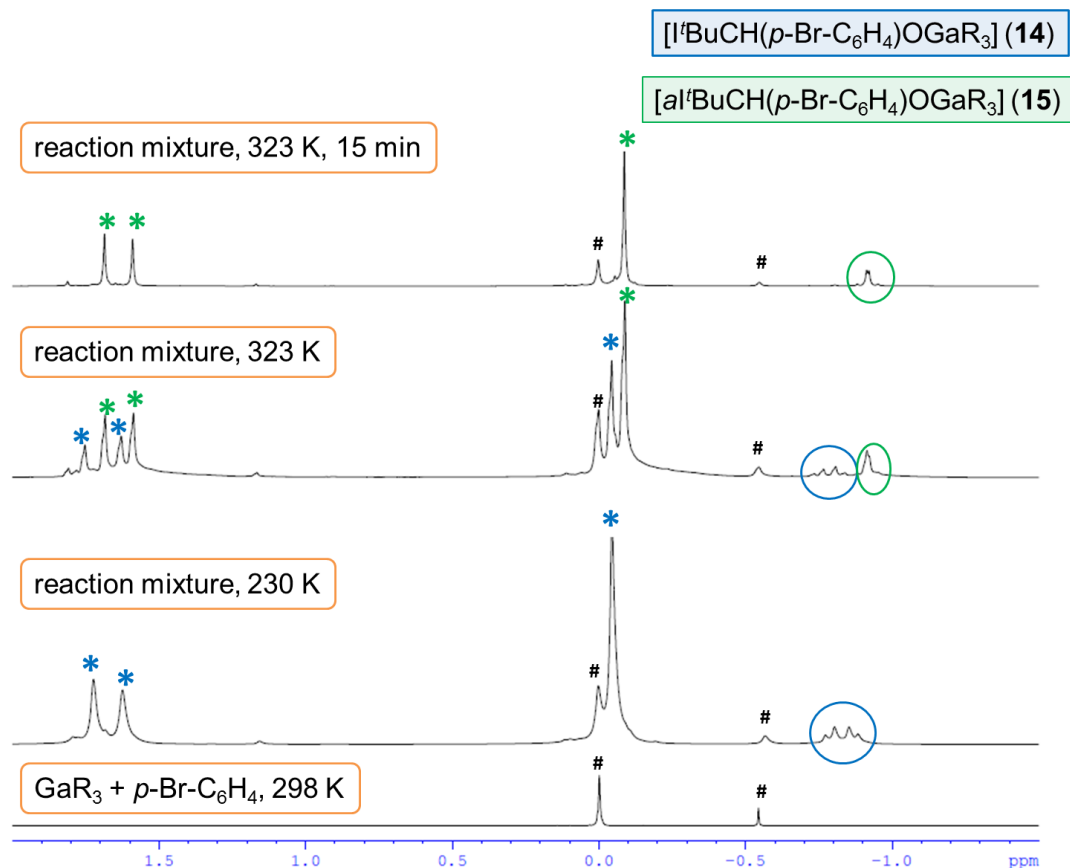


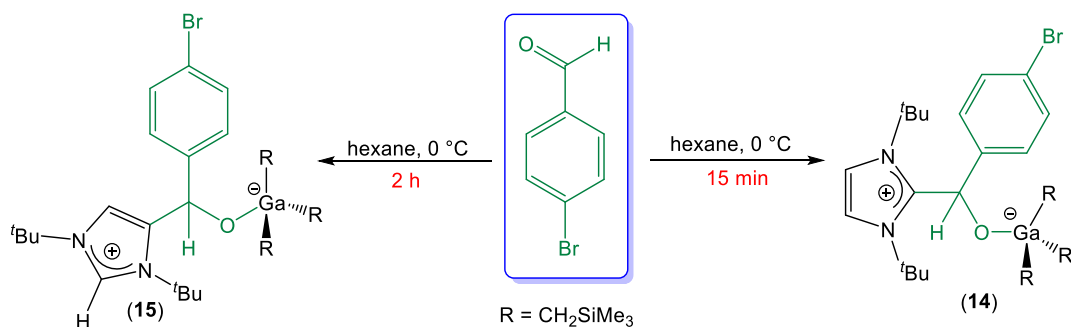
**Figure 3.6:** High field region of  $^1\text{H}$  NMR spectra of reaction mixture at different temperatures in  $d_8$ -THF. Blue labels represent resonances assigned to **14** and green those of **15**.

During these solution studies, the persistent presence of small amounts of the three components of these complexes,  $I^t\text{Bu}$ ,  $\text{GaR}_3$  and  $\text{ArCHO}$ , suggested that all these species co-exist in equilibrium. Further support was found by dissolving isolated crystals of **15** in  $d_8$ -THF the resulting  $^1\text{H}$  NMR spectrum of which showed, once again, the presence of resonances for the three starting materials. These findings are consistent with the reversible cleavage in solution of the newly formed C-C and Ga-O bond in both adducts **14** and **15**. It should be noted that a similar equilibrium has been reported previously by



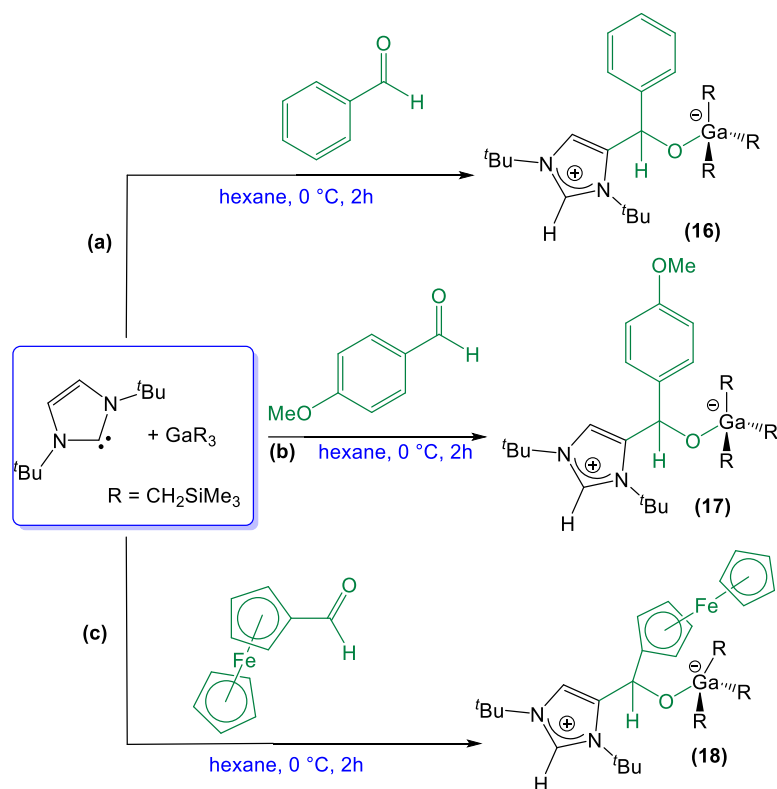
Erker for the reactions of geminal P/B FLP systems with benzaldehyde and *trans*-cinammic aldehyde.<sup>[14]</sup>

By irrefutably establishing interconversion of **14** into **15**, it was possible to prepare **15** rationally from starting materials in hexane at 0 °C simply by extending the reaction time from 15 minutes to two hours (**Scheme 3.9**).



**Scheme 3.9:** Comparison of synthetic methods to prepare kinetic (**14**) and thermodynamic (**15**) products of reaction of <sup>t</sup>Bu/GaR<sub>3</sub> pair with 4-bromobenzaldehyde.

Furthermore, this approach to access C4-substituted abnormal adducts can be successfully extended to other aldehydes, including benzaldehyde, 4-anisaldehyde and ferrocenecarboxaldehyde affording alkoxo derivatives [<sup>a</sup>tBuCH(C<sub>6</sub>H<sub>5</sub>)OGaR<sub>3</sub>] (**16**), [<sup>a</sup>tBuCH(*p*-OMe-C<sub>6</sub>H<sub>4</sub>)OGaR<sub>3</sub>] (**17**) and [<sup>a</sup>tBuCH(FeCp<sub>2</sub>)OGaR<sub>3</sub>] (**18**) in 62, 56 and 48% isolated crystalline yields respectively (**Scheme 3.10**).



**Scheme 3.10:** FLP-induced synthesis of compounds **16-18**.

Multinuclear NMR spectroscopic studies confirmed that in all cases the insertion of the substrate has taken place *via* the *t*Bu C4-position (**Table 3.1**).

**Table 3.1:** Selected  $^1\text{H}$  and  $^{13}\text{C}$  NMR shifts ( $\delta/\text{ppm}$ ) for compounds **15-18** in  $d_8$ -THF solution.

$\delta/\text{ppm}$	<b>15</b>		<b>16</b>		<b>17</b>		<b>18</b>	
	$^1\text{H}$	$^{13}\text{C}$	$^1\text{H}$	$^{13}\text{C}$	$^1\text{H}$	$^{13}\text{C}$	$^1\text{H}$	$^{13}\text{C}$
<b>CH<sub>2</sub>SiMe<sub>3</sub></b>	-0.92	1.9	-0.92	1.9	-0.93	1.9	-0.86	2.0
<b>SiMe<sub>3</sub></b>	-0.10	3.5	-0.09	3.5	-0.10	3.6	-0.03	3.6
<b>CHO</b>	6.14	72.7	6.17	73.3	6.12	72.9	6.24	100.7
<b>CH</b> (imidazole backbone)	7.84	121.8	7.85	121.8	7.83	121.7	7.67	120.0
<b>NCHN</b>	8.45	131.8	8.43	131.4	8.41	131.3	8.36	130.6
<b>C<sub>im</sub>-CHO</b>	-	149.0	-	149.3	-	147.7	-	148.0

Mimicking the situation with **15**, activation products **16-18** are in equilibrium with their free components when dissolved in  $d_8$ -THF. Interestingly, the position of this dissociative equilibrium seems to correlate with the electronic nature of the Ar group substituents of the aldehyde. Thus, by replacing the electron-withdrawing bromide with H (in **16**) or electron-donating OMe (in **17**) leads to higher ratios of free  $t$ Bu,  $\text{GaR}_3$  and the relevant aldehyde. On the other hand, with **18**, which contains a ferrocenyl substituent, no measurable sign of dissociation is observed.

An interesting solvent effect was also evident in these processes. Contrasting with the studies using  $d_8$ -THF, when  $\text{C}_6\text{D}_6$  was employed compound **16** (which is the only one partially soluble in this arene solvent), showed no evidence of being in equilibrium with its free components (**Fig. 3.7**) suggesting that donor solvents such as THF favour complex cleavage.

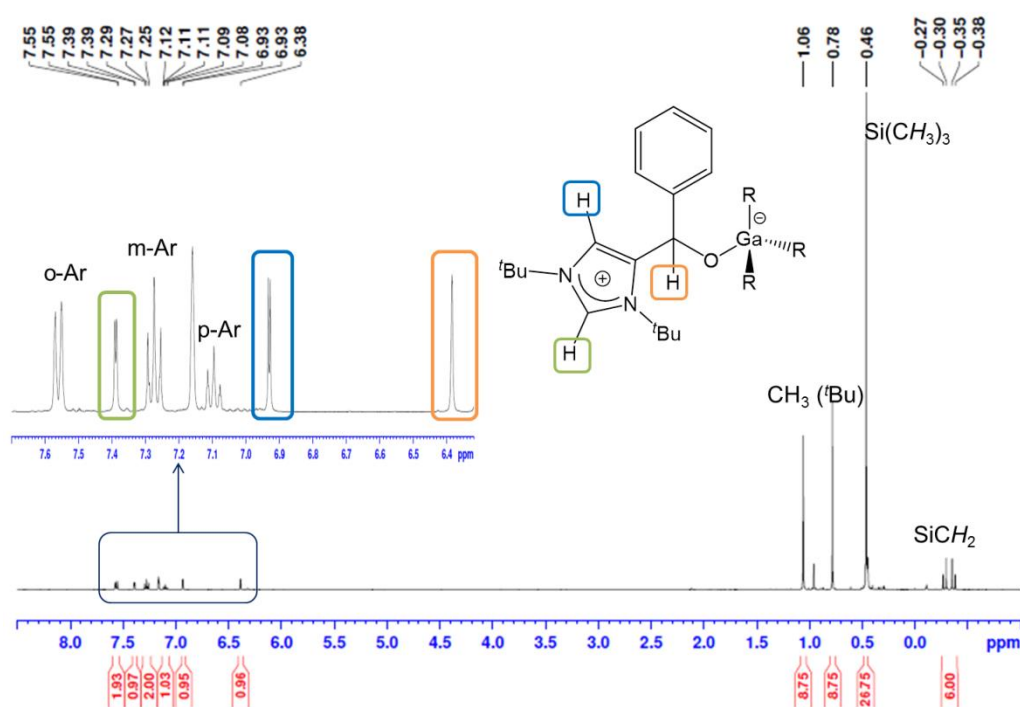


**Figure 3.7:**  $^1\text{H}$  NMR spectrum of **16** in  $\text{C}_6\text{D}_6$  solution.

### 3.4. Mechanistic implications and DFT calculations

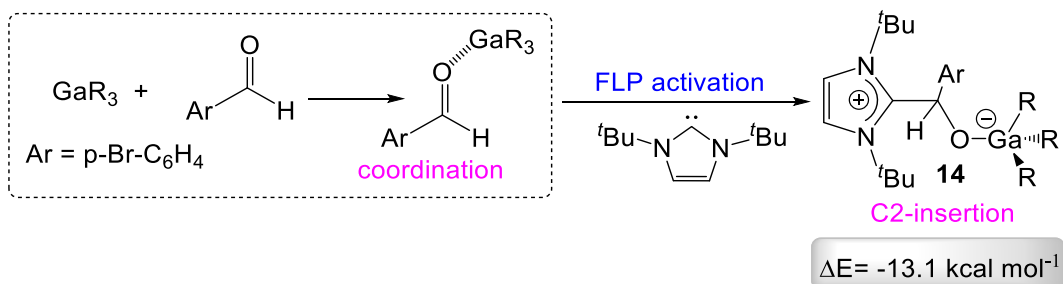
Previous studies using NHC-based FLP systems containing B<sup>[16,53]</sup> and Al<sup>[33,54]</sup> Lewis acids have shown their ability to reduce CO<sub>2</sub> and other carbonyl compounds using either the C2 or C4 position of their NHC component. However, as far as we are aware, this is the first time that both possible constitutional isomers (i.e., **14** and **15**) have been isolated and structurally defined. Furthermore, our investigations also indicate that the formation of the C4-inserted products is thermodynamically controlled. It should also be stressed that *t*Bu is not capable of activating any of the studied substrates on its own. Also despite the fact that our solution studies evidence the presence of variable amounts of free *t*Bu and GaR<sub>3</sub>, the abnormal complex [(*a**t*Bu)GaR<sub>3</sub>] (which is observed as the only product when both reagents are mixed in the absence of the aldehyde, see **Chapter 2**)<sup>[50]</sup> has not been detected.

Intrigued by these findings DFT calculations<sup>[55]</sup> were carried out employing the B3LYP method<sup>[56,57]</sup> and the 6-311G(d,p) basis set<sup>[58]</sup> to optimise structures and cast light on the thermodynamics involved in these processes. Geometrical parameters of optimised structures [*t*BuCH(p-Br-C<sub>6</sub>H<sub>4</sub>)OGaR<sub>3</sub>] (**II<sub>Ar</sub>**) and [*a**t*BuCH(p-Br-C<sub>6</sub>H<sub>4</sub>)OGaR<sub>3</sub>] (**III<sub>Ar</sub>**) are in excellent agreement with those obtained experimentally by X-ray determination of **14** and **15**, respectively (**Table 3.2**), with only a slight underestimation of the strength of the Ga-O interaction ( $\Delta[d(\text{Ga-O})_{\text{calc}}-d(\text{Ga-O})_{\text{exp}}] = 0.063$  and  $0.057 \text{ \AA}$  for **II<sub>Ar</sub>** and **III<sub>Ar</sub>** respectively). Interestingly, consistent with experimental observations, model **III<sub>Ar</sub>** was computed to be more stable than **II<sub>Ar</sub>**, although only by a modest margin of  $3.9 \text{ kcal mol}^{-1}$  (**Table 3.2**).

**Table 3.2:** Modelled structures and relative energies of inserted products **14** and **15**.

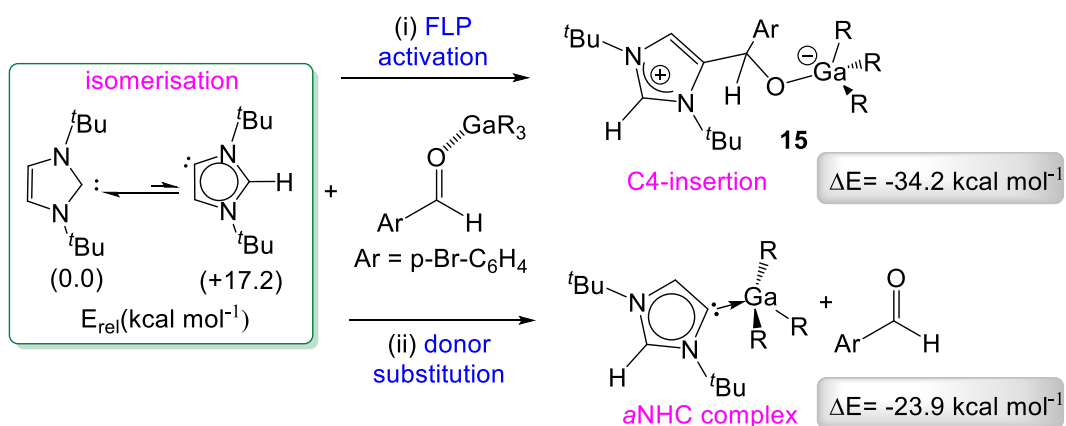
$E_{\text{relative}}$	+ 3.9 kcal mol <sup>-1</sup>		0.0 kcal mol <sup>-1</sup>	
	calculated ( <b>II</b> <sub>Ar</sub> )	experimental ( <b>14</b> )	calculated ( <b>III</b> <sub>Ar</sub> )	experimental ( <b>15</b> )
<b>C</b> <sub>NHC</sub> - <b>C</b> <sub>Ar</sub> (Å)	1.547	1.525(3)	1.532	1.541(10)
<b>Ga</b> - <b>O</b> <sub>Ar</sub> (Å)	2.016	1.9522(16)	2.000	1.943(5)
<b>N</b> - <b>C</b> - <b>N</b> (°)	107.8	107.8(2)	110.4	109.9(7)

NMR analysis of mixture of GaR<sub>3</sub> and the aldehyde revealed formation of the donor-acceptor complex in non-polar solvents (*i.e.*, C<sub>6</sub>D<sub>6</sub>) as all resonances are slightly shifted upfield when compared to those of the free starting materials. This observation suggests that formation of **14** takes place *via* initial coordination of 4-bromobenzaldehyde to Lewis acidic GaR<sub>3</sub>, which increases the polarity of the C=O bond and facilitates its nucleophilic attack by I<sup>t</sup>Bu. Supporting this interpretation, both steps were found to be exothermic, with an overall energy gain of 13.1 kcal mol<sup>-1</sup> (**Scheme 3.11**). Contrastingly, illustrating the relevance of GaR<sub>3</sub>, the reaction of I<sup>t</sup>Bu with 4-bromobenzaldehyde was found to be endothermic by 12.4 kcal mol<sup>-1</sup>, which is consistent with lack of reactivity witnessed experimentally. The activation of the aldehyde by forming a donor-acceptor intermediate is reminiscent to that proposed by Tamm for the fixation of CO<sub>2</sub> and N<sub>2</sub>O by NHC/B(C<sub>6</sub>F<sub>5</sub>)<sub>3</sub> FLP combinations.<sup>[53]</sup>



**Scheme 3.11:** Proposed scenario for the formation of **14**.

Formation of C4-substituted **15** could happen *via* a similar pathway, although in this case, abnormal *aI*<sup>t</sup>Bu should act as the Lewis base in the activation process (**Scheme 3.12**). Having just one N-atom adjacent to their carbenic position, abnormal NHCs are significantly less stabilised than their normal isomers as well as being significantly better donors.<sup>[59–61]</sup> Although usually considered as transient species, Bertrand has succeeded in the isolation of a stable free *a*NHC derived from a 1,2,3,4-tetraarylated imidazolium salt.<sup>[59]</sup>

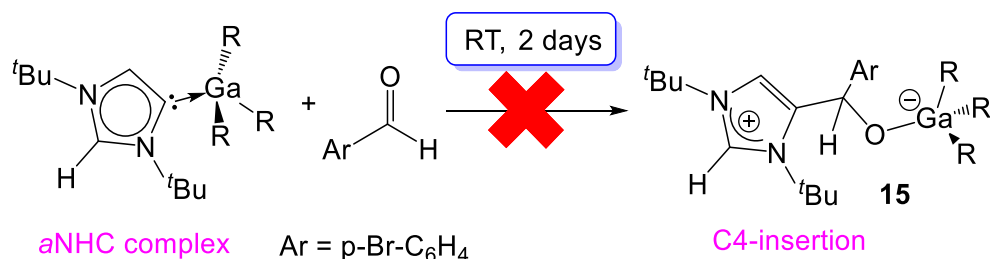


**Scheme 3.12:** Proposed scenarios for the reaction of aldehyde  $\text{GaR}_3$  donor-acceptor complex with *I*<sup>t</sup>Bu.

The computed energy difference between free *aI*<sup>t</sup>Bu and *I*<sup>t</sup>Bu is +17.2 kcal mol<sup>-1</sup> and is in a good agreement with the +13.9 kcal mol<sup>-1</sup> value obtained by Dagorne at the M06/def2-SVP level in solution (PCM with THF).<sup>[54]</sup> Assuming a fast *I*<sup>t</sup>Bu/*aI*<sup>t</sup>Bu isomerisation equilibrium, as soon as more nucleophilic *aI*<sup>t</sup>Bu is formed in solution (even as a minor product in comparison to *I*<sup>t</sup>Bu), it can react with the aldehyde· $\text{GaR}_3$  donor-acceptor complex furnishing **15** (**Scheme 3.12i**). This C4-insertion is found to be significantly more energetically

favoured (by  $10.3 \text{ kcal mol}^{-1}$ ) than the competitive formation of abnormal complex  $[(aI^t\text{Bu})\text{GaR}_3]$ , resulting from substitution of 4-bromobenzaldehyde as a donor to the  $\text{GaR}_3$  fragment (**Scheme 3.12ii**).

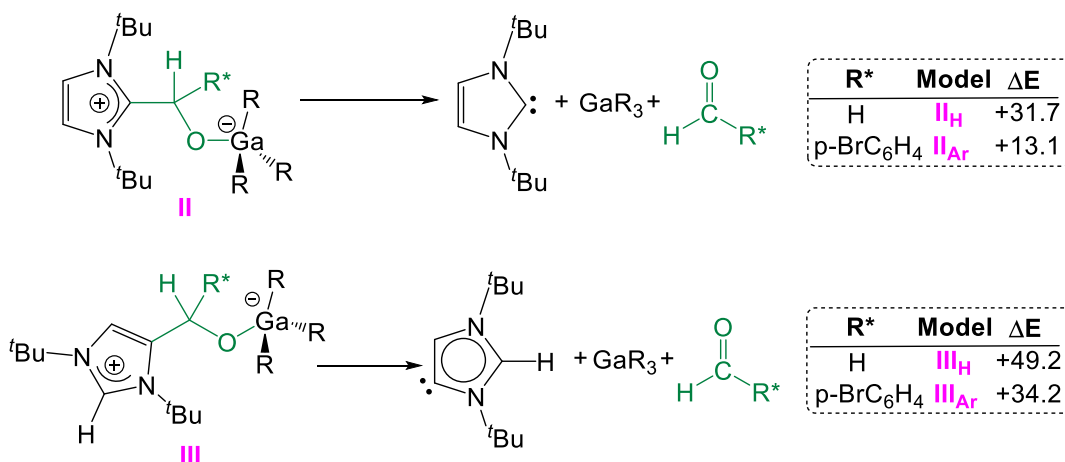
Nevertheless, a plausible alternative reaction pathway for the formation of **15** could be the insertion of 4-bromobenzaldehyde into this *a*NHC Ga complex. This possibility was investigated experimentally by dissolving isolated crystals of  $[(aI^t\text{Bu})\text{GaR}_3]$  and the aldehyde  $\text{ArCHO}$  in  $d_8$ -THF (**Scheme 3.13**).  $^1\text{H}$  NMR monitoring of the reaction mixture showed that at room temperature, after 2 days no reaction was observed between the reagents, which suggests that  $[(aI^t\text{Bu})\text{GaR}_3]$  is actually a deactivation product and once it is formed, any possible FLP reactivity with unsaturated substrates is inhibited. This is in line with previous studies in other related FLP systems containing B or Al Lewis acids for which it has been reported that the relevant abnormal NHC complexes fail to exhibit FLP reactivity.<sup>[14,16–18,54,62,63]</sup>



**Scheme 3.13:** Lack of reactivity of *aI*<sup>t</sup>Bu·GaR<sub>3</sub> towards 4-bromobenzaldehyde in  $d_8$ -THF observed experimentally.

The lability of complex **14**, which is in dynamic equilibrium with its free components, is also key in promoting the formation of **15**, as it enables over time the *I*<sup>t</sup>Bu/*aI*<sup>t</sup>Bu isomerisation. Thus complex **13**, resulting from the formal C2-insertion of formaldehyde, displays no signs of dissociation in solutions over prolonged period of time and does not seem to readily form the relevant C4-insertion isomer. Offering further support to these experimental findings, DFT calculations on the optimised structures [*I*<sup>t</sup>BuCH<sub>2</sub>OGaR<sub>3</sub>] (**II<sub>H</sub>**) and [*aI*<sup>t</sup>BuCH<sub>2</sub>OGaR<sub>3</sub>] (**III<sub>H</sub>**), showed that in this case there is not a clear thermodynamic drive for the C2/C4 isomerisation. Both models have almost identical energies (**III<sub>H</sub>** being just  $0.2 \text{ kcal mol}^{-1}$  more stable than **II<sub>H</sub>**). The

small size of the reduced aldehyde in **13** may also contribute to the lack of lability observed for this complex. In this regard, the dissociation energy of model **II<sub>H</sub>** into *t*Bu, GaR<sub>3</sub> and CH<sub>2</sub>O (**Scheme 3.14**) was found to be +31.7 kcal mol<sup>-1</sup> (18.6 kcal mol<sup>-1</sup> greater than for **II<sub>Ar</sub>**).



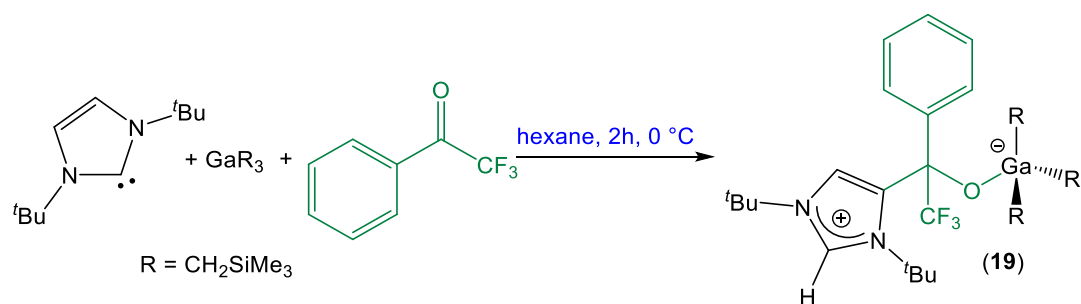
**Scheme 3.14:** Estimated dissociation energies of complexes **II** and **III**.

### 3.5. Reactions with ketones: C4 insertion vs C-H activation

Attention was next turned to the reactivity of these NHC/Ga combinations towards ketones. Initial studies using benzophenone led to the formation of the deactivation complex [(*aI*<sup>*t*</sup>Bu)GaR<sub>3</sub>]. This was best discerned in <sup>13</sup>C NMR spectrum by the observation of informative resonances at 196.1 and 159.42 ppm which can be assigned to the C=O group of benzophenone and C-Ga bond of [*aI*<sup>*t*</sup>Bu·GaR<sub>3</sub>] complex, respectively. Trying to circumvent this problem, the same reaction using the saturated version of *I*<sup>*t*</sup>Bu, namely bis(*tert*-butyl)imidazolin-2-ylidene (*SI*<sup>*t*</sup>Bu) was next probed. However even under forcing reaction conditions (60 °C, 12h), formation of an insertion product could not be detected.

Moving to the more electrophilic  $\alpha,\alpha,\alpha$ -trifluoroacetophenone, containing the strong electron withdrawing CF<sub>3</sub> group, furnished [*aI*<sup>*t*</sup>BuC(Ph)(CF<sub>3</sub>)OGaR<sub>3</sub>] (**19**) in a 63% isolated crystalline yield (**Scheme 3.15**).





**Scheme 3.15:** FLP-induced synthesis of **19**.

Established by X-ray crystallographic studies, the molecular structure of **19** (**Fig. 3.8**) bears a resemblance to that of **15** (**Fig. 3.4**), revealing that the *t*Bu has added across the C=O group of the ketone by its abnormal C4-position (*i.e.*, C2 in **Fig. 3.8**). The C<sub>3</sub>O-tetracoordinated Ga atom once again displays a distorted tetrahedral geometry (average angle 108.99°) with the newly formed Ga-O bond having a distance (1.9692(14) Å) towards the longer end of the range, but within the scope of other reported values.<sup>[51,52]</sup>

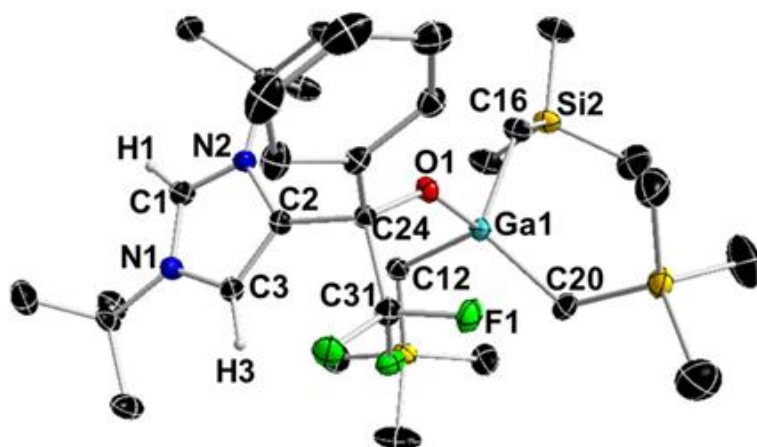


**Figure 3.8:** Molecular structure of **19** with 50% probability displacement ellipsoids. All hydrogen atoms except those on the imidazole ring are omitted for clarity. Selected bond distances (Å) and bond angles (°): Ga(1)-O(1) 1.9692(14), Ga(1)-C(12) 2.022(2), Ga(1)-C(16) 2.012(2), Ga(1)-C(20) 2.010(2), O(1)-C(24) 1.361(2), C(2)-C(24) 1.544(3), O(1)-Ga(1)-C(20) 107.81(9), O(1)-Ga(1)-C(12) 104.63(8), C(20)-Ga(1)-C(12) 116.46(9), O(1)-Ga(1)-C(16) 96.37(8), C(20)-Ga(1)-C(16) 115.00(10), C(12)-Ga(1)-C(16) 113.70(10), N(1)-C(1)-N(2) 110.93(18).

Multinuclear NMR studies are consistent with the retention of the solid-state structure of **19** in *d*<sub>8</sub>-THF solution. As observed for compounds **15-18**, two

singlets appear in the  $^1\text{H}$  NMR spectrum at 8.67 and 7.21 ppm for the imidazole hydrogen atoms, which is consistent with the lack of symmetry in the heterocyclic ring (**Fig. 3.9**).  $^{13}\text{C}$  NMR spectrum showed an informative resonance at 81.7 ppm belonging to the reduced C=O group (which resonates at 191.2 ppm in the starting material). Interestingly though, the transformation of the ketone into the gallium alkyl(alkoxide) **19** has little effect on the  $^{19}\text{F}$  NMR spectrum where a broadening of the resonance is evident, most probably caused by a hindered rotation around the O-C bond in the chiral alkoxide, but with little significant difference in the chemical shift (-69.9 ppm in **19** vs -72.4 ppm in free trifluoroacetophenone).

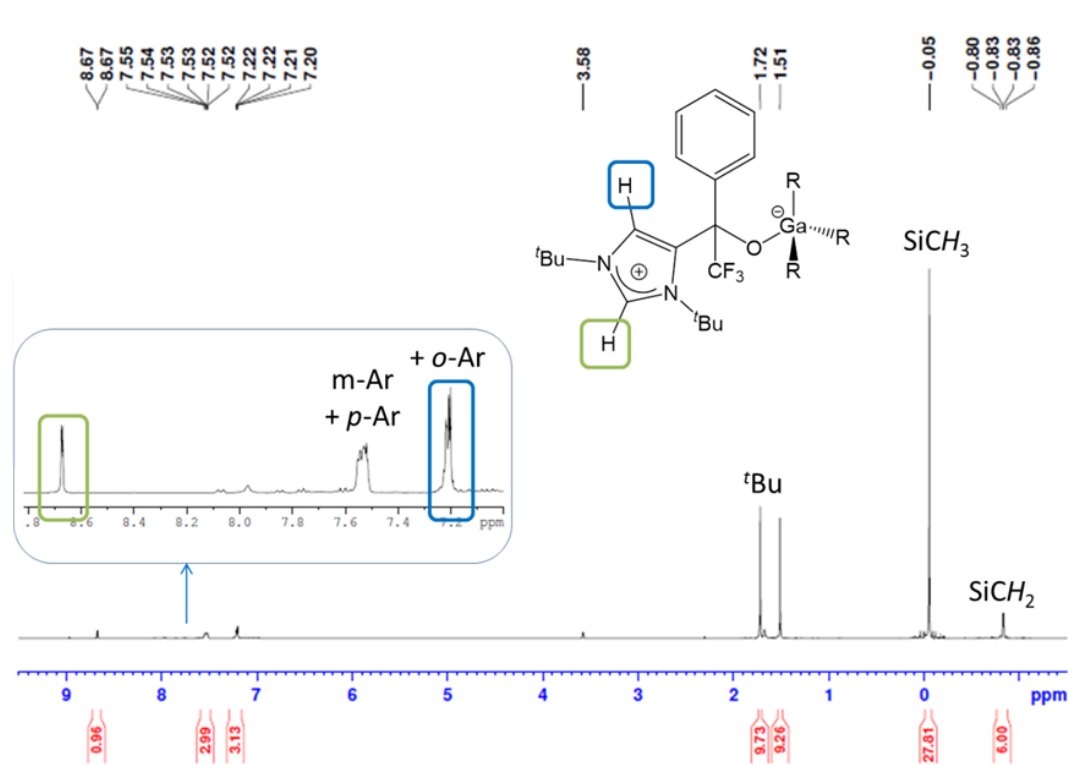
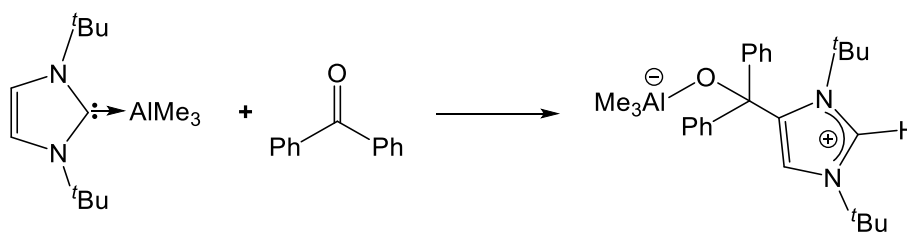


**Figure 3.9:**  $^1\text{H}$  NMR spectrum of **19** in  $d_8$ -THF solution.

Contrasting with the reactivity studies on aldehydes,  $^1\text{H}$  NMR monitoring of the reaction of  $t\text{Bu}$ ,  $\text{GaR}_3$  and  $\text{PhC(O)CF}_3$  did not detect the initial formation of a C2 insertion isomer or an equilibrium between the starting materials and adduct **19**. A plausible explanation may lie in the large steric hindrance of electron withdrawing  $\text{CF}_3$ , which has been described as intermediate in size between  $t\text{Pr}$  and  $t\text{Bu}$  substituents,<sup>[64,65]</sup> which may make difficult the approach of normal  $t\text{Bu}$  to the electrophilic C=O group of the substrate. The reduced

steric congestion on *a*I'Bu, having just one N'Bu-fragment adjacent to its carbenic position, seems to be sufficient to promote instead formation of C4-insertion adduct **19**. Further support was found by DFT calculations, where the reaction of I'Bu, GaR<sub>3</sub> and PhC(O)CF<sub>3</sub> to give [*a*I'BuC(Ph)(CF<sub>3</sub>)OGaR<sub>3</sub>] (**III**<sub>CF<sub>3</sub></sub>) was calculated to be exergonic by 14.5 kcal mol<sup>-1</sup>. The rearrangement of the free carbene, and subsequent reaction with the substrate was also suggested by Dagorne in a recent report on the activation of benzophenone with AlMe<sub>3</sub>/I'Bu pair (**Scheme 3.16**).<sup>[54]</sup>



**Scheme 3.16:** Reaction of AlMe<sub>3</sub>-I'Bu adduct with benzophenone.<sup>[54]</sup>

Geometrical parameters of the optimised structure **III**<sub>CF<sub>3</sub></sub> (**Fig. 3.10**) are in excellent agreement with those found experimentally by X-ray analysis of **19** (**Table 3.3**).

**Table 3.3:** Comparison of calculated and experimentally found structural parameters for compound **19**.

Structural parameters	<i>a</i> I'BuC(CF <sub>3</sub> )(C <sub>6</sub> H <sub>4</sub> )OGaR <sub>3</sub> ( <b>19</b> )	
	calculated ( <b>III</b> <sub>CF<sub>3</sub></sub> )	experimental ( <b>19</b> )
C <sub>NHC</sub> -C <sub>substrate</sub> (Å)	1.552	1.544(3)
Ga-O <sub>substrate</sub> (Å)	2.061	1.9692(14)
N-C-N (°)	110.7	110.93(18)

Contrastingly, attempts to model the structure of the C2-insertion product analogous to **II**<sub>Ar</sub> and **II**<sub>H</sub>, led to the optimisation of a structure where the normal carbenic position is located at 5.708 Å of the C=O group of the ketone, evidencing the steric incompatibility of the reagents to promote a C2 addition



constitution of these compounds.  $^1\text{H}$  NMR spectrum of **20** confirmed the presence of an imidazolium cation with singlets at 8.72 and 7.78 ppm for the imidazole protons integrating one and two hydrogen atoms respectively, as well as the formation of an enolate anion with olefinic protons resonating at 3.86 and 4.12 ppm. The enolate form of anion was further established by observing two resonances at 163.3 and 79.9 ppm in the  $^{13}\text{C}$  NMR spectrum belonging to the  $\text{C}=\text{CH}_2$  fragment.

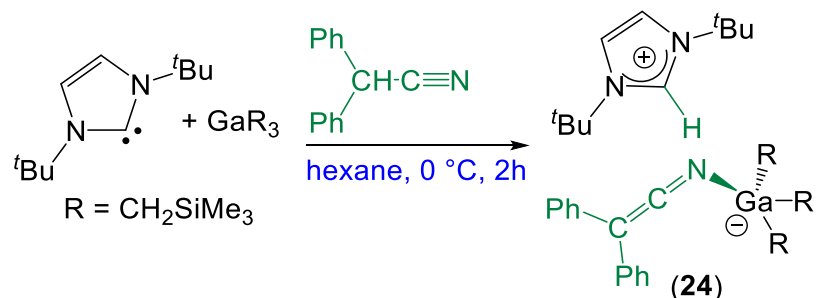
Spectroscopic analyses of compounds **20-23** have revealed their structural similarity on a molecular level (**Table 3.4**) with differences arising only from the nature of the carbene and/or substituent used.

**Table 3.4:** Selected  $^1\text{H}$  and  $^{13}\text{C}$  NMR shifts ( $\delta/\text{ppm}$ ) for compounds **20-23** in  $d_8$ -THF.

$\delta/\text{ppm}$	<b>20</b>		<b>21</b>		<b>22</b>		<b>23</b>	
	$^1\text{H}$	$^{13}\text{C}$	$^1\text{H}$	$^{13}\text{C}$	$^1\text{H}$	$^{13}\text{C}$	$^1\text{H}$	$^{13}\text{C}$
NCHN	8.72	131.9	8.75	132.0	7.43	152.9	7.87	152.8
$\text{CH}_2=\text{C}$	3.86	79.9	3.13	81.4	3.85	79.8	3.16	81.7
	4.12		3.85		4.13		3.86	
$\text{CH}_2=\text{C}-\text{O}-\text{Ga}$	-	163.3	-	165.7	-	163.0	-	165.6

The isolation of **20-23** uncovers the ability of these NHC/Ga systems for the activation of acidic C-H bonds. Evidencing their cooperative behaviour, neither the carbenes employed nor  $\text{GaR}_3$  can activate these substrates independently. This approach can be extended to other unsaturated organic substrates containing  $\alpha$ -acidic protons. Thus  $i\text{Bu}/\text{GaR}_3$  readily deprotonates diphenylacetonitrile, affording novel  $[\{i\text{BuH}\}^+\{\text{Ph}_2\text{C}=\text{C}=\text{NGaR}_3\}^-]$  (**24**) in 64% yield (**Scheme 3.18**), with  $i\text{Bu}$  abstracting the  $\alpha$ -proton of the substrate while the alkyl groups on Ga are mere spectators in the reaction. This reactivity contrasts with that observed by Mizel for the reaction of 4-ethynyl-2,6-lutidine with  $\text{GaMe}_3$  where metalation of the ethynyl groups is observed along with methane elimination (see **Scheme 3.3**).<sup>[37]</sup> Replacing  $i\text{Bu}$  by  $\text{Si}i\text{Bu}$

furnished the analogous compound  $[\{SI^tBuH\}^+\{Ph_2C=C=NGaR_3\}^-]$  (**25**) in 86% yield.



**Scheme 3.18:** Deprotonation of diphenylacetonitrile by  $I^tBu/GaR_3$  and formation of **24**.

Elucidated by a single crystal X-ray diffraction analysis, the molecular structure of **24** shows a salt-like ion-pair structure comprised of a protonated imidazolium cation charge-balanced by a heteroleptic gallate anion containing a 3:1 ratio of monosilyl groups to keteniminate ligands (**Fig. 3.11**).

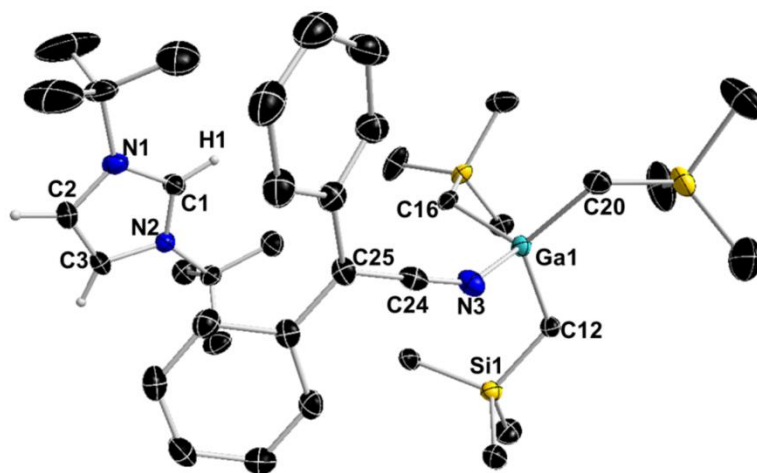


**Figure 3.11:** Molecular structure of **24** with 50% probability displacement ellipsoids. All hydrogen atoms except those on the imidazole ring and minor disorder in one of two <sup>t</sup>Bu substituents are omitted for clarity. Selected bond distances (Å) and bond angles (°): Ga(1)-N(3) 2.0726(19), Ga(1)-C(12) 2.000(2), Ga(1)-C(16) 1.988(2), Ga(1)-C(20) 1.999(3), N(3)-C(24) 1.171(3), C(24)-C(25) 1.378(3), N(3)-Ga(1)-C(20) 101.08(9), N(3)-Ga(1)-C(12) 100.57(9), C(20)-Ga(1)-C(12) 113.75(11), N(3)-Ga(1)-C(16) 103.06(9), C(20)-Ga(1)-C(16) 117.63(10), C(12)-Ga(1)-C(16) 116.82(10), N(1)-C(1)-N(2) 109.7(2).

The heteroallene nature of the keteniminate ligand is evident from the shortening of the C24-C25 bond (1.378(3) Å) and elongation of the N3-C24 bond (1.171(3) Å) compared to those in the free nitrile Ph<sub>2</sub>CHCN (1.470(2) Å and 1.147(2) Å, respectively).<sup>[66]</sup> These bond distances as well as the near linearity of the C25-C24-N3 angle (175.26°) are in close agreement with other structurally characterised metal-keteniminate complexes.<sup>[66–70]</sup> As far as is ascertained, this is the first example of a structurally characterised Ga-keteniminate complex. Its <sup>1</sup>H NMR spectrum in d<sub>8</sub>-THF displays three singlets for the imidazolium cation at 8.68, 7.59 and 1.56 ppm for the N<sub>2</sub>CH, NCH and <sup>t</sup>Bu groups respectively. In agreement with previous literature values, the newly formed ketenimine ligand gives rise to two low intensity resonances in the <sup>13</sup>C NMR spectrum, at 55.7 and 143.4 ppm for the Ph<sub>2</sub>C and C=N groups respectively. The ν(C=C=N) stretch, which is the most characteristic vibrational mode in the IR spectrum for the ketenimine ligand is visible at 2073.5 cm<sup>-1</sup>.<sup>[67–70]</sup> Molecularly analogous **25** displays in its <sup>13</sup>C NMR spectrum two low intensity resonances for Ph<sub>2</sub>C and C=N groups at 55.6 and 143.1 ppm respectively, whilst the imidazolinium cation can be best characterised by a sharp singlet at 3.75 ppm in <sup>1</sup>H NMR spectrum integrating to four protons corresponding to olefinic backbone.

Similarly as it was found for ketones, the <sup>t</sup>Bu/GaR<sub>3</sub> pair was not reactive enough to achieve addition across the C≡N bond in nitrile compounds such as benzonitrile. The analysis of the reaction mixture revealed the deactivation of the pair by formation of a<sup>t</sup>Bu·GaR<sub>3</sub> best evidenced by a resonance at 159.3 ppm in <sup>13</sup>C NMR spectrum corresponding to the C<sub>im</sub>-Ga bond (**Figure 3.12**).

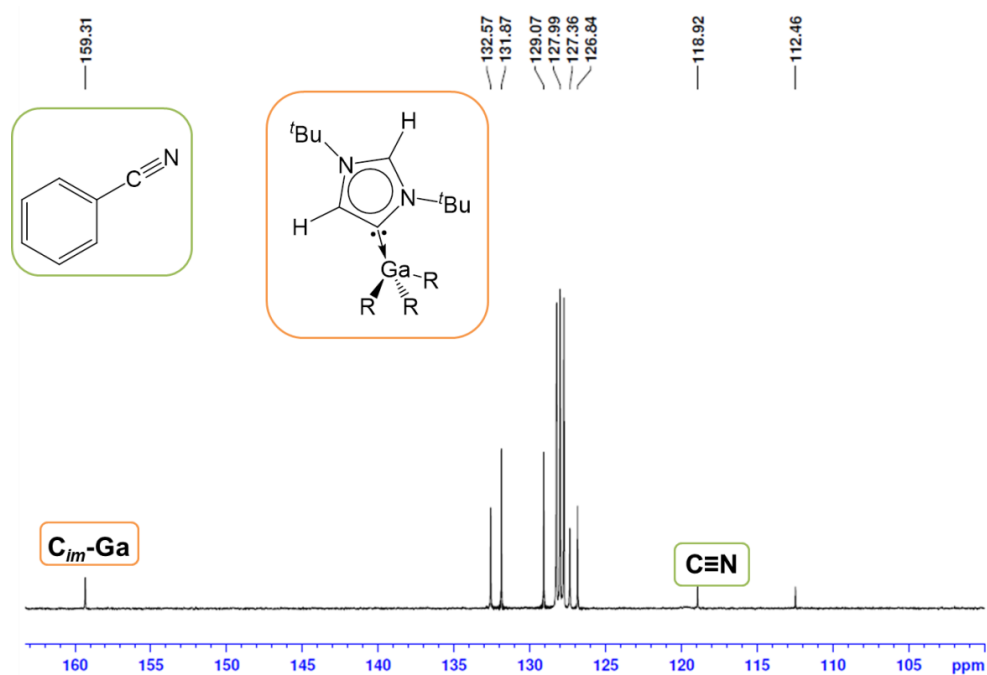
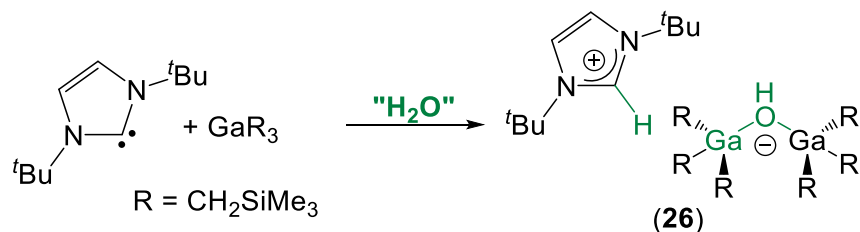


**Figure 3.12:**  $^{13}\text{C}$  NMR spectrum of reaction mixture of  $\text{GaR}_3$ ,  $t\text{Bu}$  and  $\text{PhCN}$  in  $\text{C}_6\text{D}_6$ .

### 3.6. C-H activation of other substrates bearing acidic protons

While studying the FLP reactivity of the  $\text{GaR}_3/t\text{Bu}$  pair towards various substrates, we isolated and structurally characterised mixed imidazolium gallate [ $\{t\text{BuH}\}^+\{(\text{GaR}_3)_2\text{OH}\}^-$ ] (**26**). This serendipitous product formation is most likely due to the reaction with trace amounts of moisture present in the reaction mixture (Scheme 3.19).



**Scheme 3.19:** Activation of the O-H bond of water with  $t\text{Bu}/\text{GaR}_3$  FLP pair affording **26**.



X-ray crystallographic studies established the salt-like ion pair structure of **26** where again imidazolium cation is counterbalanced with a gallate anion, however this time the anion is a dinuclear species (**Figure 3.13**). The hydroxy group acts as a bridge between the two GaR<sub>3</sub> units with bond lengths of 1.976(2) Å for Ga1-O1 and 1.962(2) Å for Ga2-O1. Both Ga atoms exhibit a distorted tetrahedral geometry with average bond angles of 108.91° and 109.10° around Ga1 and Ga2, respectively and mean Ga-C bond lengths of 2.007 Å and 1.989 Å all of which are in good agreement with other tetracoordinated Ga complexes.<sup>[50–52]</sup>

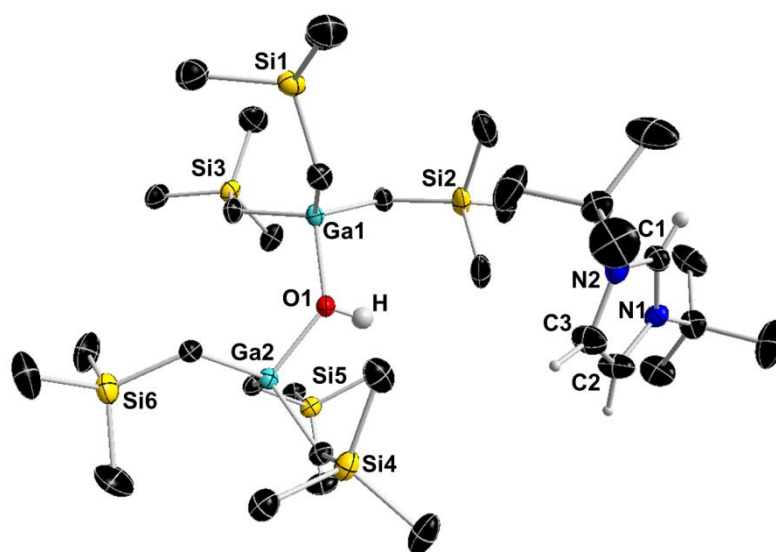
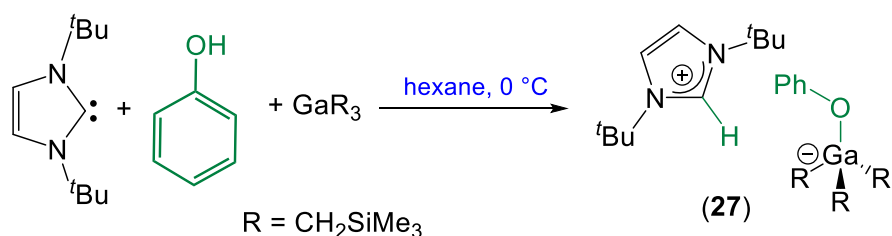


**Figure 3.13:** Molecular structure of **26** with 50% probability displacement ellipsoids. All hydrogen atoms except those on the imidazole ring and hydroxy ligand are omitted for clarity. Selected bond distances (Å) and bond angles (°): Ga(1)-O(1) 1.976(2), Ga(1)-C(12) 2.005(3), Ga(1)-C(16) 2.012(3), Ga(1)-C(20) 2.004(3), Ga(2)-O(1) 1.962(2), Ga(2)-C(24) 2.007(3), Ga(2)-C(28) 1.999(3), Ga(2)-C(32) 1.962(2).

This outcome is significant because it illustrates the cooperativity of GaR<sub>3</sub> and carbene, both of which are moisture sensitive. The decomposition of NHCs, caused by reaction with water which leads to ring opening and formation of formamide,<sup>[71]</sup> is more pronounced in the case of saturated NHC (*i.e.*, SI<sup>t</sup>Bu) due to the lack of aromatic stabilisation. However, even SI<sup>t</sup>Bu/GaR<sub>3</sub> pair was found to afford compound analogous to **26** (but incorporating {SI<sup>t</sup>BuH}<sup>+</sup> cation).

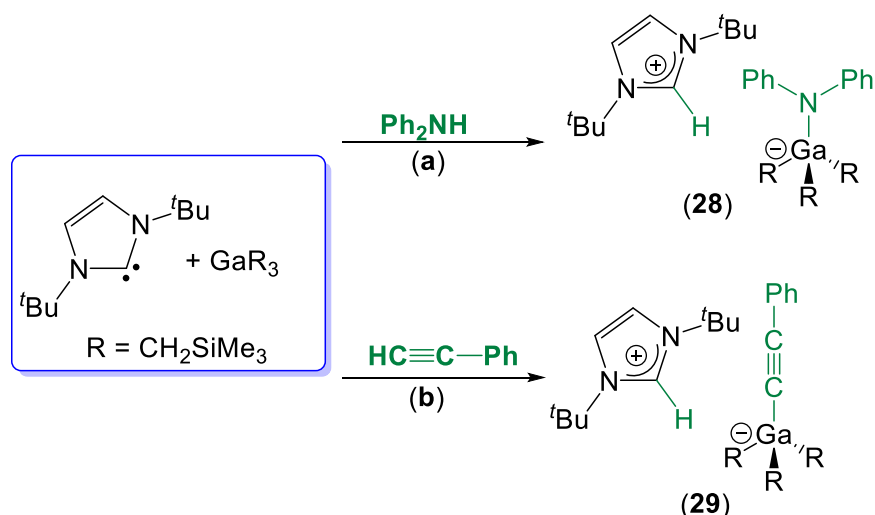
Despite its reproducibility when the solvent is not perfectly dry, targeted synthesis of **26** using stoichiometric amounts of H<sub>2</sub>O has not yet been achieved, however we were

able to prepare a closely related complex in  $[\{t\text{BuH}\}^+\{\text{GaR}_3\text{OPh}\}^-]$  (**27**) by deprotonation of phenol in hexane. Considering the relatively high acidity of phenol, this deprotonation can be achieved by either of the two components on their own (*i.e.*,  $t\text{Bu}$  or  $\text{GaR}_3$ ), as evidenced by the mixture of products obtained when phenol was added to the hexane suspension of the  $t\text{Bu}/\text{GaR}_3$  pair. However, if phenol was added to the hexane suspension of  $t\text{Bu}$ , followed by the addition of  $\text{GaR}_3$ , a more controlled deprotonation was achieved and **27** was isolated in 76% yield (**Scheme 3.20**). The clean synthesis of **27** was confirmed by elemental and  $^1\text{H}$  NMR spectroscopic analysis which unambiguously revealed a 1:3 phenoxy:monosilyl ratio.



**Scheme 3.20:** FLP-induced synthesis of **27**.

The O-H activation of phenol led us to consider the reactivity of the  $t\text{Bu}/\text{GaR}_3$  pair towards diphenylamine ( $\text{Ph}_2\text{NH}$ ) and phenylacetylene ( $\text{PhC}\equiv\text{CH}$ ). Thus, by following the same order of addition established for the synthesis of **27**, N-H and C-H activation of diphenylamine and phenylacetylene respectively was accomplished, affording  $[\{t\text{BuH}\}^+\{\text{GaR}_3\text{NPh}_2\}^-]$  (**28**) and  $[\{t\text{BuH}\}^+\{\text{GaR}_3\text{C}\equiv\text{CPh}\}^-]$  (**29**) (**Scheme 3.21**).



**Scheme 3.21:** FLP-induced synthesis of **28** and **29**.

NMR spectroscopic analysis of isolated solid revealed that **28** was only one of the products in a mixture. In attempts to obtain **28** as the sole product or at least to separate it from the mixture, the order of addition of reagents was varied, as well as temperature and introducing polar solvent (THF). However, these changes were not successful and thus only intractable mixtures were obtained. One potential explanation for complications encountered in this reaction could be due to the fact that amines as Lewis bases can form a Lewis adduct with  $\text{GaR}_3$  or even a new, competing FLP system. This is further supported by previous reports on FLP systems incorporating amine as a Lewis base component.<sup>[72–74]</sup>

On the other hand, the formation of **29** (isolated in 46% yield) was clean and controlled as evidenced from  $^1\text{H}$  NMR spectroscopic data and elemental analysis. The FLP-induced C-H activation affording **29** is in sharp contrast with the reactivity of the  $\text{GaMe}_3$  and 4-ethynyl-2,6-lutidine pair (**Scheme 3.3**) where deprotonation of terminal alkyne by  $\text{GaMe}_3$  took place. The most informative resonance in  $^1\text{H}$  NMR spectrum of **29** is a singlet at 8.80 ppm corresponding to the imidazolium cation confirming that the *t*Bu abstracts the proton and not  $\text{GaR}_3$ , which is further supported by the 3:1 relative ratio of monosilyl:phenyl groups.

Compounds **27-29** could all be isolated as crystals and their structures were elucidated by X-ray diffraction analysis. These displayed similar gross structural features of a salt-like ion-pair structure comprised of a protonated imidazolium

cation charge-balanced by a heteroleptic gallate anion. The gallate anion contains three monosilyl groups and the relevant anionic fragment stemming from the deprotonation of the substrate, that is, alkoxo,  $\text{PhO}^-$  (**27**), amido  $\text{Ph}_2\text{N}^-$  (**28**) and alkynyl  $\text{PhC}\equiv\text{C}^-$  (**29**) ligand (**Figure 3.14**).

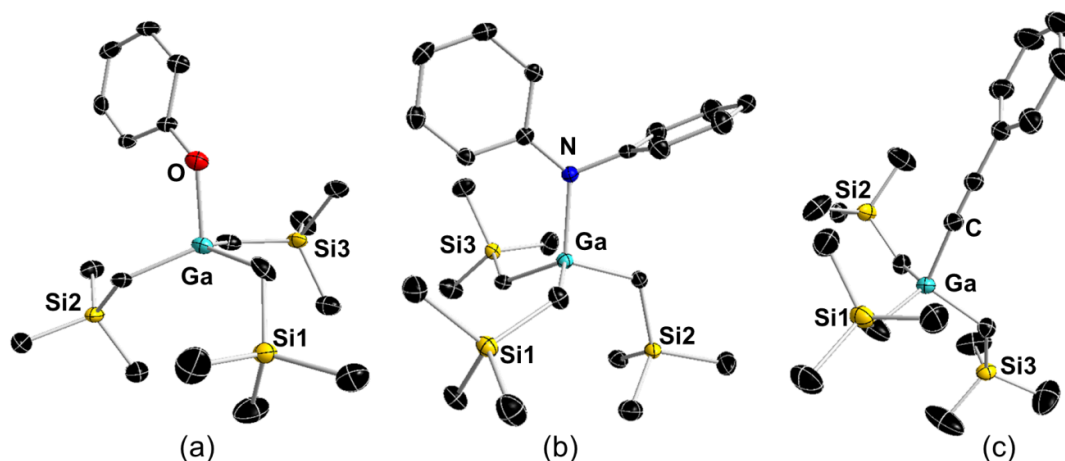


**Figure 3.14:** Anionic moiety of molecular structures of a) **27**, b) **28** and c) **29** with 50% probability displacement ellipsoids. All hydrogen atoms and disorder components are omitted for clarity.

In all three structures, as in **24**, Ga-centre adopts a distorted tetrahedral geometry as evidenced by C-Ga-X bond angles ( $X = \text{C}, \text{O}$  or  $\text{N}$ ) ranging from  $95.4(2)^\circ$  to  $115.6(2)^\circ$  [average angle  $108.87^\circ$  in **27**,  $109.33^\circ$  in **28** and  $109.36^\circ$  in **29**]. The Ga-C<sub>alkyl</sub> distances (**Table 3.5**) show little variation [mean  $2.016 \text{ \AA}$  in **27**,  $2.023 \text{ \AA}$  in **28** and  $2.022 \text{ \AA}$  in **29**] and are in excellent agreement with values of other tetracoordinated Ga species.<sup>[50–52]</sup> The Ga-O bond distance in **27** ( $1.981(4) \text{ \AA}$ ) shows good agreement with literature values for Ga complexes containing terminal alkoxy ligands.<sup>[51]</sup> The Ga-N bond length of  $2.0150(17) \text{ \AA}$  in **28** is only slightly shorter than the Ga-N distance reported for the lithium gallate<sup>[75]</sup> incorporating  $[\{\text{Ph}_3\text{Ga}(\mu\text{-NMe}_2)\text{GaPh}_3\}^-]$  anion (Ga-N =  $2.051(1) \text{ \AA}$ ) consistent with the terminal *vs* bridging mode of amido ligand. The Ga-C1 bond in **29** (**Fig 3.14c**) of  $2.031(3) \text{ \AA}$  is only slightly elongated in comparison with the Ga-C bond distance found in anionic  $[\{\text{Ga}(\text{CCSiMe}_3)_3(2,6\text{-}^i\text{Pr}_2\text{C}_6\text{H}_3\text{N}(\text{SiMe}_3))\}^-]$  (average Ga-C =  $1.969 \text{ \AA}$ ),<sup>[76]</sup> whilst the bond angle Ga-C1-C2 of  $175.7(2)^\circ$  illustrates the near linearity of the alkynyl ligand.

The bond length of 1.205(4) Å for C1-C2 (Fig 12c) in **29** is consistent with a triple bond.

**Table 3.5:** Selected bond lengths (Å) and bond angles (°) for compounds **27-29**.

	27 (X = O)	28 (X = N)	29 (X = C)
Ga-C <sub>alkyl</sub>	2.000(6)	2.022(2)	2.011(3)
Ga-C <sub>alkyl</sub>	2.029(6)	2.031(2)	2.038(4)
Ga-C <sub>alkyl</sub>	2.020(5)	2.015(2)	2.018(4)
Average Ga-C <sub>alkyl</sub>	2.016	2.023	2.022
Ga-X	1.981(4)	2.0150(17)	2.031(3)
Average angle around	108.87	109.33	109.36

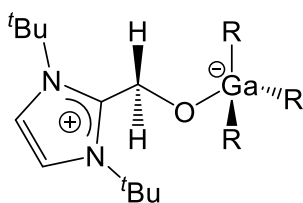
### 3.7. Conclusions and future work

Breaking new ground in organogallium chemistry, bulky trisalkylgallium, Ga(CH<sub>2</sub>SiMe<sub>3</sub>)<sub>3</sub>, has been found to be a viable, effective Lewis acid for promoting small molecule activation when combined with a strong base such as 1,3-bis(*tert*-butyl)imidazol-2-ylidene (I<sup>t</sup>Bu) forming a new Frustrated Lewis pair. The activation of carbonyl compounds can be achieved either by reduction of the C=O functionality affording zwitterionic compounds such as [I<sup>t</sup>BuCH<sub>2</sub>OGaR<sub>3</sub>] (**13**) by forming a new C-C bond, or by C-H bond activation yielding [I<sup>t</sup>BuH]<sup>+</sup>{Ph<sub>2</sub>C=C=NGaR<sub>3</sub>}<sup>-</sup> (**24**), for instance. The unprecedented isolation of constitutional isomers [I<sup>t</sup>BuCH(*p*-Br-C<sub>6</sub>H<sub>4</sub>)OGaR<sub>3</sub>] (**14**) and [*a*I<sup>t</sup>BuCH(*p*-Br-C<sub>6</sub>H<sub>4</sub>)OGaR<sub>3</sub>] (**15**), resulting from the activation of 4-bromobenzaldehyde by this novel FLP system, has revealed that I<sup>t</sup>Bu can effectively act as a Lewis base not only *via* its normal C2 position (kinetic product) but alternatively *via* its C4 (abnormal) site (thermodynamic product). Evidencing the synergistic behaviour of these NHC/GaR<sub>3</sub> pairings, when separated from each other, neither component is able to activate these carbonyl compounds. The C-H bond activation was extended to terminal alkynes affording [I<sup>t</sup>BuH]<sup>+</sup>{(PhCC)GaR<sub>3</sub>}<sup>-</sup> (**29**), as well as to O-H and N-H bond activation as evidenced by the isolation of [I<sup>t</sup>BuH]<sup>+</sup>{(PhO)GaR<sub>3</sub>}<sup>-</sup> (**27**) and

$[\{t\text{BuH}\}^+\{(\text{Ph}_2\text{N})\text{GaR}_3\}^-]$  (**28**). The serendipitous isolation of  $[\{t\text{BuH}\}^+\{\text{OH}(\text{GaR}_3)_2\}^-]$  (**26**) instead of decomposition products discloses the cooperative sedation of highly sensitive components of the pair. These results open up new possibilities for using gallium compounds in FLP activation of other types of bonds such as Si-H or B-H or even apolar E-E bonds (E = H, S, P etc.).

### 3.8. Experimental procedures

**3.8.1. Synthesis of  $[\text{tBuCH}_2\text{OGaR}_3]$  (**13**)** A solution of  $\text{Ga}(\text{CH}_2\text{SiMe}_3)_3$  (0.17 g,



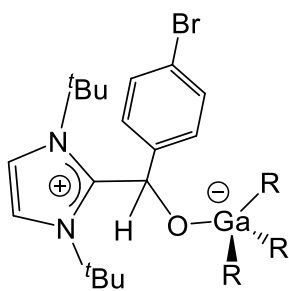
0.5 mmol in 10 mL hexane) was cooled on an ice bath. Paraformaldehyde (0.015 g, 0.5 mmol) was then added, followed by the addition of bis(*tert*-butyl)imidazol-2-ylidene (*t*Bu) (0.09 g, 0.5 mmol). Obtained white

suspension was stirred for 2 h at 0 °C. Toluene was added (1 mL) and the mixture was gently heated until all of the visible solid had dissolved. Slow cooling of the resulting solution afforded a crop of colourless crystals (0.18 g, 66%). Anal. Calcd for  $\text{C}_{24}\text{H}_{55}\text{N}_2\text{OSi}_3\text{Ga}$ : C, 53.21; H, 10.23; N, 5.17. Found: C, 53.11; H, 10.31; N, 5.39.

$^1\text{H}$  NMR (**298 K**,  $\text{C}_6\text{D}_6$ )  $\delta$ (ppm) -0.28 (6H, s,  $\text{CH}_2\text{SiMe}_3$ ), 0.44 (27H, s,  $\text{Si}(\text{CH}_3)_3$ ), 1.30 (18H, s, C ( $\text{CH}_3$ )<sub>3</sub>), 5.01 (2H, s,  $\text{OCH}_2$ ), 6.09 (2H, s, imidazole backbone CH).  $^{13}\text{C}\{^1\text{H}\}$  NMR (**298 K**,  $\text{C}_6\text{D}_6$ )  $\delta$ (ppm) 1.4 ( $\text{CH}_2\text{SiMe}_3$ ), 3.7 ( $\text{Si}(\text{CH}_3)_3$ ), 30.3 (C( $\text{CH}_3$ )<sub>3</sub>), 58.1 ( $\text{OCH}_2$ ), 62.2 (C( $\text{CH}_3$ )<sub>3</sub>), 116.5 (imidazole backbone CH), 152.7 (C- $\text{OCH}_2$ ).

$^1\text{H}$  NMR (**298 K**,  $d_8$ -THF)  $\delta$ (ppm) -0.82 (6H, s,  $\text{CH}_2\text{SiMe}_3$ ), -0.06 (27H, s,  $\text{Si}(\text{CH}_3)_3$ ), 1.81 (18H, s, C ( $\text{CH}_3$ )<sub>3</sub>), 5.05 (2H, s,  $\text{OCH}_2$ ), 7.50 (2H, s, imidazole backbone CH).  $^{13}\text{C}\{^1\text{H}\}$  NMR (**298 K**,  $d_8$ -THF)  $\delta$ (ppm) 1.3 ( $\text{CH}_2\text{SiMe}_3$ ), 3.5 ( $\text{Si}(\text{CH}_3)_3$ ), 31.0 (C( $\text{CH}_3$ )<sub>3</sub>), 58.6 ( $\text{OCH}_2$ ), 63.1 (C( $\text{CH}_3$ )<sub>3</sub>), 118.6 (imidazole backbone CH), 153.2 (C- $\text{OCH}_2$ ).

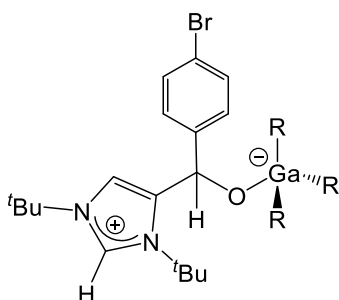
**3.8.2. Synthesis of  $[\text{tBuCH}(p\text{-Br-C}_6\text{H}_4)\text{OGaR}_3]$  (**14**)** To a cooled solution of  $\text{Ga}(\text{CH}_2\text{SiMe}_3)_3$  (0.165 g, 0.5 mmol in 10 mL hexane) 4-bromobenzaldehyde (92 mg,



0.5 mmol) was added forming a bright yellow solution. Bis(*tert*-butyl)imidazol-2-ylidene (*t*Bu) (0.09 g, 0.5 mmol) was then added and the obtained white suspension was stirred for **15 min at 0 °C**. The solvent was exchanged *in vacuo* for 5 mL of hexane and 5 mL of toluene and the resulting solution was placed at -33 °C yielding a crop of colourless crystals (0.145 g, 42%). Anal. Calcd for C<sub>30</sub>H<sub>58</sub>N<sub>2</sub>OSi<sub>3</sub>GaBr: C, 51.72; H, 8.39; N, 4.02. Found: C, 52.33; H, 8.84; N, 4.01.

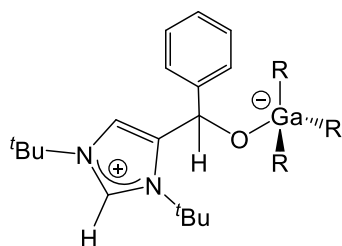
**<sup>1</sup>H NMR (298 K, d<sub>8</sub>-THF)** δ(ppm) -0.81 (6H, mult, CH<sub>2</sub>SiMe<sub>3</sub>), -0.06 (27H, s, Si(CH<sub>3</sub>)<sub>3</sub>), 1.62 (9H, s, C(CH<sub>3</sub>)<sub>3</sub>), 1.74 (9H, s, C(CH<sub>3</sub>)<sub>3</sub>), 6.79 (1H, s, CHO), 7.29 (4H, mult, Ar-CH), 7.76 (2H, s, imidazole backbone CH). **<sup>13</sup>C{<sup>1</sup>H} NMR (298 K, d<sub>8</sub>-THF)** δ(ppm) 2.9 (CH<sub>2</sub>SiMe<sub>3</sub>), 3.5 (Si(CH<sub>3</sub>)<sub>3</sub>), 31.7 (C(CH<sub>3</sub>)<sub>3</sub>), 31.9 (C(CH<sub>3</sub>)<sub>3</sub>), 64.1 (C(CH<sub>3</sub>)<sub>3</sub>), 66.3 (C(CH<sub>3</sub>)<sub>3</sub>), 72.3 (CHO), 119.0 (imidazole backbone CH), 121.8 (C-Br), 131.7 (Ar-CH), 133.2 (Ar-CH), 148.5 (Ar-C<sub>ipso</sub>), 154.2 (C<sub>imidazole</sub>-CHO).

### 3.8.3. Synthesis of [a*t*BuCH(*p*-Br-C<sub>6</sub>H<sub>4</sub>)OGaR<sub>3</sub>] (15)



To a cooled solution of Ga(CH<sub>2</sub>SiMe<sub>3</sub>)<sub>3</sub> (0.165 g, 0.5 mmol in 10 mL hexane) 4-bromobenzaldehyde (92 mg, 0.5 mmol) was added forming a bright yellow solution. Bis(*tert*-butyl)imidazol-2-ylidene (*t*Bu) (0.09 g, 0.5 mmol) was then added and the obtained white suspension was stirred for **2 h at 0 °C** and concentrated *in vacuo* to approximately 5 mL hexane. Toluene was added (3 mL) and the mixture was gently heated until all of the visible solid had dissolved. Slow cooling of the resulting solution afforded a crop of colourless crystals (0.20 g, 57%). Anal. Calcd for C<sub>30</sub>H<sub>58</sub>N<sub>2</sub>OSi<sub>3</sub>GaBr: C, 51.72; H, 8.39; N, 4.02. Found: C, 51.20; H, 8.41; N, 4.23.

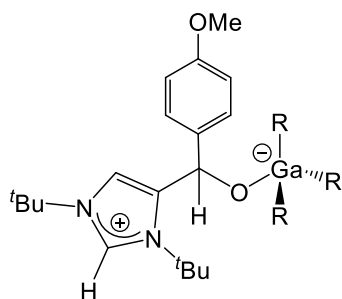
**<sup>1</sup>H NMR (298 K, d<sub>8</sub>-THF)** δ(ppm) -0.92 (6H, mult, CH<sub>2</sub>SiMe<sub>3</sub>), -0.10 (27H, s, Si(CH<sub>3</sub>)<sub>3</sub>), 1.59 (9H, s, C(CH<sub>3</sub>)<sub>3</sub>), 1.69 (9H, s, C(CH<sub>3</sub>)<sub>3</sub>), 6.14 (1H, s, CHO), 7.32 (4H, mult, Ar-CH), 7.84 (1H, s, imidazole backbone, CH), 8.45 (1H, s, C2-H). **<sup>13</sup>C{<sup>1</sup>H} NMR (298 K, d<sub>8</sub>-THF)** δ(ppm) 1.9 (CH<sub>2</sub>SiMe<sub>3</sub>), 3.5 (Si(CH<sub>3</sub>)<sub>3</sub>), 29.7 (C(CH<sub>3</sub>)<sub>3</sub>), 30.9 (C(CH<sub>3</sub>)<sub>3</sub>), 60.2 (C(CH<sub>3</sub>)<sub>3</sub>), 63.3 (C(CH<sub>3</sub>)<sub>3</sub>), 72.7 (CHO), 120.2 (C-Br), 121.8 (imidazole backbone CH), 129.9 (Ar-CH), 131.2 (Ar-CH), 131.8 (NCHN), 146.3 (Ar-C<sub>ipso</sub>) 149.0 (C<sub>imidazole</sub>-CHO).

**3.8.4. Synthesis of [aI<sup>t</sup>BuCH(C<sub>6</sub>H<sub>5</sub>)OGaR<sub>3</sub>] (16)**

A solution of Ga(CH<sub>2</sub>SiMe<sub>3</sub>)<sub>3</sub> (0.165 g, 0.5 mmol in 10 mL hexane) was cooled on an ice bath. Benzaldehyde (51 μL, 0.5 mmol) was then added, followed by the addition of bis(*tert*-butyl)imidazol-2-ylidene (I<sup>t</sup>Bu) (0.09 g, 0.5 mmol). The obtained light yellow suspension was stirred for 2 h at 0 °C. Toluene was added (2 mL) and the mixture was gently heated until all of the visible solid had dissolved. Cooling of the resulting solution at -33 °C afforded a colourless microcrystalline solid (0.19 g, 62 %). Anal. Calcd for: C<sub>30</sub>H<sub>59</sub>N<sub>2</sub>GaOSi<sub>3</sub>: C, 58.32; H, 9.63; N, 4.53. Found: C, 57.89; H, 9.39; N, 4.24.

**<sup>1</sup>H NMR (298 K, C<sub>6</sub>D<sub>6</sub>)** δ(ppm) -0.32 (6H, mult, CH<sub>2</sub>SiMe<sub>3</sub>), 0.46 (27H, s, Si(CH<sub>3</sub>)<sub>3</sub>), 0.78 (9H, s, C(CH<sub>3</sub>)<sub>3</sub>), 1.06 (9H, s, C(CH<sub>3</sub>)<sub>3</sub>), 6.38 (2H, s, CHO), 6.93 (1H, s, imidazole backbone CH), 7.09 (1H, t, *p*-CH), 7.28 (2H, t, *m*-CH), 7.39 (1H, s, C2-H), 7.55 (2H, d, *o*-CH).

**<sup>1</sup>H NMR (298 K, *d*<sub>8</sub>-THF)** δ(ppm) -0.92 (6H, mult, CH<sub>2</sub>SiMe<sub>3</sub>), -0.09 (27H, s, Si(CH<sub>3</sub>)<sub>3</sub>), 1.56 (9H, s, C(CH<sub>3</sub>)<sub>3</sub>), 1.69 (9H, s, C(CH<sub>3</sub>)<sub>3</sub>), 6.17 (1H, s, OCH), 7.07 (1H, t, *p*-CH), 7.16 (2H, t, *m*-CH), 7.34 (2H, d, *o*-CH), 7.85 (1H, s, imidazole backbone CH), 8.43 (1H, s, C2-H). **<sup>13</sup>C{<sup>1</sup>H} NMR (298 K, *d*<sub>8</sub>-THF)** δ(ppm) 1.9 (CH<sub>2</sub>SiMe<sub>3</sub>), 3.5 (Si(CH<sub>3</sub>)<sub>3</sub>), 29.7 (C(CH<sub>3</sub>)<sub>3</sub>), 30.8 (C(CH<sub>3</sub>)<sub>3</sub>), 60.1 (C(CH<sub>3</sub>)<sub>3</sub>), 63.1 (C(CH<sub>3</sub>)<sub>3</sub>), 73.3 (OCH), 121.8 (imidazole backbone CH), 126.5 (Ar-CH), 128.0 (Ar-CH), 128.1 (Ar-CH), 131.4 (NCHN), 147.2 (Ar-C<sub>ipso</sub>) 149.3 (C<sub>im</sub>-OCH).

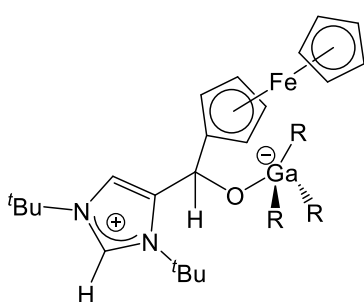
**3.8.5. Synthesis of [aI<sup>t</sup>BuCH(*p*-OMe-C<sub>6</sub>H<sub>4</sub>)OGaR<sub>3</sub>] (17)**

To a cooled solution of Ga(CH<sub>2</sub>SiMe<sub>3</sub>)<sub>3</sub> (0.165 g, 0.5 mmol in 10 mL hexane) *p*-anisaldehyde (61 μL, 0.5 mmol) was added followed by bis(*tert*-butyl)imidazol-2-ylidene (I<sup>t</sup>Bu) (0.09 g, 0.5 mmol) and the obtained white suspension was stirred for 2 h at 0 °C. Toluene was added (3 mL) and the mixture was gently heated until all of the visible solid had dissolved. Slow cooling of the resulting solution afforded colourless microcrystalline solid (0.183g, 56%). Anal. Calcd for C<sub>31</sub>H<sub>61</sub>GaN<sub>2</sub>O<sub>2</sub>Si<sub>3</sub>: C, 57.48; H, 9.49; N, 4.32. Found: C, 57.65; H, 8.69; N, 4.39.



**<sup>1</sup>H NMR (298 K, *d*<sub>8</sub>-THF)** δ(ppm) -0.93 (6H, mult, CH<sub>2</sub>SiMe<sub>3</sub>), -0.10 (27H, s, Si(CH<sub>3</sub>)<sub>3</sub>), 1.68 (9H, s, C(CH<sub>3</sub>)<sub>3</sub>), 1.69 (9H, s, C(CH<sub>3</sub>)<sub>3</sub>), 3.70 (1H, s, OCH<sub>3</sub>), 6.12 (1H, s, CHO), 6.72 (2H, d, Ar-CH), 7.22 (2H, d, Ar-CH), 7.83 (1H, s, imidazole backbone CH), 8.41 (1H, s, C2-H), **<sup>13</sup>C{<sup>1</sup>H} NMR (298 K, *d*<sub>8</sub>-THF)** δ(ppm) 1.9 (CH<sub>2</sub>SiMe<sub>3</sub>), 3.6 (Si(CH<sub>3</sub>)<sub>3</sub>), 29.7 (C(CH<sub>3</sub>)<sub>3</sub>), 30.8 (C(CH<sub>3</sub>)<sub>3</sub>), 55.2 (OCH<sub>3</sub>), 60.0 (C(CH<sub>3</sub>)<sub>3</sub>), 63.0 (C(CH<sub>3</sub>)<sub>3</sub>), 72.9 (OCH), 113.6 (Ar-CH), 121.7 (imidazole backbone CH), 129.0 (Ar-CH), 131.3 (NCHN), 141.3 (Ar-C<sub>ipso</sub>) 147.7 (C<sub>im</sub>-OCH), 159.1 (C-OMe).

**3.8.6. Synthesis of [a<sup>t</sup>BuCH(FeCp<sub>2</sub>)OGaR<sub>3</sub>] (18)** To a cooled solution of

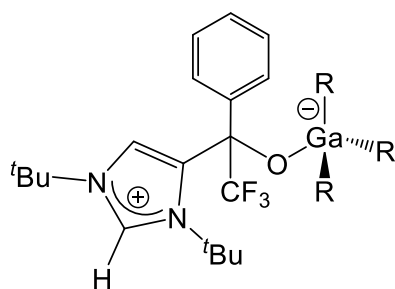


Ga(CH<sub>2</sub>SiMe<sub>3</sub>)<sub>3</sub> (0.165 g, 0.5 mmol in 10 mL hexane) ferrocenecarboxaldehyde (0.107 g, 0.5 mmol) was added forming a bright red solution. Bis(*tert*-butyl)imidazol-2-ylidene (<sup>t</sup>Bu) (0.09 g, 0.5 mmol) was then added and the obtained orange suspension was stirred for 2 h at 0 °C. Toluene was added (3 mL) and

the mixture was gently heated until all of the visible solid had dissolved. Slow cooling of the resulting solution afforded a crop of orange crystals (0.173g, 48%). Anal. Calcd for C<sub>34</sub>H<sub>63</sub>FeGaN<sub>2</sub>O<sub>2</sub>Si<sub>3</sub>: C, 56.27; H, 8.75; N, 3.86. Found: C, 53.75; H, 8.42; N, 3.99. Sample consistently shows low value of the carbon content.

**<sup>1</sup>H NMR (298 K, *d*<sub>8</sub>-THF)** δ(ppm) -0.86 (6H, mult, CH<sub>2</sub>SiMe<sub>3</sub>), -0.03 (27H, s, Si(CH<sub>3</sub>)<sub>3</sub>), 1.65 (9H, s, C(CH<sub>3</sub>)<sub>3</sub>), 1.69 (9H, s, C(CH<sub>3</sub>)<sub>3</sub>), 3.75 (1H, s, FeCp<sub>2</sub>), 3.89 (1H, s, FeCp<sub>2</sub>), 3.94 (1H, s, FeCp<sub>2</sub>), 4.14 (5H, s, FeCp<sub>2</sub>), 4.42 (1H, s, FeCp<sub>2</sub>), 6.24 (1H, s, OCH), 7.67 (1H, s, imidazole backbone CH), 8.36 (1H, s, C2-H). **<sup>13</sup>C{<sup>1</sup>H} NMR (298 K, *d*<sub>8</sub>-THF)** δ(ppm) 2.0 (CH<sub>2</sub>SiMe<sub>3</sub>), 3.6 (Si(CH<sub>3</sub>)<sub>3</sub>), 29.7 (C(CH<sub>3</sub>)<sub>3</sub>), 31.3 (C(CH<sub>3</sub>)<sub>3</sub>), 60.0 (C(CH<sub>3</sub>)<sub>3</sub>), 63.4 (C(CH<sub>3</sub>)<sub>3</sub>), 66.7 (FeCp<sub>2</sub>-C), 67.4 (FeCp<sub>2</sub>-C), 67.5 (FeCp<sub>2</sub>-C), 69.4 (FeCp<sub>2</sub>-C), 69.5 (FeCp<sub>2</sub>-C), 70.3 (FeCp<sub>2</sub>-C), 100.7 (CHO), 120.2 (imidazole backbone CH), 130.6 (NCHN) 148.0 (C<sub>im</sub>-CHO).

**3.8.7. Synthesis of [a<sup>t</sup>BuC(Ph)(CF<sub>3</sub>)OGaR<sub>3</sub>] (19)** A solution of Ga(CH<sub>2</sub>SiMe<sub>3</sub>)<sub>3</sub> (0.165 g, 0.5 mmol in 10 mL hexane) was cooled on an ice bath. α,α,α-trifluoroacetophenone (70 μL, 0.5 mmol) was then added, followed by the addition of bis(*tert*-butyl)imidazol-2-ylidene (<sup>t</sup>Bu) (0.09 g, 0.5 mmol). The obtained white suspension was stirred for 2 h at 0 °C. Toluene was added (2 mL) and the mixture

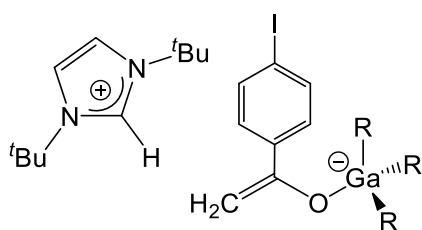


was gently heated until all of the visible solid had dissolved. Slow cooling of the resulting solution afforded an oil which upon cooling at  $-33\text{ }^{\circ}\text{C}$  afforded a crop of colourless crystals (0.215 g, 63%). Anal. Calcd for  $\text{C}_{31}\text{H}_{58}\text{F}_3\text{N}_2\text{OSi}_3\text{Ga}$ : C, 54.29; H, 8.52; N, 4.08. Found: C, 54.11; H, 7.97;

N, 4.56.

**$^1\text{H}$  NMR (298 K,  $d_8$ -THF)**  $\delta$ (ppm) -0.83 (6H, s,  $\text{CH}_2\text{SiMe}_3$ ), -0.05 (27H, s,  $\text{Si}(\text{CH}_3)_3$ ), 1.51 (9H, s,  $\text{C}(\text{CH}_3)_3$ ), 1.72 (9H, s,  $\text{C}(\text{CH}_3)_3$ ), 7.21 (3H, mult, imidazole backbone  $\text{CH}$  +  $o$ - $\text{CH}$ ), 7.53 (3H, mult,  $m$ - $\text{CH}$  +  $p$ - $\text{CH}$ ), 8.67 (1H, s, C2- $\text{H}$ ).  **$^{13}\text{C}\{^1\text{H}\}$  NMR (298 K,  $d_8$ -THF)**  $\delta$ (ppm) 3.2 ( $\text{CH}_2\text{SiMe}_3$ ), 3.5 ( $\text{Si}(\text{CH}_3)_3$ ), 29.4 ( $\text{C}(\text{CH}_3)_3$ ), 32.1 ( $\text{C}(\text{CH}_3)_3$ ), 60.6 ( $\text{C}(\text{CH}_3)_3$ ), 66.6 ( $\text{C}(\text{CH}_3)_3$ ), 81.7 (q,  $\text{OC}(\text{Ph})\text{CF}_3$ ), 119.1 (imidazole backbone  $\text{CH}$ ), 127.6 (Ar- $\text{CH}$ ), 128.1 (Ar- $\text{CH}$ ), 129.4 (Ar- $\text{CH}$ ), 134.1 (NCHN), 141.5 (Ar- $\text{C}_{ipso}$ ), 145.8 ( $\text{C}_{im}$ - $\text{OC}(\text{Ph})\text{CF}_3$ ).  $\text{CF}_3$  could not be confidentially assigned due to the low intensity of its resonances and noise in the baseline.  **$^{19}\text{F}$  NMR (298 K,  $d_8$ -THF)**  $\delta$ (ppm) -69.92 br s (additional resonances arising from the decomposition of this sensitive substrate are observed in the  $^{19}\text{F}$  NMR spectrum of both product and starting material).

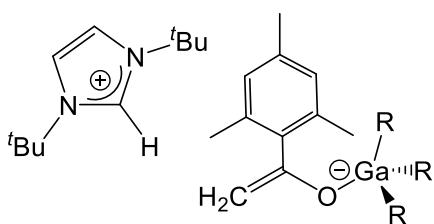
### 3.8.8. Synthesis of $[(\text{tBuH})^+\{p\text{-I-C}_6\text{H}_4\}\text{C}(\text{CH}_2)\text{OGaR}_3]$ (20)



To a cooled solution of  $\text{Ga}(\text{CH}_2\text{SiMe}_3)_3$  (0.165 g, 0.5 mmol in 10 mL hexane) 4'-iodoacetophenone (0.123 g, 0.5 mmol) was added followed by bis(*tert*-butyl)imidazol-2-ylidene ( $\text{tBu}$ ) (0.09 g, 0.5 mmol) and the obtained yellow suspension was

stirred for 2 h at  $0\text{ }^{\circ}\text{C}$  and protected from light. Straw solid (282 mg, 74%) was isolated by filtration. Anal. Calcd for  $\text{C}_{31}\text{H}_{60}\text{GaIN}_2\text{OSi}_3$ : C, 49.14; H, 7.98; N, 3.70. Found: C, 49.07; H, 7.81; N, 3.40.

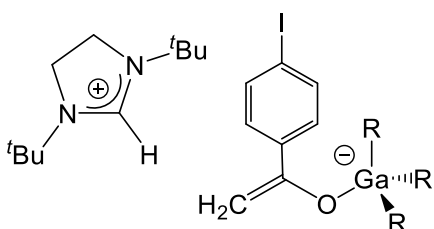
**$^1\text{H}$  NMR (298 K,  $d_8$ -THF)**  $\delta$ (ppm) -0.74 (6H, s,  $\text{CH}_2\text{SiMe}_3$ ), -0.06 (27H, s,  $\text{Si}(\text{CH}_3)_3$ ), 1.62 (18H, s,  $\text{C}(\text{CH}_3)_3$ ), 3.86 (s, 1H,  $\text{CH}_2$ ), 4.12 (s, 1H,  $\text{CH}_2$ ), 7.41 (2H, d, Ar- $\text{CH}$ ), 7.55 (2H, d, Ar- $\text{CH}$ ), 7.78 (2H, s, imidazole backbone  $\text{CH}$ ), 8.72 (1H, s, C2- $\text{H}$ ).  **$^{13}\text{C}\{^1\text{H}\}$  NMR (298 K,  $d_8$ -THF)**  $\delta$ (ppm) 2.3 ( $\text{CH}_2\text{SiMe}_3$ ), 3.5 ( $\text{Si}(\text{CH}_3)_3$ ), 29.7 ( $\text{C}(\text{CH}_3)_3$ ), 61.2 ( $\text{C}(\text{CH}_3)_3$ ), 79.9 ( $\text{CH}_2=\text{C}$ ), 90.8 ( $\text{C-I}$ ), 121.5 (imidazole backbone  $\text{CH}$ ), 129.2 (Ar- $\text{CH}$ ), 131.9 (NCHN), 136.3 (Ar- $\text{CH}$ ), 145.8 (Ar- $\text{C}_{ipso}$ ), 163.3 ( $\text{C-O}$ ).

**3.8.9. Synthesis of  $[(t\text{Bu})\text{Imidazol-2-ylidene}]^+\{(\text{Me}_3\text{C}_6\text{H}_2)\text{C}(\text{CH}_2)\text{OGaR}_3\}^-$  (21)**

solution of  $\text{Ga}(\text{CH}_2\text{SiMe}_3)_3$  (0.165 g, 0.5 mmol in 10 mL hexane) 2',4',6'-trimethylacetophenone (0.081 g, 0.5 mmol) was added followed by bis(*tert*-butyl)imidazol-2-ylidene (*t*Bu) (0.09 g, 0.5 mmol) and the obtained yellow suspension

was stirred for 2 h at 0 °C. The off-white solid (203 mg, 60%) was isolated by filtration. Anal. Calcd for  $\text{C}_{34}\text{H}_{67}\text{N}_2\text{OSi}_3\text{Ga}$ : C, 60.60; H, 10.02; N, 4.16. Found: C, 58.15; H, 9.62 N, 3.88. The sample shows consistently low value for carbon content. Small amounts of unreacted ketone are observed in NMR spectra.

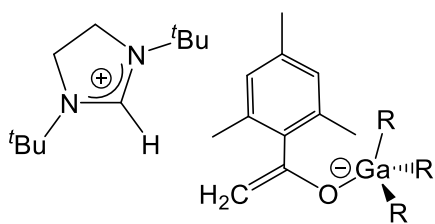
$^1\text{H}$  NMR (298 K, *ds*-THF)  $\delta$ (ppm) -0.72 (6H, s,  $\text{CH}_2\text{SiMe}_3$ ), -0.08 (27H, s,  $\text{Si}(\text{CH}_3)_3$ ), 1.63 (18H, s,  $\text{C}(\text{CH}_3)_3$ ), 2.13 (3H, s,  $\text{CH}_3$ ), 2.33 (6H, s,  $\text{CH}_3$ ), 3.13 (s, 1H,  $\text{CH}_2$ ), 3.85 (s, 1H,  $\text{CH}_2$ ), 6.57 (2H, s, Ar-CH), 7.81 (2H, s, imidazole backbone CH), 8.75 (1H, s, C2-H).  $^{13}\text{C}\{^1\text{H}\}$  NMR (298 K, *ds*-THF)  $\delta$ (ppm) 2.3 ( $\text{CH}_2\text{SiMe}_3$ ), 3.5 ( $\text{Si}(\text{CH}_3)_3$ ), 21.00 (Ar- $\text{CH}_3$ ), 21.3 (Ar- $\text{CH}_3$ ), 29.7 ( $\text{C}(\text{CH}_3)_3$ ), 61.2 ( $\text{C}(\text{CH}_3)_3$ ), 81.4 ( $\text{CH}_2=\text{C}$ ), 121.6 (imidazole backbone CH), 127.6 (Ar-CH), 132.0 (NCHN), 133.3 (Ar-C), 135.8 (Ar-C), 145.1 (Ar-*C*<sub>ipso</sub>), 165.7 (C-O).

**3.8.10. Synthesis of  $[(\text{SI}^t\text{Bu})\text{Imidazol-2-ylidene}]^+\{(p\text{-I-C}_6\text{H}_4)\text{C}(\text{CH}_2)\text{OGaR}_3\}^-$  (22)**

solution of  $\text{Ga}(\text{CH}_2\text{SiMe}_3)_3$  (0.165 g, 0.5 mmol in 10 mL hexane) 4'-iodoacetophenone (0.123 g, 0.5 mmol) was added followed by bis(*tert*-butyl)imidazol-2-ylidene (*SI*<sup>*t*</sup>Bu) (0.09 g, 0.5 mmol) and the obtained off-white suspension was

stirred for 2 h at 0 °C and protected from light. The peach-coloured solid (211 mg, 62%) was isolated by filtration. Anal. Calcd for  $\text{C}_{31}\text{H}_{62}\text{N}_2\text{IOSi}_3\text{Ga}$ : C, 49.01; H, 8.23; N, 3.69. Found: C, 48.26; H, 7.69; N, 3.41.

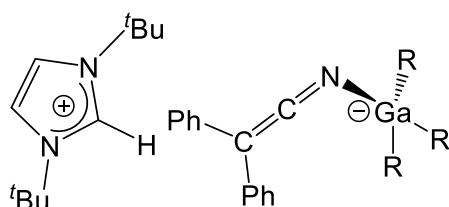
$^1\text{H}$  NMR (298 K, *ds*-THF)  $\delta$ (ppm) -0.74 (6H, s,  $\text{CH}_2\text{SiMe}_3$ ), -0.05 (27H, s,  $\text{Si}(\text{CH}_3)_3$ ), 1.37 (18H, s,  $\text{C}(\text{CH}_3)_3$ ), 3.85 (s, 1H,  $\text{CH}_2$ ), 3.92 (s, 4H,  $\text{CH}_2$  backbone), 4.13 (s, 1H,  $\text{CH}_2$ ), 7.43 (2H, d, Ar-CH), 7.56 (2H, d, Ar-CH), 7.88 (1H, s, C2-H).  $^{13}\text{C}\{^1\text{H}\}$  NMR (298 K, *ds*-THF)  $\delta$ (ppm) 2.3 ( $\text{CH}_2\text{SiMe}_3$ ), 3.5 ( $\text{Si}(\text{CH}_3)_3$ ), 27.9 ( $\text{C}(\text{CH}_3)_3$ ), 46.2 (NCH<sub>2</sub>CH<sub>2</sub>N), 57.5 ( $\text{C}(\text{CH}_3)_3$ ), 79.8 ( $\text{CH}_2=\text{C}$ ), 90.9 (C-I), 129.1 (Ar-CH), 136.4 (Ar-CH), 145.8 (Ar-*C*<sub>ipso</sub>), 152.9 (NCHN), 163.2 (C-O).

**3.8.11. Synthesis of  $[(SI^tBuH]^+[(Me_3C_6H_2)C(CH_2)OGaR_3]^-]$  (23)**

solution of  $Ga(CH_2SiMe_3)_3$  (0.165 g, 0.5 mmol in 10 mL hexane) 2',4',6'-trimethylacetophenone (0.081 g, 0.5 mmol) was added followed by bis(*tert*-butyl)imidazol-2-ylidene ( $SI^tBu$ ) (0.09 g, 0.5 mmol) and the obtained white suspension

was stirred for 2 h at 0 °C after which a white solid was isolated by filtration (272 mg, 80%). Anal. Calcd for  $C_{34}H_{67}N_2OSi_3Ga$ : C, 60.42; H, 10.29; N, 4.14. Found: C, 60.66; H, 10.16; N, 4.65.

$^1H$  NMR (298 K,  $d_8$ -THF)  $\delta$ (ppm) -0.72 (6H, s,  $CH_2SiMe_3$ ), -0.06 (27H, s,  $Si(CH_3)_3$ ), 1.37 (18H, s,  $C(CH_3)_3$ ), 2.15 (3H, s,  $CH_3$ ), 2.34 (6H, s,  $CH_3$ ), 3.16 (s, 1H,  $CH_2$ ), 3.85 (s, 4H,  $CH_2$  backbone), 3.86 (s, 1H,  $CH_2$ ), 6.60 (2H, s, Ar-CH), 7.87 (1H, s, C2-H).  $^{13}C\{^1H\}$  NMR (298 K,  $d_8$ -THF)  $\delta$ (ppm) 2.3 ( $CH_2SiMe_3$ ), 3.6 ( $Si(CH_3)_3$ ), 21.0 (Ar- $CH_3$ ), 21.3 (Ar- $CH_3$ ), 28.0 ( $C(CH_3)_3$ ), 46.2 ( $NCH_2CH_2N$ ), 57.5 ( $C(CH_3)_3$ ), 81.7 ( $CH_2=C$ ), 127.16 (Ar-CH), 133.6 (Ar-C), 135.9 (Ar-C), 145.1 (Ar- $C_{ipso}$ ), 152.8 (NCHN), 165.6 (C-O).

**3.8.12. Synthesis of  $[(I^tBuH]^+[(Ph)_2C=C=NGaR_3]^-]$  (24)**

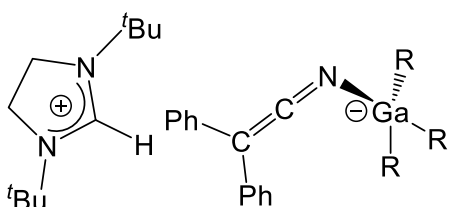
$Ga(CH_2SiMe_3)_3$  (0.165 g, 0.5 mmol in 10 mL hexane) diphenylacetone nitrile (97 mg, 0.5 mmol) was added followed by bis(*tert*-butyl)imidazol-2-ylidene ( $I^tBu$ ) (0.09 g, 0.5 mmol) and the obtained yellow suspension

was stirred for 2 h at 0 °C. Toluene was added (3 mL) and the mixture was gently heated until all of the visible solid had dissolved. Slow cooling of the resulting solution afforded yellow oil which upon standing provided X-ray quality crystals (0.225 g, 64%). Anal. Calcd for  $C_{37}H_{64}GaN_3Si_3$ : C, 63.04; H, 9.15; N, 5.96. Found: C, 61.12; H, 8.51; N, 6.04. The sample consistently shows low values for carbon content. Small amounts of unreacted diphenylacetone nitrile are observed in NMR spectra.

$^1H$  NMR (298 K,  $d_8$ -THF)  $\delta$ (ppm) -0.69 (6H, s,  $CH_2SiMe_3$ ), -0.02 (27H, s,  $Si(CH_3)_3$ ), 1.56 (18H, s,  $C(CH_3)_3$ ), 6.46 (2H, mult, *p*-CH), 6.92 (4H, t, *m*-CH), 7.28 (4H, t, *o*-CH), 7.59 (2H, s, imidazole backbone CH), 8.68 (1H, s, C2-H).  $^{13}C\{^1H\}$  NMR (298 K,  $d_8$ -THF)  $\delta$ (ppm) 2.7 ( $CH_2SiMe_3$ ), 3.1 ( $Si(CH_3)_3$ ), 29.7 ( $C(CH_3)_3$ ),

55.7 (Ph<sub>2</sub>C=C=N), 61.1 (C(CH<sub>3</sub>)<sub>3</sub>), 117.9 (Ar-CH), 121.4 (imidazole backbone CH), 123.1 (Ar-CH), 128.4 (Ar-CH), 131.9 (NCHN), 143.4 (Ph<sub>2</sub>C=C=N), 144.2 (Ar-C<sub>ipso</sub>).

### 3.8.13. Synthesis of [(SI'BuH)<sup>+</sup>{Ph<sub>2</sub>C=C=NGaR<sub>3</sub>}<sup>-</sup>] (25)

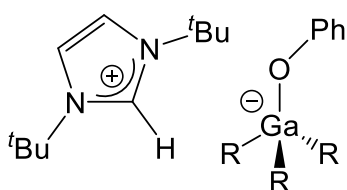


Ga(CH<sub>2</sub>SiMe<sub>3</sub>)<sub>3</sub> (0.165 g, 0.5 mmol in 10 mL hexane) diphenylacetonitrile (96 mg, 0.5 mmol) was added followed by bis(*tert*-butyl)imidazolin-2-ylidene (SI'Bu) (0.09 g, 0.5 mmol) and the obtained yellow suspension was

stirred for 2 h at 0 °C. The yellow solid was isolated by filtration (305 mg, 86%). Anal. Calcd for C<sub>37</sub>H<sub>66</sub>N<sub>3</sub>Si<sub>3</sub>Ga: C, 62.86; H, 9.41; N, 5.94. Found: C, 62.15; H, 9.06; N, 6.28.

<sup>1</sup>H NMR (298 K, d<sub>8</sub>-THF) δ(ppm) -0.68 (6H, s, CH<sub>2</sub>SiMe<sub>3</sub>), 0.00 (27H, s, Si(CH<sub>3</sub>)<sub>3</sub>), 1.28 (18H, s, C(CH<sub>3</sub>)<sub>3</sub>), 3.75 (s, 4H, CH<sub>2</sub>), 6.48 (t, 2H, *p*-CH), 6.95 (t, 4H, *m*-CH), 7.30 (4H, d, *o*-CH), 7.78 (1H, s, C2-*H*). <sup>13</sup>C{<sup>1</sup>H} NMR (298 K, d<sub>8</sub>-THF) δ(ppm) 2.8 (CH<sub>2</sub>SiMe<sub>3</sub>), 3.1 (Si(CH<sub>3</sub>)<sub>3</sub>), 27.9 (C(CH<sub>3</sub>)<sub>3</sub>), 46.0 (NCH<sub>2</sub>CH<sub>2</sub>N), 55.6 (Ph<sub>2</sub>C=C=N), 57.5 (C(CH<sub>3</sub>)<sub>3</sub>), 118.0 (Ar-CH), 123.0 (Ar-CH), 128.4 (Ar-CH), 143.1 (Ph<sub>2</sub>C=C=N), 144.0 (Ar-C<sub>ipso</sub>), 152.6 (NCHN).

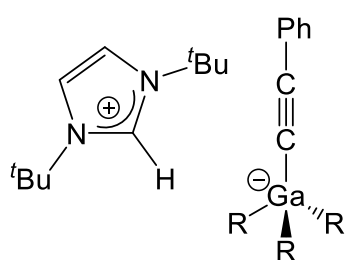
### 3.8.14. Synthesis of [(I'BuH)<sup>+</sup>{GaR<sub>3</sub>OPh}]<sup>-</sup> (27)



To a hexane suspension of I'Bu (0.5 mmol, 0.09 g in 5 mL hexane) phenol (47 mg, 0.5 mmol) was added *via* solid addition tube followed by a hexane solution of Ga(CH<sub>2</sub>SiMe<sub>3</sub>)<sub>3</sub> (0.165 g, 0.5 mmol in 5 mL hexane). The obtained white, thick suspension

was stirred for an hour at room temperature and subsequently solubilised by addition of toluene (3 mL) and gentle heating. Slow cooling of the resulting solution afforded X-ray quality crystals (230 mg, 76%). Anal. Calcd for C<sub>29</sub>H<sub>59</sub>N<sub>2</sub>Si<sub>3</sub>OGa: C, 57.50; H, 9.82; N, 4.62. Found: C, 57.85; H, 9.46; N, 5.33.

<sup>1</sup>H NMR (298 K, C<sub>6</sub>D<sub>6</sub>) δ(ppm) -0.15 (6H, s, CH<sub>2</sub>SiMe<sub>3</sub>), 0.48 (27H, s, Si(CH<sub>3</sub>)<sub>3</sub>), 1.08 (18H, s, C(CH<sub>3</sub>)<sub>3</sub>), 6.27 (s, 2H, imidazole backbone CH), 6.70 (t, 1H, *p*-CH), 7.00 (d, 2H, *o*-CH), 7.28 (2H, t, *m*-CH), 9.64 (1H, s, C2-*H*).

**3.8.15. Synthesis of  $[(t\text{BuH})^+\{\text{GaR}_3\text{C}\equiv\text{CPh}\}^-]$  (29)**

(0.5 mmol, 0.09 g in 5 mL hexane) phenylacetylene (47 mg, 0.5 mmol) was added followed by a hexane solution of  $\text{Ga}(\text{CH}_2\text{SiMe}_3)_3$  (0.165 g, 0.5 mmol in 5 mL hexane). The obtained white, thick suspension was stirred for an hour at room temperature after which the

solvent was exchanged *in vacuo* for benzene (5 mL). Gentle heating afforded a solution which upon cooling afforded X-ray quality crystals (140 mg, 46%). Anal. Calcd for  $\text{C}_{31}\text{H}_{59}\text{N}_2\text{Si}_3\text{Ga}$ : C, 60.66; H, 9.69; N, 4.56. Found: C, 60.73; H, 9.49; N, 4.89.

$^1\text{H}$  NMR (298 K,  $d_8$ -THF)  $\delta$ (ppm) -1.01 (6H, s,  $\text{CH}_2\text{SiMe}_3$ ), -0.02 (27H, s,  $\text{Si}(\text{CH}_3)_3$ ), 1.66 (18H, s,  $\text{C}(\text{CH}_3)_3$ ), 6.93 (t, 1H, *p*-CH), 7.04 (t, 2H, *m*-CH), 7.21 (2H, d, *o*-CH), 7.86 (s, 2H, imidazole backbone CH), 8.80 (1H, s, C2-H).

**3.9. Bibliography**

- [1] G. N. Lewis, *Valence and the Structure of Atoms and Molecules*, Chemical Catalogue Company, Inc., New York, **1923**.
- [2] H. C. Brown, H. I. Schlesinger, S. Z. Cardon, *J. Am. Chem. Soc.* **1942**, *64*, 325-329.
- [3] G. Wittig, E. Benz, *Chem. Ber.* **1959**, *92*, 1999–2013.
- [4] G. Wittig, A. Ruckert, *Justus Liebigs Ann. Chem.* **1950**, *566*, 101–113.
- [5] W. Tochtermann, *Angew. Chem. Int. Ed.* **1966**, *5*, 351–371.
- [6] G. C. Welch, R. R. San Juan, J. D. Masuda, D. W. Stephan, *Science* **2006**, *314*, 1124–1126.
- [7] D. W. Stephan, *Acc. Chem. Res.* **2015**, *48*, 306–316.
- [8] D. W. Stephan, G. Erker, *Angew. Chem. Int. Ed.* **2015**, *54*, 6400-6441.
- [9] D. W. Stephan, G. Erker, *Angew. Chem. Int. Ed.* **2010**, *49*, 46–76.
- [10] G. Erker, D. W. Stephan (Eds.), *Frustrated Lewis Pairs I: Uncovering and Understanding*, Springer, **2013**.
- [11] D. W. Stephan, *Dalton Trans.* **2009**, 3129–3136.
- [12] Z. Mo, A. Rit, J. Campos, E. L. Kolychev, S. Aldridge, *J. Am. Chem. Soc.* **2016**, *138*, 3306–3309.

- [13] M. N. Hopkinson, F. Glorius, *Nature* **2014**, *510*, 485–496.
- [14] D. Holschumacher, T. Bannenberg, C. G. Hrib, P. G. Jones, M. Tamm, *Angew. Chem. Int. Ed.* **2008**, *47*, 7428–7432.
- [15] P. A. Chase, D. W. Stephan, *Angew. Chem. Int. Ed.* **2008**, *47*, 7433–7437.
- [16] E. L. Kolychev, T. Bannenberg, M. Freytag, C. G. Daniliuc, P. G. Jones, M. Tamm, *Chem. Eur. J.* **2012**, *18*, 16938–16946.
- [17] D. Holschumacher, T. Bannenberg, K. Ibrom, C. G. Daniliuc, *Dalton Trans.* **2010**, *39*, 10590–10592.
- [18] S. Kronig, E. Theuergarten, D. Holschumacher, T. Bannenberg, C. G. Daniliuc, P. G. Jones, M. Tamm, *Inorg. Chem.* **2011**, *50*, 7344–7359.
- [19] M. A. Dureen, C. C. Brown, D. W. Stephan, *Organometallics* **2010**, *29*, 6594–6607.
- [20] A. Jana, I. Objartel, H. W. Roesky, D. Stalke, *Inorg. Chem.* **2009**, *48*, 7645–7649.
- [21] Y. Zhang, G. M. Miyake, E. Y. X. Chen, *Angew. Chem. Int. Ed.* **2010**, *49*, 10158–10162.
- [22] B. Ines, S. Holle, R. Goddard, M. Alcarazo, *Angew. Chem. Int. Ed.* **2010**, *49*, 8389–8391.
- [23] C. Appelt, H. Westenberg, F. Bertini, A. W. Ehlers, J. C. Slootweg, K. Lammertsma, W. Uhl, *Angew. Chem. Int. Ed.* **2011**, *50*, 3925–3928.
- [24] C. Appelt, J. C. Slootweg, K. Lammertsma, W. Uhl, *Angew. Chem. Int. Ed.* **2012**, *51*, 5911–5914.
- [25] C. Appelt, J. C. Slootweg, K. Lammertsma, W. Uhl, *Angew. Chem. Int. Ed.* **2013**, *52*, 4256–4259.
- [26] W. Uhl, C. Appelt, *Organometallics* **2013**, *32*, 5008–5014.
- [27] W. Uhl, C. Appelt, J. Backs, H. Westenberg, A. Wollschläger, J. Tannert, *Organometallics* **2014**, *33*, 1212–1217.
- [28] M. A. Dureen, D. W. Stephan, *J. Am. Chem. Soc.* **2009**, *131*, 8396–8397.
- [29] G. Ménard, L. Tran, J. S. J. McCahill, A. J. Lough, D. W. Stephan, *Organometallics* **2013**, *32*, 6759–6763.
- [30] G. Menard, D. W. Stephan, *Angew. Chem. Int. Ed.* **2012**, *51*, 4409–4412.
- [31] G. Ménard, D. W. Stephan, *J. Am. Chem. Soc.* **2010**, *132*, 1796–1797.
- [32] G. Ménard, D. W. Stephan, *Angew. Chem. Int. Ed.* **2011**, *50*, 8396–8399.

- [33] T. G. Ong, *Organometallics* **2009**, *28*, 1060–1067.
- [34] T. Jurca, G. P. A. Yap, T. G. Ong, *Organometallics* **2012**, *31*, 637–643.
- [35] T. E. Stennett, J. Pahl, H. S. Zijlstra, F. W. Seidel, S. Harder, *Organometallics* **2016**, *35*, 207–217.
- [36] G. Schnee, D. Specklin, J. Djukic, S. Dagorne, *Organometallics* **2016**, *35*, 1726–1734.
- [37] D. Winkelhaus, B. Neumann, H.-G. Stammler, N. W. Mitzel, *Dalton Trans.* **2012**, *41*, 9143–9150.
- [38] J. A. B. Abdalla, I. M. Riddlestone, R. Tirfoin, S. Aldridge, *Angew. Chem. Int. Ed.* **2015**, *54*, 5098–50102.
- [39] W. Uhl, J. Tannert, M. Layh, A. Hepp, S. Grimme, T. Risthaus, *Organometallics* **2013**, *32*, 6770–6779.
- [40] C. Ganesamoorthy, M. Matthias, D. Bläser, C. Wölper, S. Schulz, *Dalton Trans.* **2016**, *45*, 11437–11444.
- [41] A. Stute, G. Kehr, C. G. Daniliuc, R. Fröhlich, G. Erker, *Dalton Trans.* **2013**, *42*, 4487–4499.
- [42] C. Rosorius, C. G. Daniliuc, R. Fröhlich, G. Kehr, G. Erker, *J. Organomet. Chem.* **2013**, *744*, 149–155.
- [43] C. Rosorius, G. Kehr, R. Fröhlich, S. Grimme, G. Erker, *Organometallics* **2011**, *30*, 4211–4219.
- [44] M. P. Boone, D. W. Stephan, *Organometallics* **2014**, *33*, 387–393.
- [45] T. Voss, J. B. Sortais, R. Fröhlich, G. Kehr, G. Erker, *Organometallics* **2011**, *30*, 584–594.
- [46] S. Schwendemann, R. Fröhlich, G. Kehr, G. Erker, *Chem. Sci.* **2011**, *2*, 1842–1849.
- [47] Y. Hasegawa, C. G. Daniliuc, G. Kehr, G. Erker, *Angew. Chem. Int. Ed.* **2014**, *53*, 12168–12171.
- [48] A. T. Normand, C. G. Daniliuc, B. Wibbeling, G. Kehr, P. Le Gendre, G. Erker, *Chem. Eur. J.* **2016**, *22*, 4285–4293.
- [49] J. Yu, G. Kehr, C. G. Daniliuc, G. Erker, *Chem. Commun.* **2016**, *52*, 1393–1396.
- [50] M. Uzelac, A. Hernán-Gómez, D. R. Armstrong, A. R. Kennedy, E. Hevia, *Chem. Sci.* **2015**, *6*, 5719–5728.
- [51] P. Horeglad, M. Cybularczyk, B. Trzaskowski, G. Z. Zukowska, M. Dranka, J. Zachara, *Organometallics* **2015**, *34*, 3480–3496.



- [52] P. Horeglad, O. Ablialimov, G. Szczepaniak, A. M. Dabrowska, M. Dranka, J. Zachara, *Organometallics* **2014**, *33*, 100–111.
- [53] E. Theuergarten, T. Bannenberg, M. D. Walter, D. Holschumacher, M. Freytag, C. G. Daniliuc, P. G. Jones, M. Tamm, *Dalton Trans.* **2014**, *43*, 1651–1662.
- [54] G. Schnee, O. Nieto Faza, D. Specklin, B. Jacques, L. Karmazin, R. Welter, C. Silva López, S. Dagorne, *Chem. Eur. J.* **2015**, *21*, 17959–17972.
- [55] W. Kohn, A. D. Becke, R. G. Parr, *J. Phys Chem* **1996**, *100*, 12974–12980.
- [56] A. D. Becke, *Phys. Rev. A* **1988**, *38*, 3098–3100.
- [57] C. Lee, W. Yang, R. G. Parr, *Phys. Rev. B* **1988**, *37*, 785–789.
- [58] A. D. McLean, G. S. Chandler, *J. Chem. Phys.* **1980**, *72*, 5639–5649.
- [59] G. Bertrand, E. Aldeco-Perez, A. J. Rosenthal, B. Donnadieu, P. Parameswaran, G. Frenking, *Science* **2009**, *326*, 556–559.
- [60] J. B. Waters, J. M. Goicoechea, *Coord. Chem. Rev.* **2015**, *293–294*, 80–94.
- [61] M. Heckenroth, E. Kluser, A. Neels, M. Albrecht, *Angew. Chem. Int. Ed.* **2007**, *46*, 6293–6296.
- [62] E. Theuergarten, J. Schlösser, D. Schlüns, M. Freytag, C. G. Daniliuc, P. G. Jones, M. Tamm, *Dalton Trans.* **2012**, *41*, 9101–9110.
- [63] D. Holschumacher, C. Taouss, T. Bannenberg, C. G. Hrib, C. G. Daniliuc, P. G. Jones, M. Tamm, *Dalton Trans.* **2009**, 6927–6929.
- [64] C. Wolf, W. A. König, C. Roussel, *Liebigs Ann.* **1995**, *1995*, 781–786.
- [65] I. De Riggi, A. Virgili, M. De Moragas, C. Jaime, *J. Org. Chem.* **1995**, *60*, 27–31.
- [66] E. Iravani, B. Neumu, *Organometallics* **2003**, *22*, 4129–4135.
- [67] D. M. Tellers, J. C. M. Ritter, R. G. Bergman, *Inorg. Chem.* **1999**, *38*, 4810–4818.
- [68] I. L. Fedushkin, A. G. Morozov, O. V. Rassadin, G. K. Fukin, *Chem. Eur. J.* **2005**, *11*, 5749–5757.
- [69] J. Zhao, S. Zhang, W. X. Zhang, Z. Xi, *Organometallics* **2011**, *30*, 3464–3467.
- [70] J. Zhao, S. Zhang, W. X. Zhang, Z. Xi, *Organometallics* **2012**, *31*, 8370–8374.
- [71] M. K. Denk, M. Rodezno, S. Gupta, A. J. Lough, *J. Organomet. Chem.* **2001**, *617–618*, 242–253.
- [72] V. Bagutski, A. Del Grosso, J. A. Carrillo, I. A. Cade, M. D. Helm, J. R. Lawson, P. J. Singleton, S. A. Solomon, T. Marcelli, M. J. Ingleson, *J. Am. Chem. Soc.* **2013**,

135, 474–487.

- [73] V. Sumerin, F. Schulz, M. Nieger, M. Leskelä, T. Repo, B. Rieger, *Angew. Chem. Int. Ed.* **2008**, *47*, 6001–6003.
- [74] T. A. Rokob, A. Hamza, A. Stirling, I. Pápai, *J. Am. Chem. Soc.* **2009**, *131*, 2029–2036.
- [75] M. Gomez-Pantoja, P. Gomez-Sal, A. Hernan-Gomez, A. Martin, M. Mena, C. Santamaria, *Inorg. Chem.* **2012**, *51*, 8964–8972.
- [76] M. Schiefer, N. D. Reddy, H.-J. Ahn, A. Stasch, H. W. Roesky, A. C. Schlicker, H.-G. Schmidt, M. Noltemeyer, D. Vidovic, *Inorg. Chem.* **2003**, *42*, 4970–4976.

## 4. Transforming LiTMP lithiation of challenging N-heterocyclic substrates via gallium alkyl trans-metal-trapping

### 4.1. Introduction

Lithium amides ( $R_2NLi$ )<sup>[1,2]</sup> are amongst the most important and reactive classes of lithium reagents and can be easily prepared by deprotonation of secondary amines such as diisopropylamine, 2,2,6,6-tetramethylpiperidine and bis(trimethylsilyl)amine affording lithium diisopropylamide (LDA), LiTMP and LiHMDS respectively (**Figure 4.1**). Of these three sterically hindered commodity amides, LiTMP has become a staple reagent for deprotonation reactions as it is more basic than LiHMDS and more stable than LDA. These valued attributes stem from the architecture of the cyclic TMP anion where the electron-donating methyl groups are positioned adjacent to nitrogen atom simultaneously enhancing the bulkiness and the basicity while precluding decomposition *via*  $\beta$ -hydride elimination (which can be encountered when working with LDA).<sup>[3]</sup>

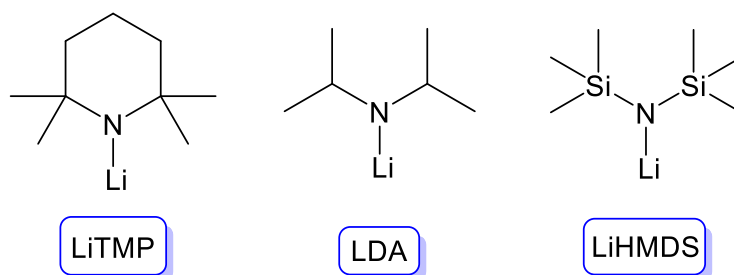


**Figure 4.1:** Simplistic representation of utility amides.

While less basic, sterically hindered lithium amides are also less nucleophilic<sup>[4]</sup> than alkyllithiums which makes them a better choice for deprotonation of substrates bearing sensitive functional groups susceptible to nucleophilic addition (*i.e.* esters<sup>[5]</sup> or nitriles<sup>[6]</sup>). This diminished nucleophilicity has also been shown to be advantageous when attempting to functionalise sensitive nitrogen heterocycles, such as pyridines, quinolines and diazines.<sup>[7-9]</sup> These important substrates represent scaffolds frequently encountered in various biologically active molecules, natural products, pharmaceuticals and agrochemicals.<sup>[10]</sup> The structural complexity of these commercial commodities requires that their syntheses need highly selective, flexible and efficient methods of functionalisation from precursors. An additional

hurdle to overcome with naked heterocycles is the lack of any directing group which could aid the control regioselectivities of such method.<sup>[11]</sup>

Diazines are derivatives of pyridines incorporating an additional N-atom which enhances their acidity (in terms of  $pK_a$  values), but also decreases the energy of their LUMO orbitals making them even more susceptible to nucleophilic addition reactions.<sup>[7]</sup> **Figure 4.2** highlights some commercially available pharmaceuticals based on structurally modified diazine scaffolds.<sup>[8,12]</sup>

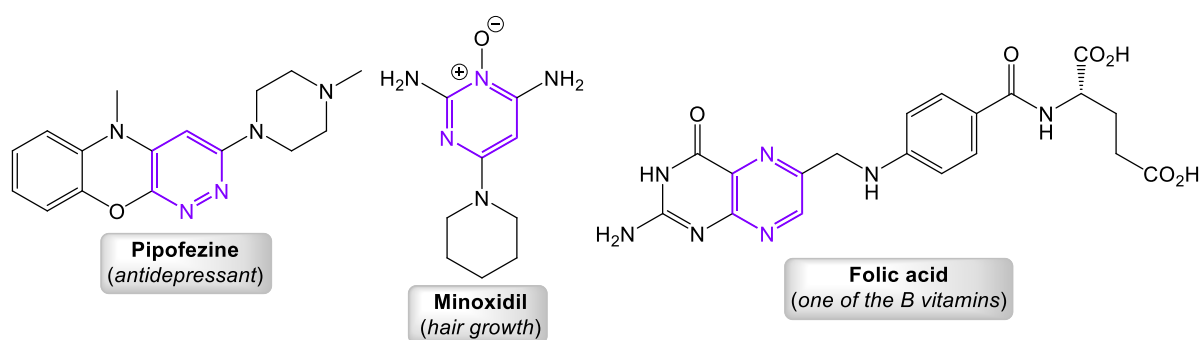
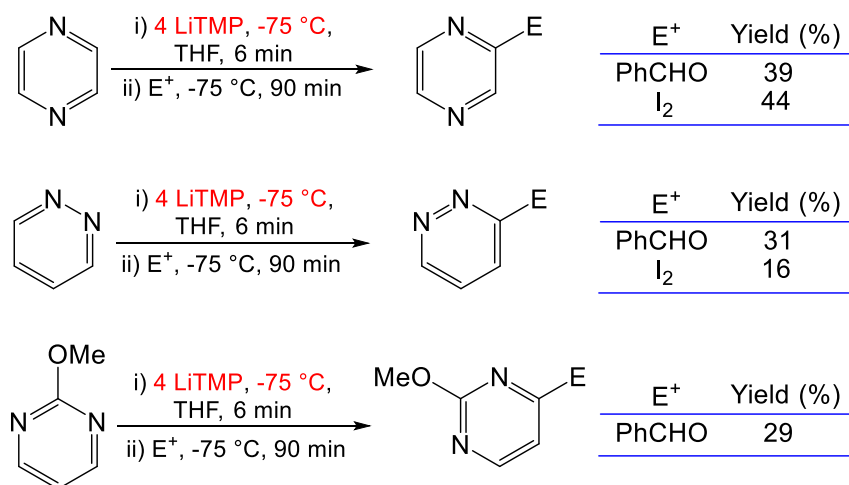


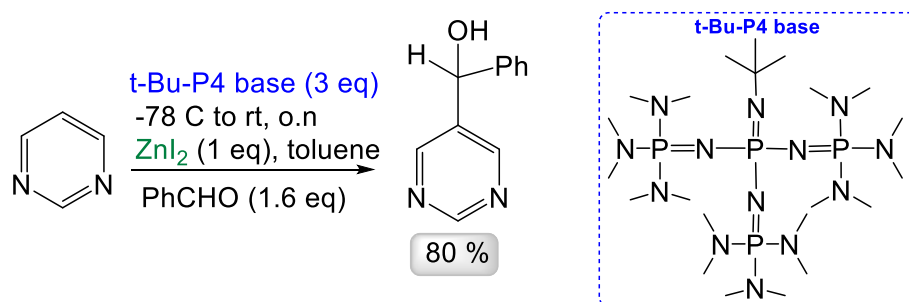
**Figure 4.2:** ChemDraw representations of selected pharmaceuticals having diazine scaffolds.<sup>[8,12]</sup>

First noted by Quéguiner, LiTMP could be employed to lithiate these sensitive substrates in moderate yields, however to achieve this, a large excess of base (4 equivalents) was required.<sup>[9]</sup> Moreover, as the lithiated diazine intermediates are generally unstable, strict cryogenic conditions, *in situ* electrophilic quenches and short reaction times are required to avoid side reactions and decomposition (**Scheme 4.1**).



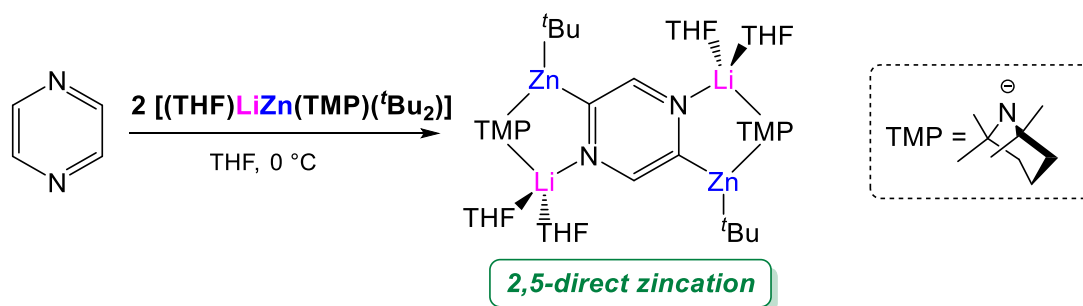
**Scheme 4.1:** Deprotonation of diazines with excess LiTMP followed by quenching.<sup>[9]</sup>

To compensate for these shortcomings, Knochel,<sup>[13]</sup> Kondo,<sup>[14]</sup> Mongin,<sup>[15]</sup> and Hevia<sup>[16]</sup> have employed coalitions of components typically but not exclusively based on the softer metal zinc (in the Pearson sense of hard and soft acids and bases, HSAB)<sup>[17]</sup> to improve stabilities and to perform metallation under milder conditions. In this context, Mongin has reported that “Li(TMP)·Zn(TMP)<sub>2</sub>” facilitates deprotonation of diazines at room temperature, whilst Knochel and Dong used (TMP)<sub>2</sub>Mg·2LiCl in the presence of ZnCl<sub>2</sub> for the regioselective α-deprotonation of pyrazine and quinoxaline. Participation of the zinc salt was found to be crucial for the success of the reaction as the reactive magnesium intermediate undergoes fast transmetalation into zincated species which are more stable and susceptible to post-metallation functionalisation. A similar role of the zinc salt was also observed by Kondo who successfully employed a nonmetallic N-alkyl oligophosphazane t-Bu-P4 base in the presence of ZnI<sub>2</sub> for deprotonative functionalisation of aromatics (**Scheme 4.2**).



**Scheme 4.2:** Deprotonation of pyrimidine by the t-Bu-P4 base.<sup>[14]</sup>

Though these organic studies made excellent progress, a lack of definitive structural information still limits the understanding of this area, which in the most extreme “black box” cases leads to a misidentification of the actual metallating base.<sup>[18]</sup> Addressing this gap in knowledge, our group employed a well-defined lithium zincate [(THF)LiZn(TMP)<sup>t</sup>Bu<sub>2</sub>] for a direct zincation of pyrazine (**Scheme 4.3**) and, going a step further, offered the first tangible information on the constitution of the organometallic intermediates involved in these reactions (**Figure 4.3**).<sup>[16]</sup>



**Scheme 4.3:** Deprotonation of pyrazine with lithium zincate [(THF)LiZn(TMP)<sup>t</sup>Bu<sub>2</sub>].<sup>[16]</sup>

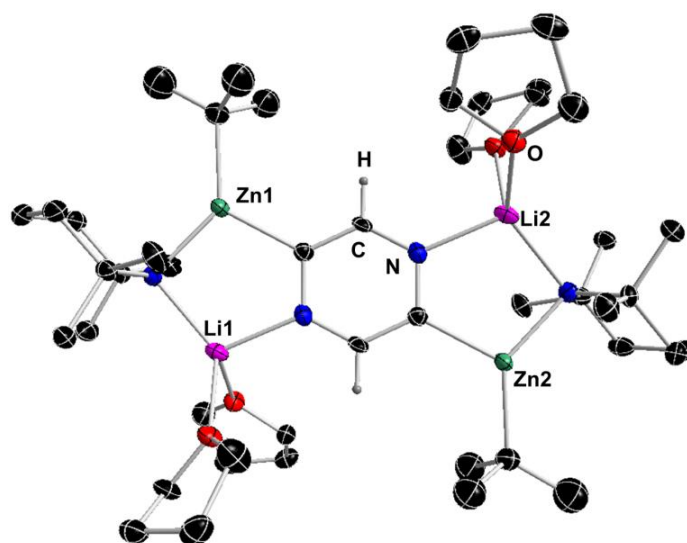
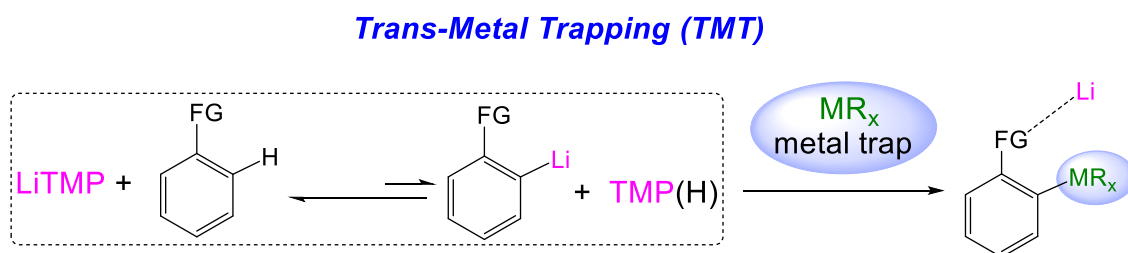


**Figure 4.3:** Molecular structure of [2,5-((THF)<sub>2</sub>LiZn(TMP)(<sup>t</sup>Bu))<sub>2</sub>(C<sub>4</sub>N<sub>2</sub>H<sub>2</sub>)] with 50% probability displacement ellipsoids. All hydrogen atoms except those on pyrazine ring have been omitted for clarity.<sup>[16]</sup>

Building on these previous studies, which all depend on the reactivity of LiTMP and presence of softer zinc, we decided to explore the trans-metal-trapping approach (see **Chapter 1**) as an alternative to existing methods. Thus, this chapter gives an account of a new trans-metal-trapping (TMT) protocol based on a mixture of LiTMP and bulky tris(trimethylsilylmethyl)gallium which leads to promising applications for the regioselective deprotonation of these sensitive heterocycles.

## 4.2. Establishing GaR<sub>3</sub> as a trapping agent

Since previous work by Quéguiner has demonstrated that LiTMP on its own can metallate diazines, albeit not very efficiently, we surmised that this system could be particularly interesting to test the ability of GaR<sub>3</sub> to engage in trans-metal trapping processes (**Scheme 4.4**).



**Scheme 4.4:** Two-step lithiation and carbanion trapping process in equilibrium controlling TMT.

On the strength of the previous work in **Chapters 2** and **3**, bulky tris(trimethylsilylmethyl)gallium (GaR<sub>3</sub>) seemed like an excellent choice of a trapping agent for several reasons. To start with, liquid GaR<sub>3</sub> exhibits good hydrocarbon solubility giving it a decided advantage over salt traps (e.g., MgCl<sub>2</sub>, ZnCl<sub>2</sub>),<sup>[19]</sup> which generally need the use of ethereal solvents and often require low temperatures to avoid competing salt metathesis reactions. More importantly, Ga is characterised by strong carbophilicity, stronger than that of zinc or aluminium, on account of which it could sedate the sensitive and unstable incipient carbanions arising from deprotonation of N-heterocyclic molecules. Apart from these intrinsic properties of GaR<sub>3</sub>, a key property of the trapping reagent, as demonstrated by the previous work,<sup>[20]</sup> is its inertness towards co-complexation with LiTMP, and therefore our first step was to establish whether GaR<sub>3</sub> is bulky enough to compromise its ability to form a weakly basic ate with LiTMP. Such separation is essential to action the lithiation step of TMT since whereas free LiTMP is a strong base, combining it with for example <sup>t</sup>Bu<sub>3</sub>Al to form aluminate LiAl(TMP)(<sup>t</sup>Bu)<sub>3</sub> greatly diminishes its deprotonating power. Unfortunately limited solubility of LiTMP in arene solvents such as benzene or toluene precluded meaningful DOSY NMR studies, however a comparison of a <sup>1</sup>H NMR spectrum of a LiTMP/GaR<sub>3</sub> mixture with those of the individual components was evidence enough that LiTMP and GaR<sub>3</sub> remain separate in benzene solution (**Figure 4.4**). The lack of co-complexation is best deduced by the informative singlet at 0.13 ppm which corresponds to

coincidentally overlapping CH<sub>2</sub> and CH<sub>3</sub> resonances of the CH<sub>2</sub>SiMe<sub>3</sub> group on gallium.<sup>[21]</sup> Furthermore, resonances for both tetrameric and trimeric LiTMP are present and identical to previously reported ones.<sup>[3]</sup>

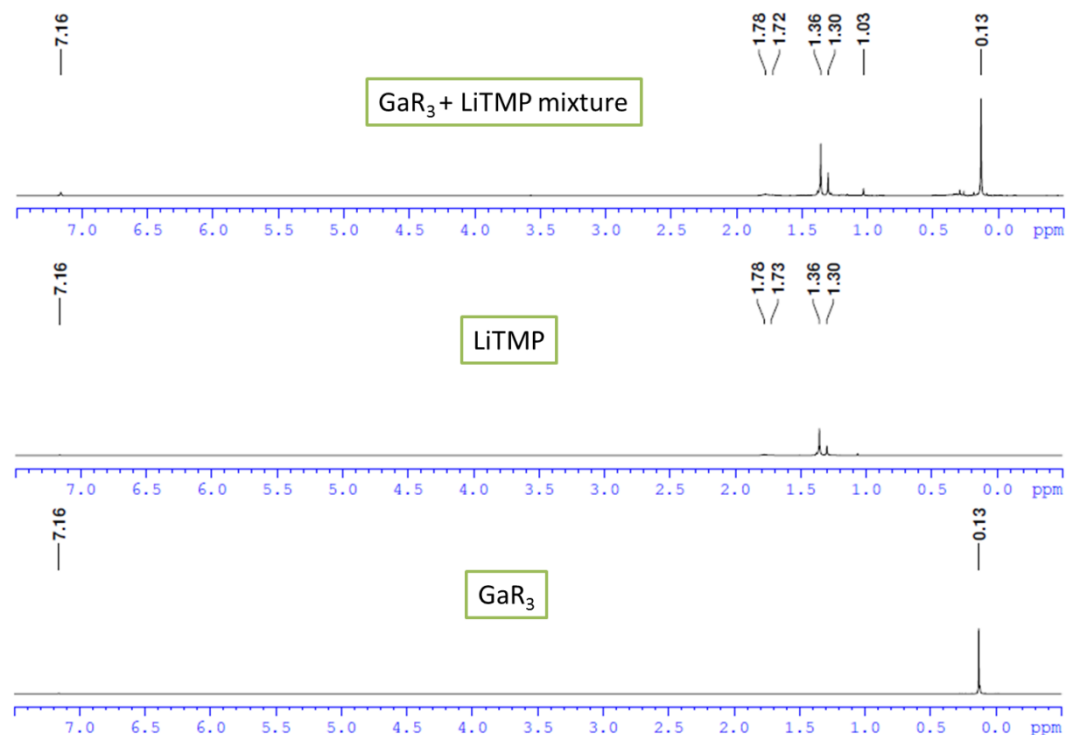


**Figure 4.4:** Comparative <sup>1</sup>H NMR spectra of free GaR<sub>3</sub> (bottom), free LiTMP (middle) and a mixture of GaR<sub>3</sub> and LiTMP in C<sub>6</sub>D<sub>6</sub>.

The ability of LiTMP and GaR<sub>3</sub> to co-complex and afford lithium gallate **I** (Figure 4.5) was further examined by performing DFT computational studies<sup>[22]</sup> employing the B3LYP method<sup>[23,24]</sup> and the 6-311G(d,p) basis set.<sup>[25]</sup>

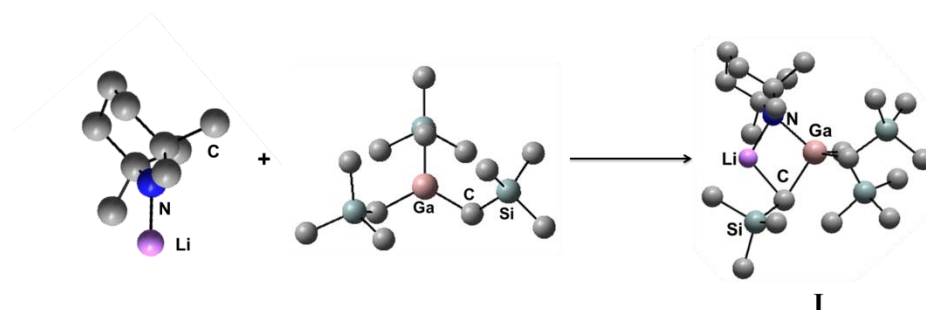


**Figure 4.5:** Modelled co-complexation process between monomeric LiTMP and GaR<sub>3</sub>.

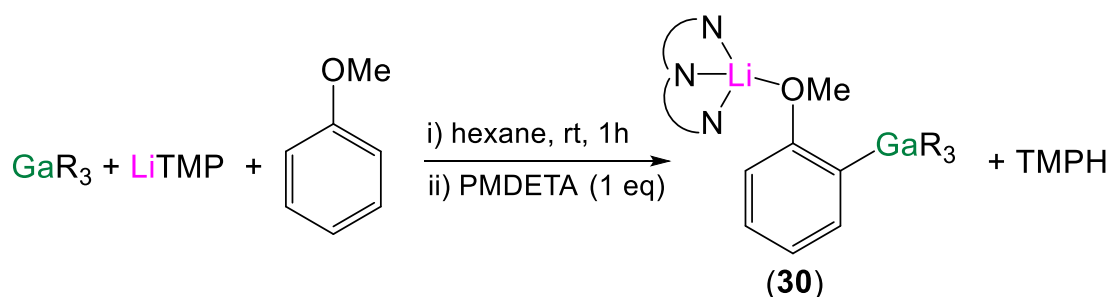


The optimised geometry of the hypothetical lithium gallate **I** contains a TMP bridge and an alkyl bridge with other two monosilyl groups terminally bonded to gallium atom. GaR<sub>3</sub> was modelled as a monomer according to its known structure in the solid state,<sup>[26]</sup> while LiTMP was modelled as a monomer, trimer and tetramer. Interestingly, it was found that the co-complexation of GaR<sub>3</sub> with LiTMP as a tetramer or trimer, which are the two known aggregates of this compound in non-polar solvent solutions,<sup>[3]</sup> were endothermic by 9.0 kcal mol<sup>-1</sup>; whereas monomeric LiTMP and GaR<sub>3</sub> was exothermic by -17.1 kcal mol<sup>-1</sup> (**Table 4.1**).

**Table 4.1:** Comparison of relative energies of co-complexation of LiTMP and GaR<sub>3</sub>.

$\frac{1}{n} (\text{LiTMP})_n + \text{GaR}_3 \rightarrow \text{LiGa}(\text{TMP})\text{R}_3$	
$n$	$\Delta E$ co-complexation/ kcal mol <sup>-1</sup>
1	-17.1
3	+9.0
4	+9.0

Confident that LiTMP and GaR<sub>3</sub> indeed remain separate in non-coordinating solvent we next decided to test this mixture as a TMT reagent using anisole as a benchmark molecule in DoM. Thus, to a hexane suspension of equimolar amounts of GaR<sub>3</sub> and LiTMP at room temperature, a molar equivalent of anisole was added to give a light yellow suspension. After stirring the mixture for an hour, an equivalent of PMDETA was added and the solution placed at -33 °C affording a crop of colourless crystals of [(PMDETA)Li(*o*-C<sub>6</sub>H<sub>4</sub>OMe)Ga(CH<sub>2</sub>SiMe<sub>3</sub>)<sub>3</sub>] (**30**) in a 55% isolated yield (**Scheme 4.5**).



**Scheme 4.5:** Synthesis of [(PMDETA)Li(*o*-C<sub>6</sub>H<sub>4</sub>OMe)Ga(CH<sub>2</sub>SiMe<sub>3</sub>)<sub>3</sub>] (**30**).

The molecular structure of **30** was elucidated by a single crystal X-ray diffraction analysis (**Figure 4.6**) which revealed the formation of a mixed-metal lithium gallate with the two metal centres connected through an ambidentate *ortho*-metallated anisole fragment giving rise to a contacted ion-pair (CIP) structure. The *ortho* carbon of metallated anisole fragment bonds to gallium forming a new Ga-C bond (Ga-C13 2.0501(15) Å in **Fig 4.6**) similar in length with the remaining Ga-C<sub>alkyl</sub> bonds ranging from 2.0279(16) Å to 2.0447(15) Å. The C4-tetracoordinated gallium atom exhibits a nearly ideal tetrahedral geometry with an average bond length of 2.0388 Å and a mean bond angle of 109.43° (angles ranging from 104.89(6)° to 113.24(7)°) which are in good agreement with those of previously discussed tetra-coordinated gallate species **3** (**Chapter 2**). Exhibiting a more distorted tetrahedral geometry with an average angle of 108.41°, the oxygen-bound lithium atom completes its coordination sphere by bonding to tridentate PMDETA ligand. Exhibiting an open structural motif, PMDETA-capped Li and GaR<sub>3</sub> are situated at the opposite sides of C17-C14-O1 plane (plane perpendicular to the aromatic ring plane) precluding any possibility for secondary interactions between Li and any methyl groups of GaR<sub>3</sub>. Whereas **30** is unprecedented in gallium chemistry, a very similar, open structural motif has been reported in the scope of zincate chemistry for the related complex [(PMDETA)Li(*o*-C<sub>6</sub>H<sub>4</sub>OMe)Zn<sup>t</sup>Bu<sub>2</sub>].<sup>[27]</sup>

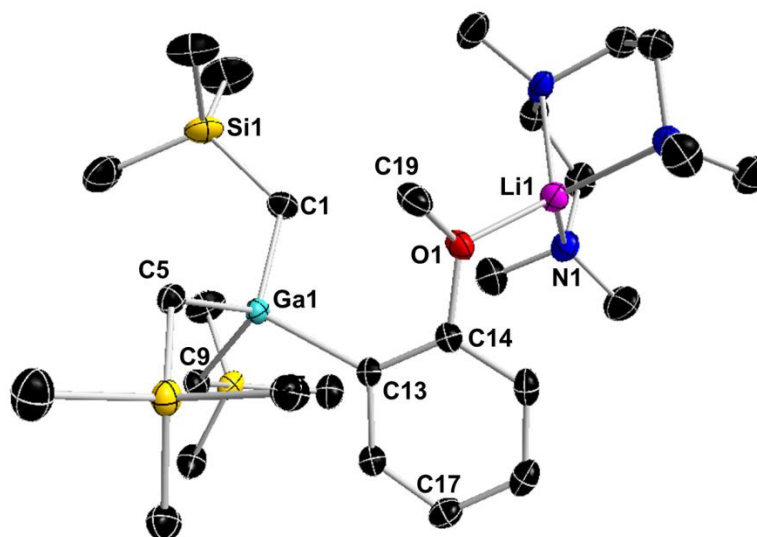
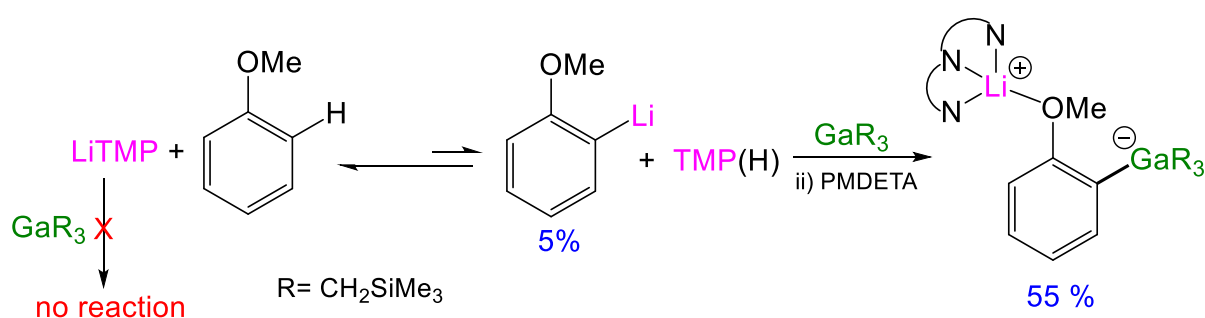


**Figure 4.6:** Molecular structure of **30** with 50% probability displacement ellipsoids. All hydrogen atoms have been omitted for clarity. Selected bond distances (Å) and bond angles (°): Ga(1)-C(1) 2.0279(16), Ga(1)-C(5) 2.0447(15), Ga(1)-C(9) 2.0324(15), Ga(1)-C(13) 2.0501(15), Li(1)-O(1) 1.910(3), Li(1)-N(1) 2.100(3), Li(1)-N(2) 2.072(3), Li(1)-N(3) 2.116(3), C(1)-Ga(1)-C(5) 113.24(7), C(1)-Ga(1)-C(9) 110.64(7), C(1)-Ga(1)-C(13) 110.19(7), C(5)-Ga(1)-C(9) 104.89(6), C(5)-Ga(1)-C(13) 109.73(6), C(9)-Ga(1)-C(13) 107.92(6).

Multinuclear ( $^1\text{H}$ ,  $^{13}\text{C}\{^1\text{H}\}$  and  $^7\text{Li}$ ) NMR spectroscopic analysis of **30** in  $d_8$ -THF solution was consistent with the solid-state structure. Thus, two doublets (7.44 and 6.40 ppm, integrating for 1H each), two triplets (6.54 and 6.78 ppm, integrating for 1H each) and a singlet at 3.67 ppm (integrating for 3H) are observed for the *ortho*-substituted anisole. The most informative resonance of this set is a doublet at 7.44 ppm corresponding to the *meta*-CH adjacent to the gallated C-atom which is significantly upfield shifted in comparison to that reported for the *ortho*-lithiated anisole (*cf.* 7.66 ppm). The presence of two distinct singlets at -0.85 and -0.19 ppm which upon integration show an overall 3:1 ratio against anisole is indicative of preservation of the three monosilyl groups on gallium. The most informative resonance in the  $^{13}\text{C}$  NMR spectrum is a low intensity signal at 155.2 ppm for the C-Ga resonance which is a good agreement with the relevant resonance in *ortho*-aluminated anisole (*cf.* 154.4 ppm),<sup>[20]</sup> reflecting the expected chemical similarity between Al and Ga.

The formation of **30** can be best interpreted as a two-step lithiation/trans-metal-trapping process synergic in efficiency as both LiTMP and  $\text{GaR}_3$  are essential for the success of the reaction. Whereas alkyllithium reactions are generally irreversible, LiTMP reactions tend to be  $pK_a$  dependent equilibria and it was previously established that LiTMP yields only about 5% lithiated anisole.<sup>[20]</sup> In TMT these equilibria can be shifted towards the wanted lithiated substrate product by its interception *via* a trapping agent. In this system, sterically voluminous  $\text{GaR}_3$  traps and stabilises the carbanion generated by deprotonative lithiation and equally as important shifts the equilibrium towards the desired anisoyl gallium product by not engaging with the free LiTMP (**Scheme 4.6**).

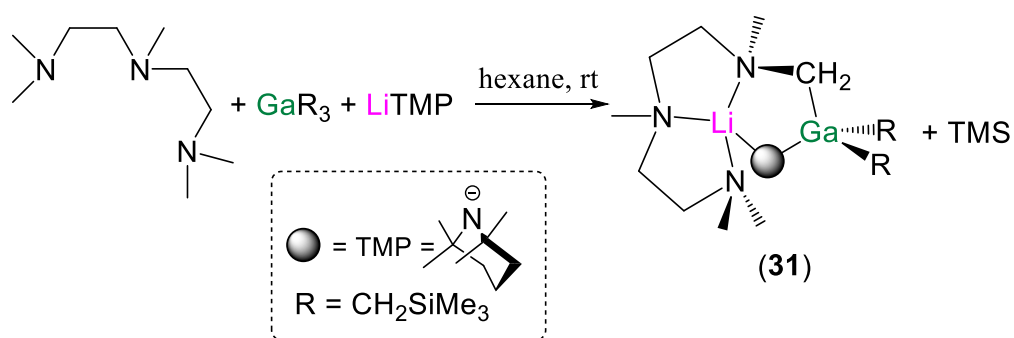


**Scheme 4.6:** Two-step lithiation/trans-metal-trapping synthesis of **30**.

Direct interception of the lithiated substrate with an electrophile such as I<sub>2</sub> would be inadequate for its non-selective nature. To elaborate, by treating the reaction mixture with iodine both lithiated anisole and LiTMP would react preventing the equilibrium in **Scheme**

**4.6** shifting towards lithiated anisole, whereas the GaR<sub>3</sub> selectively targets lithiated anisole and leaves bulkier LiTMP untouched and available to undergo further reaction.

Tridentate PMDETA proved to be the perfect donor molecule to stabilise the sensitive metallo-species and to help the crystallisation by chelating to lithium. We previously attempted to employ THF or TMEDA, however these donors led to the formation of oily mixtures. During the course of these investigations it became apparent that it is important to add PMDETA at a later stage of the reaction to avoid undergoing competing deprotonation itself as we have unambiguously established by isolating a fortuitous product [Li{Me<sub>2</sub>NCH<sub>2</sub>CH<sub>2</sub>N(Me)CH<sub>2</sub>CH<sub>2</sub>N(Me)CH<sub>2</sub>}(TMP)GaR<sub>2</sub>] (**31**) (Scheme 4.7).



**Scheme 4.7:** Synthesis of [Li{Me<sub>2</sub>NCH<sub>2</sub>CH<sub>2</sub>N(Me)CH<sub>2</sub>CH<sub>2</sub>N(Me)CH<sub>2</sub>}(TMP)GaR<sub>2</sub>] (**31**).

Determined by X-ray crystallography, the molecular structure of **31** (Figure 4.7) reveals a closed CIP arrangement where the two metal centres connect through two anions, namely TMP bridge and an ambidentate NCH<sub>2</sub> fragment of metallated PMDETA. This double bridge closes a five-membered {LiNCGaN} ring, while gallium's tetrahedral coordination sphere is completed by two terminal monosilyl groups. Interestingly, note that the three Ga-C bonds (ranging from 2.043(5) Å to 2.047(5) Å) and the Ga-N bond (2.052(4) Å) are the same length within the experimental error. The lithium centre completes its coordination sphere by bonding to the remaining two PMDETA N-donor atoms with an average Li-N bond length of 2.264 Å.

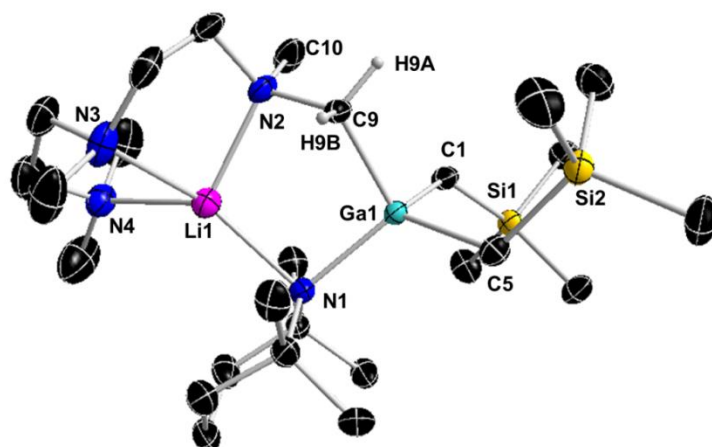


**Figure 4.7:** Molecular structure of **31** with 50% probability displacement ellipsoids. All hydrogen atoms except those on metallated CH<sub>2</sub> group of PMDETA have been omitted for clarity. Selected bond distances (Å) and bond angles (°): Ga(1)-C(1) 2.047(5), Ga(1)-C(5) 2.043(5), Ga(1)-C(9) 2.047(5), Ga(1)-N(1) 2.052(4), Li(1)-N(1) 2.187(10), Li(1)-N(2) 2.128(10), Li(1)-N(3) 2.267(9), Li(1)-N(4) 2.474(10), C(1)-Ga(1)-C(5) 105.3(2), C(1)-Ga(1)-C(9) 107.0(2), C(1)-Ga(1)-N(1) 119.53(19), C(5)-Ga(1)-C(9) 109.0(2), C(5)-Ga(1)-N(1) 114.90(18), C(9)-Ga(1)-N(1) 100.38(18).

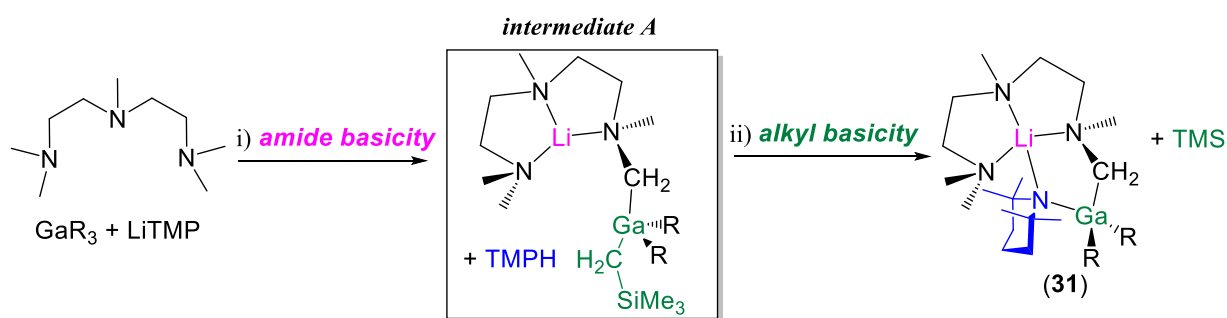
Closer inspection of the bond angles subtending Li [N-Li-N angles ranging from 79.3(3)° to 138.8(4)°, mean 108.2°] reveals a significantly distorted tetrahedral geometry which can further be quantified by calculating a Houser geometry index for four-coordinate complex ( $\tau_4$ ) which defines the molecular shape and the alignment of the structure to the perfect tetrahedron (**Equation 1**).<sup>[28]</sup>

$$\tau_4 = \frac{360^\circ - (\alpha + \beta)}{141^\circ}$$

**Equation 4.1:** Houser geometry index parameter for four-coordinate complex,  $\tau_4$ , where  $\alpha$  and  $\beta$  are the two largest bond angles around the atom of interest.<sup>[28]</sup>

Based on the value of the largest angles around the atom ( $\alpha$  and  $\beta$ ), the value of  $\tau_4$  can vary between 1 for a perfect tetrahedron ( $\alpha=\beta=109.5^\circ$ ) to 0 for a square planar geometry ( $\alpha=\beta=180^\circ$ ). Thus, with the largest bond angles around Li of 138.8(4)° and 128.4(4)°, applying **Equation 1** affords a  $\tau_4$  value of 0.66 which corroborates a significant distortion from tetrahedral geometry that must be imposed by the coordination modes of the metallated PMDETA. In comparison, the same calculation for the Ga centre ( $\alpha=119.53(19)^\circ$ ,  $\beta=114.90(18)^\circ$ ) yields a  $\tau_4$  value of 0.89 revealing a coordination geometry only slightly distorted from tetrahedral.

A quick glance at the structure might suggest that it is  $\text{GaR}_3$  that deprotonated the substrate as the structure incorporates a TMP anion and only two monosilyl groups on gallium. However  $\text{GaR}_3$  on its own is not a sufficiently strong base to metallate PMDETA, therefore the  $\alpha$ -deprotonation is based on the stepwise cooperation between LiTMP and  $\text{GaR}_3$ . LiTMP deprotonates the triamine followed by the fast trans-metal-trapping process with  $\text{GaR}_3$  yielding a proposed intermediate **A** (Scheme 4.8i) where concomitantly produced TMPH helps to fill the coordination sphere of lithium and is thus in close proximity to  $\text{GaR}_3$ . The sterically encumbered intermediate and enhanced acidity of coordinated TMPH makes it possible for otherwise inert gallium alkyl to react affording **31** and TMS (Scheme 4.8ii).



**Scheme 4.8:** Proposed reaction sequence for the surprising formation of **31**.

Although we have no direct evidence for the proposed mechanism, it is supported indirectly by the notion that triorganogallium reagents cannot deprotonate coordinating additives such as PMDETA or TMEDA as C-H bonds adjacent to N centres in tertiary amines are only weakly acidic (see below). In addition, it was found that the bulkiness of a reagent such as  $\text{GaR}_3$  precludes chelation and instead, it acts as a bridging ligand as observed in the crystal structure of  $\text{R}_3\text{Ga-TMEDA-GaR}_3$ .<sup>[29]</sup> Further, to an extent, experimental support for the proposed pathway came from the addition of a similar, but smaller diamine TMEDA to the mixture of LiTMP and  $\text{GaR}_3$  from which we have isolated  $[(\text{TMEDA})\text{Li}\{\text{Me}_2\text{NCH}_2\text{CH}_2\text{N}(\text{Me})\text{CH}_2\}\text{GaR}_3]$  (**32**) (Figure 4.8). Displaying an open CIP structure with three alkyl groups on gallium and no TMP anion incorporation, the molecular structure of **32** is reminiscent of the proposed intermediate **A**. Here, due to the smaller size of the used diamine,  $\text{N}_4$ -tetracoordinated lithium is capped with two molecules of TMEDA one of which is metallated and the other one is neutral, completing the coordination sphere and avoiding the close proximity of TMPH and  $\text{GaR}_3$  which would induce alkyl basicity.

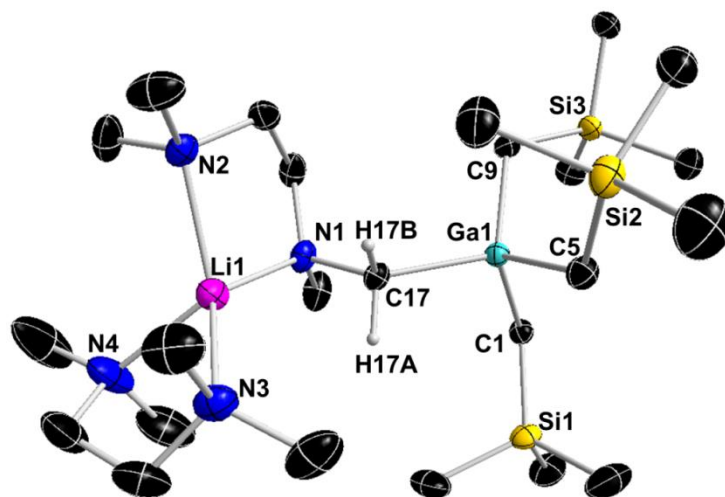


**Figure 4.8:** Molecular structure of **32** with 50% probability displacement ellipsoids. All hydrogen atoms except those on metallated CH<sub>2</sub> group of TMEDA have been omitted for clarity. Selected bond distances (Å) and bond angles (°): Ga(1)-C(1) 2.0451(19), Ga(1)-C(5) 2.032(2), Ga(1)-C(9) 2.029(2), Ga(1)-C(17) 2.0646(19), Li(1)-N(1) 2.049(4), Li(1)-N(2) 2.164(4), Li(1)-N(3) 2.202(4), Li(1)-N(4) 2.117(4), C(9)-Ga(1)-C(5) 112.62(9), C(9)-Ga(1)-C(1) 108.32(8), C(1)-Ga(1)-C(5) 110.02(8), C(9)-Ga(1)-C(17) 112.35(8), C(5)-Ga(1)-C(17) 102.76(8), C(1)-Ga(1)-C(17) 100.71(8).

The direct  $\alpha$ -metallation of tertiary amines is typically hampered by the destabilization arising from the repulsion between the developing carbanion and the lone pair electron density of the adjacent nitrogen atom.<sup>[4]</sup> There are few examples of such metallations with different organoalkali reagents such as <sup>t</sup>BuLi, <sup>n</sup>BuLi or LICKOR,<sup>[30–32]</sup> however isolation and structural characterisation of **31** and **32** is rather unusual, with the only other similar examples stemming from deprotonation by employing the LiTMP and Al<sup>t</sup>Bu<sub>3</sub> mixture.<sup>[33]</sup>

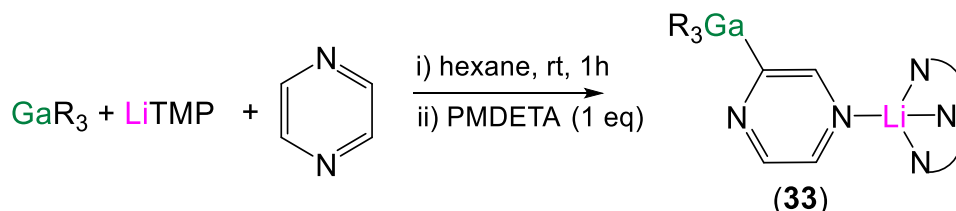
Despite the formation of **31** and **32** being reproducible, a clean and controlled synthesis has yet to be achieved, thus no further characterisation (neither NMR spectroscopic nor elemental analysis) has been obtained. Nonetheless, the formation of **31** and **32** further supports our notion that LiTMP and GaR<sub>3</sub> do not co-complex, even if a donor molecule is offered, but rather exist as separate species and react with substrates in a sequential manner.

### 4.3. Applying TMT for pyrazine functionalisation

Studies on the metallation of pyrazine have shown that four molar equivalents of LiTMP are required in THF at -75°C, affording only modest yields of 2-substituted derivatives (39–65%



depending on the electrophile) along with variable amounts of 2,5-disubstituted product (16%).<sup>[9]</sup> Performed at room temperature in hexane solution our new LiTMP/GaR<sub>3</sub> TMT approach in a 1:1:1 stoichiometry with pyrazine afforded selectively [1-(PMDETA)Li-3-(GaR<sub>3</sub>)-C<sub>4</sub>H<sub>3</sub>N<sub>2</sub>] (**33**) isolated in 61% crystalline yield (**Scheme 4.9**) and its molecular structure was established by X-ray crystallography.



**Scheme 4.9:** Synthesis of pyrazine derived [1-(PMDETA)Li-3-(GaR<sub>3</sub>)-C<sub>4</sub>H<sub>3</sub>N<sub>2</sub>] (**33**).

The formally monogallated pyrazine complex (**33**) exhibits an open CIP motif with a 1,3-separation of (PMDETA)Li and GaR<sub>3</sub> units bonded to N and C atoms, respectively (**Figure 4.9**).

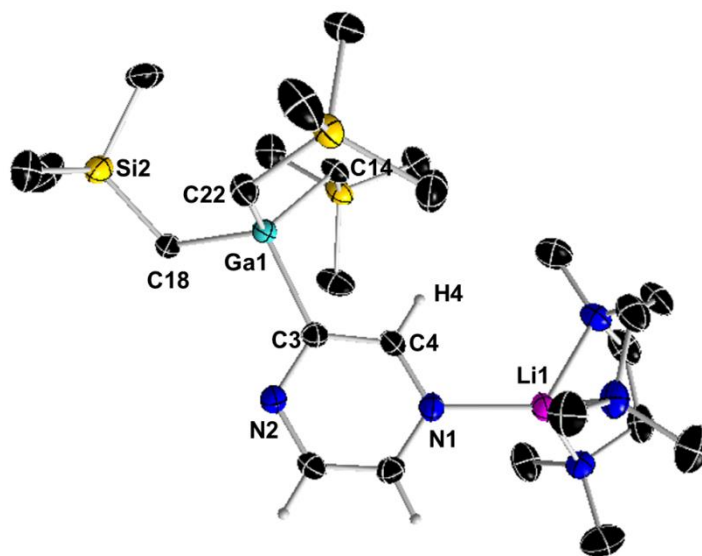


**Figure 4.9:** Molecular structure of **33** with 50% probability displacement ellipsoids. All hydrogen atoms except those on pyrazine have been omitted for clarity. Selected bond distances (Å) and bond angles (°): Ga(1)-C(3) 2.043(2), Ga(1)-C(14) 2.031(2), Ga(1)-C(18) 2.028(2), Ga(1)-C(22) 2.027(2), Li(1)-N(1) 2.020(4), Li(1)-N(3) 2.079(4), Li(1)-N(4) 2.098(4), Li(1)-N(5) 2.047(4), C(22)-Ga(1)-C(18) 110.40(9), C(22)-Ga(1)-C(14) 113.88(9), C(18)-Ga(1)-C(14) 112.94(9), C(22)-Ga(1)-C(3) 104.19(9), C(18)-Ga(1)-C(3) 108.29(9), C(14)-Ga(1)-C(3) 106.55(9).



The N<sub>4</sub>-tetracoordinated Li-atom once again exhibits a distorted tetrahedral geometry determined by bond angles ranging from 122.7(2)° to 88.02(16)° [mean angle 108.6°] and an average bond length of 2.061 Å, however a  $\tau_4$  value of 0.84 reflects a significantly reduced level of distortion than that observed in **31**. Showing very little variation in length (varying from 2.027(2) Å to 2.043(2) Å), the four Ga-C bonds are in excellent agreement with other related tetracoordinated gallium species discussed throughout this thesis (*e.g.*, compound **30**). It is remarkable that this is, as far as we can ascertain, the first example of a structurally characterised monometallated unsubstituted pyrazine obtained by direct metallation. There are two other reported structures incorporating Ir<sup>[34]</sup> and Pd<sup>[35]</sup> but they have been obtained *via* a halogen displacement methodology.

The <sup>1</sup>H NMR spectrum of **33** in d<sub>8</sub>-THF solution was consistent with the monosubstituted pyrazine displaying three distinct resonances at 7.76, 8.48 and 8.56 ppm integrating for 1H each, as opposed to the solitary singlet at 8.55 ppm for a symmetrical free pyrazine. The preserved integrity of **33** in solution is further indicated by the presence of two singlets at -0.82 and -0.18 ppm corresponding to the CH<sub>2</sub> and CH<sub>3</sub> groups of the monosilyl group, as well as by the appearance of four broadened resonances between 2.20 and 2.60 ppm for coordinated PMDETA (**Figure 4.10**).

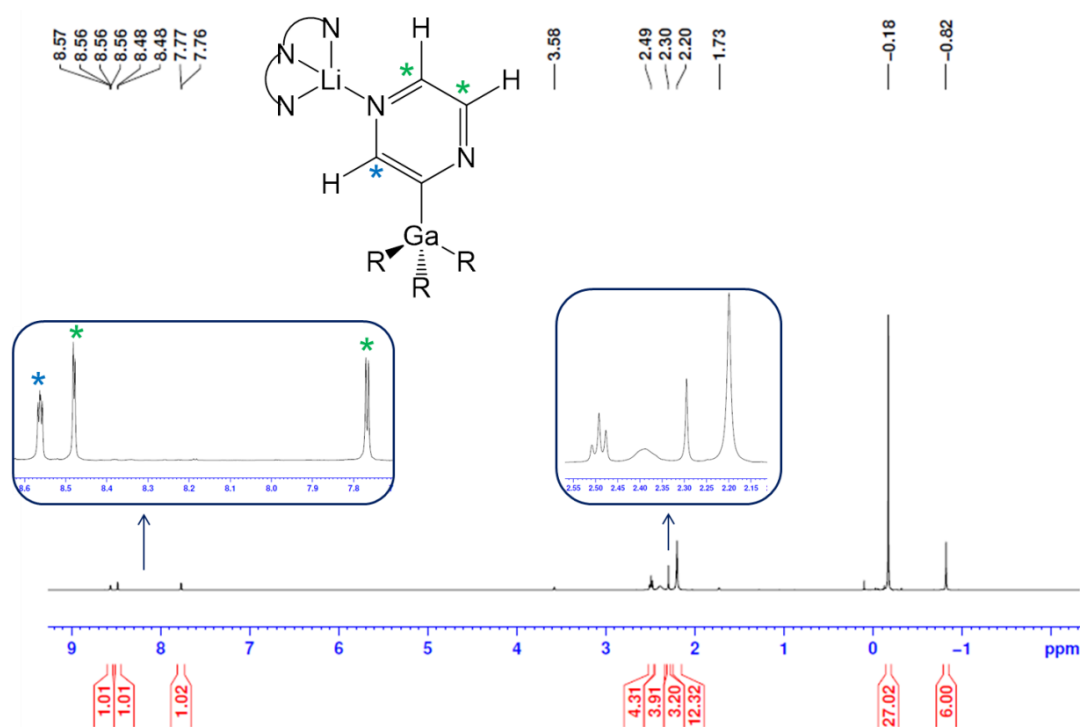
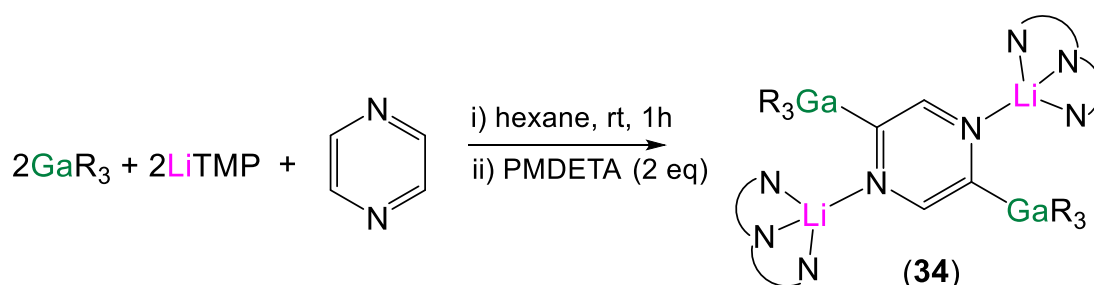


**Figure 4.10:** <sup>1</sup>H NMR spectrum of **33** in d<sub>8</sub>-THF solution.

The most informative resonance in the  $^{13}\text{C}$  NMR spectrum is the one for C-Ga located at 198.8 ppm displaying a significant downfield chemical shift when compared to that of free pyrazine (*cf.* 146.1 ppm).

Although **33** was isolated in only 61% crystalline yield, NMR monitoring of the reaction and integration against an internal standard revealed a quantitative formation in solution. In addition to excellent efficiency, our TMT protocol displayed remarkable selectivity as no dimetallated species has been observed. This observation prompted us to increase the base:trap:substrate ratio to 2:2:1, again in hexane at room temperature, affording dimetallated [1,4-((PMDETA)Li) $_2$ -2,5-(GaR $_3$ ) $_2$ -C $_4$ H $_2$ N $_2$ ] (**34**) in 43.6 % yield (**Scheme 4.10**).



**Scheme 4.10:** Synthesis of pyrazine derived [1,4-((PMDETA)Li) $_2$ -2,5-(GaR $_3$ ) $_2$ -C $_4$ H $_2$ N $_2$ ] (**34**).

The centrosymmetric molecular structure of **34** revealed a two-fold deprotonation of pyrazine incorporating two (PMDETA)Li and two GaR $_3$  units cooperatively stabilising the dianion by tying up the lone pairs of the N and C atoms respectively (**Figure 4.11**). The Ga-C bond lengths and C-Ga-C bond angles show very little variation amongst each other or to the ones reported for **33**, however a notably more congested structure of tetranuclear complex **34** with its GaR $_3$  and (PMDETA)Li units in proximal disposition, is revealed in enhanced distortion of tetrahedral geometry around the Li-atom. Having a  $\tau_4$  value of 0.63, the Li atom in **34** displays a significant level of distortion, greater even than the distortion found in **31** (*cf.*  $\tau_4=0.66$ ). Additionally, the Li-N<sub>pyrazine</sub> bond (Li1-N1, 2.138(3) Å in **Figure 4.11**) is elongated (by approximately 6%) in comparison to the analogous bond witnessed in **33** (Li1-N1, 2.020(4) Å in **Figure 4.9**). The molecular structure adopted by **34** is comparable with the relevant two-fold zincated pyrazine (*vide supra*) with the main structural difference being the open CIP motif most probably directed by the lack of bridging TMP ligands.

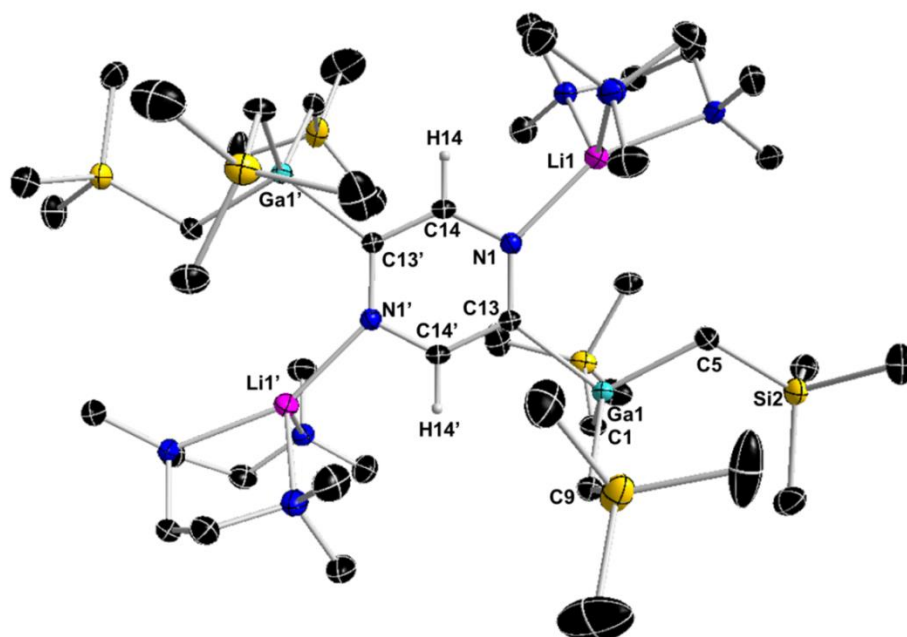
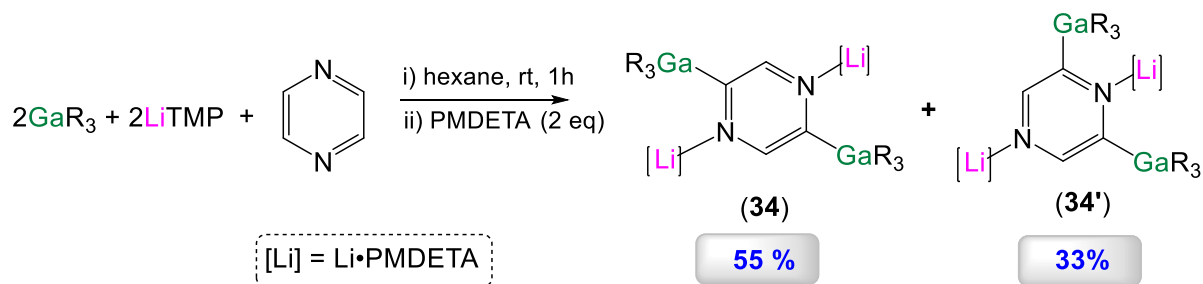


**Figure 4.11:** Molecular structure of **34** with 50% probability displacement ellipsoids. All hydrogen atoms except those on the pyrazine ring have been omitted for clarity. Symmetry operator:  $-x, -y, -z$ . Selected bond distances (Å) and bond angles ( $^{\circ}$ ): Ga(1)-C(1) 2.022(3), Ga(1)-C(5) 2.021(2), Ga(1)-C(9) 2.018(3), Ga(1)-C(13) 2.062(3), Li(1)-N(1) 2.106(5), Li(1)-N(2) 2.197(5), Li(1)-N(3) 2.224(5), Li(1)-N(4) 2.144(5), C(5)-Ga(1)-C(13) 104.22(10), C(1)-Ga(1)-C(13) 100.99(10), C(9)-Ga(1)-C(5) 119.36(12), C(9)-Ga(1)-C(1) 114.86(10), C(5)-Ga(1)-C(1) 108.11(10), C(9)-Ga(1)-C(13) 107.12(12), N(1)-Li(1)-N(4) 108.2(2), N(1)-Li(1)-N(2) 103.7(2), N(4)-Li(1)-N(2) 126.8(2), N(1)-Li(1)-N(3) 154.5(3), N(4)-Li(1)-N(3) 84.22(18), N(2)-Li(1)-N(3) 84.74(17).

From the NMR data in  $d_8$ -THF solutions, the two-fold deprotonation and formation of the symmetric complex is identified by a singlet at 8.58 ppm in the  $^1\text{H}$  NMR spectrum for the  $\text{C}_4\text{H}_2\text{N}_2$  fragment and a resonance at 184.9 for the C-Ga in the  $^{13}\text{C}$  NMR spectrum.

Interestingly, NMR monitoring of the reaction revealed **34** is formed in a 55% yield, along with a second isomer (**34'**) formed in 33% which appears to be the analogous product of 2,6-digallation (**Scheme 4.11**).



**Scheme 4.11:** Synthesis of digallated pyrazine regioisomers **34** and **34'**.

Regioisomer **34'** could not be obtained as a crystalline solid; however its constitution was confirmed unambiguously by multinuclear NMR spectroscopic analysis in  $d_8$ -THF solution. Confirming the symmetrical nature of the complex, only one singlet in the aromatic region of the  $^1\text{H}$  NMR spectrum is observed at 8.14 ppm, significantly upfield shifted in comparison to the corresponding resonance of **34**. Similarly, in the  $^{13}\text{C}$  NMR spectrum two resonances at 146.6 and 194.5 are observed attributed to the C-H and C-Ga atoms of the pyrazine scaffold (**Figure 4.12**).

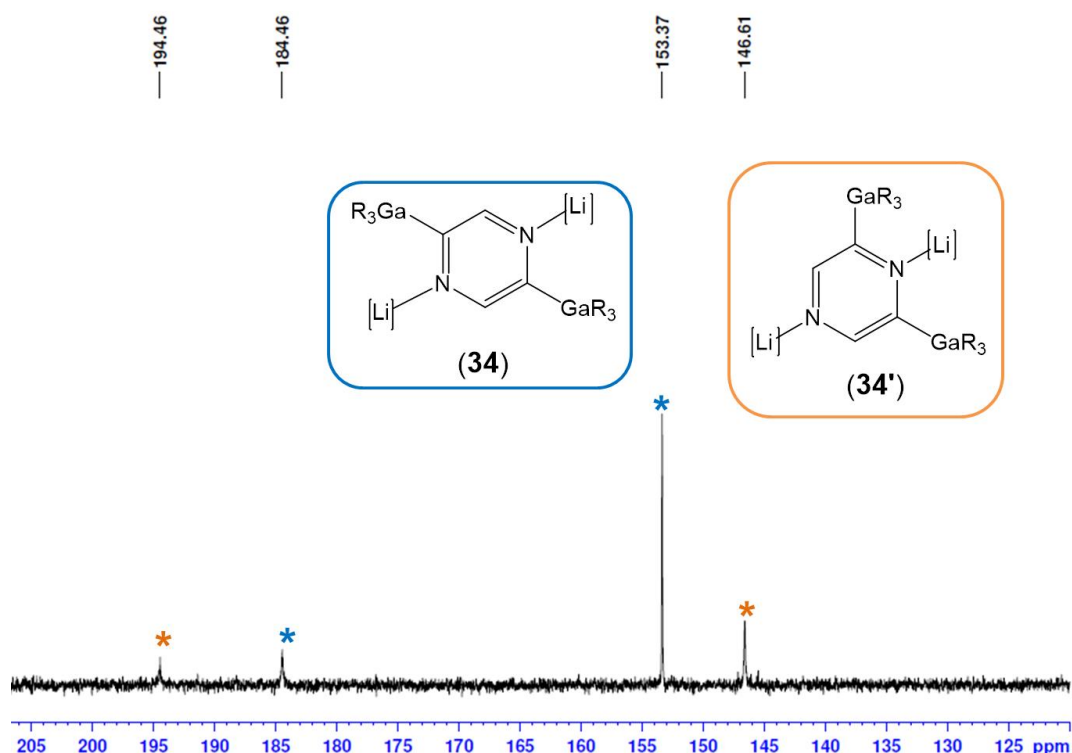
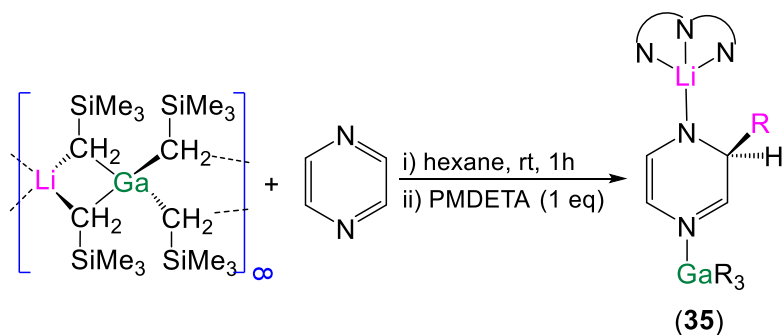


**Figure 4.12:** Low field region of the  $^{13}\text{C}$  NMR spectrum in  $d_8$ -THF solution of the crude reaction mixture affording formation of **34** and **34'**.

The stoichiometric control achieved by this TMT approach where depending on the base stoichiometry it is possible to mono- and digallate pyrazine contrasts with the performance of zincate  $[(\text{THF})\text{LiZn}(\text{TMP})^t\text{Bu}_2]$ . This operates through a synchronised bimetallic synergy distinct to that of stepwise TMT, as it affords only the 2,5-disubstituted pyrazine even with a 1:1, base:substrate stoichiometry (**Scheme 4.3**).<sup>[16]</sup> Previously, excess LiTMP (1.5 equivalents) dispensed as 0.5  $\text{ZnCl}_2 \cdot \text{TMEDA}/1.5$  LiTMP in THF produced 59% of the isolated 2-iodopyrazine that reportedly decomposes at room temperature, but in hexane a significant amount of coupled dimer product was also seen.<sup>[15]</sup>

Finally, for comparison, we have performed a control reaction, employing the same reaction conditions, between pyrazine and gallate  $\text{LiGaR}_4$ <sup>[21]</sup> which exists as a polymeric bimetallic species (**Scheme 4.12**). The reaction proceeded with a formation of orange suspension which upon addition of one equivalent of PMDETA afforded a deep red solution.



**Scheme 4.12:** Synthesis of **35** by nucleophilic addition of one monosilyl arm of  $\text{LiGaR}_4$ .

Despite several attempts, no crystalline material was obtained, that notwithstanding  $^1\text{H}$  NMR spectroscopic analysis of the crude reaction mixture in  $d_8$ -THF solution disclosed that a chemoselective addition of the R group, with concomitant dearomatization of the heterocycle has taken place affording **35** as evidenced by the appearance of four broad resonances in the region between 2.5 and 6.5 ppm (**Figure 4.13**).

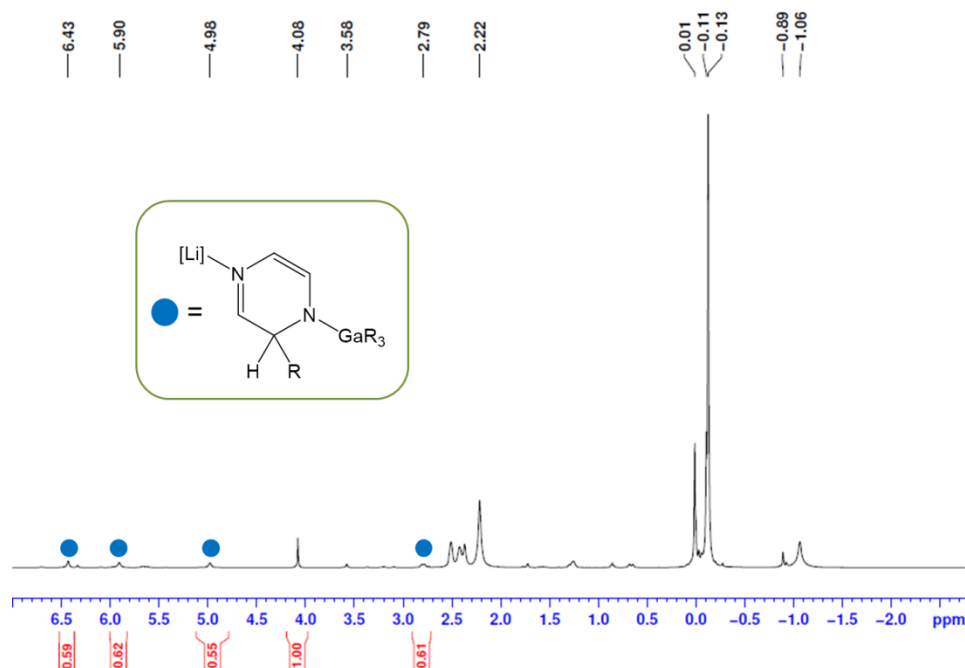
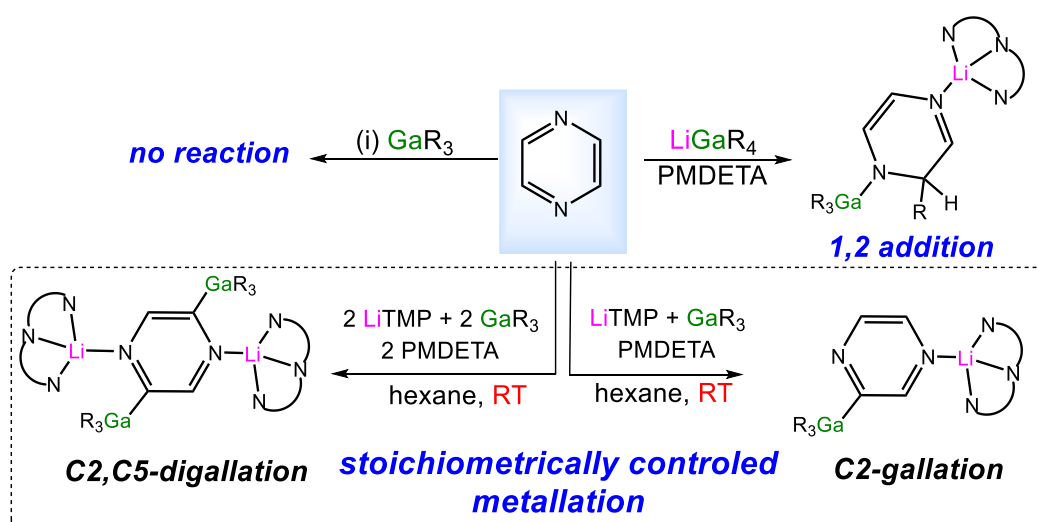


**Figure 4.13:**  $^1\text{H}$  NMR spectrum of the crude reaction mixture of affording **35** in  $d_8$ -THF.

Integration against a ferrocene internal standard has revealed a 55% yield of **35** with the remaining unreacted pyrazine removed under vacuum. Further studies were not successful due to the instability of the reaction mixture with a drastic colour change from red to deep blue and purple over a short time period hinting at a radical formation in the reaction mixture.

Using pyrazine as a case study it is possible to compare the reactivity of single metal reagents with the bimetallic lithium gallate and tandem LiTMP and GaR<sub>3</sub> reagent mixture (**Scheme 4.13**). Thus, polar LiTMP is reactive towards pyrazine but requires excess base and employment of cryogenic conditions, GaR<sub>3</sub> shows no reactivity towards pyrazine but only coordination is expected to occur, while the tetraalkyl lithium gallate will undergo nucleophilic addition. However, a mixture of LiTMP and GaR<sub>3</sub> operating in a tandem manner will perform a chemoselective metallation and with the additional benefit of good stoichiometric control.

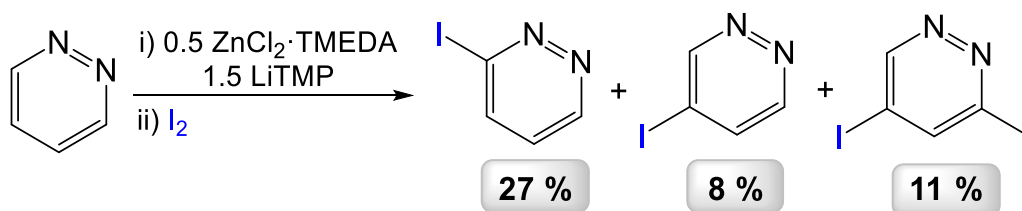


**Scheme 4.13:** Contrasting reactivities of LiTMP and different lithium-gallium combinations towards pyrazine.

#### 4.4. Expanding the scope of TMT to other sensitive heterocycles

With the well-established reactivity towards symmetrical pyrazine, it was decided to expand the scope to the next diazine, in particular pyridazine which with its 1,2-placement of N atoms, offers a choice of metallation sites. Site selectivity in its metallation is exceptionally challenging as evident from previous work using excess LiTMP in 0.5 ZnCl<sub>2</sub>·TMEDA/1.5LiTMP/I<sub>2</sub>, which in hexane at room temperature achieved only 27% of the

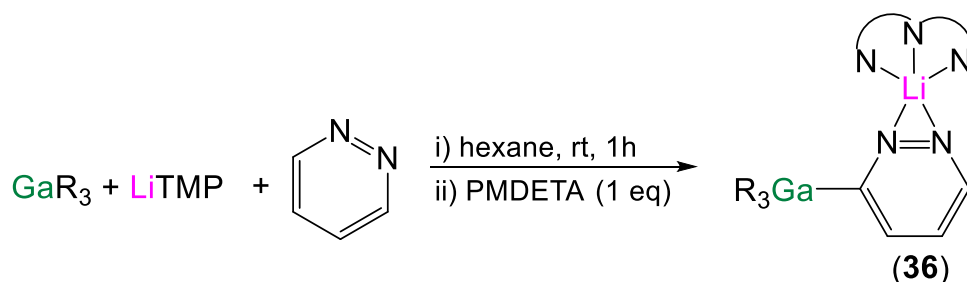
3-iodo product mixed with the 4-iodo, and 3,5-diiido derivatives as well as 54% unreacted pyridazine (**Scheme 4.14**).<sup>[15]</sup>



**Scheme 4.14:** Complexity of the deprotonation of pyridazine with  $\text{ZnCl}_2 \cdot \text{TMEDA} / 1.5 \text{ LiTMP}$  mixture followed by iodine quench.<sup>[15]</sup>

In THF the yield of the 3-iodo product rises to 66% but only under extreme reflux conditions. On its own, LiTMP (4 equivalents) in THF at  $-75^\circ\text{C}$  produced only 16-32% yields of 3-substituted pyridazines following quenching with different electrophiles.<sup>[9]</sup>

Run in hexane solution at room temperature, our TMT reaction afforded  $[1,2\text{-}(\text{PMDETA})\text{Li-}3\text{-}(\text{GaR}_3)\text{-C}_4\text{H}_3\text{N}_2]$  (**36**) in a 51% crystalline yield (**Scheme 4.15**).



**Scheme 4.15:** Synthesis of pyridazine-derived  $[1,2\text{-}(\text{PMDETA})\text{Li-}3\text{-}(\text{GaR}_3)\text{-C}_4\text{H}_3\text{N}_2]$  (**36**).

The unit cell of **36** contains two crystallographically independent molecules with identical connectivity, one of which contains minor disorder in the PMDETA ligand, thus structural discussion is focused on the non-disordered molecule. The molecular structure of **36** (**Figure 4.14**) shows C4-tetracoordinated  $\text{GaR}_3$  elects to sit at the most acidic 3-position adjacent to one N-atom, exhibiting again nearly ideal tetrahedral geometry with the average bond length of  $2.032 \text{ \AA}$  and a mean bond angle of  $109.1^\circ$ . A novel feature is the  $\text{Li}(\text{PMDETA})$  unit bridging the two diazine N atoms [ $\text{Li-N}$  bond lengths  $2.093(5)$  and  $2.043(5) \text{ \AA}$  for the non-disordered molecule of the  $Z'=2$  structure] leading to the five-coordinate spiro Li centre connecting the 3- and 2 x 5-atom rings.

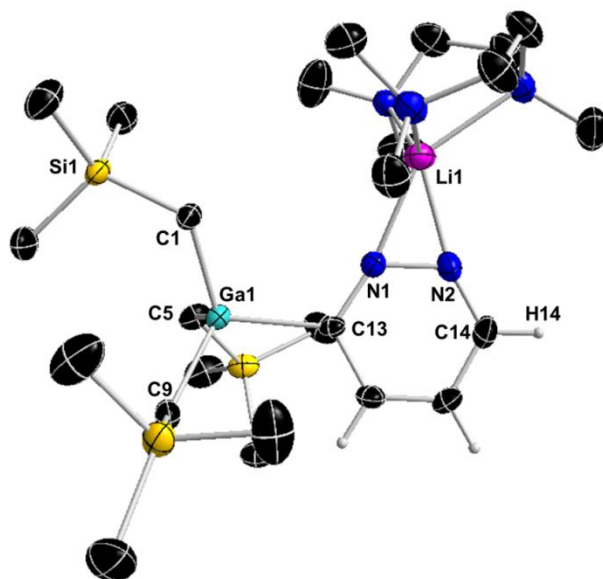
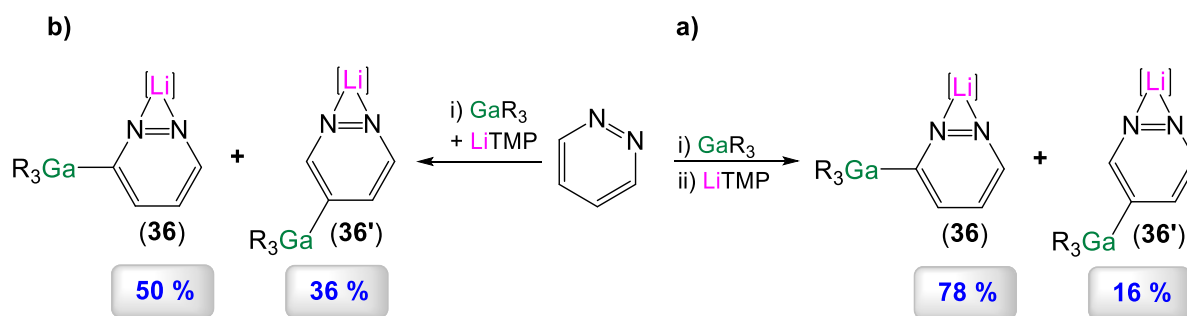


**Figure 4.14:** Molecular structure of **36** with 50% probability displacement ellipsoids. All hydrogen atoms except those on the pyridazine ring have been omitted for clarity. The unit cell of **36** contains two crystallographically independent molecules with identical connectivity. One molecule contains minor disorder in its PMDETA ligand, thus structural discussion is limited to the non-disordered molecule. Selected bond distances (Å) and bond angles (°): Ga(1)-C(1) 2.018(2), Ga(1)-C(9) 2.023(2), Ga(1)-C(5) 2.031(2), Ga(1)-C(13) 2.056(2), Li(1)-N(1) 2.093(5), Li(1)-N(2) 2.043(5), Li(1)-N(3) 2.129(5), Li(1)-N(4) 2.169(5), Li(1)-N(5) 2.107(5), C(1)-Ga(1)-C(9) 113.96(9), C(1)-Ga(1)-C(5) 112.79(10), C(9)-Ga(1)-C(5) 107.71(10), C(1)-Ga(1)-C(13) 105.11(9), C(5)-Ga(1)-C(13) 110.16(9), C(9)-Ga(1)-C(13) 104.91(9), N(2)-Li(1)-N(1) 38.40(11), N(2)-Li(1)-N(5) 121.2(2), N(1)-Li(1)-N(5) 109.8(2), N(2)-Li(1)-N(3) 113.8(2), N(1)-Li(1)-N(3) 107.4(2), N(5)-Li(1)-N(3) 124.3(2), N(2)-Li(1)-N(4) 109.0(2), N(1)-Li(1)-N(4) 147.4(2), N(5)-Li(1)-N(4) 84.38(18), N(3)-Li(1)-N(4) 85.94(18).

$^1\text{H}$  NMR spectroscopic analysis of **36** in  $d_8$ -THF exhibits three distinct multiplets (7.16, 7.84 and 8.66 ppm) characteristic for the C3-monosubstituted pyridazine. The most diagnostic resonance in the  $^{13}\text{C}$  NMR spectrum is a low intensity C-Ga signal at 199.9 ppm.

Interestingly,  $^1\text{H}$  NMR monitoring of the reaction revealed an important effect of the order of metal reagent addition on reaction regioselectivity. Thus, when LiTMP is added as a solid to the hexane solution of  $\text{GaR}_3$  and pyridazine, **36** is obtained in a 78% yield, along with small amounts of the C4-gallated regioisomer **36'** (16% yield), **Scheme 4.16a**. Contrastingly, if the substrate is added to the hexane suspension of LiTMP and  $\text{GaR}_3$ , the yield of **36** decreases to 50%, and more C4 metallated product **36'** is seen (36%), **Scheme 4.16b** and **Figure 4.15**. These contrasting results suggest an activating effect of the  $\text{GaR}_3$  component, which perhaps can initially coordinate to the Lewis basic N atoms of the heterocycle, facilitating its lithiation at the C3 position.





**Scheme 4.16:** a) Regioselectivity observed when LiTMP is added to the solution of GaR<sub>3</sub> and pyridazine; b) Regioselectivity observed when pyridazine is added to the suspension of LiTMP and GaR<sub>3</sub>.

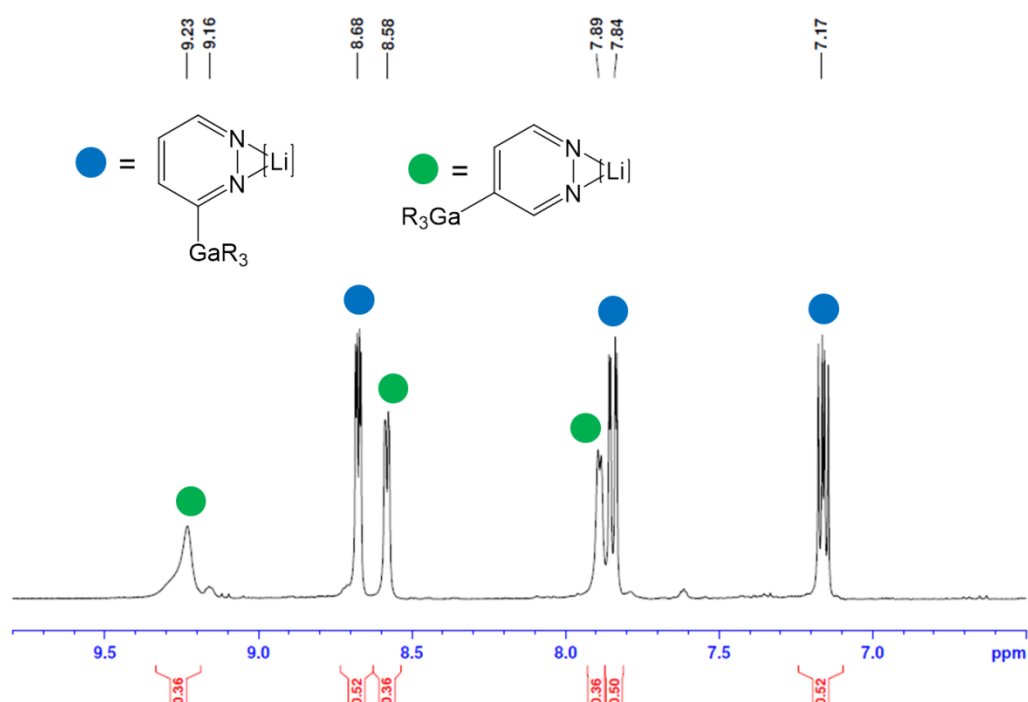
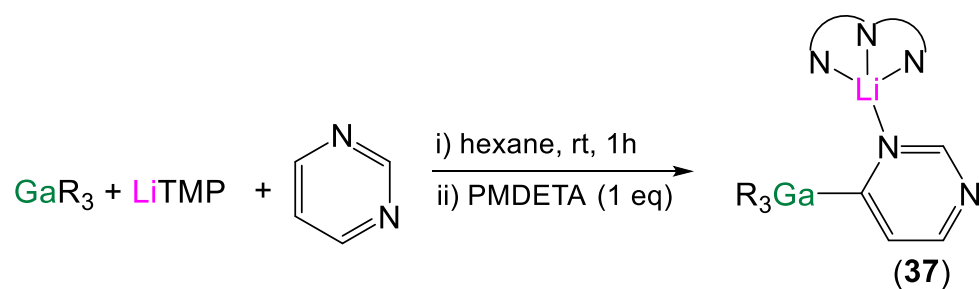


**Figure 4.15:** Aromatic region of <sup>1</sup>H NMR spectrum of **36** and **36'** in d<sub>8</sub>-THF solution.

As previous work had established that 1,3-diazine (pyrimidine) was found to be totally inert to LiTMP from 0°C to reflux temperatures,<sup>[15]</sup> it seemed the greatest challenge to TMT. However, TMT was again successful, demonstrated tangibly through isolation and structural authentication of the metallated pyrimidine [1-(PMDETA)Li-6-(GaR<sub>3</sub>)-C<sub>4</sub>H<sub>3</sub>N<sub>2</sub>] (**37**) which was produced in a 27% isolated crystalline yield (**Scheme 4.17**).



**Scheme 4.17:** Synthesis of pyrimidine-derived [1-(PMDETA)Li-6-(GaR<sub>3</sub>)-C<sub>4</sub>H<sub>3</sub>N<sub>2</sub>] (**37**).

Its structure (**Figure 4.16**) exhibits many of the features previously observed in complexes **33**, **34** and **36** with the proximal 1,6-separation of its GaR<sub>3</sub> and (PMDETA)Li fragments, akin to that found in dimetallated pyrazine **34**. As is commonly observed in the beforehand examples, again both metals display tetrahedral geometry with an average Ga-C and Li-N bond length of 2.033 Å and 2.158 Å, respectively.

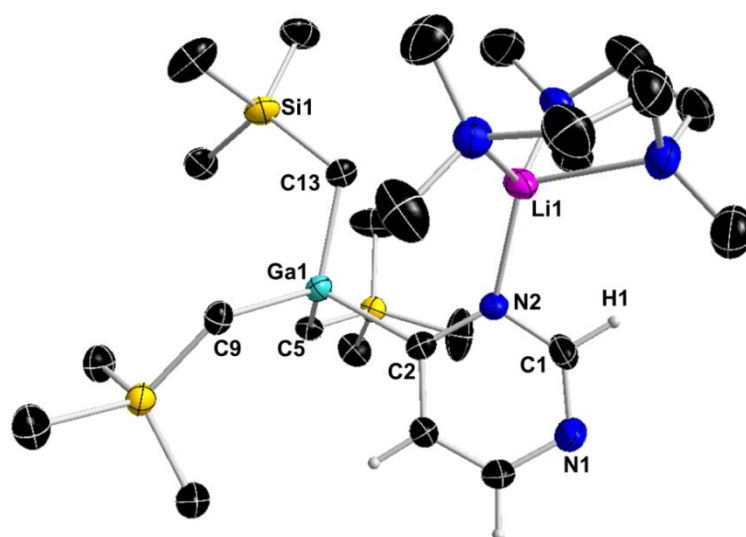


**Figure 4.16:** Molecular structure of **37** with 50% probability displacement ellipsoids. All hydrogen atoms except those on the pyrimidine ring have been omitted for clarity. Selected bond distances (Å) and bond angles (°): Ga(1)-C(2) 2.052(3), Ga(1)-C(5) 2.031(3), Ga(1)-C(9) 2.030(3), Ga(1)-C(13) 2.020(3), Li(1)-N(2) 2.067(6), Li(1)-N(3) 2.157(7), Li(1)-N(4) 2.246(7), Li(1)-N(5) 2.162(7), C(5)-Ga(1)-C(2) 113.00(13), C(9)-Ga(1)-C(2) 108.09(13), C(13)-Ga(1)-C(2) 107.52(13), C(9)-Ga(1)-C(5) 113.97(13), C(13)-Ga(1)-C(5) 111.77(13), C(13)-Ga(1)-C(9) 111.84(14), N(2)-Li(1)-N(3) 111.8(3), N(2)-Li(1)-N(5) 123.0(3), N(3)-Li(1)-N(5) 123.9(3), N(2)-Li(1)-N(4) 113.9(3), N(3)-Li(1)-N(4) 85.0(2), N(5)-Li(1)-N(4) 83.5(2).

Multinuclear NMR spectroscopic analysis in  $d_8$ -THF is in excellent agreement with the solid-state structure, most notably in the  $^1\text{H}$  NMR spectrum where a singlet at 8.87 ppm is observed that can be attributed to the *CH* between the two nitrogen atoms (i.e. C1 in **Figure 4.16**). Interestingly, the C-Ga resonance in the  $^{13}\text{C}$  NMR spectrum is observed at 219.3 ppm (**Figure 4.17**) significantly downfield shifted in comparison to that of other gallated diazines reported here (*vide supra*), alluding at the more carbenic nature of this particular bond in **37**. Additionally, the  $^7\text{Li}$  NMR spectrum displays a broad resonance at 2.41 ppm which could suggest a dynamic process taking place whereby Li shuttles between the two nitrogen atoms of pyrimidine, causing signal broadening.

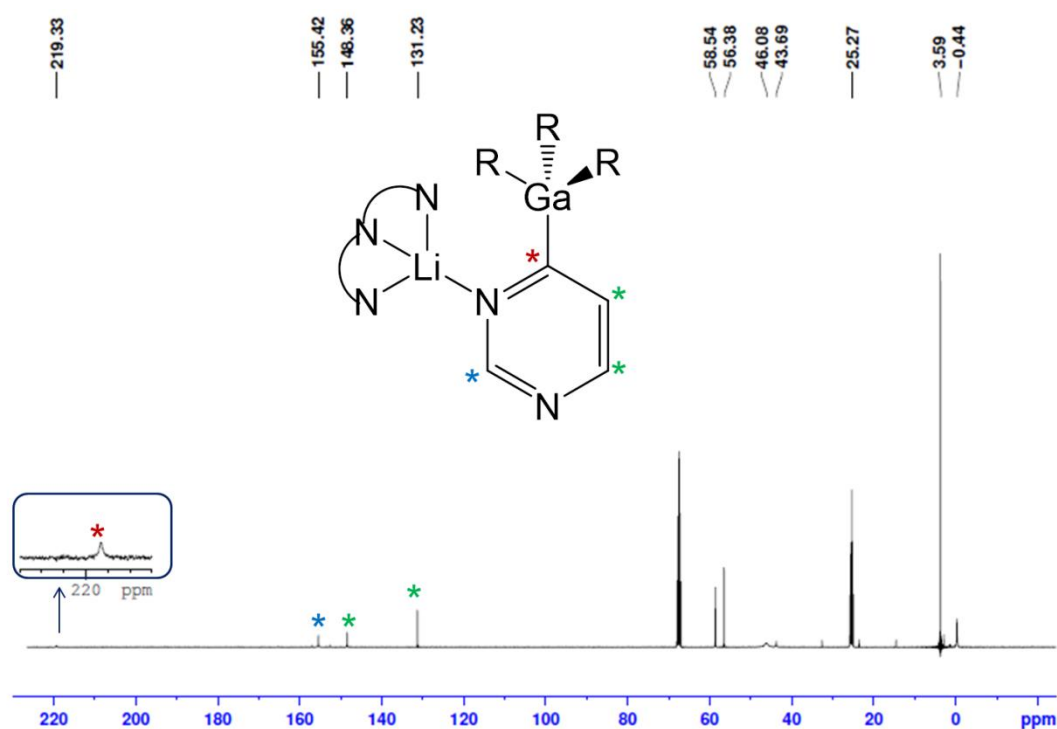
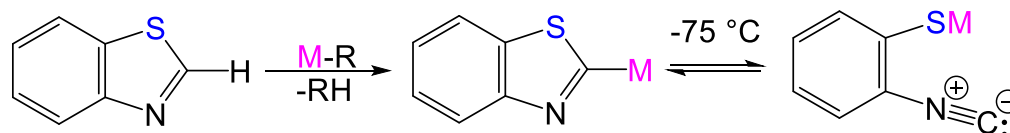


**Figure 4.17:**  $^{13}\text{C}$  NMR spectrum of **37** in  $d_8$ -THF solution.

NMR monitoring of the reaction revealed that in the solution this yield is increased to 59%. However unlike in the synthesis of **36** where the order of addition could help improve regioselectivity, here no significant difference is observed.

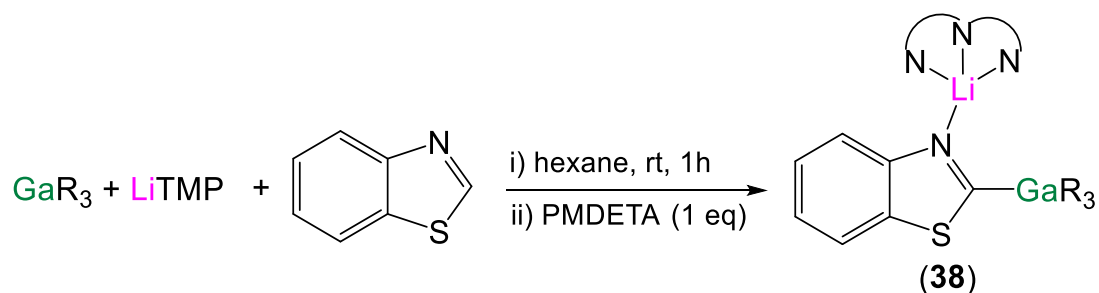
Pleased by these results, we were intrigued to see if this TMT approach could be utilized for the metallation of other families of heterocycles, as for example benzothiazole (btz). This fused heterocycle is easier to deprotonate at its C2 site due to its higher acidity ( $pK_a = 27.3$  vs  $37.3$   $pK_a$  of pyrazine, in DMSO),<sup>[36]</sup> however the formed 2-lithio derivative is well known to

exist simultaneously in ring-closed and ring-opened forms, as best evidenced by Boche's seminal  $^{13}\text{C}$  NMR studies in  $\text{d}_8\text{-THF}$  at  $-75^\circ\text{C}$  (**Scheme 4.18**).<sup>[37]</sup>



**Scheme 4.18:** Equilibrium between the ring-opened isonitrile tautomer and ring-closed benzothiazole tautomer upon metallation.

Carried out at room temperature, an addition of an equimolar amount of benzothiazole to the hexane suspension of  $\text{LiTMP}$  and  $\text{GaR}_3$ , followed by addition of PMDETA for the purpose of crystallization, produced crystalline complex  $[\text{2-(GaR}_3\text{)-3-\{Li(PMDETA)\}-C}_6\text{H}_4\text{NCS}]$  **38** in a remarkably high isolated yield of 84% (**Scheme 4.19**).



**Scheme 4.19:** Synthesis of  $[\text{2-(GaR}_3\text{)-3-\{Li(PMDETA)\}-C}_6\text{H}_4\text{NCS}]$  (**38**).

The molecular structure of **38** follows the connectivity pattern observed in the diazine series with the  $\text{Ga}(\text{R}_3)$  and  $\text{Li}(\text{PMDETA})$  units adjacent on deprotonated C and N atoms respectively with a small  $\text{Ga1-C13-N1-Li1}$  torsion angle of  $-13.9(4)^\circ$  (**Figure 4.18**). There is only a handful of C2-metal bonded benzothiazole structures reported in the CCDC of which only two are with main group metals, namely magnesium<sup>[38]</sup> and tin.<sup>[39]</sup> The magnesiated benzothiazole exhibits a dimeric structure and was prepared by direct magnesiation of free benzothiazole with the magnesium amide base,<sup>[38]</sup> while the relevant tin compound was prepared by lithiation at low temperature followed by transmetalation to  $\text{SnPh}_3$ .<sup>[39]</sup>

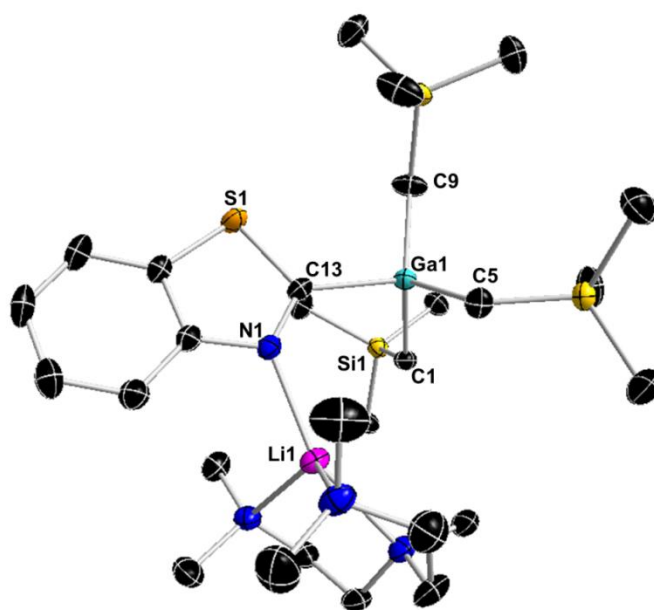


**Figure 4.18:** Molecular structure of **38** with 50% probability displacement ellipsoids. All hydrogen atoms have been omitted for clarity. Selected bond distances (Å) and bond angles (°): Ga(1)-C(1) 2.022(3), Ga(1)-C(5) 2.021(2), Ga(1)-C(9) 2.018(3), Ga(1)-C(13) 2.062(3), Li(1)-N(1) 2.016(5), Li(1)-N(2) 2.197(5), Li(1)-N(3) 2.224(5), Li(1)-N(4) 2.144(5), C(9)-Ga(1)-C(5) 119.36(12), C(9)-Ga(1)-C(1) 114.86(10), C(5)-Ga(1)-C(1) 108.11(10), C(9)-Ga(1)-C(13) 107.12(12), C(5)-Ga(1)-C(13) 104.22(10), C(1)-Ga(1)-C(13) 100.99(10), N(1)-Li(1)-N(4) 108.2(2), N(1)-Li(1)-N(2) 103.7(2), N(4)-Li(1)-N(2) 126.8(2), N(1)-Li(1)-N(3) 154.5(3), N(4)-Li(1)-N(3) 84.22(18), N(2)-Li(1)-N(3) 84.74(17)

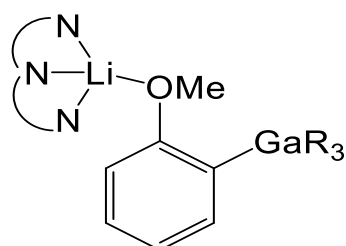
Deprotonative gallation of the C2 centre (i.e. C13 in **Figure 4.18**) was evident in  $^1\text{H}$  NMR spectrum in  $\text{C}_6\text{D}_6$  by the disappearance of the diagnostic singlet at 8.45 ppm and by the significantly downfield-shifted resonance at 209.5 ppm in the  $^{13}\text{C}$  NMR spectrum, consistent with the ring closed structure.<sup>[40]</sup> Significantly, NMR monitoring of the reaction revealed the formation of **38** to be quantitative in solution with no ring-opened metallo(2-isocyano)thiophenolate isomer detected. This first Ga TMT reaction of a N-S heterocycle is competitive with Mongin's LiTMP/ $\text{CdCl}_2$ ·TMEDA in THF solution approach, which used excess (1.5) base equivalents for a 97% yield of 2-iodobenzothiazole after  $\text{I}_2$  quenching, though no metallo-intermediate was identified.<sup>[40]</sup> These findings show a new application of TMT, enabling regioselective metallations to be carried out at RT as opposed to conventional lithium chemistry where btz has to be reacted at  $-78^\circ\text{C}$  to avoid its ring opening.

## 4.5. Conclusion and future work

This chapter has seen the emergence of a new trans-metal-trapping (TMT) protocol based on a mixture of LiTMP (the base) and tris(trimethylsilylmethyl)gallium [GaR<sub>3</sub>] (the trap) that, operating in a tandem manner, is effective for the regioselective deprotonation of diazines sensitive to conventional metallation in hydrocarbon solution. As well as launching the concept of gallium TMT, this study reports the first crystal structures of metallodiazine complexes made by metallation (C-H to C-metal) reactions for gallium and indeed, bar a single exception for zinc, for any metal. Furthermore, the study highlights that two-metal synergistic reactions are not confined to concerted, synchronised processes where the metals belong within the same reagent, but can be extended to tandem, stepwise processes involving two separately added reagents that do not form a reaction inhibiting co-complex. Work presented here could potentially open the floodgates to a general improvement in many other metallation reactions with various sensitive and non-sensitive substrates where LiTMP and related bulky bases give only low-to-moderate yields of products. In addition to extending the scope of substrates metallated by this system, future work should look at extending the range the electrophilic quenching studies as well as exploring the potential compatibility of organogallium intermediates with transition-metal coupling methodologies. Another avenue of development for future work is finding new TMT protocols incorporating a different gallium source as a trap, as well as trying some other bulky amides as base components.

## 4.6. Experimental procedures

### 4.6.1. Synthesis of [(PMDETA)Li(*o*-C<sub>6</sub>H<sub>4</sub>OMe)Ga(CH<sub>2</sub>SiMe<sub>3</sub>)<sub>3</sub>] (30)

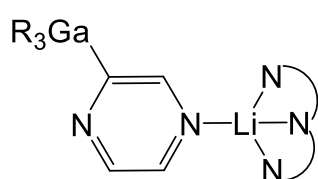


To a suspension of LiTMP (0.074g, 0.5 mmol) and Ga(CH<sub>2</sub>SiMe<sub>3</sub>)<sub>3</sub> (0.165 g, 0.5 mmol) in hexane (10 mL), an equivalent of anisole (0.054 g, 0.5 mmol, 54μL) was added at room temperature. As soon as anisole was added, a yellow fine suspension was formed which persisted during stirring for 1 hour at room temperature. PMDETA was

added (0.11 mL, 0.5 mmol), the solvent was exchanged *in vacuo* for toluene and the yellow solution placed in freezer to obtain X-ray suitable crystals (0.17 g, 55%). Anal. Calcd for C<sub>28</sub>H<sub>63</sub>GaLiN<sub>3</sub>OSi<sub>3</sub>: C, 54.35; H, 10.26; N, 6.79. Found: C, 54.95; H, 9.94; N, 7.55.

**$^1\text{H}$  NMR (298 K,  $d_8$ -THF)  $\delta$ (ppm)** -0.85 (6H, s,  $\text{CH}_2\text{SiMe}_3$ ), -0.19 (27H, s,  $\text{Si}(\text{CH}_3)_3$ ), 2.20 (12H, s,  $\text{N}(\text{CH}_3)_2$ ), 2.26 (3H, s,  $\text{NCH}_3$ ), 2.37 (4H, mult,  $\text{NCH}_2\text{CH}_2\text{N}$ ), 2.47 (4H, mult,  $\text{NCH}_2\text{CH}_2\text{N}$ ), 3.59 (3H, s,  $\text{OCH}_3$ ), 6.40 (1H, d, Ar-H), 6.53 (1H, t,  $p$ -CH), 6.78 (1H, t, Ar-H), 7.44 (1H, d, Ar-H).  **$^{13}\text{C}\{^1\text{H}\}$  NMR (298 K,  $d_8$ -THF)  $\delta$ (ppm)** 0.5 ( $\text{CH}_2\text{SiMe}_3$ ), 3.9 ( $\text{Si}(\text{CH}_3)_3$ ), 43.7 (PMDETA), 46.0 (PMDETA), 54.3 ( $\text{OCH}_3$ ), 56.2 (PMDETA), 58.5 (PMDETA), 107.5 (Ar-C), 119.4 (Ar-C), 120.9 (Ar-C), 125.0 (Ar-C), 138.8 (Ar-C), 155.2 (C-Ga), 166.7 (Ar-C).  **$^7\text{Li}$  NMR (298 K,  $d_8$ -THF, reference LiCl in  $\text{D}_2\text{O}$  at 0.00 ppm):  $\delta$**  0.14.

#### 4.6.2. Synthesis of [1-(PMDETA)Li-3-(GaR<sub>3</sub>)-C<sub>4</sub>H<sub>3</sub>N<sub>2</sub>] (33)

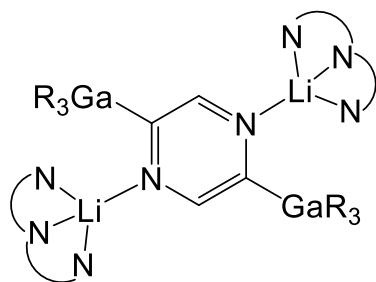


(0.074g, 0.5 mmol) and  $\text{Ga}(\text{CH}_2\text{SiMe}_3)_3$  (0.165 g, 0.5 mmol) in hexane (10 mL), 1 equivalent of pyrazine (0.04 g, 0.5 mmol) was added *via* solid addition tube at room temperature. As soon as pyrazine was added, a yellow solution was formed which quickly

evolved into orange and then red suspension. After stirring for 30 min at room temperature, PMDETA was added (0.11 mL, 0.5 mmol) which induced even stronger precipitation. Addition of 2 mL of toluene and gentle heating afforded a solution which upon slow cooling deposited X-ray suitable crystals (0.18 g, 61%). Anal. Calcd for  $\text{C}_{25}\text{H}_{59}\text{GaLiN}_5\text{Si}_3$ : C, 50.83; H, 10.07; N, 11.86. Found: C, 50.05; H, 9.74; N, 11.87.

**$^1\text{H}$  NMR (298 K,  $d_8$ -THF)  $\delta$ (ppm)** -0.82 (6H, s,  $\text{CH}_2\text{SiMe}_3$ ), -0.18 (27H, s,  $\text{Si}(\text{CH}_3)_3$ ), 2.20 (12H, s,  $\text{N}(\text{CH}_3)_2$ ), 2.30 (3H, s,  $\text{NCH}_3$ ), 2.39 (4H, br s,  $\text{NCH}_2\text{CH}_2\text{N}$ ), 2.49 (4H, mult,  $\text{NCH}_2\text{CH}_2\text{N}$ ), 7.76 (1H, s, pyrazine), 8.48 (1H, s, pyrazine), 8.56 (1H, s, pyrazine).  **$^{13}\text{C}\{^1\text{H}\}$  NMR (298 K,  $d_8$ -THF)  $\delta$ (ppm)** -0.3 ( $\text{CH}_2\text{SiMe}_3$ ), 3.5 ( $\text{Si}(\text{CH}_3)_3$ ), 43.7, 45.9, 56.1, 58.4 PMDETA, 137.5 (CH-pyrazine), 146.4(CH-pyrazine), 150.0 (CH-pyrazine), 198.8 (C-Ga).  **$^7\text{Li}$  NMR (298 K,  $d_8$ -THF, reference LiCl in  $\text{D}_2\text{O}$  at 0.00 ppm):  $\delta$**  2.35.

#### 4.6.3. Synthesis of [1,4-((PMDETA)Li)<sub>2</sub>-2,5-(GaR<sub>3</sub>)<sub>2</sub>-C<sub>4</sub>H<sub>2</sub>N<sub>2</sub>] (34)



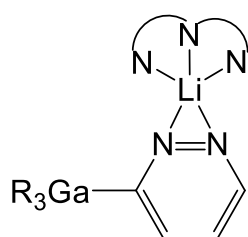
LiTMP (0.074 g, 0.5 mmol) and  $\text{Ga}(\text{CH}_2\text{SiMe}_3)_3$  (0.165 g, 0.5 mmol) in hexane (10 mL), 0.5 equivalent of pyrazine (0.02 g, 0.25 mmol) was added *via* solid addition tube at room temperature. As soon as pyrazine was added, a yellow solution was formed which quickly evolved into orange and then red suspension and finally a green solution. After

stirring for 30 min at room temperature, PMDETA was added (0.11 mL, 0.5 mmol) which induced precipitation and a change of colour to orange. Addition of 2 mL of toluene and

gentle heating afforded solution which upon slow cooling deposited X-ray suitable crystals (0.12 g, 43.6 %). Anal. Calcd for  $C_{46}H_{114}Ga_2Li_2N_8Si_6$ : C, 50.17; H, 10.43; N, 10.17. Found: C, 50.47; H, 10.44; N, 9.98.

$^1H$  NMR (298 K,  $d_8$ -THF)  $\delta$ (ppm) -0.91 (12H, s,  $CH_2SiMe_3$ ), -0.15 (54H, s,  $Si(CH_3)_3$ ), 2.17 (24H, s, PMDETA- $CH_3$ ), 2.26 (6H, s, PMDETA- $CH_3$ ), 2.34 (8H, mult, PMDETA- $CH_2$ ), 2.45 (8H, mult, PMDETA- $CH_2$ ), 8.58 (2H, s,  $H$ -pyrazine).  $^{13}C\{^1H\}$  NMR (298 K,  $d_8$ -THF) -0.3 ( $CH_2SiMe_3$ ), 3.7 ( $Si(CH_3)_3$ ), 43.8, 46.2, 56.9, 58.7 PMDETA, 153.48 (CH-pyrazine), 184.9 (C-Ga).  $^7Li$  NMR (298 K,  $d_8$ -THF, reference LiCl in  $D_2O$  at 0.00 ppm):  $\delta$  2.47.

#### 4.6.4. Synthesis of [1,2-(PMDETA)Li-3-(GaR<sub>3</sub>)-C<sub>4</sub>H<sub>3</sub>N<sub>2</sub>] (36)

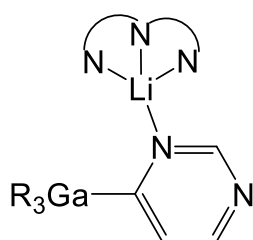


mL) of  $Ga(CH_2SiMe_3)_3$  (0.165 g, 0.5 mmol) and pyridazine (0.04 g, 0.5 mmol), LiTMP (0.074 g, 0.5 mmol) was added *via* solid addition tube at room temperature. As soon as LiTMP was added, a yellow suspension was formed which evolved into orange and then red solution. After stirring for 15 min at room temperature, PMDETA was added (0.11 mL,

0.5 mmol) which induced instant, but short-lived precipitation. The dark red solution was placed at  $-33$  °C to obtain X-ray suitable crystals (0.15 g, 51%). Anal. Calcd for  $C_{25}H_{59}GaLiN_5Si_3$ : C, 50.83; H, 10.07; N, 11.86. Found: C, 50.34; H, 9.67; N, 12.00.

$^1H$  NMR (298 K,  $d_8$ -THF)  $\delta$ (ppm) -0.75 (6H, s,  $CH_2SiMe_3$ ), -0.16 (27H, s,  $Si(CH_3)_3$ ), 2.17 (12H, s,  $N(CH_3)_2$ ), 2.41 (7H, mult,  $NCH_3 + NCH_2CH_2N$ ), 2.54 (4H, mult,  $NCH_2CH_2N$ ), 7.17 (1H, s, pyridazine), 7.84 (1H, s, pyridazine), 8.67 (1H, s, pyridazine).  $^{13}C\{^1H\}$  NMR (298 K,  $d_8$ -THF)  $\delta$ (ppm) -0.3 ( $CH_2SiMe_3$ ), 3.6 ( $Si(CH_3)_3$ ), 44.1, 45.9, 55.5, 58.1 PMDETA, 122.9 (CH-pyridazine), 136.7 (CH-pyridazine), 147.4 (CH-pyridazine), 199.9 (C-Ga).  $^7Li$  NMR (298 K,  $d_8$ -THF, reference LiCl in  $D_2O$  at 0.00 ppm):  $\delta$  2.80.

#### 4.6.5. Synthesis of [1-(PMDETA)Li-6-(GaR<sub>3</sub>)-C<sub>4</sub>H<sub>3</sub>N<sub>2</sub>] (37)



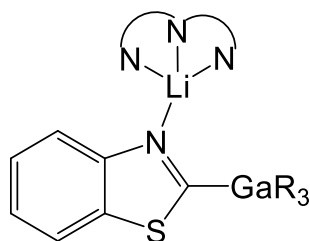
(0.074 g, 0.5 mmol) and  $Ga(CH_2SiMe_3)_3$  (0.165 g, 0.5 mmol) in hexane (10 mL), a hexane solution of pyrimidine (0.04 g, 0.5 mmol in 10 mL hexane) was added *via* syringe at room temperature. As soon as pyrimidine was added, a yellow suspension was formed which evolved into orange and then brown suspension. After stirring for 15 min at

room temperature, PMDETA was added (0.11 mL, 0.5 mmol) which induced instant, but short-lived precipitation. The suspension was filtered with cannula and a dark red solution was placed at  $-33$  °C to obtain X-ray suitable crystals overnight (0.08 g, 27%). Anal. Calcd for  $C_{25}H_{59}GaLiN_5Si_3$ : C, 50.83; H, 10.07; N, 11.86. Found: C, 50.91; H, 10.02; N, 11.82.



**<sup>1</sup>H NMR (298 K, d<sub>8</sub>-THF) δ(ppm)** -0.83 (6H, s, CH<sub>2</sub>SiMe<sub>3</sub>), -0.16 (27H, s, Si(CH<sub>3</sub>)<sub>3</sub>), 2.20 (12H, s, N(CH<sub>3</sub>)<sub>2</sub>), 2.29 (3H, mult, NCH<sub>3</sub>), 2.38 (4H, mult, NCH<sub>2</sub>CH<sub>2</sub>N), 2.49 (4H, mult, NCH<sub>2</sub>CH<sub>2</sub>N), 7.67 (1H, d, pyrimidine), 7.92 (1H, d, pyrimidine), 8.87 (1H, s, pyrimidine). **<sup>13</sup>C{<sup>1</sup>H} NMR (298 K, d<sub>8</sub>-THF) δ(ppm)** -0.4 (CH<sub>2</sub>SiMe<sub>3</sub>), 3.6 (Si(CH<sub>3</sub>)<sub>3</sub>), 43.7, 46.1, 56.4, 55.8 PMDETA, 131.2 (CH-pyrimidine), 148.4 (CH-pyrimidine), 155.4 (CH-pyrimidine), 219.3 (C-Ga). **<sup>7</sup>Li NMR (298 K, d<sub>8</sub>-THF, reference LiCl in D<sub>2</sub>O at 0.00 ppm):** δ 2.41.

**4.6.6. Synthesis of [2-(GaR<sub>3</sub>)-3-{Li(PMDETA)}-C<sub>6</sub>H<sub>4</sub>NCS] (38)** To a suspension of



LiTMP (0.074 g, 0.5 mmol) and Ga(CH<sub>2</sub>SiMe<sub>3</sub>)<sub>3</sub> (0.165 g, 0.5 mmol) in hexane (10 mL), 1 equivalent of benzothiazole (0.067 g, 0.5 mmol, 55 μL) was added at room temperature. As soon as benzothiazole was added, a yellow solution was formed which slowly evolved into orange solution. After stirring for 1 hour at room temperature, PMDETA was added (0.11 mL, 0.5 mmol) which induced precipitation. Vigorous heating of the mixture afforded solution which upon slow cooling deposited X-ray suitable crystals (0.27 g, 83.6 %). Anal. Calcd for C<sub>28</sub>H<sub>60</sub>GaLiN<sub>4</sub>SSi<sub>3</sub>: C, 52.08; H, 9.37; N, 8.68. Found: C, 52.28; H, 9.15; N, 8.60.

**<sup>1</sup>H NMR (298 K, d<sub>8</sub>-THF) δ(ppm)** -0.73 (6H, s, CH<sub>2</sub>SiMe<sub>3</sub>), -0.10 (27H, s, Si(CH<sub>3</sub>)<sub>3</sub>), 2.17 (12H, s, PMDETA-CH<sub>3</sub>), 2.24 (3H, s, PMDETA-CH<sub>3</sub>), 2.34 (4H, mult, PMDETA-CH<sub>2</sub>), 2.44 (4H, mult, PMDETA-CH<sub>2</sub>), 7.02 (1H, t, CH-btz), 7.13 (1H, t, CH-btz), 7.78 (2H, mult, CH-btz). **<sup>13</sup>C{<sup>1</sup>H} NMR (298 K, d<sub>8</sub>-THF) δ(ppm)** 0.9 (CH<sub>2</sub>SiMe<sub>3</sub>), 3.5 (Si(CH<sub>3</sub>)<sub>3</sub>), 43.6 (PMDETA-CH<sub>3</sub>), 46.0 (PMDETA-CH<sub>3</sub>), 56.2 (PMDETA-CH<sub>2</sub>), 58.5 (PMDETA-CH<sub>2</sub>), 121.4 (CH-btz), 121.6 (CH-btz), 121.9 (CH-btz), 123.3 (CH-btz), 139.2 (C quaternary), 158.6 (C quaternary), 209.5 (C-Ga). **<sup>7</sup>Li NMR (298 K, d<sub>8</sub>-THF, reference LiCl in D<sub>2</sub>O at 0.00 ppm):** δ 1.87.

#### 4.7. Bibliography

- [1] R. E. Mulvey, S. D. Robertson, *Angew. Chem. Int. Ed.* **2013**, *52*, 11470–11487.
- [2] M. F. Lappert, P. P. Power, A. Protchenko, A. Seeber, *Metal Amide Chemistry*, Wiley, Chichester, UK, **2009**.
- [3] E. Hevia, A. R. Kennedy, R. E. Mulvey, D. L. Ramsay, S. D. Robertson, *Chem. Eur. J.* **2013**, *19*, 14069–14075.
- [4] J. Clayden, *Organolithiums: Selectivity for Synthesis*, Pergamon, Oxford, **2002**.
- [5] M. Hamell, R. Levine, *J. Org. Chem.* **1950**, *15*, 162–168.

- [6] G. Stork, L. Maldonado, *J. Am. Chem. Soc.* **1971**, *93*, 5286–5287.
- [7] G. Queguiner, F. Marsais, V. Snieckus, J. Epszajn, *Adv. Heterocycl. Chem.* **1991**, *52*, 187–304.
- [8] G. Queguiner, *J. Heterocycl. Chem.* **2000**, *37*, 615–621.
- [9] N. Ple, A. Turck, K. Couture, G. Queguiner, *J. Org. Chem.* **1995**, *60*, 3781–3786.
- [10] A. R. Katritzky, *Handbook of Heterocyclic Chemistry*, Pergamon, New York, **1985**.
- [11] F. Chevallier, F. Mongin, *Chem. Soc. Rev.* **2008**, *37*, 595–609.
- [12] M. Asif, *SOP Trans. Org. Chem.* **2014**, *1*, 1–17.
- [13] A. Krasovskiy, V. Krasovskaya, P. Knochel, *Angew. Chem. Int. Ed.* **2006**, *45*, 2958–2961.
- [14] T. Imahori, Y. Kondo, *J. Am. Chem. Soc.* **2003**, *125*, 8082–8083.
- [15] A. Seggio, F. Chevallier, M. Vaultier, F. Mongin, *J. Org. Chem.* **2007**, *72*, 6602–6605.
- [16] S. E. Baillie, V. L. Blair, D. C. Blakemore, D. Hay, A. R. Kennedy, D. C. Pryde, E. Hevia, *Chem. Commun.* **2012**, *48*, 1985–1987.
- [17] C. E. Housecroft, A. G. Sharpe, *Inorganic Chemistry*, Pearson Education Limited, Essex, **2005**.
- [18] D. R. Armstrong, A. R. Kennedy, R. E. Mulvey, J. A. Parkinson, S. D. Robertson, *Chem. Sci.* **2012**, *3*, 2700–2707.
- [19] A. Frischmuth, M. Fernández, N. M. Barl, F. Achraimer, H. Zipse, G. Berionni, H. Mayr, K. Karaghiosoff, P. Knochel, *Angew. Chem. Int. Ed.* **2014**, *53*, 7928–7932.
- [20] D. R. Armstrong, E. Crosbie, E. Hevia, R. E. Mulvey, D. L. Ramsay, S. D. Robertson, *Chem. Sci.* **2014**, *5*, 3031–3045.
- [21] D. R. Armstrong, E. Brammer, T. Cadenbach, E. Hevia, A. R. Kennedy, *Organometallics* **2013**, *32*, 480–489.
- [22] W. Kohn, A. D. Becke, R. G. Parr, *J. Phys Chem* **1996**, *100*, 12974–12980.
- [23] A. D. Becke, *Phys. Rev. A* **1988**, *38*, 3098–3100.
- [24] C. Lee, W. Yang, R. G. Parr, *Phys. Rev. B* **1988**, *37*, 785–789.
- [25] A. D. McLean, G. S. Chandler, *J. Chem. Phys.* **1980**, *72*, 5639–5649.
- [26] M. U. Kramer, D. Robert, Y. Nakajima, U. Englert, T. P. Spaniol, J. Okuda, *Eur. J. Inorg. Chem.* **2007**, *2007*, 665–674.
- [27] W. Clegg, B. Conway, E. Hevia, M. D. McCall, L. Russo, R. E. Mulvey, *J. Am. Chem. Soc.* **2009**, *131*, 2375–2384.
- [28] L. Yang, D. R. Powell, R. P. Houser, *Dalton Trans.* **2007**, 955–964.

- [29] R. B. Hallock, W. E. Hunter, J. L. Atwood, O. T. Beachley Jr., *Organometallics* **1985**, *4*, 547–549.
- [30] F. H. Kohler, N. Hertkorn, J. Bluemel, *Chem. Ber.* **1987**, *120*, 2081–2082.
- [31] S. Harder, M. Lutz, *Organometallics* **1994**, *13*, 5173–5176.
- [32] C. Strohmman, V. H. Gessner, *Angew. Chem. Int. Ed.* **2007**, *46*, 4566–4569.
- [33] B. Conway, J. García-Álvarez, E. Hevia, A. R. Kennedy, R. E. Mulvey, S. D. Robertson, *Organometallics* **2009**, *28*, 6462–6468.
- [34] W.-B. Yu, Y.-J. Lin, G.-X. Jin, *Organometallics* **2011**, 3905–3907.
- [35] Y.-J. Tu, H.-F. Wang, G.-H. Lee, K.-H. Yih, X.-Y. Tang, *Acta Crystallogr. Sect. E Struct. Reports Online* **2012**, *68*, m1419–m1420.
- [36] K. Shen, Y. Fu, J.-N. Li, L. Liu, Q.-X. Guo, *Tetrahedron* **2007**, *63*, 1568–1576.
- [37] C. Hilf, F. Bosold, K. Harms, M. Marsch, G. Boche, *Chem. Ber.* **1997**, *130*, 1213–1221.
- [38] S. E. Baillie, V. L. Blair, T. D. Bradley, W. Clegg, J. Cowan, R. W. Harrington, A. Hernández-Gómez, A. R. Kennedy, Z. Livingstone, E. Hevia, *Chem. Sci.* **2013**, *4*, 1895–1905.
- [39] M. F. Mahon, K. C. Molloy, P. C. Waterfield, *J. Organomet. Chem.* **1989**, *365*, 61–73.
- [40] J.-M. L’Helgoual’ch, G. Bentabed-Ababsa, F. Chevallier, M. Yonehara, M. Uchiyama, A. Derdour, F. Mongin, *Chem. Commun.* **2008**, *42*, 5375–5377.

## 5. Structural and magnetic diversity in alkali-metal manganate chemistry: Evaluating donor and alkali-metal effects in co-complexation processes

### 5.1. Introduction

As mentioned in **Chapter 1**, despite the widespread interest that mixed-metal (ate) compounds have attracted over the last decade, the vast majority of these studies are focused on s/p block metals,<sup>[1-4]</sup> with only a few examples using transition-metals.<sup>[5-7]</sup> Interestingly, prominent work by Mulvey has already shown the great potential of alkali-metal manganates for deprotonative metallation of aromatic substrates.<sup>[8-10]</sup> Insightful studies have demonstrated that these reactivities are genuine examples of direct manganation. On the other hand, the structures and magnetic properties of homo(alkyl) alkali-metal manganates have remained virtually unexplored.<sup>[11-15]</sup> This is particularly surprising considering their possible implication in C-C bond forming processes discussed in **Chapter 1**.

### 5.2. Aim of the chapter

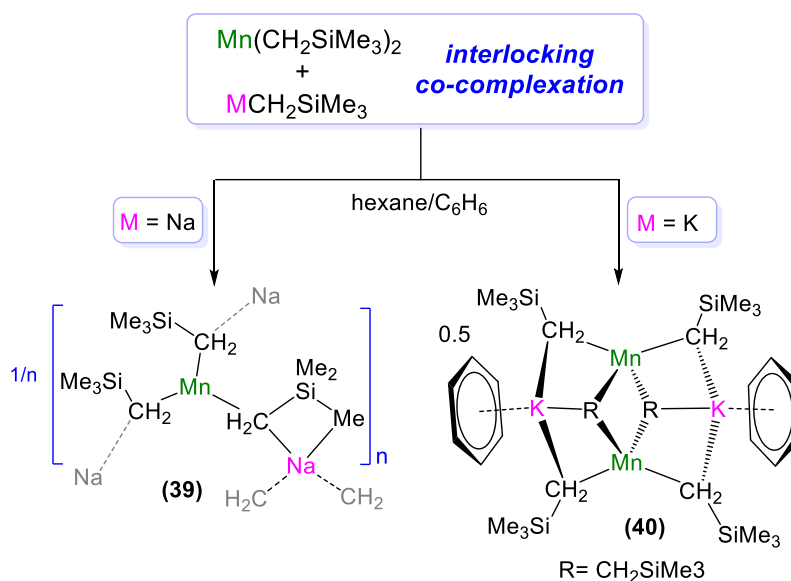
Building on our previous work on main-group heterobimetallic (ate) compounds,<sup>[16-18]</sup> this chapter presents the investigations into the synthesis of a series of homoleptic alkyl alkali-metal manganates. By systematically probing the co-complexation reactions of  $[MCH_2SiMe_3]$  ( $M = Na$  or  $K$ ) with  $[Mn(CH_2SiMe_3)_2]$  in a variety of solvent combinations, containing in some cases Lewis donors of different hapticities and coordinative properties, a new family of tris(alkyl) alkali-metal manganates is presented. The influence that the alkali-metal and these Lewis donors impose on the structures and magnetic properties of these bimetallic species has been quantified by combining X-ray crystallography with SQUID magnetization measurements and EPR spectroscopy. At the end of the chapter we extended the investigations on the synthesis, structure and reactivity of higher order tetraalkyl lithium manganate.

### 5.3. Syntheses

#### 5.3.1. Synthesis of lower order sodium and potassium manganates

Following previous successes in the synthesis of solvent-free alkali-metal magnesiates and zincates, we started our investigations assessing the co-complexation reactions between Wilkinson's Mn(II) dialkyl compound  $Mn(CH_2SiMe_3)_2$ <sup>[19]</sup> and the heavier

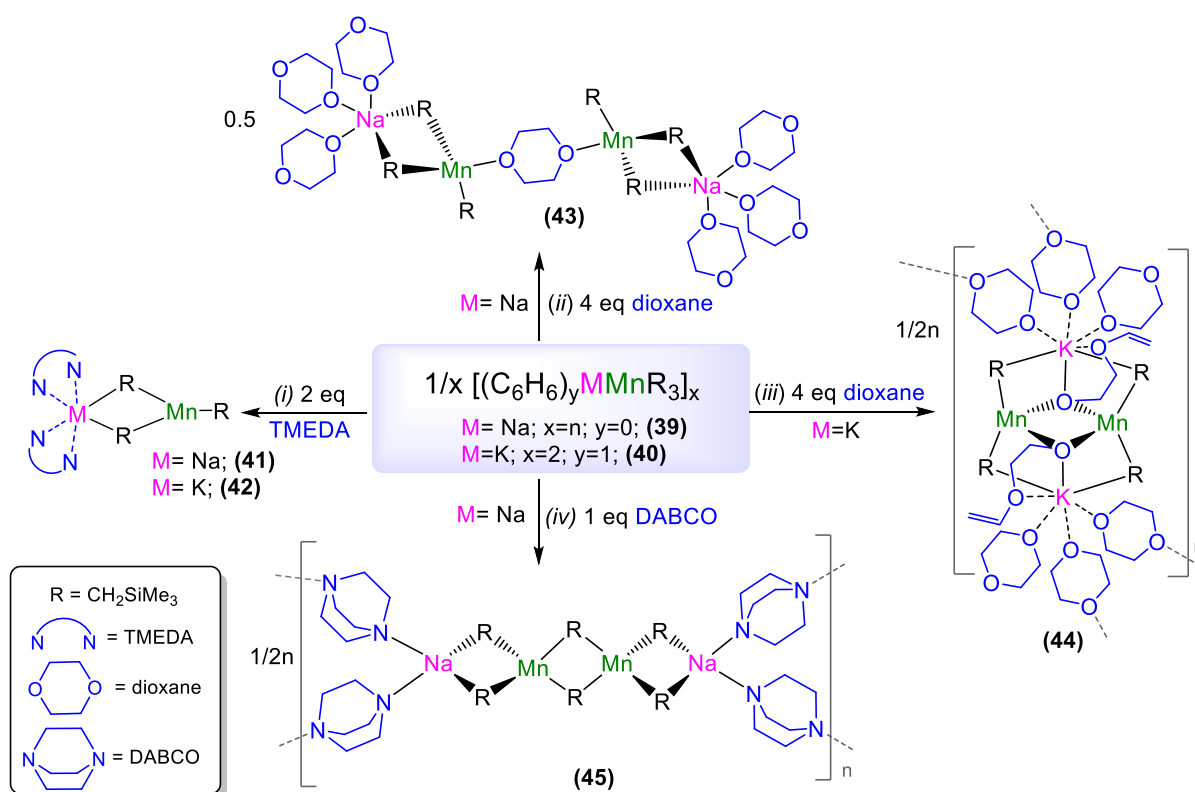
alkali-metal alkyls  $M(\text{CH}_2\text{SiMe}_3)$  ( $M = \text{Na}, \text{K}$ )<sup>[20–22]</sup> in the non-coordinating solvent hexane. As mentioned before (**Chapter 2**), the heteroneopentyl ligand  $\text{Me}_3\text{SiCH}_2^-$  was selected primarily due to its lack of  $\beta$ -hydrogen atoms, considerable steric bulk and electronic stabilization when compared to carbon-only-based alkyl groups that are prone to decomposition processes.<sup>[23,24]</sup> Addition of the arene solvent and gentle heating of the resulting suspensions resulted in the formation of orange solutions that on cooling deposited crystals of the homoleptic alkali-metal manganates  $[\{\text{NaMn}(\text{CH}_2\text{SiMe}_3)_3\}_\infty]$  (**39**) and  $[\{\text{KMn}(\text{CH}_2\text{SiMe}_3)_3 \cdot \text{C}_6\text{H}_6\}_2]$  (**40**) in yields of 68 and 67% respectively (**Scheme 5.1**).



**Scheme 5.1:** Synthesis of homoleptic, trisalkyl alkali-metal manganates **39** and **40**.

As it has been well established that the presence of Lewis donors determines the aggregation and subsequently influences the reactivity of s-block metals, the effect of adding Lewis donors 1,4-dioxane, TMEDA and 1,4-diazabicyclo[2.2.2]octane (DABCO) to manganates **39** and **40** was investigated (**Scheme 5.2**). Using two molar equivalents of bidentate N-donor TMEDA allowed the isolation of complexes  $[(\text{TMEDA})_2\text{MMn}(\text{CH}_2\text{SiMe}_3)_3]$  ( $M = \text{Na}$ , **41**;  $M = \text{K}$ , **42**) in 65% and 69% yields respectively. Interestingly, disclosing an important alkali-metal effect, the reactions of **39** and **40** with 1,4-dioxane (four equivalents) produced an entirely different outcome (**Scheme 5.2**). Thus while the sodium manganate **39** formed coordination adduct  $[\{\text{NaMn}(\text{CH}_2\text{SiMe}_3)_3\}_2(\text{dioxane})_7]$  (**43**) (52% yield), potassium manganate **40** yielded heteroleptic species  $[\{(\text{dioxane})_6\text{K}_2\text{Mn}_2(\text{CH}_2\text{SiMe}_3)_4(\text{O}(\text{CH}_2)_2\text{OCH}=\text{CH}_2)_2\}_\infty]$  (**44**) (45% yield), which contains two alkyl groups, three solvating molecules of dioxane

and surprisingly an alkoxy vinyl ether ligand (**Scheme 5.2**), resulting from the alpha metallation and ring opening of the remaining molecule of dioxane (*vide infra*). Adding bicyclic diamine donor DABCO to a solution of **39** in hexane afforded a white precipitate that could be dissolved in hot toluene, giving a brown solution that deposited colorless crystals of  $[\{\text{Na}_2\text{Mn}_2(\text{CH}_2\text{SiMe}_3)_6(\text{DABCO})_2\}_\infty]$  (**45**) on cooling to room temperature in a 43% yield. Attempts to isolate a product from the same reaction using potassium manganate **40** led to the isolation of a white microcrystalline material which was not amenable for X-ray analysis.



**Scheme 5.2:** Reactivity of donor-solvent free manganates **39** and **40** with selected Lewis bases.

Alkali-metal manganates **39-45** were characterized by X-ray crystallography, EPR spectroscopy and elemental analysis and they also had their magnetic susceptibilities measured on a SQUID magnetometer.

Unsolvated sodium manganate **39** displays an infinitely aggregated structure, comprising dinuclear  $\{\text{NaMn}(\text{CH}_2\text{SiMe}_3)_3\}$  units (**Figure 5.1a**) where each alkyl group acts as a bridge between Mn and Na centers *via* their methylene group, giving rise to an intricate two-dimensional network (**Fig. 5.1c**). Its basic repeat unit features a distorted trigonal-planar Mn (sum of angles around Mn=359.03°) bonded to three

monosilyl  $\text{CH}_2\text{SiMe}_3$  groups, one of which bridges to sodium (**Fig. 5.1b**). The two remaining alkyl ligands bond to Na atoms of a neighbouring unit, building a 2D honeycomb sheet structure which contains 12-membered  $\{(\text{NaCMnC})_3\}$  fused rings with the  $\text{SiMe}_3$  groups alternately pointing to opposite faces of the sheet. Each of these rings accommodates 6 metals (3 Na, 3 Mn) and 6 monosilyl ligands (**Fig. 5.1b**) and is interconnected with another six rings within the polymeric structure (**Fig. 5.1c**). Additionally, each Na gains further stabilization by forming a secondary electrostatic interaction with the methyl group of one  $\text{CH}_2\text{SiMe}_3$  ligand [ $\text{Na1}\cdots\text{C8}$ , 3.020(1) Å], which induces a slight pyramidalisation in its geometry (sum of bond angles around Na = 352.9°).

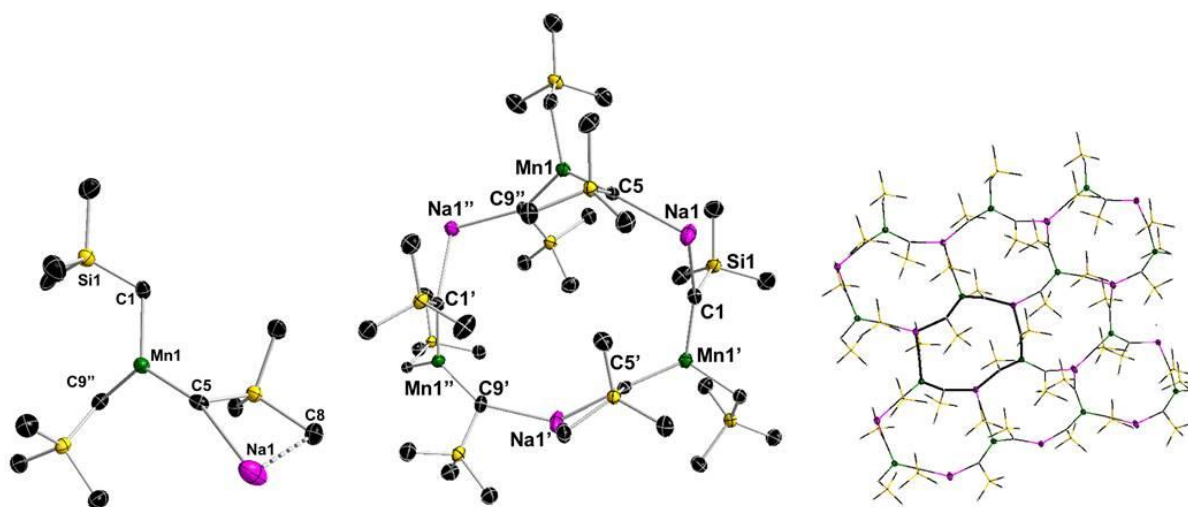


**Figure 5.1:** (a) Asymmetric unit of **39**; (b) section of polymeric **39** showing a 12-membered  $\{(\text{NaCMnC})_3\}$  ring; and (c) wire representation of polymeric sheet network of **39**. In all figures hydrogen atoms have been omitted for clarity and ellipsoids are drawn in 50% probability. Symmetry operators ('):  $x+0.5, y, -z+0.5$ ; (''):  $-x+0.5, y+0.5, z$ ; (''''):  $-x+0.5, y-0.5, z$ ; (''''):  $x-0.5, y, -z+0.5$ .

Inspection of the sodium-carbon distances within **39** (**Table 5.1**) shows that there is no significant variation that would define a specific molecular unit. Thus all three Na-C distances in **39** lie within relatively small range [2.653(4) to 2.705(4) Å]. Similarly, no significant difference is found between the three Mn-C bond lengths of **39** [range: 2.166(4)-2.180(4) Å].

**Table 5.1:** Selected bond distances (Å) for manganates **39**, **41**, **42**, **43** and **45**.

	M = Na ( <b>39</b> )	M = Na ( <b>41</b> )	M = K ( <b>42</b> )	M = Na, X = O ( <b>43</b> )	M = Na, X = N ( <b>45</b> )
<b>Mn1 – C1</b>	2.166(4)	2.176(2)	2.174(3)	2.170(2)	2.254(3)
<b>Mn1 – C5</b>	2.180(4)	2.171(2)	2.176(3)	2.230(2)	2.214(3); 2.419(3) <sup>[c]</sup>
<b>Mn1 – C9</b>	2.177(4) <sup>[a]</sup>	2.155(2)	2.156(3)	2.208(2)	2.202(3)
<b>Mn1 – X1</b>	n/a	n/a	n/a	2.3271(12)	n/a
<b>Average Mn1 – C</b>	2.174	2.167	2.169	2.203	2.272
<b>M – C1</b>	2.705(4) <sup>[b]</sup>	3.079(2)	3.163(3)	n/a	2.558(1)
<b>M – C5</b>	2.653(4)	3.025(2)	3.199(3)	2.694(2)	n/a
<b>M – C9</b>	2.664(4)	n/a	n/a	2.719(2)	2.721(1)
<b>Average M – C</b>	2.674	3.052	3.181	2.706	2.639
<b>M – Mn1</b>	n/a	3.5513(9)	3.6468(8)	3.3150(8)	3.0919(10)

[a] This distance represents Mn1-C9'' (symmetry operator: -x+0.5, y+0.5, z). [b] This distance represents Mn1-C5' (symmetry operator: x, -y - 0.5, z - 0.5). [c] This distance represents Mn1-C5' (symmetry operator: -x, -y, -z).

These values are slightly elongated compared to those reported for the discrete monomeric NHC-complex [(IPr)Mn(CH<sub>2</sub>SiMe<sub>3</sub>)<sub>2</sub>] (IPr = 1,3-bis(2,6-diisopropylphenyl)imidazol-2-ylidene), which also contains a tricoordinated Mn center (Mn-C<sub>alkyl</sub> bond length, 2.129(1) Å).<sup>[25]</sup> Reflecting the structural similarities previously noticed between organomagnesium and organomanganese (II) compounds,<sup>[13,25,26]</sup> the intriguing 2D honeycomb assembly of **39**, although unique in manganate chemistry, is isostructural to that previously reported by our group for magnesiate [{NaMg(CH<sub>2</sub>SiMe<sub>3</sub>)<sub>3</sub>]<sub>∞</sub>}.<sup>[16]</sup> This ring-fused structure contrasts with those found for the monometallic components of **39**, which are also highly aggregated but display polymeric chain arrangements made up in each case by association of {Mn<sub>2</sub>(CH<sub>2</sub>SiMe<sub>3</sub>)<sub>2</sub>} dimers<sup>[7]</sup> or {Na(CH<sub>2</sub>SiMe<sub>3</sub>)<sub>4</sub>} tetramers.<sup>[16]</sup>

In general, donor free alkali-metal ate structures are rare in heterobimetallic chemistry due to solubility issues or difficulty in generating X-ray quality crystals. In manganate chemistry, Ernst has reported the structure of the substituted tris(dienyl) [K{Mn(3-Me-1,5-(Me<sub>3</sub>Si)C<sub>5</sub>H<sub>4</sub>)<sub>3</sub>}] which forms a discrete monomer, where K is trapped within the three dienyl ligands, through π-engaging with the C=C bonds (**Figure 5.2**).<sup>[27]</sup>



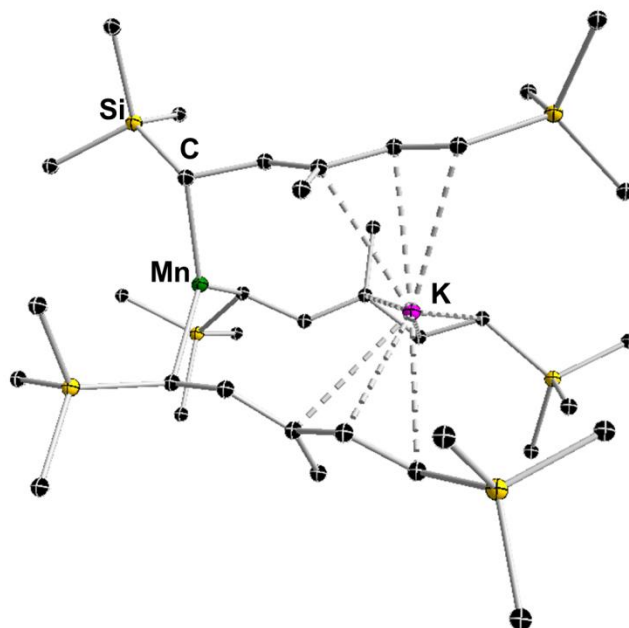


**Figure 5.2:** Molecular structure of  $[\text{K}\{\text{Mn}(3\text{-Me-1,5-(Me}_3\text{Si)C}_5\text{H}_4)_3\}]$  with 50% probability displacement ellipsoids. All hydrogen atoms have been omitted for clarity.<sup>[27]</sup>

As far as we can ascertain, **39** constitutes the first example of an unsolvated alkali-metal manganate with an extended structure as well as the first homo(alkyl) sodium manganate to be structurally defined. Switching to the heavier alkali-metal potassium facilitated the synthesis and isolation of benzene-solvated manganate **40**, which, contrasting with polymeric **39**, features a discrete dimeric arrangement and has incorporated two molecules of benzene in its constitution, each of them  $\pi$ -engaging with a K center. Centrosymmetric **40** can be described as a cationic octagonal  $[(\text{KCMnC})_2]^{2+}$  ring hosting two monosilyl anion guests that are  $\mu_3$ -capped at the top and bottom of the ring by binding to two Mn and one K (C11 and C11' in **Fig. 5.3b**). Within **40**, tetracoordinated Mn exhibits a distorted tetrahedral geometry, bonded to four alkyl groups [range of CMnC bond angles,  $103.04(12)^\circ$ - $119.97(12)^\circ$ ; mean  $109.16^\circ$ ]. Unsurprisingly, the Mn-C distances for the  $\mu_2$ -alkyls that are part of the eight-membered ring and coordinate to K and Mn are shorter [2.186(3) and 2.198(3) Å] than those for the  $\mu_3$ -guest alkyls [Mn1-C11, 2.235(3) Å], this difference being particularly noticeable for Mn1-C11' [2.488(3) Å, **Table 5.2**]. These Mn-C bond distances are within the same range as those reported for  $[\{\text{Mn}(\text{CH}_2\text{SiMe}_3)_2\}_\infty]$  where the Mn atoms also exhibit a distorted tetrahedral  $C_4$  geometry, (Mn-C bond lengths ranging from 2.2023(17) to 2.4358(17) Å).<sup>[7]</sup> This trend is even more evident for the K-C distances, with the  $\mu_2$ -alkyls (C7 and C15, **Fig. 5.3a**) forming significantly shorter

bonds [mean value, 3.030(4) Å] than the remaining  $\mu_3$ -ligands [K1-C11, 3.374(4) Å]. The observed values for K1-C7 and K1-C15 (Table 5.2) are in the same range as those in the homometallic alkyl  $[\{(PMDETA)K(CH_2SiMe_3)\}_\infty]$  (PMDETA = *N,N,N',N'',N'''*-pentamethyldiethylenetriamine; mean K-C, 2.975 Å).<sup>[22]</sup>

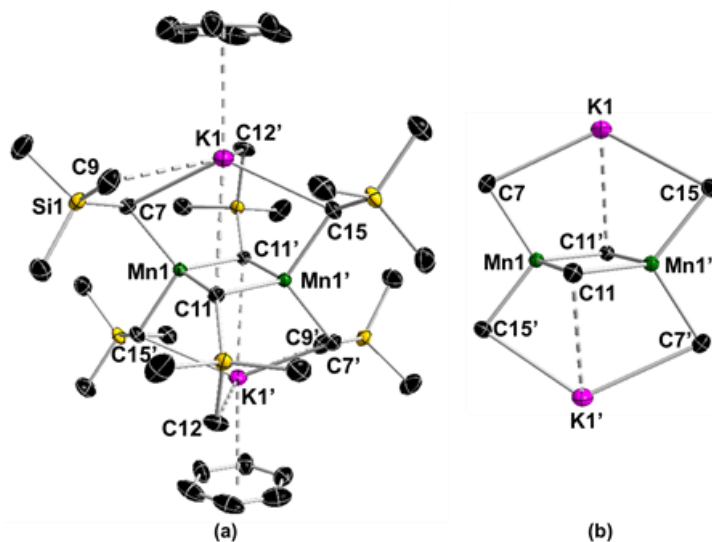


**Figure 5.3:** (a) Molecular structure of **40**. (b) Framework of **40** with benzene molecules and SiMe<sub>3</sub> substituents omitted for clarity. In all figures hydrogen atoms have been omitted for clarity and ellipsoids are drawn in 50% probability. Dotted lines represent secondary K-C interactions. Symmetry operator:  $-x, -y, -z+1$ .

In addition, two further long-distance stabilizing secondary interactions are observed for each K with the Me groups of two different SiMe<sub>3</sub> units [K1-C12', 3.3738(6) Å and K1-C9, 3.2462(4) Å]. Potassium completes its coordination by engaging with the C=C  $\pi$ -bonds of a molecule of benzene which coordinates in an essentially  $\eta^6$ -fashion [K-C distances lie in the relatively narrow range 3.285(13)-3.407(12) Å].<sup>[28–30]</sup>

**Table 5.2:** Selected bond distances (Å) for potassium manganate **40**.

<b>Mn1-C7</b>	<b>2.186(3)</b>	<b>K1-C7</b>	<b>3.011(4)</b>
<b>Mn1-C15'</b>	2.198(3)	<b>K1-C15</b>	3.050(4)
<b>Mn1-C11'</b>	2.235(3)	<b>K1-C12'</b>	3.374(4)
<b>Mn1-C11</b>	2.488(3)	<b>K1-C11</b>	3.375(3)
<b>Mn1'-C11</b>	2.235(3)	<b>Average K-C</b>	3.202
<b>Mn1'-C15</b>	2.198(3)	<b>Mn1-K1</b>	3.4712(10)
<b>Average Mn1-C</b>	2.277	<b>Mn1-K1'</b>	3.5202(10)
<b>Mn1···Mn1</b>	2.8716(10)		

The internuclear Mn $\cdots$ Mn separation in **40** [2.8716(10) Å] is comparable with those found for homometallic  $[\{\text{Mn}(\text{CH}_2\text{SiMe}_3)_2\}_\infty]$  [mean, 2.8885 Å] and  $[\{\text{Mn}(\text{Mesityl})_2\}_3]$  [mean 2.8515 Å]<sup>[31]</sup> and is considerably more elongated than that recently reported by Hayton in the ketimide-bridged dimer  $[\text{Li}([\text{12}]\text{crown-4})_2][\text{Mn}_2(\text{N}=\text{C}^t\text{Bu}_2)_5]$  [Mn $\cdots$ Mn 2.5965(7) Å], which exhibits strong metal-metal electronic communication between the two Mn centers as determined by solid state magnetic susceptibility measurements using SQUID magnetometry.<sup>[32]</sup>

The basic motif of **40**, alternatively described as a face-fused double heterocubane structure with two missing corners or as some type of inverse crown complex has been previously found in a variety of s-block homo- and heterobimetallic compounds.<sup>[33–44]</sup> However, we believe it is unique for a homo(alkyl) ate system.<sup>[45]</sup> Unlike sodium manganate **39**, the structure of **40** is strikingly different to that of its magnesiate analogue  $[\{\text{KMg}(\text{CH}_2\text{SiMe}_3)_3\cdot\text{C}_6\text{H}_6\}_\infty]$  which forms an infinitely aggregated 2D network.<sup>[46]</sup>

Addition of two equivalents of bidentate nitrogen donor TMEDA to manganates **39** and **40** caused their deaggregation forming discrete monomeric triorganomanganates  $[(\text{TMEDA})_2\text{MMn}(\text{CH}_2\text{SiMe}_3)_3]$  **41** (M = Na) and **42** (M = K) respectively with the same ring-closed contacted ion pair motif (**Figure 5.4**).

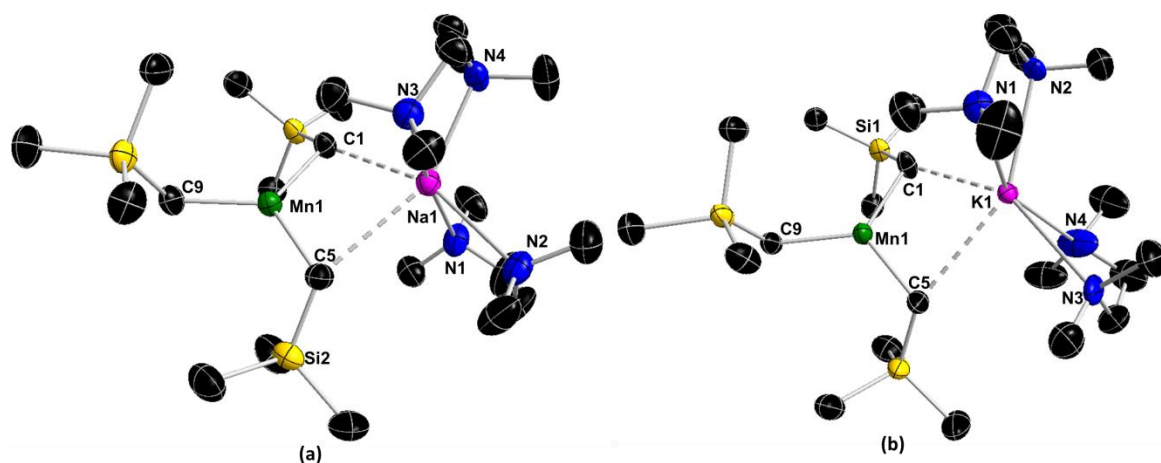


**Figure 5.4:** Molecular structure of **41** (a) and of **42** (b) with displacement ellipsoids drawn in 50% probability. In all figures hydrogen atoms and in **42** the minor disorder component in one of the TMEDA ligands have been omitted for clarity.

Both compounds display a C<sub>3</sub>-tricoordinated Mn atom (sum of the angles around Mn, 360.00° for both **41** and **42**), where two alkyl groups bridge to the doubly chelated cation  $\{(\text{TMEDA})_2\text{M}\}^+$  (M= Na or K). As shown in **Table 5.1**, the Mn-C bond distances in **41** and **42** are very similar [ranging from 2.155(2) to 2.176(3)Å] and show

almost no variation to those found in unsolvated sodium manganate **39** which also contains a tricoordinated Mn center [mean value, 2.173 Å, see **Table 5.1** for details]. Contrastingly, a comparison between the Na-C distances in **39** and **41** revealed a significant elongation for the latter [mean values, 2.676 vs 3.052 Å]. A different trend is observed for the K-C distances in **40** and **42** which are relatively well matched [mean values, 3.202 vs 3.181 Å] and can be attributed to the fact that in both structures the potassium cations are hexacoordinated. The formation of potassium triorganomanganate **42** contrast sharply with the reactivity recently reported for magnesiate [ $\{ \text{KMg}(\text{CH}_2\text{SiMe}_3)_3 \cdot \text{C}_6\text{H}_6 \}_\infty$ ] where the bidentate ligand TMEDA not only induces the deaggregation of its polymeric structure but also causes a redistribution process forming higher-order tetraorganomagnesiate [ $(\text{TMEDA})_2\text{K}_2\text{Mg}(\text{CH}_2\text{SiMe}_3)_4$ ] along with the elimination of  $[\text{Mg}(\text{CH}_2\text{SiMe}_3)_2]$ .<sup>[46]</sup>

Addition of O-donor dioxane to manganates **39** and **40** led to the isolation of  $[\{\text{NaMn}(\text{CH}_2\text{SiMe}_3)_3\}_2(\text{dioxane})_7]$  (**43**) and  $[\{(\text{dioxane})_6\text{K}_2\text{Mn}_2(\text{CH}_2\text{SiMe}_3)_4(\text{O}(\text{CH}_2)_2\text{OCH}=\text{CH}_2)_2\}_\infty]$  (**44**) respectively which exhibit completely different constitutions and structural motifs. Possessing two oxygen atoms at positions 1 and 4, which generally precludes this bidentate donor from acting as a chelating ligand, dioxane is well-known to facilitate aggregation by linking metal atoms together through  $\text{M}-\text{O}(\text{CH}_2)_4\text{O}-\text{M}$  bridges.<sup>[47–51]</sup> Displaying a discrete dimeric arrangement (**Figure 5.5**), **43** contains two  $\{(\text{dioxane})_3\text{NaMn}(\text{CH}_2\text{SiMe}_3)_3\}$  units which are connected by an additional bridging dioxane that solvates the Mn centers.

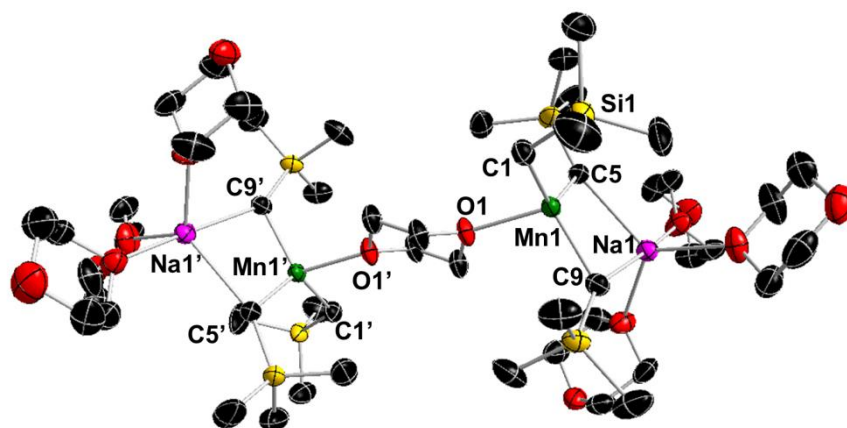


**Figure 5.5:** Dimeric structure of **43** with 50% probability displacement ellipsoids. All hydrogen atoms and minor disorder in two terminal 1,4-dioxane molecules have been omitted for clarity. Symmetry operator:  $-x, -y, -z+2$ .

In each of these units, the Na and Mn atoms are connected by two alkyl groups, closing four-membered  $\{\text{NaCMnC}\}$  rings, with a remaining alkyl bonded terminally to

Mn. Interestingly, despite the higher coordination number of Mn in **43** (coordinated to three C atoms and to one O atom), its mean Mn-C bond distance is just slightly elongated [2.203 Å] to those found in supramolecular **39** [2.173 Å] and discrete monomer **41** [2.167 Å] (See **Table 5.1** for details).

Showing a more marked effect, pentacoordinated distorted trigonal bipyramidal Na centers form significantly stronger (shorter) bonds with the alkyl groups [2.706 Å] than those found for **39** [3.052 Å] where Na is in a distorted octahedral environment (*vide supra*).

X-ray crystallographic studies of **44** uncovered its heteroleptic anionic constitution, containing a 2:1 ratio of monosilyl groups and alkoxy vinyl ether residues, with the latter resulting from fragmentation of 1,4-dioxane. Exhibiting a similar core structure to that of precursor **40**, the asymmetric unit in **44** is made up by a cationic octagonal [(KCMnC)<sub>2</sub>]<sup>2+</sup> ring which is now hosting two alkoxy vinyl ether anion {OCH<sub>2</sub>CH<sub>2</sub>OCH=CH<sub>2</sub>}<sup>-</sup> guests (**Figure 5.6b**).

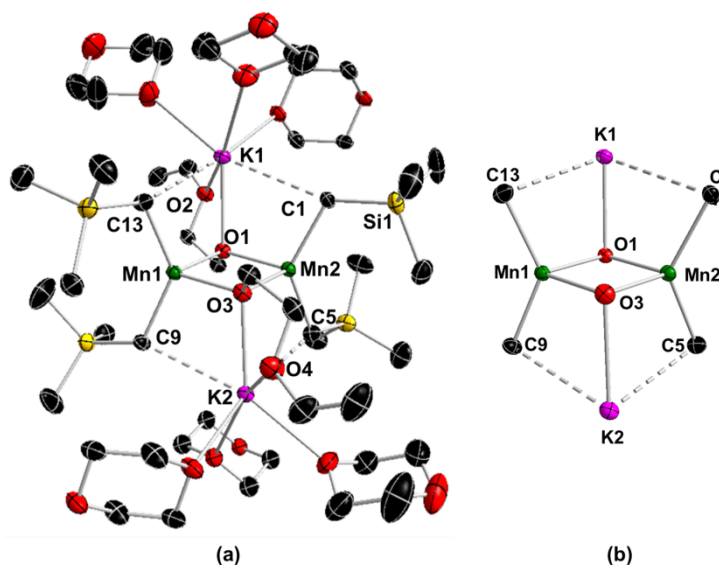


**Figure 5.6:** (a) Asymmetric unit of **44**. (b) Framework of **44** with dioxane molecules, SiMe<sub>3</sub> substituents and alkoxy vinyl substituents omitted for clarity. In all figures hydrogen atoms and minor disorder in two coordinated 1,4-dioxane molecules have been omitted for clarity and displacement ellipsoids are drawn in 50% probability. Dotted lines represent secondary K-C interactions.

Each alkoxy anion interconnects two Mn atoms with one K (*via* O1 and O3, **Fig. 5.6**) and uses its ether oxygen (O2 and O4 respectively) to chelate a K center. Each K atom is further solvated by three molecules of dioxane, two of which are bridging to other K centers from neighboring {K<sub>2</sub>Mn<sub>2</sub>(CH<sub>2</sub>SiMe<sub>3</sub>)<sub>4</sub>(OR)<sub>2</sub>} (R = CH<sub>2</sub>CH<sub>2</sub>OCH=CH<sub>2</sub>) units assembling a 2D network (**Figure 5.7**).

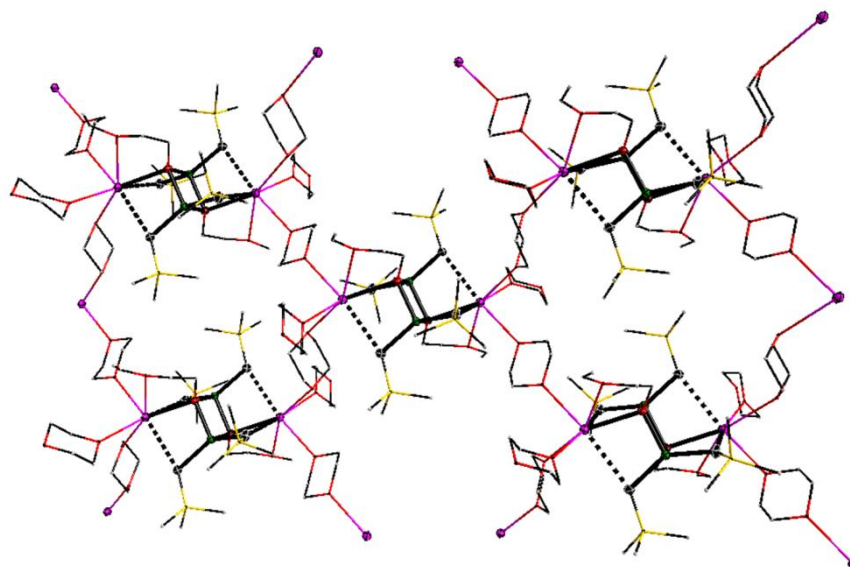


**Figure 5.7:** Wire model representation of polymeric structure of **44** with core atoms drawn in 50% probability displacement ellipsoids. All hydrogen atoms and minor disorder in coordinating 1,4-dioxane molecules have been omitted for clarity. Symmetry operators #1:  $-x+1, -y+1, -z+2$ ; #2:  $-x, -y+1, -z+2$ ; #3:  $-x, -y+2, -z+3$ ; #4:  $-x+1, -y+2, -z+3$ . Dotted lines represent secondary K-C interactions.

A comparison of the main geometrical parameters of **40** and **44** revealed that while replacing the alkyl guests by alkoxide groups in the eight-membered  $[(KCMnC)_2]^{2+}$  ring has little effect on the Mn-C distances [mean value 2.175 Å in **44** vs 2.186(3) and 2.198(3) Å in **40**], it imposes a significant elongation on the intermetallic Mn...Mn separation which is now 3.1447(4) Å [2.8716(10) Å for **40**] as well as on the K-C(alkyl) bonds [mean value 3.219 Å in **44** vs 3.011(4) and 3.050(4) Å in **40**] see **Table 5.3**.

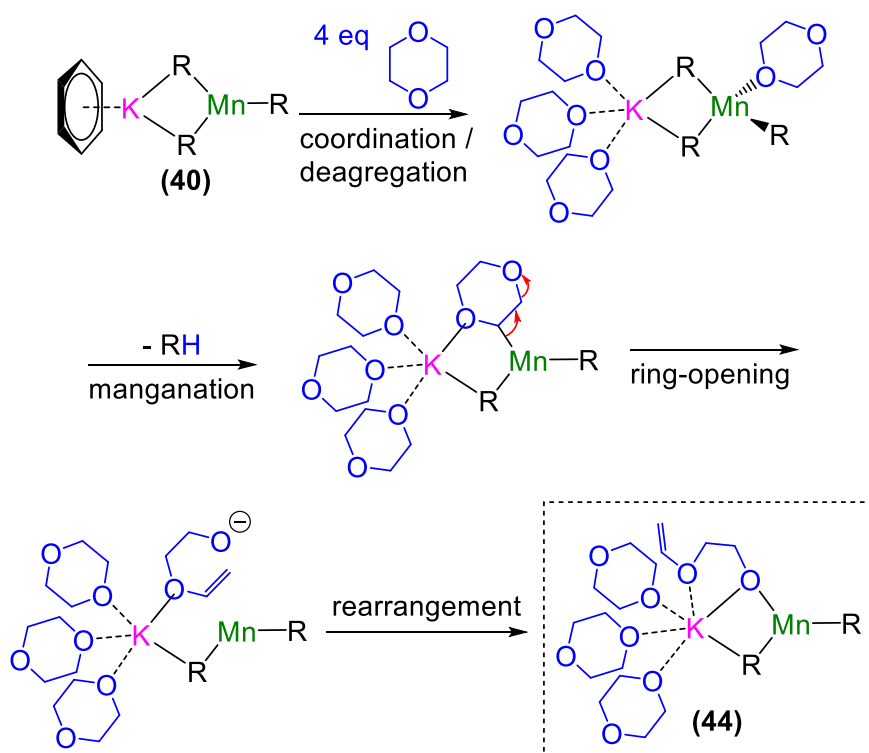
**Table 5.3:** Selected bond distances (Å) for potassium manganate **44**.

<b>Mn1 – C9</b>	<b>2.172(2)</b>	<b>K1 – C1</b>	<b>3.279(1)</b>
<b>Mn1 – C13</b>	2.175(2)	<b>K1 – C13</b>	3.182(1)
<b>Mn2 – C1</b>	2.180(2)	<b>K2 – C5</b>	3.156(1)
<b>Mn2 – C5</b>	2.175(2)	<b>K2 – C9</b>	3.261(1)
<b>Mn1...Mn2</b>	3.1447(4)	<b>K1...Mn1</b>	3.6171(5)

Despite ether cleavage being a problematic side reaction in organometallic chemistry,<sup>[52]</sup> and 1,4-dioxane a common solvent in synthesis, the number of structurally defined intermediates resulting from this process is surprisingly scarce. In one example, Henderson has trapped the alkoxy-vinyl fragment present in **44** as a result of the cleavage of dioxane by  $t\text{BuLi}$ <sup>[53]</sup> as well as by the action of a

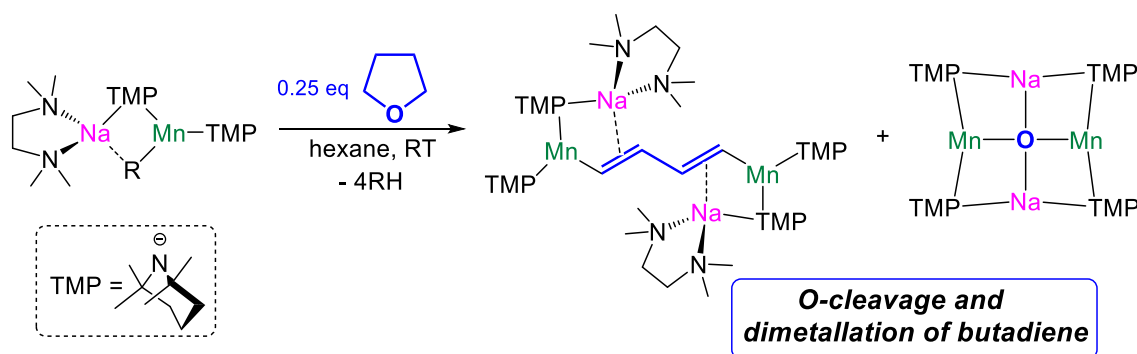


Bu<sub>2</sub>Mg/diisopropylaniline mixture.<sup>[54]</sup> Closer to **44** is the fragmentation of this cyclic ether mediated by lithium aluminate [ $\{\text{PhC(=O)N}^i\text{Pr}_2\}\text{LiAl}^i\text{Bu}_3$ ], where the heteroleptic system metallates dioxane at its alpha position, to form a transient intermediate that can rapidly undergo ring-opening and rearrange to a vinyl modification.<sup>[55]</sup> A similar process could be in operation in forming **44** (**Scheme 5.3**), suggesting an enhanced metallating power for potassium manganate **40** over its Na analogue **39** (where addition of dioxane only induces deaggregation of the manganate structure to form dimer **43**, *vide supra*).  $\alpha$ -Manganation of one molecule of dioxane can be facilitated by its coordination to the Mn center (as seen in **43**) which would bring it into close proximity to the ate activated monosilyl groups. Transformation of this proposed intermediate into final product **44** involves ring-opening of the coordinated deprotonated dioxane molecule followed by a rearrangement step to its vinyl form (**Scheme 5.3**).



**Scheme 5.3:** Proposed stepwise mechanism for formation of **44**.

Also pertinent is the ability of alkali-metal manganates to promote the metallation and cleavage of cyclic ethers previously demonstrated by Mulvey using [(TMEDA)NaMn(TMP)<sub>2</sub>(CH<sub>2</sub>SiMe<sub>3</sub>)], which induces the “catastrophic” cleavage of THF, breaking its two C-O bonds and four C-H bonds to form oxo and butadiene anions that are trapped by the residue of the bimetallic system (**Scheme 5.4**).<sup>[56]</sup>



**Scheme 5.4:** Cleavage of THF molecule by  $[(\text{TMEDA})\text{NaMn}(\text{TMP})_2(\text{CH}_2\text{SiMe}_3)]$  affording an inverse-crown ether and 1,4-dimanganated butadiene.<sup>[56]</sup>

Finally, utilizing DABCO as a Lewis donor, which akin to 1,4-dioxane has its donor atoms arranged at geometrically opposing sites led to the isolation of sodium manganese  $[\{\text{Na}_2\text{Mn}_2(\text{CH}_2\text{SiMe}_3)_6(\text{DABCO})_2\}_\infty]$  (**45**) where a new supramolecular assembly was revealed (**Fig. 5.8** and **5.9**).

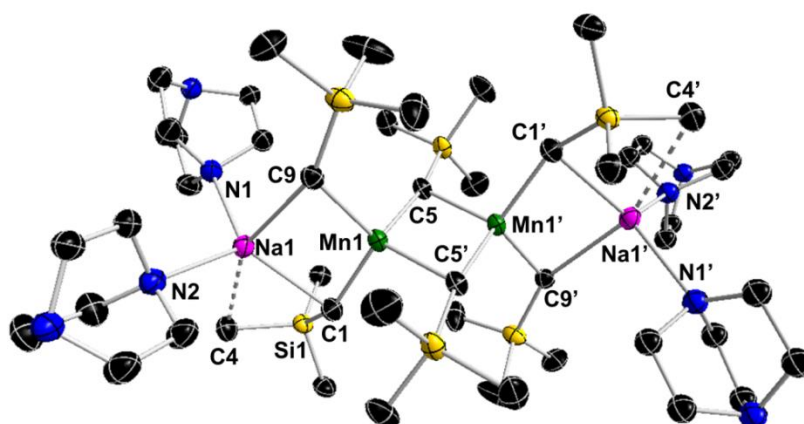


**Figure 5.8:** Molecular structure of dimeric **45** with 50% probability displacement ellipsoids. All hydrogen atoms have been omitted for clarity. Dotted lines represent secondary Na-C interactions. Symmetry operator:  $-x, -y, -z$ .

The basic organometallic core in centrosymmetric **45** comprises a tetranuclear  $\text{Na}\cdots\text{Mn}\cdots\text{Mn}\cdots\text{Na}$  chain arrangement connected by six bridging alkyl groups. This gives rise to three planar four-membered rings, made up of two outer  $\{\text{NaCMnC}\}$  heterobimetallic rings which are linked through a central  $\{\text{MnCMnC}\}$  ring that is orthogonal to the outer rings. The sum of internal angles  $\{\text{Na1C9Mn1C1}\}$  and  $\{\text{Mn1C5Mn1'C1'}\}$  are  $357.93$  and  $359.34^\circ$  respectively. While this core motif is unprecedented in manganese chemistry, it has been previously reported in magnesiate chemistry,<sup>[57–60]</sup> and is reminiscent to the  $\text{Li}\cdots\text{Mn}\cdots\text{Li}$  trinuclear arrangement reported



by Girolami in a series of  $[(\text{TMEDA})_2\text{Li}_2\text{MnR}_4]$  ( $\text{R} = \text{Me}, \text{Et}, \text{CH}_2\text{CH}_2\text{CMe}_3$ ) complexes which contains two orthogonal heterometallic  $\{\text{LiMnC}\}$  four membered rings fused by their Mn vertex.<sup>[11,13]</sup> Each Mn atom in **45** is bonded to four alkyl groups with Mn-C distances [mean value, 2.272 Å] similar to those found in **40** [mean value, 2.272 Å], which also contains a Mn in four-carbon coordination sphere, although in this case the manganate exhibits a ring-structure instead of a linear arrangement. Two nitrogens and two carbons from DABCO and alkyl ligands respectively bond to the Na center, which is further stabilized by a medium-long electrostatic interaction involving a methyl from one  $\text{SiMe}_3$  group [ $\text{Na}\cdots\text{C4}$ , 2.9947(1) Å]. This secondary contact translates into a significantly shorter Na-CH<sub>2</sub> bond for this alkyl group [ $\text{Na1-C1}$ , 2.5584(1) Å], which formally coordinates in an ambidentate fashion closing a four-membered  $\{\text{NaCSiC}\}$  ring, than that observed for the alkyl that binds to Na *via* only its methylene group [ $\text{Na-C9}$ , 2.7206(1) Å]. Each DABCO ligand on the Na atoms coordinates to another Na from a neighboring tetranuclear  $\{\text{Na}_2\text{Mn}_2\text{R}_4\}$  ( $\text{R} = \text{CH}_2\text{SiMe}_3$ ) fragment, giving rise to the formation of an eye-catching 2D network (**Fig. 5.9**). This supramolecular assembly can be envisaged as a network of  $\{\text{Na-DABCO-Na-DABCO}\}_n$  chains in a zig-zag disposition, connected by  $\{\text{Mn}_2\text{R}_4\}^{2-}$  linkers which bind to each Na in a chelating fashion by a combination of Na-CH<sub>2</sub> and  $\text{Na}\cdots\text{Me-SiMe}_2$  interactions (**Figure 5.9**).

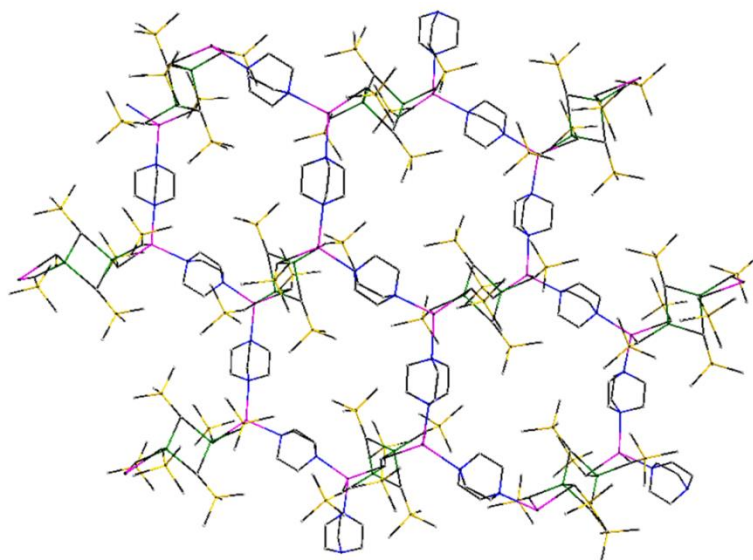


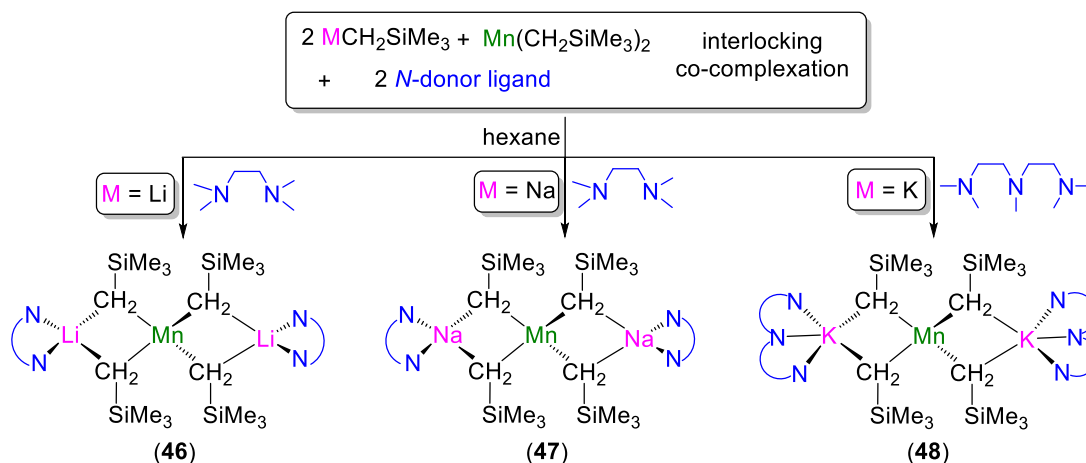
**Figure 5.9:** Wire model representation of polymeric sheet network of **45**. Hydrogen atoms have been omitted for clarity. Symmetry operators #1:  $-x, -y, -z$ ; #2:  $-x+0.5, y+0.5, z$ ; #3:  $-x+0.5, y-0.5, z$ .

The closely-contacted ion-pair structure of **45** contrasts with that reported for disodium tetrabutylmagnesiate  $[[[\text{Na}_2(\text{DABCO})_3(\text{toluene})]^{2+}(\text{Mg}^n\text{Bu}_4)^{2-}]_\infty]$ , which

also displays a supramolecular assembly but one that is exclusively made up of a 3D network of DABCO and toluene-solvated sodium cations storing in its interstices discrete  $\{Mg^nBu_4\}^{2-}$  dianions.<sup>[61]</sup>

### 5.3.2. A homologous series of tetraorgano alkali-metal manganates

Having prepared and established the structural diversity in lower order alkali-metal manganates we decided to expand the scope and prepare homologous series of higher order manganates. Thus, by employing once again a co-complexation approach and mixing relevant alkali-metal alkyl  $M(CH_2SiMe_3)$  ( $M = Li, Na, K$ ) with  $Mn(CH_2SiMe_3)_2$  in hexane at room temperature this time in 2:1 stoichiometric ratio, followed by the addition of 2 molar equivalents of Lewis donor TMEDA (for Li and Na congeners) or PMDETA (for K) afforded fine orange suspensions. Gentle heating produced solutions which upon slow cooling yielded crystals of  $[(TMEDA)_2M_2Mn(CH_2SiMe_3)_4]$  ( $M=Li$ , **46**;  $M=Na$ , **47**) and  $[(PMDETA)_2K_2Mn(CH_2SiMe_3)_4]$  (**48**) in 72, 88 and 63% crystalline yields, respectively (**Scheme 5.5**).



**Scheme 5.5:** Synthesis of homoleptic higher-order alkali-metal manganates **46-48**.

Their structures were elucidated by X-ray crystallographic studies which confirmed their bimetallic, alkali-metal rich constitution based on the 2:1 ratio of alkali-metal:Mn within the molecule (**Fig. 5.10** and **5.11**).

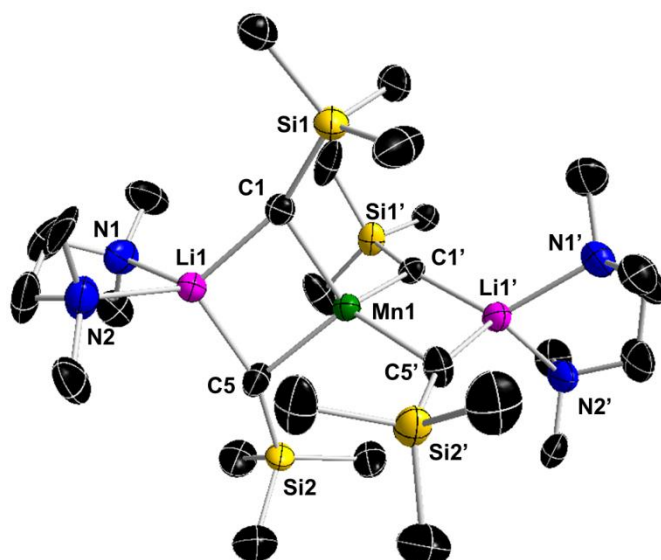


**Figure 5.10:** Molecular structure of **46** with 50% probability displacement ellipsoids. All hydrogen atoms and minor disorder components in TMEDA ligand and SiMe<sub>3</sub> group have been omitted for clarity. Symmetry operator:  $x-1, y+1, -z+2$ . Selected bond distances (Å) and angles (°): Mn(1)-C(1) 2.277(5), Mn(1)-C(5) 2.272(5), Li(1)-C(1) 2.230(5), Li(1)-C(5) 2.229(5), C(5')-Mn(1)-C(5) 113.3(3), C(5')-Mn(1)-C(1') 100.17(18), C(5)-Mn(1)-C(1') 116.37(17), C(5')-Mn(1)-C(1) 116.37(17), C(5)-Mn(1)-C(1) 100.17(18), C(1')-Mn(1)-C(1) 111.3(3).

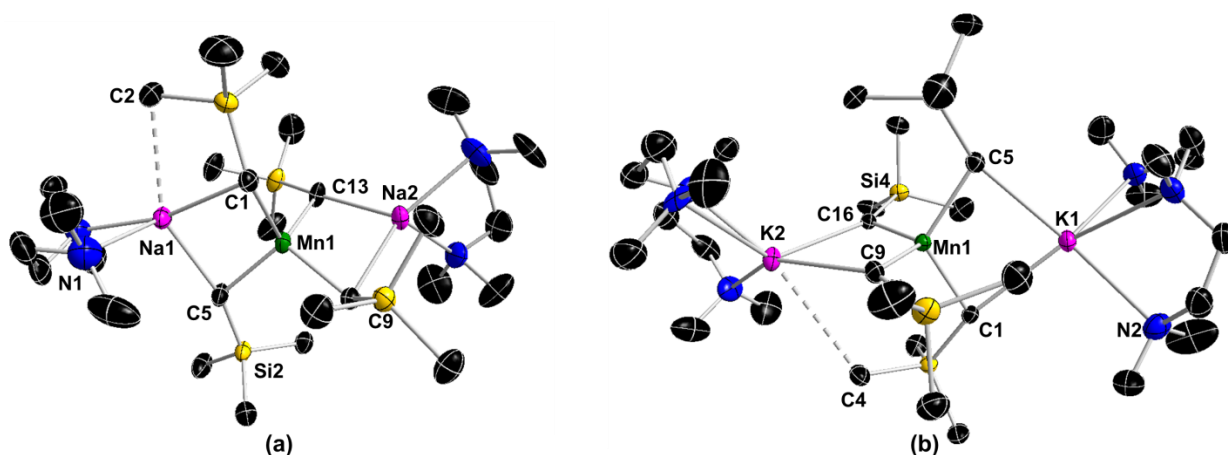


**Figure 5.11:** Molecular structure of **47** (a) and **48** (b) with 50% probability displacement ellipsoids. All hydrogen atoms and minor disorder components in TMEDA (a) and one PMDETA (b) ligand have been omitted for clarity. Selected bond distances (Å) and angles (°): a) Mn(1)-C(1) 2.302(2), Mn(1)-C(5) 2.233(2), Mn(1)-C(9) 2.284(2), Mn(1)-C(13) 2.253(2), Na(1)-C(1) 2.563(5), Na(1)-C(5) 2.643(5), Na(2)-C(9) 2.567(5), Na(2)-C(13) 2.608(5), C(1)-Mn(1)-C(5) 110.81(8), C(5)-Mn(1)-C(9) 107.43(8), C(9)-Mn(1)-C(13) 110.37(8), C(13)-Mn(1)-C(1) 107.09(8), C(1)-Mn(1)-C(9) 105.74(7), C(5)-Mn(1)-C(13) 115.04(9); b) Mn(1)-C(1) 2.275(5), Mn(1)-C(5) 2.265(5), Mn(1)-C(9) 2.259(5), Mn(1)-C(16) 2.248(5), K(1)-C(1) 2.999(2), K(1)-C(5) 3.010(5), K(2)-C(9) 3.045(2), K(2)-C(16) 2.990(5), C(5)-Mn(1)-C(1) 115.8(2), C(9)-Mn(1)-C(1) 107.61(19), C(1)-Mn(1)-C(16) 106.2(2), C(5)-Mn(1)-C(9) 107.5(2), C(5)-Mn(1)-C(16) 106.34(18), C(9)-Mn(1)-C(16) 113.70(19).

These discrete monomeric, contacted ion-pair structures display a classical “Weiss motif”<sup>[45,62]</sup> where the four alkyl groups form bridges between the central Mn atom

and the N-donor capped alkali-metal and are isostructural on molecular level with the series reported by Girolami (*vide supra*).<sup>[11,13]</sup> The arrangement between the metals, determined by the AM1...Mn1...AM2 angle, is nearly linear in **46** (Li1...Mn1...Li2 176.082(2)°) and in **48** (K1...Mn1...K2 174.396(3)°), while **47** exhibits a more bent arrangement (Na1...Mn1...Na2 154.993(1)°). Related to this, Mn adopts marginally distorted tetrahedral geometry with a narrow range of angles between 100.17(18)° and 116.37(17)° for **46** [mean 109.61°], 105.79° to 115.03° for **47** [mean 109.41°] and 106.2(2) to 115.8(2) for **48** [mean 109.53°]. In all three structures there is very little variation in Mn-C bond distances (**Table 5.4**) which suggests these are anchoring bonds forming the {[MnR<sub>4</sub>]<sup>2-</sup>} framework and the M<sup>I</sup>-C interactions are ancillary bond and more electrostatic in nature. The Mn-C bond distances are in good agreement with other examples of C4-tetracoordinated Mn-species as for instance in [(TMEDA)<sub>2</sub>Li<sub>2</sub>MnEt<sub>4</sub>] or [(TMEDA)<sub>2</sub>Li<sub>2</sub>Mn(CH<sub>2</sub>CH<sub>2</sub><sup>t</sup>Bu)<sub>4</sub>], 2.249 and 2.28 Å respectively.<sup>[13]</sup> Even better agreement is observed when compared with the previously discussed **45** (mean Mn-C 2.272 Å) in which central Mn-atom adopts a very similar coordination environment surrounded by exactly the same alkyl group.

**Table 5.4:** A comparison of selected bond distances (Å) and angles (°) for **46**, **47** and **48**.

	M = Li ( <b>46</b> )	M = Na ( <b>47</b> )	M = K ( <b>48</b> )
Mn-C <sub>av</sub>	2.274	2.268	2.262
M-C <sub>av</sub>	2.230	2.595	3.011
(C-Mn-C) <sub>av</sub>	109.61	109.41	109.53
(M...Mn) <sub>av</sub>	2.847	3.008	3.546

A more notable difference is observed in the alkali-metal-C bond lengths which are elongating from mean Li-C 2.230 Å (**46**) over mean Na-C 2.595 Å (**47**) to mean K-C 3.011 Å (**48**) (**Table 5.4**) in agreement with the increased radii of the alkali-metal incorporated. Furthermore, the increase in the size and electropositivity of the alkali-metal in question is also accompanied by the increase in the coordination number from four in **46** up to six in **48**. Capped by a bidentate TMEDA ligand, the C<sub>2</sub>N<sub>2</sub>-tetracoordinated Li exhibits a distorted tetrahedral geometry [bond angles spanning from 84.904(2)° to 123.934(2)°] with an average angle of 109.65°. Sodium capped with the same bidentate ligand, however, forms an additional secondary electrostatic

interaction with the methyl group of one alkyl group [Na1...C2, 2.9374(1) Å and Na2...C12, 3.1448(1) Å] increasing its coordination number to five and exhibiting a distorted square pyramidal geometry. The potassium congener was crystallised by employing the tridentate PMDETA, affording **48** which is isostructural with the magnesiate derivative [(PMDETA)<sub>2</sub>K<sub>2</sub>Mg(CH<sub>2</sub>SiMe<sub>3</sub>)<sub>4</sub>].<sup>[46]</sup> Thus, the K atom in **48** is chelated by PMDETA, bridged by two monosilyl groups and by engaging in secondary electrostatic interaction with the methyl group of one monosilyl ligand [K2...C4, 3.6117(2) Å and K1...C10, 3.8962(2) Å] achieves further stabilisation.

## 5.4. EPR and magnetic susceptibility

With the [Ar]3d<sup>5</sup> electronic configuration, Mn(II) compounds contain unpaired electrons making them paramagnetic and incompatible with NMR techniques which is one of the reasons why these compounds are often poorly characterized. Thus, in order to shed some light on the electronic structure of the Mn(II) centers in the various coordination environments unveiled in this family of compounds, in collaboration with the group of Prof Aromí in Universitat de Barcelona, we have conducted variable temperature magnetization and EPR spectroscopy measurements. In this part of the chapter, the information obtained as a part of this collaboration will be presented and discussed.

### 5.4.1. Lower order manganates

Molar paramagnetic susceptibility ( $\chi_M$ ) data were collected from microcrystalline samples in the 2 to 300 K temperature range together with isothermal magnetization measurements at 2 K in the field range of 0–5 T.

Lower order manganates containing one isolated magnetic metal centre (**39**, **41** and **42**) display almost identical behaviour, fully consistent with the presence of one high-spin ( $S=5/2$ ) Mn(II) ion (**Figure 5.12**). In all cases, the  $\chi_M T$  product at 300 K (3.96, 4.02 and 4.19 cm<sup>3</sup> mol<sup>-1</sup> K for **39**, **41** and **42**, respectively) is slightly lower than the theoretical prediction (4.375 cm<sup>3</sup> mol<sup>-1</sup> K,  $g = 2.0$  and  $S=5/2$ ). The small deviation from a Curie-behaviour observed when reaching the higher temperature range is caused by slight decomposition of the samples or their oxidation to Mn(III) analogues occurring at these stages. However, below 250 K the values of  $\chi_M T$  are closer to those

expected and the  $\chi_M T$  vs  $T$  curves feature a small positive slope, before experiencing a sharp decrease below 7 K.

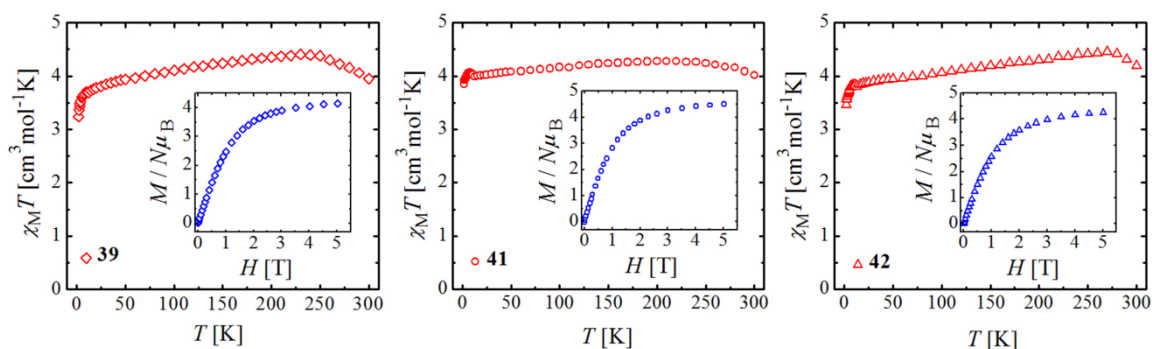


**Figure 5.12:**  $\chi_M T$  vs  $T$  curves of compounds **39**, **41** and **42**. Measurement setup: 2→300 K,  $B=0.3$  T.

The latter is due to zero-field splitting, which inhibits also the saturation of the reduced magnetization, even in high fields. The positive slope, which lies beyond the reasonable contribution of temperature independent paramagnetism, is often observed in organometallic Mn(II) compounds and has been attributed to the contribution of low-spin states to the susceptibility.<sup>[15,63]</sup> An additional explanation could be the contribution of a very small amount of antiferromagnetically coupled impurities, one of which could be the starting material  $\text{Mn}(\text{CH}_2\text{SiMe}_3)_2$  for which antiferromagnetic coupling between the spin carriers is reported.<sup>[7,19]</sup>

Variable temperature X-band EPR spectra of a powdered sample of compound **39** show two very broad transitions centred at  $g = 5.49$  and  $g = 2.03$  (**Fig. 5.13a**). The broadness is caused by intermolecular dipole-dipole interactions and  $D$  strain, which prevents the observation of the hyperfine interaction with the Mn nuclei ( $I=5/2$ ).<sup>[64]</sup> The large deviation from  $g = 2$  of the main spectral feature indicates the influence of the zero-field splitting. The simplicity of the spectrum suggests a large degree of rhombicity ( $E/D \approx 1/3$ ).<sup>[65]</sup> The intensity of the spectra increases upon cooling, while their shape remains unchanged. The EPR spectra of compounds **41** and **42** (**Fig. 15b,c**) exhibit a much higher degree of complexity, featuring three main resonances centred at  $g \approx 6.7$ ,  $g = 4.45/4.32$  (the strongest one) and  $2.06/2.11$  which indicates a smaller degree of rhombicity contributions ( $E/D < 1/3$ ). In both cases, the overall intensity increases with cooling while the relative peak intensities remain practically unchanged in the whole temperature range. Interestingly, despite the similar coordination environment (a  $C_3$  ligand field), the spectra and the zero-field splitting of compound



**39** differ significantly from those observed for **41** and **42**. The similarity of the latter is expected, while the differences with **39** could be due to a different ligand field of the donors or to dissimilarity in coordination spheres.

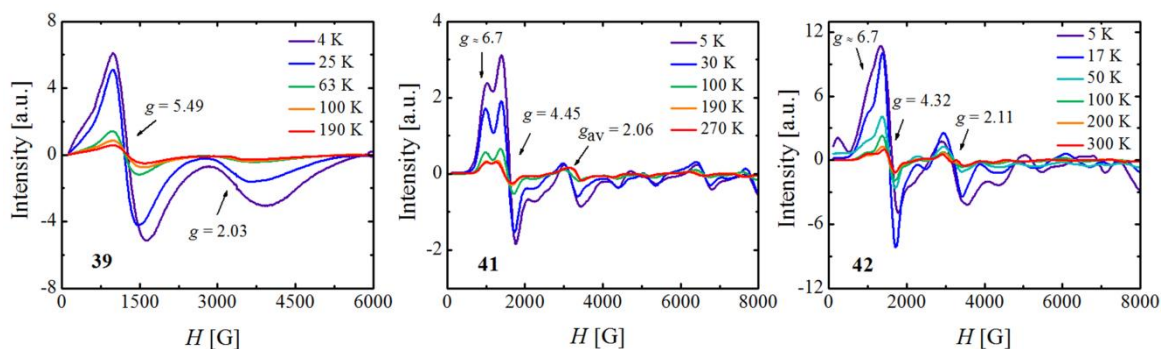


**Figure 5.13:** Variable temperature (4-280 K) X-band EPR spectra ( $f = 9.422$  GHz) of powdered sample of compounds **39**, **41** and **42**.

The magnetic behaviour of dinuclear compound **43** is analogous to that of the mononuclear species. The measured  $\chi_M T$  product at 300 K ( $8.42 \text{ cm}^3 \text{ mol}^{-1} \text{ K}$ ) is only slightly below the theoretical value of  $8.75 \text{ cm}^3 \text{ mol}^{-1} \text{ K}$  ( $g = 2.0$  and  $S=5/2$ ) for two non-interacting high-spin Mn(II) ions in the structure (**Fig. 5.14**). As described above, near 250 K, the value of the  $\chi_M T$  product is more coincident with the expected one;  $9.11 \text{ cm}^3 \text{ mol}^{-1} \text{ K}$ .

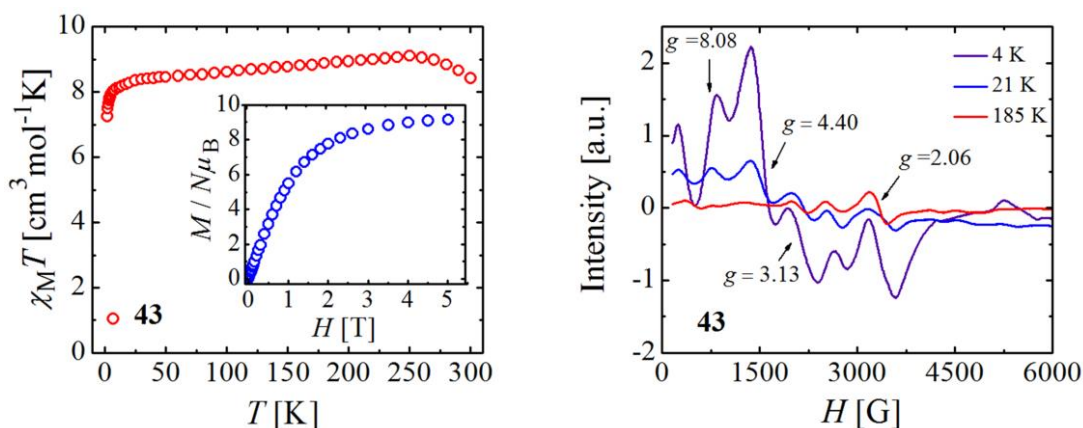


**Figure 5.14:** a)  $\chi_M T$  vs  $T$  curves of compound **43** (measurement setup:  $2 \rightarrow 300$  K,  $B=0.5$  T); b) Variable temperature (4-185 K); b) X-band EPR spectra ( $f=9.422$  GHz) of powdered sample.

The higher temperature observations and the slight positive slope below 250 K are caused by the same causes as discussed previously for compounds **39**, **41** and **42**, whereas the pronounced drop below near 8 K is a consequence of the zero-field splitting. The reduced magnetization at 2 K confirms indeed the  $S=5/2$  spin states of

the Mn(II) centres of **43**, subject to a small degree of zero field splitting ( $M/N\mu_B = 9.16$  at 5 T). X-band EPR spectra at 185 K on a powdered sample shows several strong resonances, the most important ones centred at  $g = 2.01$ ,  $g = 2.57$ ,  $g = 3.18$ ,  $g = 4.4$  and  $g = 8$ , some of which change their relative intensities with varying temperature (**Fig. 5.14b**). The ensemble is consistent with the presence of zero-field splitting with a high axial character.

Dinuclear systems with short Mn...Mn distances (compounds **40**, **44** and **45**) display different magnetic properties as a result of the coupling between spin magnetic moments. Compound **44** displays the typical behaviour of a dinuclear complex with antiferromagnetic interactions between both manganese(II) centres. The  $\chi_M T$  value at 300 K is significantly lower than expected for two non-interacting high-spin Mn(II) ions (measured of  $4.20 \text{ cm}^3 \text{ mol}^{-1} \text{ K}$  compared with the expected value of  $8.75 \text{ cm}^3 \text{ mol}^{-1} \text{ K}$  for  $g = 2.0$  and  $S=5/2$ ). Additionally, a pronounced decrease of the  $\chi_M T$  product upon lowering the temperature is observed, reaching a plateau of  $0.1 \text{ cm}^3 \text{ mol}^{-1} \text{ K}$  at 20 K (**Figure 5.15**).

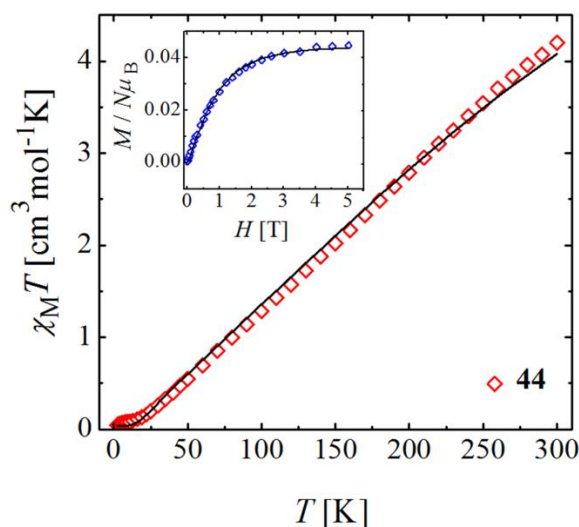


**Figure 5.15:**  $\chi_M T$  vs  $T$  curve of compound **44**. Measurement setup: 2→300 K,  $B = 0.3$  T. Solid line represents the results of the fit.

The small magnetic response below this temperature is caused by a trace amount of paramagnetic impurity, made evident on the  $\chi_M$  vs  $T$  plot, which exhibits a sharp increase below 15 K. The data of the  $\chi_M$  vs  $T$  plot were fitted using the program PHI<sup>[66]</sup> by matrix diagonalization of the isotropic spin Hamiltonian defined in **Equation 5.1**:

$$\hat{H} = -2J(\hat{S}_1\hat{S}_2) + g\mu_B B\hat{S} \quad (5.1)$$



where  $J$  is the exchange constant,  $\widehat{S}$  is the total spin operator,  $\widehat{S}_1 = \widehat{S}_2 = 5/2$  are the spin operators of the individual Mn(II) ions,  $B$  is the magnetic induction and  $\mu_B$  is the Bohr magneton. A simultaneous fit of the magnetization and the molar susceptibility data using a fixed  $g$  factor ( $g = 2.05$ ), yielded the exchange constant  $J = -24.18 \text{ cm}^{-1}$  and 0.9% of paramagnetic impurity ( $S=5/2$ ). As it can be seen from **Figure 5.15**, the proposed model slightly overestimates the  $\chi_M T$  product in the temperature region of 50-200 K. Thus, additional fits on a restricted dataset corresponding to the temperatures below 200 K led to a slightly more negative coupling;  $J = -25.10 \text{ cm}^{-1}$ . Minor temperature variations of the exchange constant have already been reported for an antiferromagnetically coupled Mn(II) dimer and it was rationalised as the consequence of small changes in the bridging geometry and the lattice expansion upon warming.<sup>[67]</sup> In any case, the observed intensity of the exchange coupling is one order of magnitude higher than reported for compounds containing the  $\{\text{Mn}^{\text{II}}_2(\mu_2\text{-O})_2\}$  unit with tetrahedral coordination environment around metal ion (**Table 5.5**).<sup>[68,69]</sup>

**Table 5.5:** Magneto-structural data of compounds containing  $\{\text{Mn}_2(\mu_2\text{-O})_2\}$  core reported in the literature.

Molecular formula	Mn...Mn (Å)	Magnetic data		
		$J$ (cm <sup>-1</sup> )	$g$	$S$
(Et <sub>4</sub> N) <sub>2</sub> [Mn <sub>2</sub> Cl <sub>4</sub> (O-C <sub>6</sub> H <sub>4</sub> - <i>p</i> -CH <sub>3</sub> ) <sub>2</sub> ] <sup>[68]</sup>	3.186(1)	-2.5	2	5/2
[Mn <sub>3</sub> (μ-OMes) <sub>4</sub> {N(SiMe <sub>3</sub> ) <sub>2</sub> } <sub>2</sub> (THF) <sub>2</sub> ] <sup>[69]</sup>	3.1820(7)	-1.2	1.93	5/2

This could be rationalised in terms of the comparatively shorter Mn...Mn distance (3.1447(4) Å) and more acute Mn–O–Mn bridging angles (average 95.36°), which provide a more efficient pathway for the superexchange interaction mechanism involving 3d orbitals of metal ion and *p*-orbitals of alkoxy oxygen atoms from the ligand, and perhaps some higher degree of direct overlap. However, the value of  $J$  obtained for compound **44** is lower than those reported for dialkyl or diamido bridged Mn(II) dimers (**Table 5.6**).<sup>[7,32,67,70,71]</sup>

**Table 5.6:** Magneto-structural data of compounds containing  $\{\text{Mn}_2(\mu_2\text{-X})_2\}$  core (X=C or N), reported in the literature.

Molecular formula	Mn...Mn (Å)	Magnetic data		
		$J$ (cm <sup>-1</sup> )	$g$	$S$
$[\{\text{Mn}(\text{CH}_2\text{SiMe}_3)_2\}_\infty]^{[7]}$	2.8874(5)	-51.4	1.97	5/2
	2.8897(5)			
$[\{\text{Mn}(\text{CH}_2\text{SiMe}_3)(\mu\text{-CH}_2\text{SiMe}_3)(\text{THF})_2\}_2]^{[70]}$	2.7878(9)	-42.5(2)	2.01(5)	5/2
$[\{(\text{THF})(\text{Mes})\text{Mn}(\mu\text{-Mes})_2\}_2]^{[71]}$	2.851(2)	-40.4	1.99	5/2
$[\{(2,6\text{-Mes-C}_6\text{H}_3)\text{Mn}(\mu\text{-NMe}_2)_2\}_2]^{[67]}$	2.9479(3)	-38(1)	2	5/2
$[\text{Li}([\text{12-crown-4}]_2)[\text{Mn}_2(\text{NC}^t\text{Bu}_2)_5]^{[32]}$	2.5965(7)	-78	2.025	5/2

The variable temperature EPR spectra of **44** mirror the reported magnetic data remarkably well (**Figure 5.16**). The intensities of most spectral features (with major resonances at  $g = 3.35$ , 2.48, 1.77 and 1.43) decline systematically in lowering the temperature while the intensity of transitions at  $g = 4.96$  and  $g = 2.20$  initially increase (100-280 K) before disappearing at the lowest temperatures. As a result, the EPR response at 4 K is silent as expected for an  $S = 0$  ground state of the dimer.

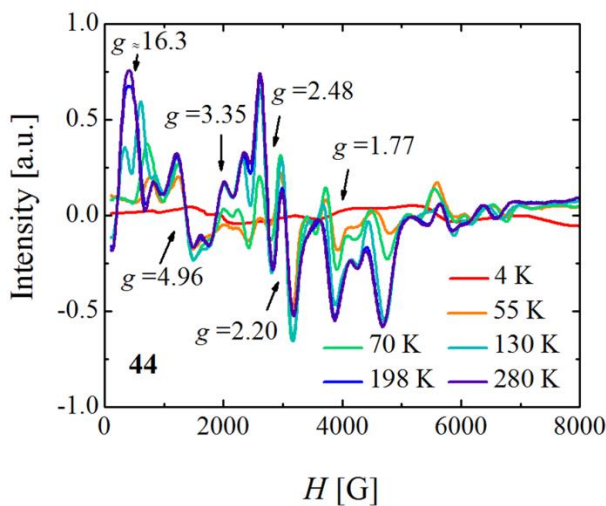


**Figure 5.16:** Variable temperature (4-280 K) X-band EPR spectra ( $f = 9.422$  GHz) of powdered sample of compound **44**.

At high temperatures (198 K and 280 K), the spectral pattern is quite complex, with numerous features in the almost entire range explored (500 to 5500 G). The Boltzmann factors of the energy levels, as extracted from the  $J$  value indicate that there is a significant population of spin states from  $S=0$  to  $S=4$  at these temperatures,

justifying a rich structure of the spectra. Upon cooling to the 100-130 K range, the dominant contributions arise from transitions related to the spin states  $S=1$  and  $S=2$ , while below 70 K, significant features arise only from the population of the  $S=1$  energy level.

The  $\chi_M T$  vs  $T$  plot for compound **40** shows a value of  $\chi_M T$  at 300 K ( $9.48 \text{ cm}^3 \text{ mol}^{-1} \text{ K}$ ,  $g = 2.08$ ) that lies just above the theoretical value of  $8.75 \text{ cm}^3 \text{ mol}^{-1} \text{ K}$  ( $g = 2.0$  and  $S=5/2$ ) for two non-interacting high-spin Mn(II) ions (**Figure 5.17**). As seen for complexes **39**, **41** and **42**, a smooth maximum is seen near 260 K ( $9.86 \text{ cm}^3 \text{ mol}^{-1} \text{ K}$ ), as a consequence of the slight degradation of the sample above that temperature. Below this point, the positive slope is only perceptible from near 160 K, whereas for temperatures close to 15 K, the decline becomes much sharper. These results indicate that the behaviour of complex **40** is more similar to that of the complexes with isolated Mn(II) centers than to the structurally related cluster **44**. Thus, the effect of the magnetic coupling between the Mn centres that could be anticipated only manifests itself very slightly by the small positive slope below 160 K, in sharp contrast to the effect seen for **44**. Consistent with this, the reduced magnetization measurements at 2 K easily saturates to the expected value for two independent Mn(II) centres ( $M/N\mu_B = 9.14$  at 5 T; expected value,  $M/N\mu_B = 10$ ).

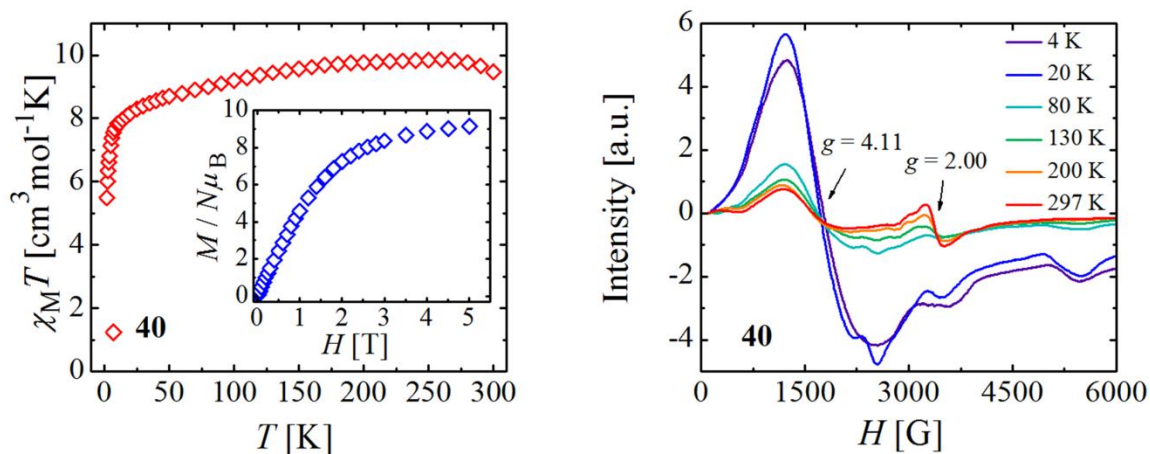


**Figure 5.17:** a)  $\chi_M T$  vs  $T$  curves of compound **40** (measurement setup: 2→300 K,  $B=0.3$  T); b) Variable temperature (4-297 K) X-band EPR spectra ( $f=9.422$  GHz) of powdered sample.

The temperature dependent X-band EPR spectra are in agreement with the SQUID measurements and resemble those for compound **39** for a highly rhombic system. The main difference is an additional feature at  $g = 2.00$  that decays and becomes barely

detectable below 130 K. Since the temperature evolution of the spectra as well as that of  $\chi_{\text{M}}T$ , are rather complex and cannot be explained with a simple coupling model, even taking into account only zero-field splitting effects, the possibility of a thermal equilibrium between different spin states ( $S=5/2$ ,  $S=3/2$ ,  $S=1/2$ ) exists, as has been invoked before.<sup>[15,63]</sup> The lack of significant coupling indicates that a super-exchange mechanism through bridging  $sp^3$  carbon atoms is not effective. This is caused by the long Mn–C bond distances within the asymmetric  $\{\text{Mn}_2(\mu_2\text{-C})_2\}$  core (especially that of 2.488(3)Å; 0.12 Å above the sum of covalent radii of the two atoms),<sup>[72]</sup> which keep both Mn(II) centers disconnected magnetically. The peculiar local ‘hypercoordination’ geometry around the bridging carbon atoms may also contribute to its inefficient exchange interaction. Conversely, compound **45** displays a behaviour closer to that of compound **44**, resulting from antiferromagnetic interactions between Mn(II) ions. At room temperature (300 K), the  $\chi_{\text{M}}T$  value (6.20 cm<sup>3</sup> mol<sup>-1</sup> K) is below expected for the two non-interacting high-spin Mn(II) ions (8.75 cm<sup>3</sup> mol<sup>-1</sup> K for  $g = 2.0$  and  $S=5/2$ ). By lowering the temperature, an almost linear decrease of  $\chi_{\text{M}}T$  is observed followed by a sharp decline below 12 K (**Figure 5.18**).

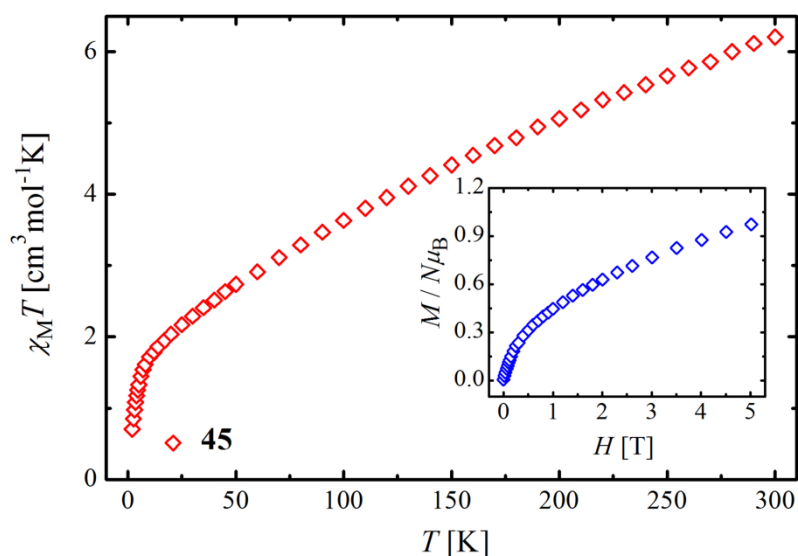


**Figure 5.18:**  $\chi_{\text{M}}T$  vs  $T$  curve of compound **45**. Measurement setup: 2→300 K,  $B = 0.3$  T.

The non-zero  $\chi_{\text{M}}T$  product at 2 K (0.71 cm<sup>3</sup> mol<sup>-1</sup> K) indicates the presence of paramagnetic impurities, which prevents fitting the data for a precise determination of  $J$ . However, the significantly larger coupling inferred from the data in comparison with compound **40** arises from shorter Mn–C bonds (2.214 and 2.419 Å (**45**) vs 2.235

and 2.489 Å for **40**) and also importantly, a lower degree of ‘hypercoordination’ which influences the directionality of the overlap and enables a better pathway for the superexchange interaction mechanism between Mn(II) ions.

#### 5.4.2. Higher order manganates

Of the three prepared higher order manganates, only [(TMEDA)<sub>2</sub>Li<sub>2</sub>Mn(CH<sub>2</sub>SiMe<sub>3</sub>)<sub>4</sub>] (**46**) was studied, while **47** and **48** are awaiting to be measured. Electronic structure of the Mn(II) centre in **46** was studied through bulk magnetization measurements and EPR spectroscopy applying the same protocol as in previous examples (*vide supra*). Displayed magnetic behaviour of [(TMEDA)<sub>2</sub>Li<sub>2</sub>Mn(CH<sub>2</sub>SiMe<sub>3</sub>)<sub>4</sub>] reflects its structure where the existence of isolated high-spin Mn(II) (*S*=5/2) metallic centers was established (Fig. 5.19).

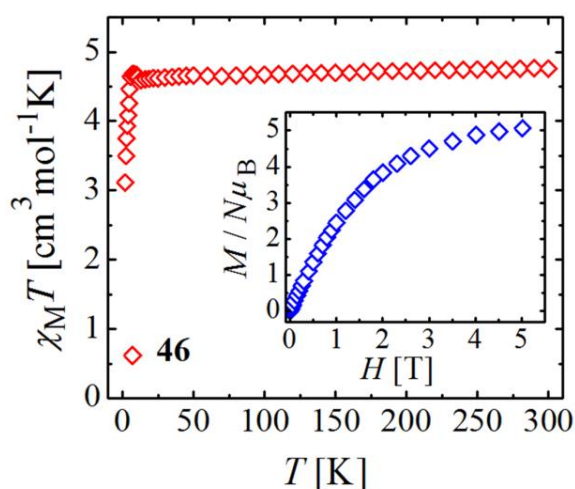


**Figure 5.19:**  $\chi_M T$  vs  $T$  curve of compound **46**. Measurement setup: 2→300 K,  $B=0.3$ T;  $T_{\text{mag}}=2$ K.

The  $\chi_M T$  product of 4.759 cm<sup>3</sup> mol<sup>-1</sup> K at the room temperature (300 K) is slightly higher than expected for one high-spin manganese(II) ion (expected value for *S*=5/2 is 4.375 cm<sup>3</sup> mol<sup>-1</sup> K taking into account *g* = 2.0) and corresponds to the calculated *g* value of 2.086 (Curie Law). Upon lowering the temperature, the  $\chi_M T$  product remains practically constant down to 6 K (minor positive slope) followed by the abrupt decrease ending at the  $\chi_M T$  value of 3.114 cm<sup>3</sup> mol<sup>-1</sup> K at 2 K. The latter could be ascribed to the effects of the zero-field splitting, weak antiferromagnetic interactions between the molecules at the low temperature or combination of both. Additionally, *S*=5/2 ground state of Mn(II) magnetic centre is confirmed by the

variable field magnetization measurements where  $M/N\mu_B$  vs  $H$  curve reaches the value of 5.067 at 5 T (expected 5.20 for  $S=5/2$  and  $g = 2.08$ ). The high-spin electron configuration for Mn(II) centre in **46** is fully consistent with previously reported Mn(II) mononuclear compounds with a tetrahedral  $-C_4$  coordination environment including even the strong-ligand field species such as anion  $[\text{Mn}(\text{CN})_4]^{2-}$ .<sup>[11,13,14,73–77]</sup>

Variable-temperature X-band EPR spectra for powdered sample of  $[(\text{TMEDA})_2\text{Li}_2\text{Mn}(\text{CH}_2\text{SiMe}_3)_4]$  show one very broad transition centered at  $g = 2.001$  (**Figure 5.20**). The intensity of observed resonance increases continuously upon lowering the temperature as expected from the Curie Law. Although the shape of the spectra is maintained in the whole temperature range, the appearance of additional broad and weakly intense feature centred at  $g \approx 4$  can be detected at 4 K. This observation along with broadness of the central resonance at  $g = 2$  indicates the existence of small anisotropy ( $D \neq 0$ ,  $E \neq 0$ ).

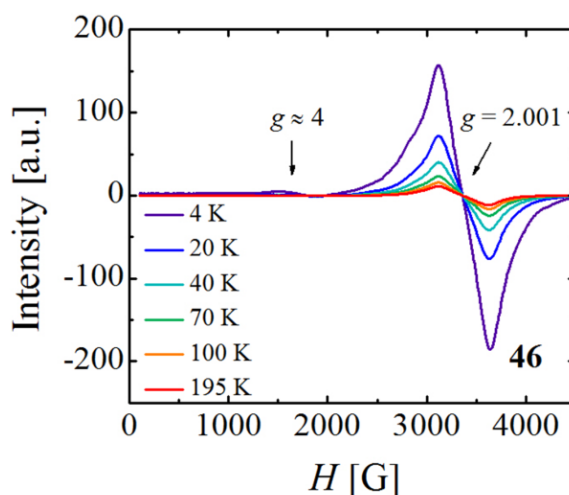
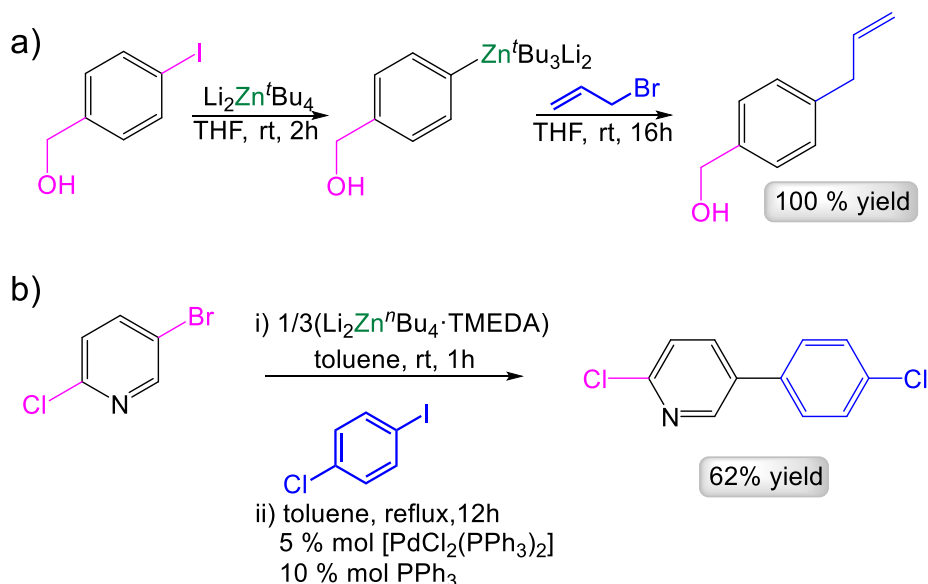


**Figure 5.20:** Variable temperature (4-195 K) X-band EPR spectra ( $f=9.417$  GHz) of **46**.

Furthermore, the absence of any hyperfine structure coming from interaction with  $^{55}\text{Mn}$  nuclei ( $I=5/2$ ) could be the consequence of intermolecular dipole-dipole interactions and/or the small changes in molecular geometry through the sample which roots the inhomogeneous line broadening.<sup>[64]</sup> Nevertheless, the reported EPR spectra is characteristic for high-spin tetrahedral Mn(II) compounds in a  $C_4$  ligand field, both in the solid state and solution.<sup>[7,13,19,78]</sup>

## 5.5. Exploring the ability of $[(\text{TMEDA})_2\text{Li}_2\text{MnR}_4]$ to promote Mn-I exchange and homocoupling processes

With a range of structurally well-defined and characterised alkali-metal manganates, next we decided to probe their potential applications in metal-halogen exchange reactions, which is one of the most powerful methods employed in organic synthesis for functionalization of aromatic molecules. In a single step a C-X bond (where X is a halogen, commonly  $\text{Br}^-$  or  $\text{I}^-$ ) is transformed to a more reactive C-M bond, but because the position of the halogen atom determines the end location of the metal atom, this methodology allows a greater regioselective control than for example deprotonative metallation.<sup>[79,80]</sup> Traditional lithium or magnesium reagents are well known to undergo direct metal-halogen exchange; however they display limitations (**Chapter 1**) which prompted the development of new reagents that can overcome these setbacks. In this context, excellent results have been achieved by employing lithium zincates, where  $\text{LiZn}^t\text{Bu}_3$ <sup>[80–83]</sup> and  $\text{Li}_2\text{Zn}^t\text{Bu}_4$ <sup>[80,84,85]</sup> have been shown to readily undergo direct Zn-I exchange when reacted with functionalised aromatic iodides, even in the presence of unprotected sensitive functionalities such as ester or nitro groups. What is more interesting, the higher order zincate could additionally undergo Zn-Br exchange and even in the presence of acidic protons such as phenolic OH protons (**Scheme 5.6a**).

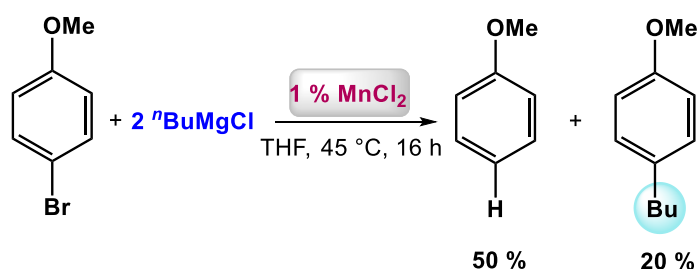


**Scheme 5.6:** a) Zn-I exchange of 4-iodobenzyl alcohol with  $\text{Li}_2\text{Zn}^t\text{Bu}_4$  followed by reaction with allyl bromide;<sup>[84]</sup> b) Related Zn-Br exchange of 2-chloro-5-bromopyridine with a substoichiometric amount of  $\text{Li}_2\text{Zn}^t\text{Bu}_4 \cdot \text{TMEDA}$  followed by Negishi cross-coupling.<sup>[86]</sup>



The closely related reagent  $\text{Li}_2\text{Zn}^n\text{Bu}_4 \cdot \text{TMEDA}$  readily undergoes Zn-Br exchange of bromopyridines in substoichiometric amounts (1/3 equivalent) which could then undergo Negishi cross-coupling (**Scheme 5.6b**).<sup>[80,86]</sup> Interestingly, organozinc reagents on their own fail to promote direct Zn-X exchange processes, evidencing the synergic behaviour of these heterobimetallic systems.

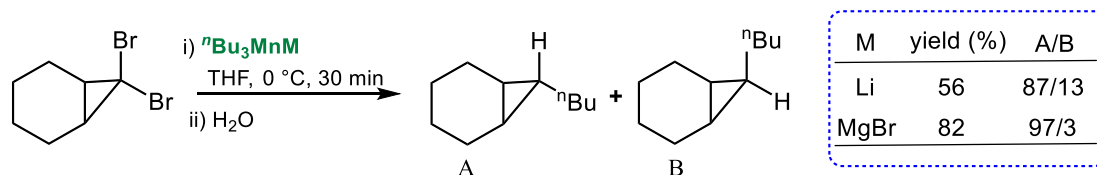
In the realm of manganese chemistry, seminal work by Cahiez and Normant have revealed a Mn-catalysed reaction between 4-bromoanisole and  $^n\text{BuMgCl}$  affording anisole as a major component and the cross-coupling product in low yields (**Scheme 5.7**).<sup>[87,88]</sup>



**Scheme 5.7:**  $\text{MnCl}_2$ -catalysed reduction and cross-coupling of 4-bromoanisole and  $^n\text{BuMgCl}$ .<sup>[87,88]</sup>

The protocol was successfully extended and proved to be more efficient for aryl halides containing electron-withdrawing groups<sup>[89]</sup> and even aromatic ortho-chloroketones.<sup>[90]</sup>

Regarding the closely related Mn-Br exchange reactions, Oshima and co-workers have reported dialkylation of gem-dibromocyclopropanes with trialkylmanganates ( $\text{MMnR}_3$ ,  $\text{M} = \text{Li}, \text{MgX}$ ) in a similar fashion as has been previously done with zincates and cuprates (**Scheme 5.8**).<sup>[80,91,92]</sup> However, dialkylation performed with manganese species was tolerant to higher temperatures ( $0^\circ\text{C}$ ) than zincates or cuprates, and more importantly, could be upgraded from stoichiometric to catalytic processes.

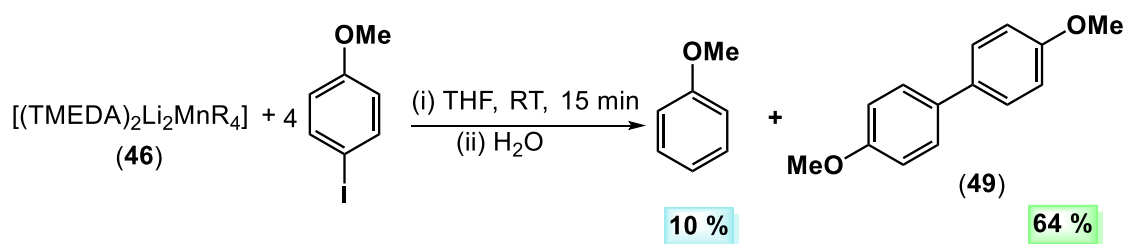


**Scheme 5.8:** Dialkylation of gem-dibromocyclopropanes with trialkylmanganates.<sup>[91]</sup>



Building on these findings and considering that in all these studies the putative manganese species are prepared in situ and remain ill-defined, it was decided to test if homoleptic lithium manganese **46** could also be involved in promoting direct metal-halogen exchange reactions.

Probing the reactivity of **46** towards four equivalents of 4-iodoanisole, in THF at room temperature, an immediate change from bright orange to dark red solution was observed. GC-analyses of hydrolysed reaction aliquots were performed and revealed that the substrate had been consumed and two different products had formed. Based on the previous work of Cahiez,<sup>[93,94]</sup> these were identified as anisole and biaryl **49** (Scheme 5.9). Subsequent NMR spectroscopic analysis of hydrolysed reaction mixture confirmed the identities of products and integration against ferrocene revealed **49** to be the main product (64 %).

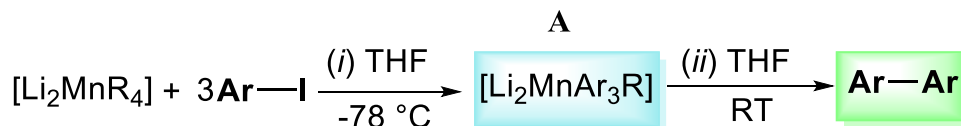


**Scheme 5.9:** Unoptimised reaction of  $[(\text{TMEDA})_2\text{Li}_2\text{MnR}_4]$  with four equivalents of 4-iodoanisole followed by aqueous work-up affording **49** and anisole.

Although some substrate was recovered, in general, the reaction displays a great promise due to the employment of mild reaction conditions, short reaction times and substoichiometric amount of **46**. Encouraged with these findings it was decided to further study the synthetic potential of **46** in synthesis of symmetrical polyaromatic compounds. The optimisation of reaction conditions and expansion of the substrate scope was developed as a part of another PhD project (Marco De Tullio), while here an inquiry into the constitution of the organometallic compounds involved in these reactions was carried out.

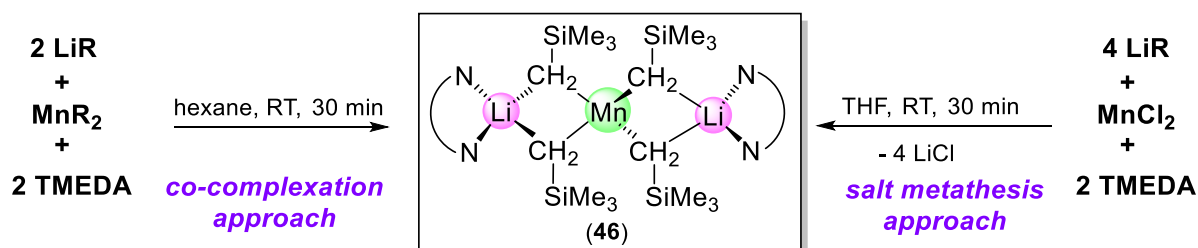
The best results were obtained when three equivalents of 4-iodoanisole were reacted with one equivalent of **46** at  $-78\text{ }^\circ\text{C}$  for 15 min and the obtained mixture further stirred at room temperature overnight. A tentative reaction pathway can be envisioned to proceed *via* Mn-I exchange reaction affording a short-lived arylmanganate transient species **A** (Scheme 5.10i) which undergoes a rapid coupling process yielding **49**

(Scheme 5.10ii). The coupling processes of manganate species were reported before,<sup>[92,93]</sup> but the exact mechanism behind these transformations is extremely complex.



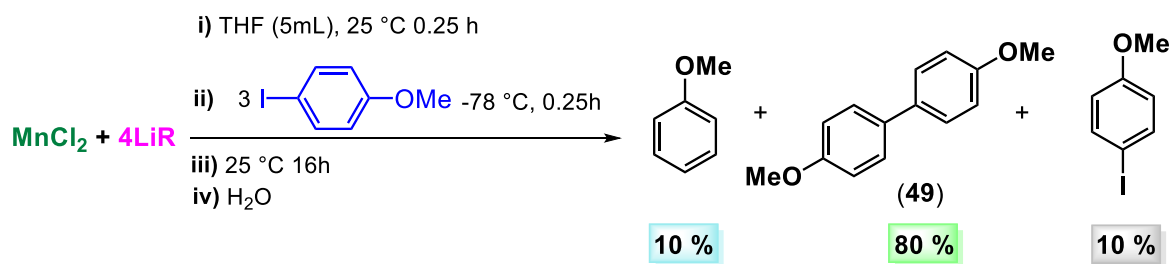
**Scheme 5.10:** Simplistic representation of the proposed two-step process behind the homocoupling of aryl iodides promoted by lithium tetraalkylmanganate.

Having originally prepared **46** by co-complexation, we pondered if the same reagent could be obtained from the commercially available manganese salt and  $\text{LiCH}_2\text{SiMe}_3$ . Thus, by turning attention to a more straightforward approach and performing a simple salt metathesis reaction, dry  $\text{MnCl}_2$  and four equivalents of alkyllithium were mixed in THF at room temperature. The reaction mixture quickly turned into an orange solution suggesting the formation of organomanganate **46**. The solvent was exchanged *in vacuo* for hexane to precipitate the presumably formed  $\text{LiCl}$ , followed by filtration and addition of two equivalents of TMEDA. The product was solubilised with toluene and crystallised at  $-33\text{ }^\circ\text{C}$ . Single crystal X-ray, SQUID magnetometric and elemental analysis revealed that the isolated product is indeed **46** (Scheme 5.11).



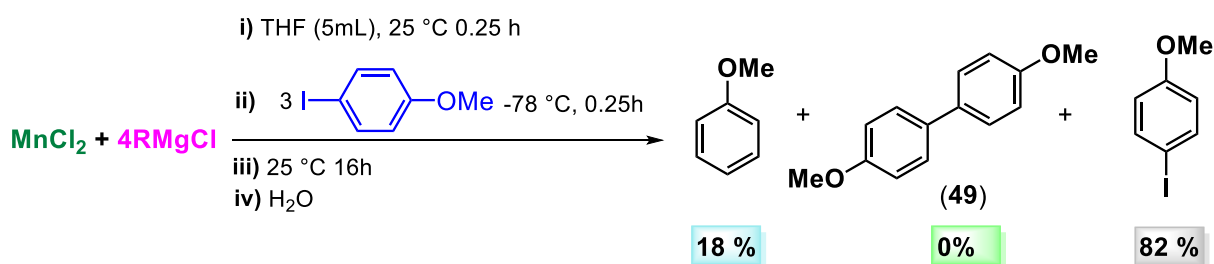
**Scheme 5.11:** Different approaches for synthesis of  $[(\text{TMEDA})_2\text{Li}_2\text{Mn}(\text{CH}_2\text{SiMe}_3)_4]$  (**46**).

Although the isolated crystalline yield for **46** using this approach was significantly lower (38%), these results confirmed that this mixed Li/Mn complex can be easily prepared *in situ* using two commercially available reagents. It should be noted that the yields for coupling product **49** when manganate **46** is treated with 4-iodoanisole are almost identical irrespectively of whether **46** was prepared by co-complexation or salt metathesis (Scheme 5.12).



**Scheme 5.12:** *In situ* preparation of lithium manganese and its subsequent reaction with three equivalents of 4-iodoanisole applying the optimised conditions.

It is well known that neutral organomanganese reagents ( $\text{MnR}_2$ ) cannot perform this type of organic transformations.<sup>[88,92]</sup> In this case we observed no reaction of  $\text{MnR}_2$  with 4-iodoanisole, however it was intriguing to establish the importance of the nature of the other metal. This line of inquiry was particularly intriguing as it builds connections between this work and the work of Oshima (**Scheme 5.8**) who equally successfully employed both  $\text{RLi}$  and  $\text{RMgX}$  with  $\text{MnCl}_2$  for Mn-Br exchange reactions. Thus, applying the same optimised conditions as previously, 4 molar equivalents of  $(\text{CH}_2\text{SiMe}_3)\text{MgCl}$  was reacted with  $\text{MnCl}_2$  in THF at room temperature, followed by the addition of three equivalents of 4-iodoanisole. After aqueous workup and column chromatography there was no evidence of formation of homocoupled product, only starting material recovered in 82% along with presumed 18% formation of anisole (**Scheme 5.13**).



**Scheme 5.13:** Reaction of  $\text{MnCl}_2$  and  $4\text{RMgCl}$ , followed by reaction with three equivalents of 4-iodoanisole applying the optimised conditions.

Surprised by this outcome, and interested in identifying the putative magnesium manganese species formed in the solution, the reaction was repeated by mixing the four equivalents of freshly prepared and titrated  $(\text{CH}_2\text{SiMe}_3)\text{MgCl}$  with  $\text{MnCl}_2$  in THF at room temperature. After stirring the resulting grey-green solution for one hour, hexane was added to the solution which was left at -33 °C overnight affording a crop of colourless crystals identified as  $\text{MgCl}_2$  by X-ray analysis. The salt was removed by

filtration and the resulting solution returned to the freezer where after a few days new colourless crystals of  $[(\text{THF})_4\text{MgCl}_2\text{Mn}(\text{CH}_2\text{SiMe}_3)_2]$  (**50**) formed, as revealed by X-ray crystallography (**Figure 5.21**).

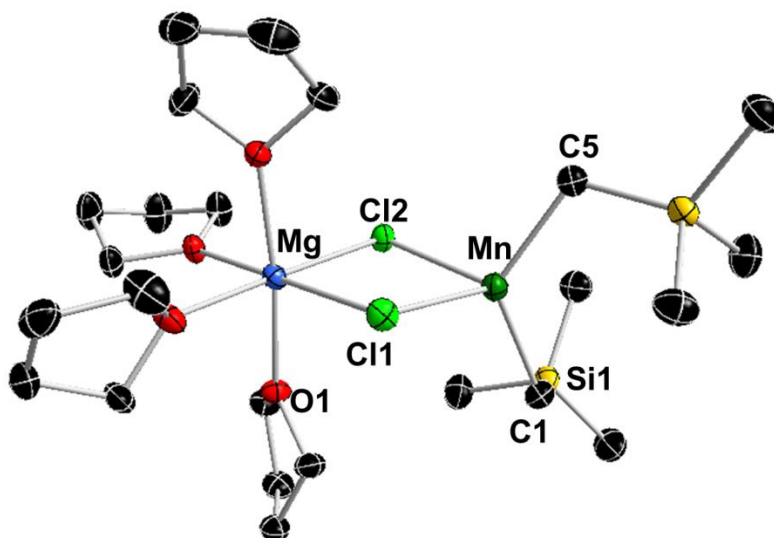
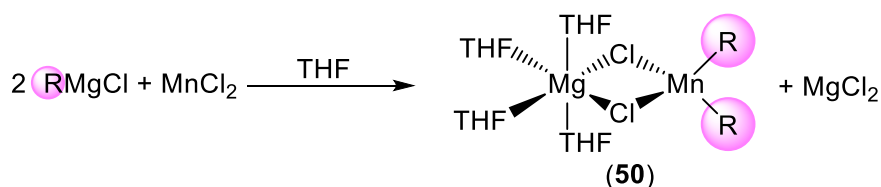


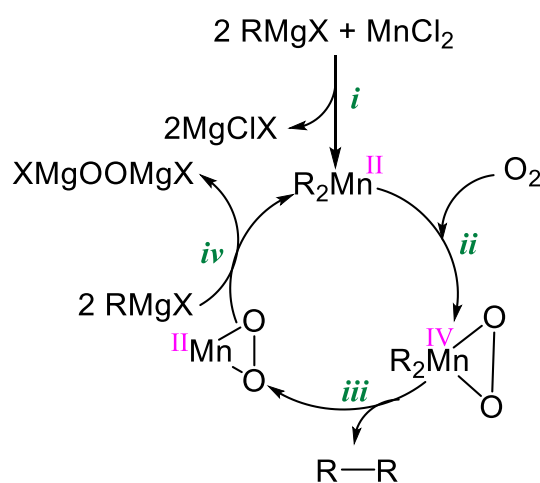
**Figure 5.21:** Molecular structure of **50** with 50% probability displacement ellipsoids. All hydrogen atoms have been omitted for clarity. The unit cell of **50** contains two crystallographically independent molecules with identical connectivity. One of these molecules contains minor disorder in THF ligands, thus structural discussion is focused on the non-disordered molecule. Selected bond distances (Å) and bond angles (°): Mn(1)-C(1) 2.160(2), Mn(1)-C(5) 2.160(2), Mn(1)-Cl(1) 2.5484(5), Mn(1)-Cl(2) 2.5368(5), Mg(1)-Cl(1) 2.4707(7), Mg(1)-Cl(2) 2.4542(7), C(5)-Mn(1)-C(1) 122.67(8), C(5)-Mn(1)-Cl(2) 110.01(5), C(1)-Mn(1)-Cl(2) 114.45(6), C(5)-Mn(1)-Cl(1) 108.78(6), C(1)-Mn(1)-Cl(1) 109.21(6), Cl(2)-Mn(1)-Cl(1) 85.206(16).

Magnesium manganate (**50**) can be envisaged as a co-complex of  $\text{MgCl}_2$  and  $\text{MnR}_2$  exhibiting a CIP structure where the two metals are held together by the two bridging chlorine ligands, forming a planar  $[\text{MgClMnCl}]$  four-membered ring (sum of angles  $359.62^\circ$ ) with the M-Cl bonds comparable to the structurally related  $[(\text{THF})_4\text{Mg}(\mu\text{-Cl})_2\text{MnCl}_2]$ .<sup>[95]</sup> Completing its coordination sphere, manganese forms two identical sigma bonds ( $\text{Mn-C} = 2.160(2)$  Å) with two alkyl groups transferred from the Grignard reagent which are terminally bound. These Mn-C bond lengths are in excellent agreement with related tetrahedral organomanganese compounds containing (trimethylsilyl)methyl fragment such as  $[\text{Mn}(\text{CH}_2\text{SiMe}_3)_2\cdot\text{TMEDA}]$  or  $[\text{Mn}(\text{CH}_2\text{SiMe}_3)_2(\text{pyridine})_2]$  (2.1379(15) and 2.150(4) Å).<sup>[7]</sup> The magnesium ion adopts a distorted octahedral geometry by bonding to additional four molecules of THF with an average Mg-O bond length of 2.1126 Å.



**Scheme 5.14:** Reaction of RMgCl and MnCl<sub>2</sub> to form **50**.

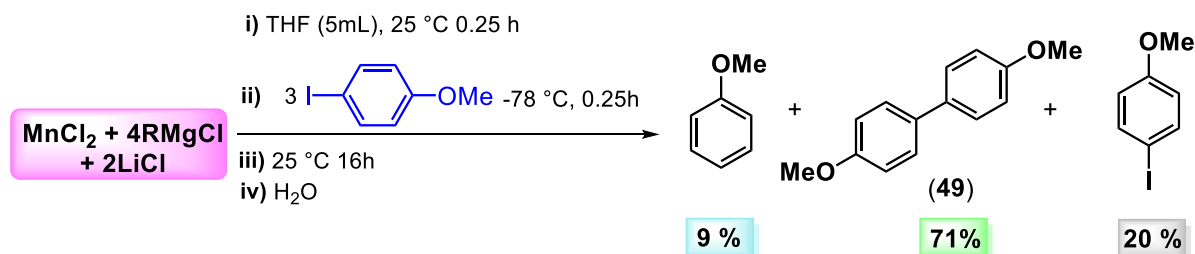
It is interesting that the outcome of this reaction was found to be independent of the reaction times (0.5 to 6 h) or stoichiometry used (1 to 4 equivalents of RMgCl), affording in all cases **50** along with variable amounts of MgCl<sub>2</sub> (**Scheme 5.14**). This observation is in stark contrast to related Mg-Zn hybrid chemistry developed by our group where the nature of the magnesium zincate species could be controlled by the stoichiometry.<sup>[96]</sup> Furthermore, even though this result does not by any means exclude the existence of other Mn-containing species in solution, it does raise a question on the bimetallic constitution of the product of salt-metathesis between Grignard reagents and MnCl<sub>2</sub> which is particularly relevant to the MnCl<sub>2</sub>-catalysed coupling of Grignard reagents where the first step is presumed formation of the diorganomanganese species (**Scheme 5.15i**).<sup>[93]</sup>



**Scheme 5.15:** Proposed mechanism for Mn-catalysed homocoupling of Grignard reactions.<sup>[93]</sup>

In light of this pronounced difference in reactivity between RMgCl and RLi when combined with MnCl<sub>2</sub> and considering the extended use of MnCl<sub>2</sub>·LiCl as a source of manganese, we then decided to examine the influence of LiCl. Thus, by reacting four molar equivalents of freshly prepared Grignard reagent with MnCl<sub>2</sub>·LiCl in THF, followed by the addition of three equivalents of 4-iodoanisole and organic work-up,

we isolated 71% of homocoupled product (**Scheme 5.16**) which is in excellent agreement with results obtained by using alkyllithium as a partner.



**Scheme 5.16:** Reaction of  $\text{MnCl}_2 \cdot \text{LiCl}$  and  $4\text{RMgCl}$ , followed by reaction with three equivalents of 4-iodoanisole applying the optimised conditions.

These results (summarised in **Table 5.7**) disclose an important activating role for LiCl, present as a part of the  $\text{MnCl}_2 \cdot \text{LiCl}$  catalyst for homo- and cross-coupling of Grignard reagents.<sup>[93,94]</sup> Whereas in every single one of these reactions LiCl was present, its presence was attributed merely to solubility reasons and was never included in proposed intermediates, however these results suggest that its presence is crucial to facilitate the Mn-X exchange and the subsequent homocoupling process. Studies trying to shed new light on the role of LiCl in these processes are currently underway in our laboratory.

**Table 5.7:** Comparison of the composition of the reaction mixture after reacting different organometallic mixtures with three equivalents of 4-iodoanisole applying the same conditions.

Reagent mixture	49 (homocoupled product)	Anisole <sup>[a]</sup> (exchange product)	4-iodoanisole (starting material)
$\text{MnCl}_2 + 4 \text{LiR}$	80	10	10
$\text{MnCl}_2 + 4 \text{RMgCl}$	0	18	82
$\text{MnCl}_2 + 2 \text{LiCl} + 4 \text{RMgCl}$	71	9	20

[a] The presence of anisole has been confirmed in the <sup>1</sup>H NMR spectra, but due to its volatility, the amount provided in the table is actually calculated as a difference up to 100 %.

## 5.6. Conclusions

This study uncovers the diversity of alkali-metal triorganomanganate structures, ranging from simple monomeric motifs to intricate supramolecular networks. Co-complexation approach of the single-metal reagents  $\text{Mn}(\text{CH}_2\text{SiMe}_3)_2$  and  $\text{M}(\text{CH}_2\text{SiMe}_3)$  (M = Na, K) in hexane/benzene solutions produced the alkali-metal triorganomanganates  $[\{\text{NaMn}(\text{CH}_2\text{SiMe}_3)_3\}_\infty]$  (**39**) and  $[\{\text{KMn}(\text{CH}_2\text{SiMe}_3)_3 \cdot \text{C}_6\text{H}_6\}_2]$

(40). X-ray crystallographic studies have revealed the structural variations of this heterobimetallic species, showing an important alkali-metal effect. Addition of common donors in synthesis, such as TMEDA, 1,4-dioxane and DABCO has allowed the isolation of novel bimetallic systems **41-45**. Interestingly, potassium manganate **40** reacts with 1,4-dioxane to furnish heteroleptic  $[\{(dioxane)_6K_2Mn_2(CH_2SiMe_3)_4(O(CH_2)_2OCH=CH_2)_2\}_\infty]$  (**44**), resulting from the  $\alpha$ -manganation/ring opening of the cyclic ether.

Noticeably, despite the contrasting structures of manganates **39**, **41**, **42** and **43**, all of them share the same  $\{Mn(CH_2SiMe_3)_3\}^-$  anchor and exhibit minimal variation in their Mn-C bond distances, providing the foundations to these heterobimetallic structures; whereas Na and K are affixed to the frameworks via M-CH<sub>2</sub> and M-CH<sub>3</sub> ancillary bonds. Manganates **40** and **45** illustrate two distinct dimeric arrangements for these bimetallic systems, in forming a cyclic eight-atom ring structure containing both  $\mu_2$ - and  $\mu_3$ -alkyl ligands or alternatively adopting a pseudo-linear, tetranuclear M $\cdots$ Mn $\cdots$ Mn $\cdots$ M arrangement where all the alkyl groups bind to the metals in a  $\mu_2$ -fashion.

By changing the stoichiometric ratio of alkali-metal alkyl MCH<sub>2</sub>SiMe<sub>3</sub> (M = Li, Na, K) and dialkylmanganese to 2:1 followed by the addition of N-Lewis donor, TMEDA or PMDETA, has led to the isolation of higher-order alkali-metal manganates **46-48**. Compound **46** can also be accessed by salt metathesis of a 4:1 LiR: MnCl<sub>2</sub> mixture. Finally, the well-defined and easily accessible lithium manganate **46** has been tested as an efficient reagent for Mn-I exchange transformation in a substoichiometric amount. Preliminary results have shown that this reagent is indeed a good choice, not only for the metal-halogen exchange but also for further homocoupling of biaryls in absence of any oxidant and under mild conditions.

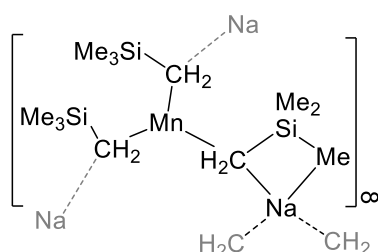
Collectively these findings advance understanding of solvent effects and aggregation in ate chemistry, an area that has received little attention in comparison to single-metal systems (e.g. organolithiums), despite the fact that recent reports have highlighted that the overall performance of these reagents can be finely tuned by introducing variable amounts of Lewis donors. Moreover, new light has been shed on the close relationship of structural/magnetic/reactivity aspects of alkali-metal manganates, which should contribute towards further development of synthetic applications of this class of organometallic reagents, which have already shown promising applications in stoichiometric and catalytic organic transformations. In particular, it is interesting to

note that ‘hypercoordination’ of bridging C atoms significantly decreases its ability to couple magnetically Mn(II) centers.

## 5.7. Experimental procedures

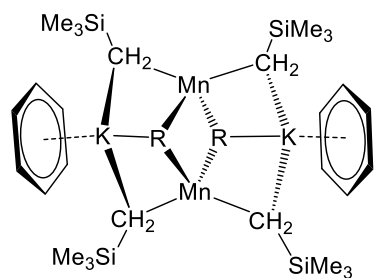
### 5.7.1. Synthesis of $[\{\text{NaMn}(\text{CH}_2\text{SiMe}_3)_3\}_\infty]$ (**39**)

$\text{Mn}(\text{CH}_2\text{SiMe}_3)_2$  (0.23 g, 1 mmol) and  $\text{NaCH}_2\text{SiMe}_3$  (0.11 g, 1 mmol) were suspended together in 10 mL of hexane followed by 3 mL of toluene in order to solubilize the product. The brown fine suspension obtained was stirred for 30 min at room temperature and gently heated in order to obtain a solution. Slow cooling to room temperature afforded X-ray quality crystals. The mixture was then kept overnight at  $-34^\circ\text{C}$  to yield a crop of needle-like, colorless crystals (0.23 g, 68%). Anal. Calcd. for  $\text{C}_{12}\text{H}_{33}\text{MnNaSi}_3$ : C 42.44; H 9.80; N 0.00; found C 42.13; H 9.67; N 0.34.



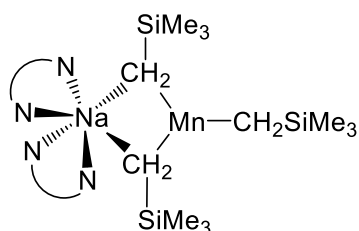
### 5.7.2. Synthesis of $[\{\text{KMn}(\text{CH}_2\text{SiMe}_3)_3\cdot\text{C}_6\text{H}_6\}_2]$ (**40**)

$\text{Mn}(\text{CH}_2\text{SiMe}_3)_2$  (0.23 g, 1 mmol) and  $\text{KCH}_2\text{SiMe}_3$  (0.13 g, 1 mmol) were suspended together in 10 mL of hexane followed by 3 mL of benzene in order to solubilize the product. The brown fine suspension obtained was stirred for 30 min at room temperature and gently heated in order to obtain a solution. Slow cooling to room temperature followed by overnight storage at  $-27^\circ\text{C}$  afforded orange, needle-like X-ray quality crystals (0.29 g, 67%). It should be noted that the two coordinated benzene molecules are lost upon drying *in vacuo*. Anal. Calcd. for  $\text{C}_{36}\text{H}_{78}\text{Mn}_2\text{K}_2\text{Si}_6$ : C 40.52; H 9.35; N 0.00; found C 40.17; H 9.20; N 0.00.



### 5.7.3. Synthesis of $[(\text{TMEDA})_2\text{NaMn}(\text{CH}_2\text{SiMe}_3)_3]$ (**41**)

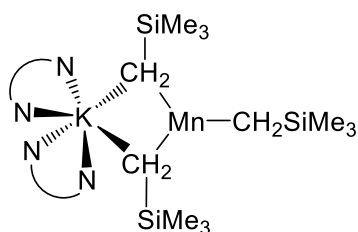
To a solution of *in situ* formed compound **39** (1 mmol) in hexane (7 mL), freshly distilled *N,N,N',N'*-tetramethylethylenediamine (TMEDA) (0.3 mL, 2 mmol) was added, affording an orange suspension that was left stirring for 30 min at room temperature. The suspension was then filtered giving an orange solution that





was left at room temperature for 24 hours to obtain colorless X-ray quality crystals (0.37 g, 65%). Anal. Calcd. for  $C_{24}H_{65}MnNaN_4Si_3$ : C 50.40, H 11.45; N 9.80; found C 50.07 H 11.09 N 10.42.

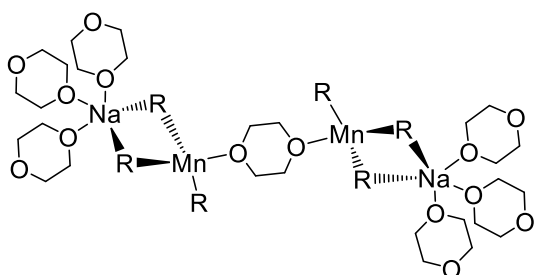
**5.7.4. Synthesis of  $[(TMEDA)_2KMn(CH_2SiMe_3)_3]$  (**42**)**



To a solution of *in situ* formed compound **40** (1 mmol) in a hexane (7 mL)/benzene (2 mL) mixture, freshly distilled *N,N,N',N'*-tetramethylethylenediamine (TMEDA) (0.3 mL, 2 mmol) was added, affording an orange suspension that was left stirring for 30 min at room temperature. The suspension was heated and then filtered while

hot, giving an orange solution that was left at room temperature for 24 hours to obtain orange X-ray quality crystals (0.40 g, 68%). Anal. Calcd. for  $C_{24}H_{65}KMnN_4Si_3$ : C 49.02, H 11.14, N 9.53; found C 48.55, H 11.45, N 9.75.

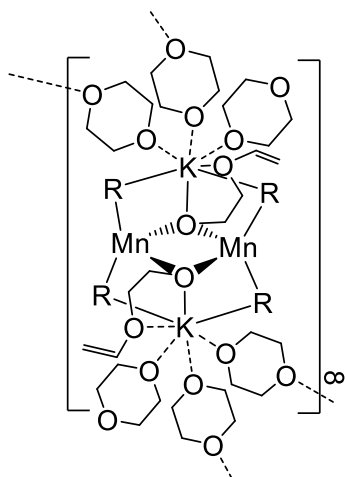
**5.7.5. Synthesis  $[\{NaMn(CH_2SiMe_3)_3\}_2(dioxane)_7]$  (**43**)**



compound **39** (1 mmol) in hexane (5 mL), freshly distilled 1,4-dioxane (0.34 mL, 4 mmol) was added, affording an orange suspension that was left stirring for 30 min at room temperature. The suspension was gently heated to obtain an orange solution which upon slow cooling to

room temperature afforded colorless X-ray quality crystals (0.34 g, 52%). Anal. Calcd. for  $C_{36}H_{90}Mn_2Na_2O_6Si_6$ : C, 45.83; H, 9.62; N, 0.00; found C,45.49; H, 9.58; N, 0.00.

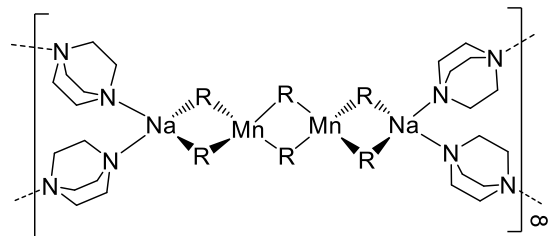
**5.7.6. Synthesis of  $[\{(dioxane)_6K_2Mn_2(CH_2SiMe_3)_4(O(CH_2)_2OCH=CH_2)_2\}_\infty]$  (**44**)**



a solution of *in situ* formed compound **40** (1 mmol) in a hexane (10 mL)/benzene (5 mL) mixture, freshly distilled 1,4-dioxane (0.34 mL, 4 mmol) was added, affording an orange suspension that was left stirring for 30 min at room temperature. The suspension was gently heated to obtain an orange solution which upon slow cooling to room temperature afforded colorless X-ray quality crystals (0.28 g, 53%). Anal. Calcd. for

$C_{32}H_{74}K_2Mn_2O_8Si_4$ : C, 43.31; H, 8.41; N, 0.00; found C, 42.42; H, 8.81; N, 0.00.

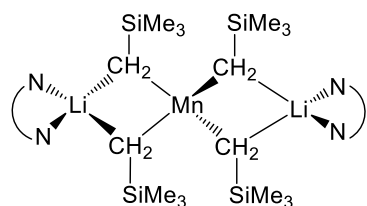
**5.7.7. Synthesis of  $[\{Na_2Mn_2(CH_2SiMe_3)_6(DABCO)_2\}_\infty]$  (45)**  $Mn(CH_2SiMe_3)_2$  (0.23 g, 1



mmol) and  $NaCH_2SiMe_3$  (0.11g, 1 mmol) were suspended in 10 mL of hexane and stirred at room temperature for 30 min. To this suspension DABCO (0.11 g, 1 mmol) was added *via* solid addition tube and the suspension was left stirring

for another 30 min at room temperature. The solvent was exchanged *in vacuo* for 15 mL of toluene and the obtained brown suspension was vigorously heated in order to obtain a solution. Slow cooling to room temperature afforded colorless X-ray quality crystals (0.18 g, 40%). Anal. Calcd. for  $C_{18}H_{45}MnN_2NaSi_3$ : C, 47.86; H, 10.04; N, 6.20; found C, 46.05; H, 9.16; N, 7.11.

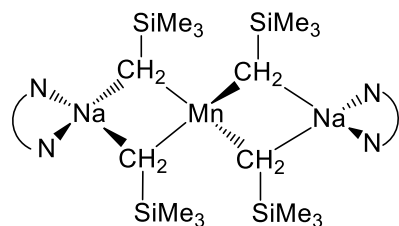
**5.7.8. Synthesis of  $[(TMEDA)_2Li_2Mn(CH_2SiMe_3)_4]$  (46)**  $Mn(CH_2SiMe_3)_2$  (0.23 g, 1



mmol) and  $LiCH_2SiMe_3$  (0.19 g, 2 mmol) were suspended in 10 mL of hexane and stirred at room temperature for 30 min. To this suspension freshly distilled *N,N,N',N'*-tetramethylethylenediamine (TMEDA) (0.3 mL, 2 mmol) was

added, affording an orange suspension that was left stirring for another 30 min at room temperature. The solvent was concentrated *in vacuo* to approximately 5 mL to which 2 mL of toluene was added and the obtained orange suspension was vigorously heated in order to obtain a solution. Slow cooling to room temperature afforded colorless X-ray quality crystals (465 mg, 72%). Anal. Calcd. for  $C_{28}H_{76}Li_2MnN_4Si_4$ : C, 51.73; H, 11.78; N, 8.62; found C, 51.34; H, 11.72; N, 9.45.

**5.7.9. Synthesis of  $[(TMEDA)_2Na_2Mn(CH_2SiMe_3)_4]$  (47)**  $Mn(CH_2SiMe_3)_2$  (0.23 g, 1



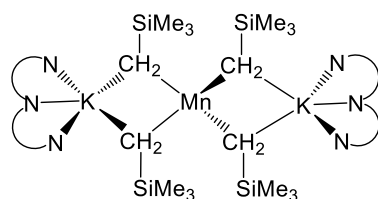
mmol) and  $NaCH_2SiMe_3$  (0.22g, 2 mmol) were suspended in 10 mL of hexane and stirred at room temperature for 30 min. To this suspension freshly distilled *N,N,N',N'*-tetramethylethylenediamine (TMEDA) (0.3 mL, 2 mmol) was added, affording an orange suspension that was left

stirring for another 30 min at room temperature. The solvent was concentrated *in vacuo* to

approximately 5 mL to which 2 mL of toluene was added and the obtained orange suspension was vigorously heated in order to obtain a solution. Slow cooling to room temperature afforded colorless X-ray quality crystals (598 mg, 88%). Anal. Calcd. for  $C_{28}H_{76}Na_2MnN_4Si_4$ : C, 49.30; H, 11.23; N, 8.21; found C, 48.55; H, 10.76; N, 8.34.

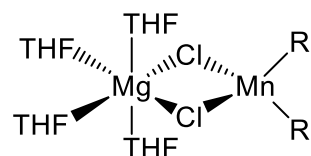
#### 5.7.10. Synthesis of $[(PMDETA)_2K_2Mn(CH_2SiMe_3)_4]$ (48)

$Mn(CH_2SiMe_3)_2$  (0.23 g, 1 mmol) and  $KCH_2SiMe_3$  (0.26g, 2 mmol) were suspended in 10 mL of hexane and stirred at room temperature for 30 min. To this suspension freshly distilled  $N,N',N'',N''',N'''$ -pentamethylethylenetriamine (PMDETA) (0.42 mL, 2 mmol) was added, affording an orange suspension that was left stirring for another 30 min at room temperature. The solvent was concentrated *in vacuo* to approximately 5 mL to which 2 mL of toluene was added and the obtained orange suspension was vigorously heated in order to obtain a solution. Slow cooling to room temperature afforded colorless X-ray quality crystals (518 mg, 63%). Anal. Calcd. for  $C_{34}H_{90}K_2MnN_6Si_4$ : C, 49.28; H, 10.95; N, 10.14. Satisfactory elemental analysis was not obtained and needs to be repeated.



#### 5.7.11. Synthesis of $[(THF)_4MgCl_2Mn(CH_2SiMe_3)_2]$ (50)

To a THF suspension of  $MnCl_2$  (0.126 g, 1mmol in 10 mL THF), freshly prepared and titrated THF solution of  $(CH_2SiMe_3)MgCl$  (0.63 M, 2 mmol, 3.16 mL) was added dropwise. After stirring for 1 hour at room temperature, the greyish solution was layered with hexane and placed at  $-33\text{ }^\circ\text{C}$  to precipitate  $MgCl_2$  which was removed by filtration. The filtrate was returned at  $-33\text{ }^\circ\text{C}$  and after several days a crop of colourless, X-ray quality crystals were isolated (0.15 g, 24.5 %). Anal. Calcd. for  $C_{24}H_{54}Cl_2MgMnO_4Si_2$ : C, 47.02; H, 8.08. Satisfactory elemental analysis was not obtained and needs to be repeated.



## 5.8. Bibliography

- [1] R. E. Mulvey, *Organometallics* **2006**, *25*, 1060–1075.
- [2] R. E. Mulvey, F. Mongin, M. Uchiyama, Y. Kondo, *Angew. Chem. Int. Ed.* **2007**, *46*, 3802–3824.
- [3] A. Harrison-Marchand, F. Mongin, *Chem. Rev.* **2013**, *113*, 7470–7562.
- [4] R. E. Mulvey, D. R. Armstrong, B. Conway, E. Crosbie, A. R. Kennedy, S. D. Robertson,

- Inorg. Chem.* **2011**, *50*, 12241–12251.
- [5] V. L. Blair, W. Clegg, R. E. Mulvey, L. Russo, *Inorg. Chem.* **2009**, *48*, 8863–8870.
- [6] R. A. Layfield, *Chem. Soc. Rev.* **2008**, *37*, 1098–1107.
- [7] A. Alberola, V. L. Blair, L. M. Carrella, A. R. Kennedy, J. Klett, R. E. Mulvey, S. Newton, E. Rentschler, L. Russo, *Organometallics* **2009**, *28*, 2112–2118.
- [8] J. Garcia-Álvarez, A. R. Kennedy, J. Klett, R. E. Mulvey, *Angew. Chem. Int. Ed.* **2007**, *46*, 1105–1108.
- [9] V. L. Blair, L. M. Carrella, W. Clegg, J. Klett, R. E. Mulvey, E. Rentschler, L. Russo, *Chem. Eur. J.* **2009**, *15*, 856–863.
- [10] V. L. Blair, W. Clegg, B. Conway, E. Hevia, A. Kennedy, J. Klett, R. E. Mulvey, L. Russo, *Chem. Eur. J.* **2008**, *14*, 65–72.
- [11] R. J. Morris, G. S. Girolami, *J. Am. Chem. Soc.* **1988**, *110*, 6245–6246.
- [12] R. A. Bartlett, M. M. Olmstead, P. P. Power, S. C. Shoner, *Organometallics* **1988**, *7*, 1801–1806.
- [13] R. J. Morris, G. S. Girolami, *Organometallics* **1989**, *8*, 1478–1485.
- [14] G. M. Yee, K. Kowolik, S. Manabe, J. C. Fettinger, L. A. Berben, *Chem. Commun.* **2011**, *47*, 11680–11682.
- [15] R. A. Layfield, S. M. Humphrey, *Angew. Chem. Int. Ed.* **2004**, *43*, 3067–3069.
- [16] S. E. Baillie, W. Clegg, P. García-Álvarez, E. Hevia, A. R. Kennedy, J. Klett, L. Russo, *Chem. Commun.* **2011**, *47*, 388–390.
- [17] T. Cadenbach, E. Hevia, *Organometallics* **2013**, *32*, 480–489.
- [18] D. R. Armstrong, H. S. Emerson, A. Hernán-Gómez, A. R. Kennedy, E. Hevia, *Dalton Trans.* **2014**, *43*, 14229–14238.
- [19] G. Wilkinson, *Dalton Trans.* **1976**, 2204–2211.
- [20] A. J. Hart, C. R. Russell, *J. Organomet. Chem.* **1974**, *72*, C19–C22.
- [21] B. Conway, D. V. Graham, E. Hevia, A. R. Kennedy, J. Klett, R. E. Mulvey, *Chem. Commun.* **2008**, 2638–2640.
- [22] W. Clegg, B. Conway, A. R. Kennedy, J. Klett, R. E. Mulvey, L. Russo, *Eur. J. Inorg. Chem.* **2011**, *2011*, 721–726.
- [23] P. J. Davidson, M. F. Lappert, R. Pearce, *Acc. Chem. Res.* **1974**, *7*, 209–217.
- [24] P. J. Davidson, M. F. Lappert, R. Pearce, *Chem. Rev.* **1976**, *76*, 219–242.
- [25] A. R. Kennedy, J. Klett, R. E. Mulvey, S. D. Robertson, *Eur. J. Inorg. Chem.* **2011**, *2011*, 4675–4679.

- [26] A. R. Kennedy, J. Klett, R. E. Mulvey, S. Newton, D. S. Wright, *Chem. Commun.* **2008**, 308–310.
- [27] M. S. Krallk, L. Stahl, A. M. Arif, C. E. Strouse, R. D. Ernst, *Organometallics* **1992**, *11*, 3617–3621.
- [28] G. W. W. Gokel, S. L. De Wall, E. S. Meadows, S. L. De Wall, *Eur. J. Org. Chem.* **2000**, 2967–2978.
- [29] G. C. Forbes, A. R. Kennedy, R. E. Mulvey, B. A. Roberts, B. Rowlings, *Organometallics* **2002**, *21*, 5115–5121.
- [30] J. C. Ma, D. A. Dougherty, *Chem. Rev.* **1997**, *97*, 1303–1324.
- [31] S. Gambarotta, C. Floriani, A. Chiesi-Villa, C. Guastini, *J. Chem. Soc. Chem. Commun.* **1983**, 1128–1129.
- [32] R. A. Lewis, S. Morochnik, A. Chapovetsky, G. Wu, T. W. Hayton, *Angew. Chem.* **2012**, *124*, 12944–12947.
- [33] K. J. Drewette, K. W. Henderson, A. R. Kennedy, R. E. Mulvey, C. T. O'Hara, R. B. Rowlings, *Chem. Commun.* **2002**, 1176–1177.
- [34] P. C. Andrikopoulos, D. R. Armstrong, A. R. Kennedy, R. E. Mulvey, C. T. O'Hara, R. B. Rowlings, *Eur. J. Inorg. Chem.* **2003**, 3354–3362.
- [35] N. D. R. Barnett, W. Clegg, A. R. Kennedy, R. E. Mulvey, S. Weatherstone, *Chem. Commun.* **2005**, 375–377.
- [36] E. Hevia, A. R. Kennedy, J. Klett, R. E. Mulvey, *Chem. Commun.* **2007**, 1641–1643.
- [37] S. E. Baillie, E. Hevia, A. R. Kennedy, R. E. Mulvey, *Organometallics* **2007**, 204–209.
- [38] J. García-Alvarez, D. V. Graham, E. Hevia, A. R. Kennedy, R. E. Mulvey, *Dalton Trans.* **2008**, *4*, 1481–1486.
- [39] Y. K. Gun'ko, U. Cristmann, V. G. Kessler, *Eur. J. Inorg. Chem.* **2002**, 1029–1031.
- [40] R. E. Mulvey, K. W. Henderson, *J. Am. Chem. Soc.* **2004**, *126*, 7444–7445.
- [41] K. Merz, S. Block, R. Schoenen, M. Driess, *Dalt. Trans.* **2003**, 3365–3369.
- [42] E. Hevia, A. R. Kennedy, R. E. Mulvey, S. Weatherstone, *Angew. Chem. Int. Ed.* **2004**, *43*, 1709–12.
- [43] M. M. Olmstead, W. J. Grigsby, D. R. Chacon, T. Hascall, P. P. Power, *Inorganica Chim. Acta* **1996**, *251*, 273–284.
- [44] S. Sakamoto, T. Imamoto, K. Yamaguchi, *Org. Lett.* **2001**, *3*, 1793–1795.
- [45] E. Weiss, *Angew. Chem. Int. Ed.* **1993**, *32*, 1501–1670.
- [46] S. E. Baillie, T. D. Bluemke, W. Clegg, A. R. Kennedy, J. Klett, L. Russo, M. de Tullio, E. Hevia, *Chem. Commun.* **2014**, *50*, 12859–12862.

- [47] J. Langer, S. Krieck, R. Fischer, H. G??rls, D. Walther, M. Wusterhausen, *Organometallics* **2009**, *28*, 5814–5820.
- [48] P. C. Andrews, R. E. Mulvey, D. R. Armstrong, D. R. Baker, W. Clegg, L. Horsburgh, Pa. A. O'Neill, D. Reed, *Organometallics* **1995**, *14*, 427–439.
- [49] D. J. MacDougall, J. J. Morris, B. C. Noll, K. W. Henderson, *Chem. Commun.* **2005**, 456–458.
- [50] J. J. Morris, B. C. Noll, K. W. Henderson, *Chem. Commun.* **2007**, *6*, 5191–5193.
- [51] A. Jaenschke, U. Behrens, *Zeitschrift fur Naturforsch. - Sect. B J. Chem. Sci.* **2014**, *69*, 655–664.
- [52] A. Maercker, *Angew. Chemie Int. Ed.* **1987**, *26*, 972–989.
- [53] J. Randazzo, J. Jacob Morris, J. a. Rood, B. C. Noll, K. W. Henderson, *Inorg. Chem. Commun.* **2008**, *11*, 1270–1272.
- [54] J. a. Rood, B. C. Noll, K. W. Henderson, *Inorg. Chem. Commun.* **2006**, *9*, 1129–1132.
- [55] J. Garcia-Alvarez, E. Hevia, A. R. Kennedy, J. Klett, R. E. Mulvey, *Chem. Commun.* **2007**, 851, 2402.
- [56] R. E. Mulvey, V. L. Blair, W. Clegg, A. R. Kennedy, J. Klett, L. Russo, *Nat. Chem.* **2010**, *2*, 588–591.
- [57] D. R. Armstrong, R. E. Mulvey, J. A. Parkinson, *Angew. Chem.* **2010**, *49*, 3185–3188.
- [58] S. C. Cole, M. P. Coles, P. B. Hitchcock, *Organometallics* **2004**, *23*, 5159–5168.
- [59] E. Hevia, K. W. Henderson, A. R. Kennedy, R. E. Mulvey, *Organometallics* **2006**, *25*, 1778–1785.
- [60] M. L. Hsueh, S. F. Hsu, *Organometallics* **2006**, *25*, 4144–4149.
- [61] P. C. Andrikopoulos, D. R. Armstrong, E. Hevia, A. R. Kennedy, R. E. Mulvey, C. T. O'Hara, *Chem. Commun.* **2005**, 1131–1133.
- [62] T. Greiser, D. Thoennes, E. Weiss, *Chem. Ber.* **1981**, *114*, 209–213.
- [63] A. D. Bond, R. a. Layfield, J. a. MacAllister, J. M. Rawson, D. S. Wright, M. McPartlin, *Chem. Commun.* **2001**, *36*, 1956–1957.
- [64] C. Duboc, M.-N. Collomb, F. Neese, *Appl. Magn. Reson.* **2010**, *37*, 229–245.
- [65] C. Duboc, V. Astier-Perret, H. Chen, J. Pecaut, R. H. Crabtree, G. W. Brudvig, M. N. Collomb, *Inorganica Chim. Acta* **2006**, *359*, 1541–1548.
- [66] N. F. Chilton, R. P. Anderson, L. D. Turner, A. Soncini, K. S. Murray, *J. Comput. Chem.* **2013**, *34*, 1164–1175.
- [67] C. Ni, G. J. Long, F. Grandjean, P. P. Power, *Inorg. Chem.* **2009**, *48*, 11594–11600.

- [68] D. Coucouvanis, K. Greiwe, A. Salifoglou, P. Challen, A. Simopoulos, A. Kostikas, *Inorg. Chem.* **1988**, *27*, 593–594.
- [69] S. K. Kondaveeti, S. Vaddypally, C. Lam, D. Hirai, N. Ni, R. J. Cava, M. J. Zdilla, *Inorg. Chem.* **2012**, *51*, 10095–10104.
- [70] P. Crewdson, S. Gambarotta, G. P. A. Yap, L. K. Thompson, *Inorg. Chem.* **2003**, *42*, 8579–8584.
- [71] E. Solari, F. Musso, E. Gallo, C. Floriani, N. Re, A. Chiesi-Villa, C. Rizzoli, *Organometallics* **1995**, *14*, 2265–2276.
- [72] B. Cordero, V. Gómez, A. E. Platero-Prats, M. Revés, J. Echeverría, E. Cremades, F. Barragán, S. Alvarez, *Dalt. Trans.* **2008**, 2832–2838.
- [73] C. Ni, J. C. Fettinger, G. J. Long, P. P. Power, *Dalton Trans.* **2010**, *39*, 10664–10670.
- [74] W. E. Buschmann, A. M. Arif, J. S. Miller, *Angew. Chem. Int. Ed.* **1998**, *37*, 781–783.
- [75] J. Langer, S. Kriech, H. Görls, M. Westerhausen, *Angew. Chem. Int. Ed.* **2009**, *48*, 5741–5744.
- [76] H. Schmidbaur, T. Costa, B. Milewski-Mahrla, F. H. Koehler, Y.-H. Tsay, C. Krueger, J. Abart, F. E. Wagner, *Organometallics* **1982**, *1*, 1266–1270.
- [77] G. Mueller, D. Neugebauer, W. Geile, F. H. Koehler, J. Pebler, H. Schmidbaur, *Organometallics* **1983**, *2*, 257–263.
- [78] R. Fischer, H. Goerls, M. Friedrich, M. Westerhausen, *J. Organomet. Chem.* **2009**, *694*, 1107–1111.
- [79] B. Haag, V. Malakhov, P. Knochel, *Angew. Chem. Int. Ed. Engl.* **2011**, *50*, 9794–9824.
- [80] D. Tilly, F. Chevallier, F. Mongin, P. C. Gros, *Chem. Rev.* **2014**, *114*, 1207–1257.
- [81] Y. Kondo, M. Fujinami, M. Uchiyama, T. Sakamoto, *J. Chem. Soc. Perkin Trans. 1* **1997**, 799–800.
- [82] M. Uchiyama, T. Miyoshi, Y. Kajihara, T. Sakamoto, Y. Otani, T. Ohwada, Y. Kondo, *J. Am. Chem. Soc.* **2002**, *124*, 8514–8515.
- [83] M. Uchiyama, Y. Kobayashi, T. Furuyama, S. Nakamura, Y. Kajihara, T. Miyoshi, T. Sakamoto, Y. Kondo, K. Morokuma, *J. Am. Chem. Soc.* **2008**, 472–480.
- [84] M. Uchiyama, T. Furuyama, M. Kobayashi, Y. Matsumoto, K. Tanaka, *J. Am. Chem. Soc.* **2006**, *128*, 8404–8405.
- [85] T. Furuyama, M. Yonehara, S. Arimoto, M. Kobayashi, Y. Matsumoto, M. Uchiyama, *Chem. Eur. J.* **2008**, *14*, 10348–10356.
- [86] N. T. T. Chau, M. Meyer, S. Komagawa, F. Chevallier, Y. Fort, M. Uchiyama, F. Mongin, P. C. Gros, *Chem. Eur. J.* **2010**, *16*, 12425–12433.
- [87] G. Cahiez, D. Bernard, J. F. Normant, *J. Organomet. Chem.* **1976**, *113*, 107–113.

- [88] G. Cahiez, C. Duplais, J. Buendia, *Chem. Rev.* **2009**, *109*, 1434–1476.
- [89] G. Cahiez, F. Lepifre, P. Ramiandrasoa, *Synthesis-Stuttgart* **1999**, 2138–2144.
- [90] G. Cahiez, D. Luart, F. Lecomte, *Org. Lett.* **2004**, *6*, 4395–4398.
- [91] K. Oshima, *J. Organomet. Chem.* **1999**, *575*, 1–20.
- [92] D. A. Valyaev, G. Lavigne, N. Lugan, *Coord. Chem. Rev.* **2015**, *308*, 191–235.
- [93] G. Cahiez, A. Moyeux, J. Buendia, C. Duplais, *J. Am. Chem. Soc.* **2007**, *129*, 13788–13789.
- [94] G. Cahiez, C. Duplais, J. Buendia, *Angew. Chem. Int. Ed.* **2009**, *48*, 6731–6734.
- [95] P. Sobota, J. Utko, L. B. Jerzykiewicz, *Inorg. Chem.* **1998**, *37*, 3428–3431.
- [96] E. Hevia, J. Z. Chua, P. García-Alvarez, A. R. Kennedy, M. D. McCall, *Proc. Natl. Acad. Sci. U. S. A.* **2010**, *107*, 5294–5299.



## 6. Conclusions and Outlook

Exploiting metal-metal and metal-ligand cooperativities, this thesis provides new insights in organogallium and organomanganese chemistry, advancing the applications of these compounds for the functionalisation of organic substrates and raising implications for small molecule activation processes.

The first part of the thesis presents new applications of trisalkylgallium in organic transformations. Studies on gallium NHC chemistry revealed a rational approach to access three distinct types of carbenes (i.e., normal, abnormal and anionic). Thus, anionic alkali-metal gallates have been shown to react with a variety of electrophiles in a controlled and selective manner affording  $\alpha$ NHC·Ga complexes under mild conditions. Interestingly,  $\alpha$ NHC·Ga complexes can also be accessed by thermal isomerisation. Combining NMR spectroscopic and kinetic studies with DFT calculations, new light has been shed on this intriguing transformation, which highlighted the importance of the donor ability of the solvent used in these thermal isomerisations as well as the steric bulk of the substituents on the NHC and gallium reagent. This reactivity was reminiscent of that reported for the  $\text{BAr}_3/\text{tBu}$  frustrated Lewis pair (FLP) system which has been used for the small molecule activation of molecules such as hydrogen or alkynes. By pursuing this line of enquiry, this thesis has also revealed the first examples of FLP activation processes using a gallium tris(alkyl) complex as an effective Lewis Acid. Using carbonyl compounds as model substrates, two different types of FLP activation processes have been uncovered: namely, (i) reduction of the C=O functionality and formation of a new C-C bond, and (ii) C-H bond activation yielding. The reduction reactions can be finely tuned to take place either at the normal (C2) or abnormal position (C4), depending on the size of the substrate and the reaction time in processes involving complex equilibria. These in-depth studies, supported by solid-state structural characterisation, have revealed the hitherto hidden ability of abnormal NHCs to promote FLP chemistry.

The cooperative behaviour of  $\text{tBu}$  and  $\text{GaR}_3$  observed in small molecule activation based on the steric incompatibility of reagents in question, led us to attempt a similar approach in the domain of bimetallic chemistry. In this context, sterically hindered lithium amide  $\text{LiTMP}$  and  $\text{GaR}_3$  were found not to undergo co-complexation to form a weakly basic ate, but rather

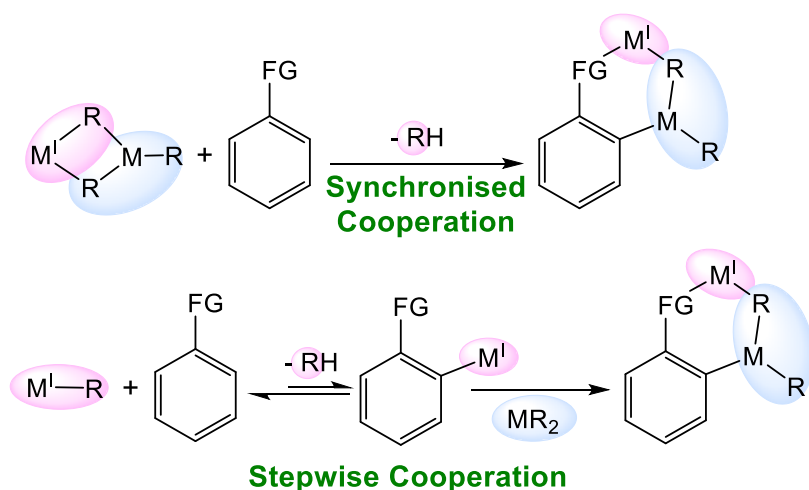
operating as a multicomponent mixture in a tandem manner, to effectively promote deprotonation of sensitive heterocycles lacking a lateral directing group. These findings introduced the concept of gallium *trans-metal-trapping* where the complementary combination of the strong basicity of free LiTMP and the strong carbophilicity of GaR<sub>3</sub> that can stabilize sensitive metallo-intermediates, facilitate challenging functionalisations can be accomplished with high selectivity under mild conditions in hydrocarbon solvent.

Moving on to the second part of the thesis, extending study to manganate chemistry, a family of rationally synthesized and fully characterized alkali-metal manganates has been presented. Paramagnetic character of organomanganate species precluded their studies by NMR spectroscopy; however in that case the picture obtained by X-ray crystallographic studies was completed with the information gleaned from EPR spectroscopic and SQUID magnetometric measurements. These studies revealed intriguing structural/synthetic/magnetic correlations where aggregation state and reactivity of different manganates was determined predominantly by the alkali-metal employed. Building on these findings, further study into the application of a well-defined alkali-metal manganate in Mn-I exchange and homocoupling reactions has been investigated, establishing a direct relationship between a well-defined manganate species and its application in synthesis.

Overall, the results presented in this PhD thesis illustrate that there are different types of synergy that can be employed for application in organic transformations. The chemistry developed for organogallium reagents highlights stepwise synergistic processes which can be based on either two metal reagents or on a single-metal reagent combined with a special ligand. Foundations set in this research could potentially open many new roads of development in organogallium chemistry. In the context of small molecule activation, not only should new types of substrate-activation be investigated (most notable examples being B-H or H-H bonds) but also a potential for variation in the components making the FLP system. Fine-tuning the skeleton of the NHC or moving to a different carbene altogether would be obvious choices, but additionally many different bulky ligands (such as phosphines or guanidines), could be potentially utilised as a base component. Similarly, the use of gallium reagent as a Lewis acid component should be further examined with the focus on other bulky alkyl groups (i.e. <sup>t</sup>Bu or even adamantyl). An interesting question to ponder is “could the variability of the gallium reagent be extended to less reactive compounds such as salts (e.g. GaCl<sub>3</sub>) or alkoxides, especially for the work in the context of *trans-metal-trapping*?” The reasoning behind this is the key characteristic of gallium reagent offering

stabilisation based on its carbophilicity, and not the requirement to actually conduct deprotonation, that is, functions as the trap not the base.

The results arising from the study of organomanganate chemistry emphasise a second type of synergy where the two metals are integrated within the same molecule and they operate in a synchronised manner. Having just scraped the surface, already a connection between a well-defined species and metal-halogen exchange and subsequent carbon-carbon bond formation has been established. Further mechanistic studies are required to determine the pathway this transformation takes place. This could move this reactivity into the realm of catalytic processes and encourage a design of reagent with improved performance. Most notable improvement would be the ability to control the outcome of the final step in reactivity, namely homocoupling *versus* heterocoupling.



To conclude, the take home message is not which type of cooperation is better, but rather that chemists have choices of methods at their disposal and that the approach should be chosen based on the specific requirements of the system.

## 7. General experimental techniques and procedures

### 7.1. Schlenk Techniques

Synthetic work was carried out using standard Schlenk techniques as most of the reactants and obtained products are air and moisture sensitive, with some, like  $\text{Ga}(\text{CH}_2\text{SiMe}_3)_3$ , even being pyrophoric. A Schlenk line contains an inert gas/vacuum manifold and has two separate compartments; one compartment is connected to a vacuum pump and the other one to a supply of dry inert, argon gas (**Figure 7.1**).



**Figure 7.1:** A typical Schlenk line.

The Schlenk line has a number of connectors, each of which have a two way tap so that either vacuum or argon can be applied when needed. From the connected piece of glassware, air can be removed by applying vacuum for twenty minutes after which it is refilled with dry argon. This procedure is employed three times to ensure there are no traces of air and moisture inside Schlenk tubes and other used glassware. Additionally, the line contains a pressure release bubbler and a trap attached to the end of the Schlenk line. The trap is cooled with liquid nitrogen ( $-196\text{ }^\circ\text{C}$ ) to condense any volatiles that are removed *in vacuo* from the reaction mixture, while the bubbler maintains the pressure inside the system.

All Schlenk glassware, including Schlenk tubes, filtersticks, and solid addition tubes contain ground-glass joints which are always lightly greased prior to any use ensuring an air tight seal. A positive flow of argon is maintained at all times to ensure no air enters the system while adding solvents and reagents. Liquids are transferred using a syringe and a needle that are flushed with argon ten times immediately prior to use.

## 7.2. Glove box

A glove box was used routinely to store reagents and products that were air and moisture sensitive. A typical glove box is made up of three chambers - the main one, where the actual work is carried out and two smaller ones that are used to take chemicals in and out of the main chamber (**Figure 7.2**). The main chamber has a gas recirculation and a purification system that ensure the minimal amounts of air and moisture are present and manipulation within the box is made possible through gloves made of semi-permeable material. The smaller chambers are called ports and they contain both inner and outer doors to allow materials to be transferred into the main chamber without the possibility of air entering. The outside door allows items to be placed in the port after which vacuum and argon can be applied. The inside door can then be opened allowing the materials to be transferred into the manipulation area.



**Figure 7.2:** A typical glove box.

### 7.3. Solvent purification

Extreme air and moisture sensitivity of the reactants and products required all solvents to be dried and degassed prior to use. This was achieved by refluxing them over benzophenone and sodium metal under an inert nitrogen atmosphere.<sup>[1]</sup> When sodium metal reacts with dissolved water, sodium hydroxide and hydrogen gas are formed; however the remaining sodium will react with the benzophenone to give a blue ketyl radical anion. The blue coloured solution is hence an indicator that the solvents are dry as this radical will react with any traces of water or oxygen and the intense blue colour will be lost.

Deuterated solvents were purchased dried and sealed, but still underwent a freeze-pump-thaw methodology<sup>[1]</sup> to remove any dissolved oxygen, which was repeated three times. Finally the degassed solvents were stored in the glove box over activated 4 Å molecular sieves.

### 7.4. Commercial reagents

Commercially available reagents were purchased from Sigma Aldrich, Alfa Aesar or Fluorochem at the highest purity available. Tetramethylpiperidine (TMPPH) was acquired from Acros Organics.

The hygroscopic liquid reagents (i.e. *N,N,N',N'*-tetramethylethylenediamine or 1,4-dioxane) were dried by heating to reflux over calcium hydride, distilled under nitrogen and stored over activated 4 Å molecular sieves in an ampoule fitted with a J Young valve.

### 7.5. Standardisation of organometallic reagents

Grignard reagents were used in the form of THF solutions and were titrated against iodine to determine the exact concentration.<sup>[2]</sup> The solution of Grignard reagent was added dropwise into the THF solution of iodine saturated with LiCl until a colour change from brown to colourless was observed which marked the end point. From the used volume of the Grignard reagent it was possible to determine the concentration.

Similarly, commercial solutions of organolithium reagents (i.e. (trimethylsilyl)methyl lithium) were titrated against salicylaldehyde phenylhydrazone in dry THF.<sup>[3]</sup> The change of colour from yellow to red indicated the end point from which the concentration of the lithium reagent could be calculated.

## 7.6. Analytical procedures

All  $^1\text{H}$  NMR spectroscopic experiments were carried out using a Bruker AV3, AV400 or DRX 500 spectrometer operating at 400.03, 400.13 or 500.13 MHz respectively. The  $^{13}\text{C}\{^1\text{H}\}$  NMR spectra were obtained on the same instruments; operating at 100.62, 100.60 and 125.77 MHz, respectively, and were always proton decoupled, while the  $^2\text{H}$  NMR spectra were recorded at 61.402 MHz. Chemical shifts are reported relative to tetramethylsilane at 0.00 ppm. The  $^7\text{Li}$  NMR spectra were recorded at 155.50 MHz and referenced against LiCl in  $\text{D}_2\text{O}$  at 0.00 ppm, whereas the  $^{19}\text{F}\{^1\text{H}\}$  NMR spectra were recorded at 376.40 MHz and referenced against  $\text{C}_6\text{H}_5\text{CF}_3$  in  $d_6$ -acetone at -63.72 ppm vs  $\text{CFCl}_3$  at 0.00 ppm. Abbreviations of NMR patterns are as follows: s (singlet), d (doublet), t (triplet), sept (septet), mult (multiplet) and br (broad signal).

The Diffusion-Order Spectroscopy (DOSY) NMR experiments were recorded on a Bruker AV400 NMR spectrometer operating at 400.13 MHz for proton resonance and the plots were generated using the DOSY processing modules with empirical optimisation of parameters.

Elemental (C, H, N) analysis was performed on a Perkin Elmer 2400 elemental analyser. Samples were prepared in the argon-filled glovebox and transported in an air-tight box in order to prevent decomposition. However, even with these precaution measures in place, some compounds were too sensitive or have exhibited difficulties in burning (*e.g.* forming metal carbides) to obtain results within 0.5% error of calculated values.

Infrared spectra were recorded on a Nicolet 360 FTIR spectrometer spanning the range 4000 – 400  $\text{cm}^{-1}$ . Samples were prepared in the glovebox as Nujol mulls on NaCl plates, using Nujol that had been dried over sodium metal, and were transferred to the spectrometer in a dessicator.

Crystallographic data were measured at 123(2) K on Oxford Diffraction Gemini S or Xcalibur E instruments with graphite-monochromated Mo ( $\lambda = 0.71073 \text{ \AA}$ ) or Cu ( $\lambda = 1.54184 \text{ \AA}$ ) radiation. All structures were refined to convergence on  $F^2$  using all unique reflections and programs from the SHELX family.<sup>[4]</sup>

## 7.7. Synthesis of common starting materials

### 7.7.1. Synthesis of Ga(CH<sub>2</sub>SiMe<sub>3</sub>)<sub>3</sub> (GaR<sub>3</sub>)<sup>[5]</sup>

In an oven-dried, argon purged 500 mL round bottom flask, Mg turnings (3.5 g, 144 mmol) were suspended in dry diethyl ether (60 mL). An ethereal solution (60 mL) of (chloromethyl)trimethylsilane (17.1 mL, 120 mmol) was added dropwise into the magnesium suspension. The resulting grey suspension was left stirring overnight after which it was filtered through celite and glass wool to remove excess magnesium. The obtained straw filtrate was slowly added into a cooled (0 °C) ethereal solution (80 mL) of gallium(III) chloride (5.0 g, 28 mmol). The resulting thick white suspension was then gradually warmed to room temperature and stirred overnight. Removal of the solvent *in vacuo* afforded a white residue which was purified by distillation at 120 °C (10<sup>-2</sup> Torr) to furnish pure GaR<sub>3</sub> as a colourless liquid (typical yield 7.5 g, 80%).

<sup>1</sup>H NMR (298 K, C<sub>6</sub>D<sub>6</sub>) δ 0.13 (11H, s, CH<sub>2</sub> and CH<sub>3</sub>). <sup>13</sup>C{<sup>1</sup>H} NMR (298 K, C<sub>6</sub>D<sub>6</sub>) δ 2.49 (CH<sub>3</sub>), 12.69 (CH<sub>2</sub>). <sup>1</sup>H NMR (298 K, d<sub>8</sub>-THF) δ -0.55 (2H, s, CH<sub>2</sub>), -0.01 (9H, s, CH<sub>3</sub>). <sup>13</sup>C{<sup>1</sup>H} NMR (298 K, d<sub>8</sub>-THF) δ 2.90 (CH<sub>3</sub>), 3.46 (CH<sub>2</sub>).

### 7.7.2. Synthesis of Mn(CH<sub>2</sub>SiMe<sub>3</sub>)<sub>2</sub> (MnR<sub>2</sub>)<sup>[6]</sup>

Mg(CH<sub>2</sub>SiMe<sub>3</sub>)<sub>2</sub> was prepared from Grignard reagent (Me<sub>3</sub>SiCH<sub>2</sub>)MgCl by manipulation of the Schlenk equilibrium and purified by sublimation.<sup>[7]</sup> Mg(CH<sub>2</sub>SiMe<sub>3</sub>)<sub>2</sub> (3 g, 15 mmol) and MnCl<sub>2</sub> (1.91 g, 15 mmol) were suspended in 60 mL of dry diethyl ether and allowed to stir for 2-3 days at room temperature. The solvent was exchanged *in vacuo* for dried toluene (160 mL) giving an orange suspension. Vigorous heating to boiling afforded an orange solution with a white precipitate (MgCl<sub>2</sub>) which was filtered hot and the bright orange filtrate allowed to cool to room temperature. Storage of the solution in the freezer (-33 °C) overnight yielded Mn(CH<sub>2</sub>SiMe<sub>3</sub>)<sub>2</sub> as orange crystals which were filtered and dried under vacuum (typical yield 2.5 g, 72 %).

### 7.7.3. Synthesis of NaCH<sub>2</sub>SiMe<sub>3</sub> (NaR)<sup>[8]</sup>

NaO<sup>t</sup>Bu (1.92 g, 20 mmol) was suspended in 40 mL of dry hexane to which LiCH<sub>2</sub>SiMe<sub>3</sub> (1 M in pentane, 20 mL, 20 mmol) was added dropwise. The resulting suspension was stirred



overnight at room temperature, and then filtered and washed with hexane (2 x 20 mL). The resulting white solid was dried *in vacuo* and isolated (typical yield 1.8 g, 82 %).

**<sup>1</sup>H NMR (298 K, C<sub>6</sub>D<sub>6</sub>)** δ -2.44 (2H, s, SiCH<sub>2</sub>), 0.15 (9H, s, Si(CH<sub>3</sub>)<sub>3</sub>). **<sup>1</sup>H NMR (298 K, d<sub>8</sub>-THF)** δ -2.20 (2H, s, CH<sub>2</sub>), -0.19 (9H, s, CH<sub>3</sub>).

#### 7.7.4. Synthesis of KCH<sub>2</sub>SiMe<sub>3</sub> (KR)<sup>[8a,9]</sup>

KO<sup>t</sup>Bu (2.24 g, 20 mmol) was suspended in 40 mL of dry hexane to which LiCH<sub>2</sub>SiMe<sub>3</sub> (1 M in pentane, 20 mL, 20 mmol) was added dropwise. The resulting suspension was stirred overnight at room temperature, and then filtered and washed with hexane (2 x 20 mL). The resulting white solid was dried *in vacuo* and isolated (typical yield 2.2 g, 87 %).

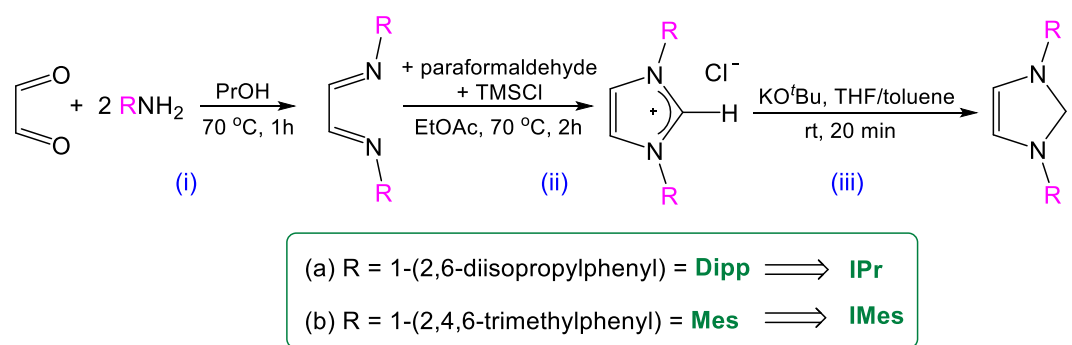
**<sup>1</sup>H NMR (298 K, C<sub>6</sub>D<sub>6</sub>)** δ -2.60 (2H, s, SiCH<sub>2</sub>), 0.18 (9H, s, Si(CH<sub>3</sub>)<sub>3</sub>). **<sup>1</sup>H NMR (298 K, d<sub>8</sub>-THF)** δ -2.24 (2H, s, CH<sub>2</sub>), -0.20 (9H, s, CH<sub>3</sub>).

#### 7.7.5. Synthesis of LiTMP<sup>[10]</sup>

To a stirring hexane (20 mL) solution of TMPH (1.7 mL, 10 mmol), <sup>n</sup>BuLi (6.3 mL, 1.6 M in hexanes, 10 mmol) was added dropwise. The resulting pale yellow solution was left stirring overnight at room temperature which afforded a suspension. After the filtration and washing with hexane (2 x 10 mL), the resulting white solid was dried *in vacuo* and isolated (typical yield 0.96 g, 65 %).

The product was analysed by comparing the NMR spectra with the literature ones and it should be noted that resonances for both trimeric and tetrameric polymorphs are evident and here reported.

**<sup>1</sup>H NMR (298 K, C<sub>6</sub>D<sub>6</sub>)** δ 1.30 and 1.36 (16H, s, CH<sub>3</sub> and H<sub>β</sub>, TMP) 1.73 and 1.78 (2H, m, H<sub>γ</sub>, TMP). **<sup>13</sup>C{<sup>1</sup>H} NMR (298 K, C<sub>6</sub>D<sub>6</sub>)** δ 20.1 and 19.9 (C<sub>γ</sub>, TMP), 37.1 and 37.0 (CH<sub>3</sub>, TMP), 43.2 and 42.8 (C<sub>β</sub>, TMP), 52.3 and 52.4 (C<sub>α</sub>, TMP). **<sup>7</sup>Li NMR (298 K, C<sub>6</sub>D<sub>6</sub>)** δ 2.47.

7.7.6. Synthesis of 1,3-diaryl-imidazol-2-ylidenes<sup>[11]</sup>

Scheme 7.1: Synthesis of IPr and IMes.

7.7.6.1. Synthesis of 1,3-bis-(2,6-diisopropylphenyl)imidazol-2-ylidene (**IPr**)

2,6-Diisopropylphenylamine (49.25 g, 52.4 mL, 280 mmol) and a 40% aqueous solution of glyoxal (18.15 g, 14.3 mL, 125 mmol) were dissolved in a mixture of 200 mL of *n*-propanol and 50 mL of water at room temperature. After stirring for 1h at 70 °C, the precipitate was collected by filtration and recrystallised from acetone to give glyoxal-bis-(2,6-diisopropylphenyl)imine (typical yield 40 g, 85 %).

The diimine (20 g, 53 mmol) and paraformaldehyde (1.59 g, 53 mmol) were added to heated (70 °C) ethyl acetate (0.5 L, technical quality, distilled in a rotary evaporator over  $\text{K}_2\text{CO}_3$ ). A solution of TMSCl (6.73 mL, 53 mmol) in ethyl acetate (20 mL) was added dropwise with vigorous stirring and the resulting yellow suspension was stirred for 2h at 70 °C. The mixture was left to cool overnight after which a colourless microcrystalline powder of 1,3-bis(2,6-diisopropylphenyl)imidazolium chloride was collected by filtration (typical yield 13.5 g, 60 %).

A Schlenk was charged with the imidazolium salt (2.9 g, 6.8 mmol) and evacuated three times after which dry THF was added (50 mL).  $\text{KO}^t\text{Bu}$  (0.9 g, 8.0 mmol) was added and the orange suspension was stirred for 2h at room temperature after which the solvent was exchanged *in vacuo* for toluene (50 mL). After filtration through celite and glass wool, all volatiles were removed to give the product as an off-white solid (average yield 2.4 g, 90%).

$^1\text{H}$  NMR (**298 K**,  $\text{C}_6\text{D}_6$ )  $\delta$  1.19 (12H, d,  $\text{CH}(\text{CH}_3)_2$ ), 1.29 (12H, d,  $\text{CH}(\text{CH}_3)_2$ ), 2.97 (sept, 4H,  $\text{CH}(\text{CH}_3)_2$ ), 6.63 (2H, s, imidazole backbone CH), 7.19 (4H, d, meta-CH), 7.29 (2H, t, para-CH).  $^{13}\text{C}\{^1\text{H}\}$  NMR (**298 K**,  $\text{C}_6\text{D}_6$ )  $\delta$  23.6 ( $\text{CH}(\text{CH}_3)_2$ ), 24.8 ( $\text{CH}(\text{CH}_3)_2$ ), 28.7

(CH(CH<sub>3</sub>)<sub>2</sub>), 121.5 (imidazole backbone, CH), 123.6 (meta-CH), 129.0 (para-CH), 139.0 (ipso-C), 146.2 (ortho-C), 220.6 (carbenic C:). <sup>1</sup>H NMR (298 K, d<sub>8</sub>-THF) δ 1.16 (12H, d, CH(CH<sub>3</sub>)<sub>2</sub>), 1.19 (12H, d, CH(CH<sub>3</sub>)<sub>2</sub>), 2.82 (sept, 4H, CH(CH<sub>3</sub>)<sub>2</sub>), 7.16 (2H, s, imidazole backbone CH), 7.25 (4H, d, meta-CH), 7.35 (2H, t, para-CH). <sup>13</sup>C{<sup>1</sup>H} NMR (298 K, d<sub>8</sub>-THF) δ 23.8 (CH(CH<sub>3</sub>)<sub>2</sub>), 24.9 (CH(CH<sub>3</sub>)<sub>2</sub>), 29.2 (CH(CH<sub>3</sub>)<sub>2</sub>), 122.5 (imidazole backbone, CH), 123.9 (meta-CH), 129.1 (para-CH), 139.7 (ipso-C), 146.8 (ortho-C), carbenic C: was not observed.

#### 7.7.6.2. Synthesis of 1,3-bis-(2,4,6-trimethylphenyl)imidazol-2-ylidene (IMes)

2,4,6-Trimethylphenylamine (67.61 g, 70.2 mL, 0.5 mol) and a 40% aqueous solution of glyoxal (36.3 g, 28.6 mL, 0.25 mol) were dissolved in a mixture of 200 mL of *n*-propanol and 50 mL of water at room temperature. After stirring overnight at room temperature and 4h at 60 °C the precipitate was collected by filtration and recrystallised from acetone to give glyoxal-*bis*-(2,4,6-trimethylphenyl)imine (typical yield 51.1 g, 70 %).

The diimine (15.49 g, 53 mmol) and paraformaldehyde (1.59 g, 53 mmol) were added to heated (70 °C) ethyl acetate (0.5 L, technical quality, distilled in a rotary evaporator over K<sub>2</sub>CO<sub>3</sub>). A solution of TMSCl (6.73 mL, 53 mmol) in ethyl acetate (20 mL) was added dropwise with vigorous stirring and the resulting yellow suspension was stirred for 2h at 70 °C. The mixture was left to cool overnight after which a colourless microcrystalline powder of 1,3-bis(2,6-diisopropylphenyl)imidazolium chloride was collected by filtration (typical yield 10.3 g, 57 %).

A Schlenk was charged with the imidazolium salt (4.3 g, 12.6 mmol) and evacuated three times after which dry THF was added (50 mL). KO<sup>t</sup>Bu (1.56 g, 13.9 mmol) was added and the orange suspension was stirred for 2h at room temperature after which the solvent was exchanged *in vacuo* for toluene (50 mL). After filtration through celite and glass wool, all volatiles were removed to give a dull orange residue which was then washed with hexane (30 mL) to yield the product as an off-white solid (average yield 2.5 g, 65%).

<sup>1</sup>H NMR (298 K, C<sub>6</sub>D<sub>6</sub>) δ 2.15 (18H, s, CH<sub>3</sub>), 6.50 (2H, s, imidazole backbone CH), 6.82 (4H, s, meta-CH). <sup>13</sup>C{<sup>1</sup>H} NMR (298 K, C<sub>6</sub>D<sub>6</sub>) δ 17.9 (ortho-CH<sub>3</sub>), 20.9 (para-CH<sub>3</sub>), 120.4

(imidazole backbone, CH), 129.0 (meta-CH), 135.3 (para-CH), 137.1 (ortho-C), 139.1 (ipso-C), 220.0 (carbenic C:).

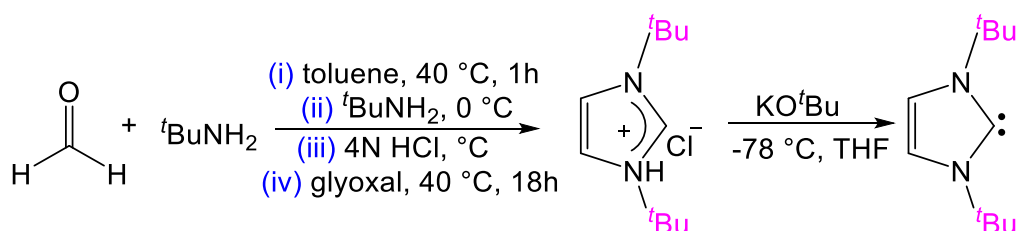
### 7.7.6.3. Synthesis of 1,3-bis-(2,6-diisopropylphenyl)-4,5-dideuteroimidazol-2-ylidene (**DIPr**)<sup>[12, 11a]</sup>

IPr•HCl (1.5 g, 3.5 mmol) and K<sub>2</sub>CO<sub>3</sub> (24.7 mg, 0.18 mmol) were added to a Schlenk followed by ~ 6 mL D<sub>2</sub>O. The reaction mixture was heated at 100 °C under argon for 24 hours. After allowing the reaction to cool, remaining solvents were removed under reduced pressure. Once dry, the product was washed with hexanes before filtering to collect a white solid (1.2 g, 80 % yield).

A Schlenk was charged with the imidazolium salt (1.2 g, 2.8 mmol) and evacuated three times after which dry THF was added (15 mL). KO<sup>t</sup>Bu (0.4 g, 3.2 mmol) was added and the white suspension was stirred for 0.5h at room temperature after which the solvent was exchanged *in vacuo* for toluene (20 mL). After filtration through celite and glass wool, all volatiles were removed to give the product as an off-white solid (average yield 750 mg, 67%).

<sup>1</sup>H NMR (**298 K**, C<sub>6</sub>D<sub>6</sub>) δ 1.19 (12H, d, CH(CH<sub>3</sub>)<sub>2</sub>), 1.29 (12H, d, CH(CH<sub>3</sub>)<sub>2</sub>), 2.97 (sept, 4H, CH(CH<sub>3</sub>)<sub>2</sub>), 7.19 (4H, d, meta-CH), 7.29 (2H, t, para-CH). <sup>2</sup>H NMR (**298 K**, C<sub>6</sub>D<sub>6</sub>) δ 6.63 (br s, imidazole backbone).

### 7.7.7. Synthesis of (**I'Bu**)<sup>[13]</sup>



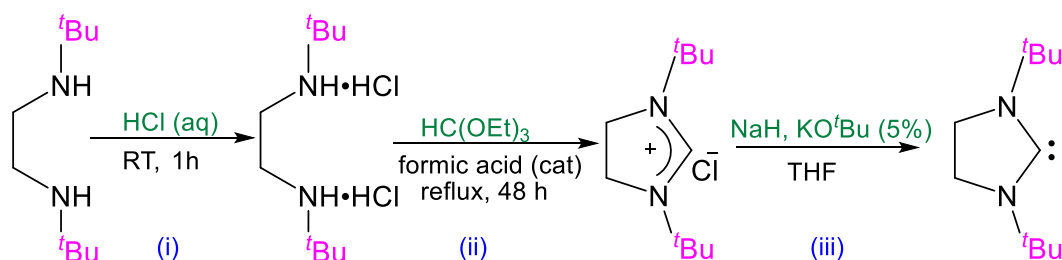
**Scheme 7.2:** Synthesis of I'Bu.

A Schlenk was charged with paraformaldehyde (0.60 g, 20 mmol) and evacuated three times after which dry toluene was added (20 mL) followed by a dropwise addition of *tert*-butylamine (1.46 g, 2.12 mL, 20 mmol). The mixture was heated at 40 °C until a clear solution was formed which was then cooled to 0 °C and another aliquot of *tert*-butylamine (2.12 mL) was added dropwise. 4N dioxane HCl (6.7 mL) was added slowly at 0 °C and then the ice bath was removed. Glyoxal (2.28 mL of a 40% solution in water) was then added and the mixture stirred overnight at 40 °C. The mixture was quenched with NaHCO<sub>3</sub> (10 mL of an aqueous solution) and the aqueous phase was washed with diethyl ether (3 x 25 mL). The water was removed *in vacuo* and the product extracted with DCM (average yield 2.03 g, 47%).

A Schlenk tube was charged with the imidazolium salt (2.0 g, 9.3 mmol) and evacuated three times after which dry THF was added (30 mL). The suspension was cooled to -78 °C and stirred for 20 minutes followed by the addition of KO<sup>t</sup>Bu (1.01 g, 9.0 mmol). The mixture was allowed to warm to room temperature over 30 minutes after which the solvent was exchanged *in vacuo* for toluene (30 mL). After filtration through celite and glass wool, all volatiles were removed to give the product as an off-white solid (average yield 1.0 g, 59%).

<sup>1</sup>H NMR (298 K, C<sub>6</sub>D<sub>6</sub>) δ 1.51 (18H, s, C(CH<sub>3</sub>)<sub>3</sub>), 6.78 (2H, s, imidazole backbone CH).  
<sup>13</sup>C{<sup>1</sup>H} NMR (298 K, C<sub>6</sub>D<sub>6</sub>) δ 32.1 (CH<sub>3</sub>), 56.5 (C(CH<sub>3</sub>)<sub>3</sub>), 115.8 (imidazole backbone, CH), 213.2 (carbenic C:).  
<sup>1</sup>H NMR (298 K, d<sub>8</sub>-THF) δ 1.51 (18H, s, C(CH<sub>3</sub>)<sub>3</sub>), 7.04 (2H, s, imidazole backbone CH).

### 7.7.8. Synthesis of 1,3-bis(*t*-butyl)imidazolin-2-ylidene (SI<sup>t</sup>Bu)<sup>[14]</sup>



**Scheme 7.3:** Synthesis of SI<sup>t</sup>Bu.

*N,N'*-bis(*t*-butylamine)ethane (5 mL, 23.24 mmol) was treated with 10M HCl (4.7 mL, 46.48 mmol) in portions yielding a colourless solution which was stirred for 1h at room

temperature. The volatiles were removed under vacuum and *N,N'*-bis(*t*-butylamine)ethane dihydrochloride was obtained as a white crystalline solid (5.65 g, 99%).

A white suspension of triethyl orthoformate (37.3 mL, 224.5 mmol), *N,N'*-bis(*t*-butylamine)ethane dihydrochloride (5.5 g, 22.44 mmol) and formic acid (4 drops) was heated to reflux for 48 h. The obtained pale yellow solution was cooled to room temperature and the solvent was removed to yield a white solid.

1.3-Bis(*t*-butyl)imidazolium chloride (5 g, 22.8 mmol) was suspended in 50 mL of dry THF and in another Schlenk NaH (3.6 g, 60% dispersion in mineral oil, 91.2 mmol) and KO<sup>t</sup>Bu (125 mg, 1 mmol) were suspended in 80 mL THF. The suspension of NaH and KO<sup>t</sup>Bu was transferred *via* cannula and the reaction mixture was stirred overnight at room temperature. The white suspension was filtered through glass wool and celite, the solvent was removed under vacuum and the oily residue dissolved in 10 mL of hexane followed by another filtration to remove any residual impurities. Due to its extreme moisture sensitivity, Si<sup>t</sup>Bu was used as a hexane solution (concentration determined against hexamethylbenzene) and stored in an ampoule fitted with the Young J valve.

<sup>1</sup>H NMR (298 K, C<sub>6</sub>D<sub>6</sub>) δ 1.33 (18H, s, C(CH<sub>3</sub>)<sub>3</sub>), 3.04 (4H, s, NCH<sub>2</sub>). <sup>13</sup>C{<sup>1</sup>H} NMR (298 K, C<sub>6</sub>D<sub>6</sub>) δ 30.1 (CH<sub>3</sub>), 44.6 (C(CH<sub>3</sub>)<sub>3</sub>), 54.0 (NCH<sub>2</sub>CH<sub>2</sub>N), 218.7 (carbenic C:).

## 7.8. Bibliography

- [1] D. F. Shriver, M. A. Drezdson, *The Manipulation of Air-Sensitive Compounds*, 2nd ed., Wiley, New York, **1986**.
- [2] A. Krasovskiy, P. Knochel, *Synthesis* **2006**, 5, 890.
- [3] B. E. Love, E. G. Jones, *J. Org. Chem.* **1999**, 64, 3755.
- [4] G. M. Sheldrick, *Acta Crystallogr.* **2008**, A64, 112.
- [5] O. T. Beachley, Jr., R. G. Simmons, *Inorg. Chem.* **1980**, 19, 1021.
- [6] A. Alberola, V. L. Blair, L. M. Carella, W. Clegg, A. R. Kennedy, J. Klett, R. E. Mulvey, S. Newton, E. Rentschler, L. Russo, *Organometallics* **2009**, 28, 2112-2118.
- [7] S. E. Baillie, T. D. Bluemke, W. Clegg, A. R. Kennedy, J. Klett, L. Russo, M. de Tullio, E. Hevia, *Chem. Commun.* **2014**, 50, 12859.

- [8] (a) A. J. Hart, D. H. O'Brien, C. R. Russell, *J. Organomet. Chem.* **1974**, 72, C19-C22; (b) W. Clegg, B. Conway, A. R. Kennedy, J. Klett, R. E. Mulvey, L. Russo, *Eur. J. Inorg. Chem.* **2011**, 721-726.
- [9] B. Conway, D. V. Graham, E. Hevia, A. R. Kennedy, J. Klett, R. E. Mulvey, *Chem. Commun.* **2008**, 2638-2640.
- [10] E. Hevia, A. R. Kennedy, R. E. Mulvey, D. L. Ramsay, S. D. Robertson, *Chem. Eur. J.* **2013**, 9, 14069.
- [11] (a) A. J. Arduengo, III, R. Krafczyk, R. Schmutzler, H. A. Craig, J. R. Goerlich, W. J. Marshall, M. Unverzagt, *Tetrahedron* **1999**, 55, 14523; (b) L. Hintermann, *Beilstein J. Org. Chem.* **2007**, 3, No. 22.
- [12] R. M. Stolley, H. A. Duong, D. R. Thomas, J. Louie, *J. Am. Chem. Soc.* **2012**, 134, 15154.
- [13] E. C. Hurst, K. Wilson, I. J. S. Fairlamb, V. Chechik, *New J. Chem.* **2009**, 33, 1837.
- [14] K. Arentsen, S. Caddick, F. G. N. Cloke, *Tetrahedron* **2005**, 61, 9710.